Characterization of integral membrane proteins using mass spectrometry : bacteriorhodopsin, rhodopsin, and neutrophil cytochrome b558
by David Robert Barnidge

A thesis submitted in partial fulfillment of the requirements for the degree of Doctor of Philosophy in Chemistry
Montana State University


Abstract:
Electrospray ionization mass spectrometry (ESI MS) and matrix assisted laser desorption/ionization mass spectrometry (MALDI MS) have been used extensively to characterize the structural properties of cytosolic proteins. However, ESI and MALDI have had limited success in determining the accurate mass of integral membrane proteins, presumably due to interference from the detergents needed to solubilize them. Therefore, mass spectrometry has had limited applicability in structural studies of integral membrane proteins.

The integral membrane protein bacteriorhodopsin (BR) was used as a model in the development of a method for determining the accurate mass of BR solubilized in the detergents cetyltrimethylammonium bromide (CTAB), octyl-β-glucoside (OG), and CHAPSO by ESI MS. Quality mass spectra were obtained by means of a phase-separation technique where BR was partitioned into a chloroform-rich layer after mixing BR solubilized in an aqueous detergent solution with a chloroform:methanol:water mixture.

Tryptic digestion of the G protein-coupled receptor rhodopsin was used as a test case for mapping the transmembrane peptides of an integral membrane protein using MALDI MS. Affinity purified rhodopsin solubilized in OG was digested with trypsin and the resulting proteolytic fragments were separated using a modified reverse-phase high performance liquid chromatography technique. Detergent was incorporated throughout the procedure. Transmembrane tryptic peptides were identified by accurate mass and confirmed by Edman microsequencing.

The heterodimeric integral membrane protein cytochrome b558 from human neutrophils is the central component of the microbicidal NADPH-oxidase enzyme system. The protein shuttles electrons across the lipid bilayer via hemes located within the hydrophobic regions of the molecule to generate superoxide anion. Little is known about the tertiary structure of the protein, including the heme binding regions. Methods were developed for isolating fragments of purified cytochrome b558 that retained heme absorbance spectra after partial digestion with either trypsin or endoprotease Glu-C (V8) for analysis by SDS-PAGE, Western Blotting, and MALDI MS. Evidence from these analyses suggested that a region of the small subunit containing histidine 94 and regions of the large subunit of cytochrome b558 is involved in binding one of the hemes.

# CHARACTERIZATION OF INTEGRAL MEMBRANE PROTEINS USING MASS SPECTROMETRY: BACTERIORHODOPSIN, RHODOPSIN, AND NEUTROPHIL CYTOCHROME $b_{558}$

by

**David Robert Barnidge**

A thesis submitted in partial fulfillment
of the requirements for the degree

of

Doctor of Philosophy

in

Chemistry

MONTANA STATE UNIVERSITY
Bozeman, Montana

July, 1998

**APPROVAL**

of a thesis submitted by

David Robert Barnidge

This thesis has been read by each member of the thesis committee and has been found to be satisfactory regarding content, English usage, format, citations, bibliographic style, and consistency, and is ready for submission to the College of Graduate Studies.

July 22, 1998
Date

Chairperson, Graduate Committee

Approved for the Major Department

July 30, 1998
Date

Head, Major Department

Approved for the College of Graduate Studies

August 4, 1998
Date

Joseph J. Fedock
Graduate Dean

## STATEMENT OF PERMISSION TO USE

In presenting this thesis in partial fulfillment of the requirements for a doctoral degree at Montana State University, I agree that the Library shall make it available to borrowers under rules of the Library. I further agree that copying of this thesis is allowable only for scholarly purposes, consistent with "fair use" as prescribed in the U.S. Copyright Law. Requests for extensive copying or reproduction of this thesis should be referred to University Microfilms International, 300 North Zeeb Road, Ann Arbor, Michigan 48106, to whom I have granted "the exclusive right to reproduce and distribute my dissertation for sale in and from microform or electronic format, along with the right to reproduce and distribute my abstract in any format in whole or in part."

Signature 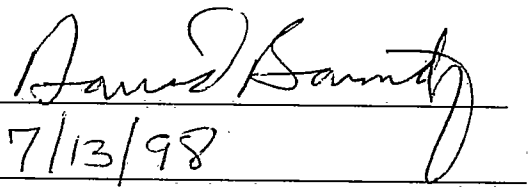

Date 7/13/98

This thesis is dedicated to my wife Phyllis who has given me the three most beautiful things in my life, Preston, Miles, and herself.

## ACKNOWLEDGEMENTS

I would like to sincerely thank Dr. Jan Sunner and Dr. Al Jesaitis for their guidance and patience. Their willingness to allow me to combine the disciplines of mass spectrometry and protein chemistry is greatly appreciated. The experience I have gained from being exposed to these two diverse fields has made me a better analytical chemist. It has also given me the opportunity to explore the fascinating world of cellular biology. I would like to thank Dr. Ed Dratz for his helpful insights and encouragement. I would also like to thank Dr. Joe Sears for sharing his knowledge of mass spectrometry with me and for allowing me to become familiar with a variety of mass spectrometers.

I am grateful to all of my coworkers in the Jesaitis Laboratory, Drs. Heini Miettinen and John Mills, Kathy Billings-Sandoval, Heather Edens, Maria Kohler, and Michael Vlases. I would like to acknowledge the patience and support that was shown to me by Dan Siemsen when I showed up in the laboratory as a 'green' analytical chemist who didn't know a SDS-PAGE gel from a Western blot. Thanks Dan, for teaching me the best gradient gel technique around.

Most notably, I am indebted to Jeannie Gripentrog, Connie MacDonald, Tom Foubert, and Dr. Jim Burritt, the 'cytochrome crew', for all their help. To all my coworkers, thank you for making my tenure as a graduate student such an enjoyable, and often times hilarious, experience.

Finally I would like to thank my wife and my two children for their never-ending support.

## TABLE OF CONTENTS

## TABLE OF CONTENTS--Continued

## TABLE OF CONTENTS--Continued

## TABLE OF CONTENTS--Continued

## TABLE OF CONTENTS--Continued

# LIST OF TABLES

## LIST OF FIGURES

## LIST OF FIGURE--Continued

## LIST OF FIGURE--Continued

## LIST OF FIGURE--Continued

## LIST OF FIGURE--Continued

## LIST OF FIGURE--Continued

## LIST OF FIGURE--Continued

## ABSTRACT

Electrospray ionization mass spectrometry (ESI MS) and matrix assisted laser desorption/ionization mass spectrometry (MALDI MS) have been used extensively to characterize the structural properties of cytosolic proteins. However, ESI and MALDI have had limited success in determining the accurate mass of integral membrane proteins, presumably due to interference from the detergents needed to solubilize them. Therefore, mass spectrometry has had limited applicability in structural studies of integral membrane proteins.

The integral membrane protein bacteriorhodopsin (BR) was used as a model in the development of a method for determining the accurate mass of BR solubilized in the detergents cetyltrimethylammonium bromide (CTAB), octyl-β-glucoside (OG), and CHAPSO by ESI MS. Quality mass spectra were obtained by means of a phase-separation technique where BR was partitioned into a chloroform-rich layer after mixing BR solubilized in an aqueous detergent solution with a chloroform:methanol:water mixture.

Tryptic digestion of the G protein-coupled receptor rhodopsin was used as a test case for mapping the transmembrane peptides of an integral membrane protein using MALDI MS. Affinity purified rhodopsin solubilized in OG was digested with trypsin and the resulting proteolytic fragments were separated using a modified reverse-phase high performance liquid chromatography technique. Detergent was incorporated throughout the procedure. Transmembrane tryptic peptides were identified by accurate mass and confirmed by Edman microsequencing.

The heterodimeric integral membrane protein cytochrome $b_{558}$ from human neutrophils is the central component of the microbicidal NADPH-oxidase enzyme system. The protein shuttles electrons across the lipid bilayer via hemes located within the hydrophobic regions of the molecule to generate superoxide anion. Little is known about the tertiary structure of the protein, including the heme binding regions. Methods were developed for isolating fragments of purified cytochrome $b_{558}$ that retained heme absorbance spectra after partial digestion with either trypsin or endoprotease Glu-C (V8) for analysis by SDS-PAGE, Western Blotting, and MALDI MS. Evidence from these analyses suggested that a region of the small subunit containing histidine 94 and regions of the large subunit of cytochrome $b_{558}$ is involved in binding one of the hemes.

# Chapter 1

## INTRODUCTION

### Electrospray Ionization and Matrix Assisted Laser Desorption/Ionization Mass Spectrometry

Over the past decade mass spectrometry has become established as an essential analytical technique for use in the characterization of proteins and peptides. This important development has resulted largely because electrospray ionization (ESI) and matrix-assisted laser desorption/ionization (MALDI) (1-7) that have been able to provide gas-phase ions for accurate mass determination of previously unionizable compounds. Fast atom bombardment, or FAB, was the first ionization technique that produced high mass ( ≤ 1,000 Da) gas-phase ions. In FAB, ions are generated from a viscous liquid, usually glycerol, by bombarding the surface with energetic atoms or ions. The generation of gas-phase ions from peptides having a mass above a few kDa was, however, unsuccessful (8). In spite of the this relatively low upper mass limit, FAB was used extensively for producing gas-phase ions from a variety of biopolymers thus starting a new field of

analytical chemistry termed 'bioanalytical' mass spectrometry.

It was not until the mid 1980's that the ionization techniques ESI and MALDI were introduced. In 1985, Fenn and coworkers in the Department of Chemical Engineering at Yale University devised a method to produce gas phase ions from a solution at atmospheric pressure for subsequent analysis by a quadrupole mass spectrometer (9). By applying a high voltage (~2,000 V) to the tip of a thin capillary, connected to a liquid introduction system, they were able to produce an 'electrospray' generating $\mu$m sized droplets that contained charged analyte molecules. The generation of a spray induced by a high electric field was not novel since others had reported the production of such 'electrosprays' much earlier, however, it was not known at the time that gas phase ions were produced. Yet, Fenn et al. were the first to couple an electrospray source at atmospheric pressure to a heated capillary backed by a multi-stage vacuum system. This advance allowed the introduction of gas-phase ions produced by the charged droplets into the mass spectrometer without overloading the high vacuum system.

The mechanism for the transfer of ions from solution into the gas-phase, derives from a competition between the Coulombic repulsion of like charges in a droplet and the surface tension of the droplet. The charge density on the surface of the droplet increases due to evaporation of neutral solvent ions until it reaches the Rayleigh limit where Coulombic repulsion becomes large enough to overcome the surface tension of the droplet. At this point the droplet becomes unstable and decomposes, producing daughter droplets. This process repeats itself until the droplets reach a small enough size such that the charge density on the surface induces a field strong enough to desorb the ion from the

droplet(10). This field induced desorption ia a 'soft' form of ionization that results in even-electron ions with low internal energies.

Frequently, clusters of analyte ions with neutral solvent molecules are produced. For accurate mass determination of the analyte, the ions must be completely desorbed. The elimination of clusters is accomplished either through the use of a heated ion transport capillary or heated counter current gas. Transporting the ions produced by the electrospray process into the high vacuum region of the mass spectrometer is achived through the use of lenses or small octopoles. Bare analyte ions are focused into the quadrupoles via ion optics then filtered by mass due to the action of the RF and DC fields applied to the quadrupole rods. A mass spectrum is produced by recording the signal from the detector as the RF and DC voltages on the quadrupoles are varied from lower to higher potential.

In the case of positively charged proteins and peptides, the extent of multiple charging observed in ESI is dependent upon the number of sites where protonation can occur. A mass spectrum of a protein electrosprayed from an acidic solution will reflect the number of solvent accessible basic sites. This has been used to probe conformational structures of proteins under different solvent conditions (11,12). Calculation of the accurate mass of the analyte is accomplished through the use of algorithms, however, the mass can easily be calculated manually. The presence of multiple peaks has the advantage of providing a more robust calculation of the accurate mass since the mass calculated for each peak is used to determine an average molecular weight. Multiple charging also has the advantage of producing ions with low m/z values. Thus, molecules with high

molecular weights (upwards of 100 kDa) may be observed using standard quadrupole mass analyzers that have a mass limit of approximately 3,000 Da for singly charged ions..

Though multiple charging in electrospray ionization has clear advantages in the determination of high molecular weight biopolymers, there are also some disadvantages. If for instance, a sample contains mutiple components, it is often difficult to interpret the spectrum, since overlapping of charge states from the different analytes can occur. Deconvoluting algorithms exist to aid in interpretation of complex spectra from heterogeneous samples. However, liquid chromatography or capillary electrophoresis is often used 'in-line' with the electrospray source to help avoid complex ES mass spectra. Since electrospray is a liquid phase atmospheric pressure ionization technique, it is superbly suited to the coupling of liquid phase separation methods to a mass spectrometer. Flow rates for routine LC (1-5 ml/min) are well above the flow rates used in electrospray (0.5-50 $\mu$l/min). Therefore, the LC flow is either split, or chromatography is performed using a 'micro' LC system. LC/ESI or CE/ESI coupled to a tandem mass spectrometer offers significant advantages. Tandem instruments are capable of determining the masses of daughter ions produced by collisional induced dissociation (CID) of electrospray generated pseudo-molecular ions. The analysis of daughter ions produced by CID is termed MS/MS. Mass spectrometers capable of performing MS/MS experiments include triple quadrupoles, ion traps, and FTICR mass spectrometers (13). The amino acid sequence of a parent or peptide ion can often be determined from a daughter ion MS/MS spectrum. MS/MS has been used extensively for sequencing of proteolytic peptides (2,5,14-21). This technique also enables sites of post-translational modifications such as

phosphorylation (22-24) and glycosylation (25-27) to be characterized using mass spectrometry.

Matrix-assisted laser desorption/ionization, or MALDI, is the second primary ionization technique used in bioanalytical mass spectrometry (28-31). In 1988 Karas and Hillenkamp at the University of Münster in Germany, found that ions are produced from a UV absorbing crystalline matrix when ablated with a UV laser in vacuum (32,33). This observation was, by itself, not surprising. However when analytes such as peptides and proteins were mixed with the matrix solution prior to crystallization, desorption/ionization of these analytes also occured. MALDI coupled to a time-of-flight mass spectrometer (TOF) is capable of detecting singly charged proteins with masses in excess of 100,000 Da. Singly charged ions of high molecular weight proteins can be observed since there is theoretically no upper mass limit for this type of mass analyzer (34).

The process of desorption/ionization in MALDI is not completely understood. However, it is recognized that the matrix used strongly affects the yield, mass resolution, and fragmentation of analyte ions (3,35,36). For each new analyte it becomes essential to try several different matrices. Some of the most commonly used matices are, dihydroxy benzoic acid (DHB), sinapininc acid (SA), and α-cyano-4-hydroxy cinnamic acid (α-CHCA). All of these matrices are small (<400 Da), conjugated organic acids having high extinction coefficients in the UV (37). Samples are prepared by combining a saturated solution of the matrix allowing the mixture to crystallize.

Many variations on this procedure have been reported in the literature. In most cases homogeneous or uniform crystal morphology upon drying results in more consistent

results. This is evident by the ability to generate analyte ions from different regions within the sample. Yet, even with optimum sample preparation, 'hot-spots' on the sample exist where analyte signal is more intense. In addition, suppression effects are seen for mixtures of analytes. An alternative method to MALDI has been described where the analyte is mixed with graphite or glycerol to produce what is known as SALDI or surface-assisted laser desorption/ionization (38). This technique has the advantage of low background from matrix ions and shows promise for adaptation to liquid systems.

Despite the problems in sample preparation, MALDI, coupled with TOF, is still a powerful technique for the accurate mass determination of proteins and peptides. Since MALDI makes use of a solid matrix, samples are introduced into the source region of a TOF mass spectrometer either on a standard insertion probe through a vacuum interlock, or on a sample plate transported through a series of pumping chambers. Once in the source, the sample is positioned to align with the focus of the pulsed laser beam. Ion extraction is obtained by applying a continuos high electric field over the sample (~30 kV/cm). Ions produced by the laser pulse that have the same polarity as the potential applied to the sample will pass through the flight tube to the detector. A photodiode provides the trigger for the digital oscilloscope that records the analog signal from the detector. The digital oscilloscope converts the analog signal to a digital signal and stores the spectra that can be downloaded to a personal computer for data manipulation. The time-of-flight for a MALDI ion is related to its mass by the formula shown below.

$$t = L \sqrt{\frac{m}{2 \cdot V_{acc} \cdot q}}$$

where t is flight time, L is the length of the flight tube, m is the mass of the ion, $V_{acc}$ is the value of the accelerating voltage, and q is the charge of the ion. The mass resolution in a linear TOF mass spectrometer is typically a few hundred. Thus an ion having a mass of 300 Da could be resolved from an ion having a mass of 301 Da (i.e. $m/\Delta m$ = resolution). A number of different modifications have been devised for increasing the mass resolution in MALDI TOF instruments. One of the most common modification is the introduction of a reflector. The reflector, or ion mirror, serves to focus ions of different kinetic energies by reflecting the ions in a potential gradient. Ions with higher kinetic energies will penetrate deeper into the gradient field and thus travel a longer distance, arriving at the detector at the same time as ions with lower kinetic energies traveling a lesser distance. A major breakthrough in the pursuit of increased mass resolution for TOF instruments is the incorporation of delayed ion extraction technology (39). Instead of continuously extracting ions, the application of the extraction field is delayed a few $\mu$s after the laser pulse. The result is that the kinetic energies of the ions in the plume are more uniform due to collisionals within the plume. This uniformity translates into mass resolution on the order of several thousands in a linear TOF.

Comparison of ESI MS and MALDI MS of Hydrophobic Proteins and Peptides

ESI and MALDI have their respective strengths and weaknesses that derive from a number of key differences between the two techniques. Generally, MALDI is more

tolerable of buffers, salts, and detergents, used in the purification of proteins and peptides, than ESI (40). MALDI also uses much less material than standard ESI to produce mass spectra of comparable quality. Sample preparation in MALDI is quite simple, and the sample stages used in many instruments have multiple sites, therefore screening of a large number of samples is less time consuming using MALDI as compared to ESI. However, the mass accuracy and resolution of ESI quadrupole instruments is superior to that of linear MALDI TOF instruments without delayed ion extraction, especially for analytes with mass above 2,000 Da. To summarize, the optimum ionization technique is dependent upon the amount of sample available and its purity.

Both ESI and MALDI have been used extensively for the characterization of protein digests (3,41-48). In addition, a large number of reports have described accurate mass determinations of intact proteins using both ESI and MALDI (2,4,14). Yet, out of thousands of publications describing mass spectral analysis of proteins and peptides, very few (roughly less than 50) involve the mass analysis of hydrophobic samples. Even fewer articles deal with the mass analysis of integral membrane proteins. The lack of mass spectral results for this class of biopolymers is due to the problems associated with sample handling and ionization. In the case of ESI, it is found that ions must first be solubilized in solvents that can be electrosprayed before they can be desorbed. Therefore, hydrophobic proteins or peptides solubilized in aqueous buffers containing high levels of salt and detergents (>50 mM) must be solubilized in non-polar solvents prior to ESI. This requires the exchange of detergent solubilized proteins and peptides into non-polar solutions without aggregating the sample. MALDI on the other hand is a solid-phase technique and

integrating the sample solubilized in detergent into the matrix is experimentally easier to accomplish. Thus, MALDI is prefered over ESI since removal of detergent is not a prerequisite for ionization.

Intact Membrane Proteins Analyzed by ESI MS and MALDI MS

Schindler et al. first desribed methods dedicated to the ESI MS analysis of hydrophobic proteins and peptides (49). These authors found that mixed polar/non-polar solvent systems, such as chloroform:methanol:water, were able to keep hydrophobic proteins and peptides solubilized and were ionizable by ESI. The report included the first published ESI mass spectrum of the integral membrane protein bacteriorhodopsin (m.w. 26,784 Da). The protein was solubilized from purple membrane using hexafluoroisopropanol and/or neat formic acid. However, no detergents were used for solubilization in this study. The first work to demonstrate the ESI analysis of bacteriorhodopsin, solubilized in detergent, was published by Le Maire et al. (50). In this case, the protein was isolated on an SDS-PAGE gel then electroeluted into solution with subsequent removal of the detergent before analysis by ESI MS. Recently, a method was described by Hufnagel et al. (51) for the isolation of bacteriorhodopsin from purple membrane using a series of non-polar solvent washes to remove excess lipid. These authors analyzed the protein by ESI MS in the chloroform:methanol:water solvent system described by Schindler et al. (49). In this study bacteriorhodopsin solubilized in detergent prior to the solvent wash was also analyzed successfully by ESI MS.

MALDI MS has also been used to analyze the integral membrane protein

bacteriorhodopsin. The first report of an accurate mass for this protein, determined by MALDI MS, was by Beavis and Chait in a paper on the applicability of MALDI MS to the accurate mass determination of proteins (30). The work by Schey et al. demonstrated that MALDI MS could be used to determine the accurate mass not only of bacteriorhodopsin, but also of the G protein-coupled receptor rhodopsin (52). They also demonstrated that accurate masses could be obtained for the large peptides generated when rhodopsin was proteolyzed in rod outer segment membranes.

The samples used by Schey et al. were derived from non-detergent solubilized sources and this represents an unusual situation relative to most membrane proteins. Although it is promising that a native membrane protein can be ionized after a brief treatment with a non-polar solvent the fact remains that bacteriorhodopsin and rhodopsin are exceptions, in the sense that most mono-disperse preparations of membrane proteins are in detergent. Since most membrane proteins must be purified prior to mass spectral analysis, any methods used to determine the accurate mass of a protein must be able to tolerate the presence of detergent. The most thorough examination on the effect of different detergents on MALDI MS spectra of membrane proteins is the work by Rosinke et al. (53). The application of different detergents were examined using the membrane proteins bacteriorhodopsin, porin and cholesterolesterase. In addition, various matrixes were evaluated with the best obtained using dihydroxybenzoic acid. The non-ionic detergents such as octylglucoside (OG) were found to degrade the MALDI spectrum to a lesser extent than ionic detergents, such as sodium dodecyl sulfate (SDS).

Proteolytic Digests of Membrane Proteins Analyzed by ESI and MALDI

A majority of the peptide mapping experiments involving integral membrane proteins have focused on the hydrophilic fragments generated and not on the hydrophobic transmembrane fragments. Much of the mapping performed on integral membrane proteins, such as the acetylcholine receptor, were performed prior to the emergence of ESI and MALDI and instead relied on FAB for ionization of the proteolytic fragments (54,55). Also, early work on the FAB analysis of peptides produced by cyanogen bromide and chymotryptic digestion of both bacteriorhodopsin and rhodopsin were performed without any prior separation of the peptides (56). This deficiency was primarily due in part to the formidable difficulties involved in separating transmembrane peptides.

Attempts to overcome this problem have been made with limited success. MALDI MS was used in a study by Machold to identify a hydrophobic tryptic fragment of the nicotinic acetylcholine receptor that had been labeled with a radioactive photo-crosslinker specific for the α-neurotoxin binding site (57). The receptor was isolated by SDS-PAGE after reacting with the ligand and digested in the gel with trypsin. Small non-transmembrane fragments were extracted from the gel and isolated using conventional RP-HPLC. A similar technique was used in the study of sarcoplasmic reticulum $Ca^{+2}$ ATPase by le Maire et al. (50) However, in this case the protein was digested with V8 while in vesicles, and SDS-PAGE was used to isolate the fragments that remained in the membrane after digestion. These authors isolation of these relatively large (>9,000 Da) hydrophobic peptides by electro-transferring the fragments into solution from select bands cut from the SDS-PAGE gel instead of isolating the fragments via RP-HPLC.

Nonetheless, the fragments, after electroelution from the gel into solution, were treated for removal of SDS prior to analysis by ESI.

Goals of This Dissertation: Advancement of Electrospray Ionization and Matrix-Assisted Laser Desorption/Ionization Mass Spectrometry Techniques for the Analysis of Hydrophobic Proteins and Peptides

It is clear from the preceeding discussion that there is a need for the development of methods designed to facilitate the accurate mass analysis of integral membrane proteins and their proteolytic peptides by ESI MS and MALDI MS. Montana State Unversity is fortunate enough to have both types of ionization techniques available in the form of a 'home-built' ESI source coupled to a VG TRIO-2 quadrupole mass spectrometer (58,59) and a Perseptive Biosystems Voyager MALDI time-of-flight mass spectrometer. The characterization of integral membrane proteins is at the forefront of research for a number of groups in the Department of Chemistry and Biochemistry, and the Department of Microbiology. Thus experiments were designed to address three questions regarding transmembrane proteins and their proteolytic fragments:

1) Can the accurate mass of the integral membrane protein bacteriorhodopsin be determined using electrospray ionization mass spectrometry, even in the presence of detergent?

2) Can transmembrane tryptic peptides from the detergent solubilized G protein-coupled receptor, rhodopsin, be isolated then analyzed using matrix-assisted laser

desorption/ionization mass spectrometry without the need for eliminating detergent?

3) Can these procedures be applied to transmembrane protein samples of lower purity?

The first part of this thesis is dedicated to the experiments that were designed to address the first two questions. The second part of the thesis focuses on the third question.

Human Phagocyte Cytochrome $b_{558}$

Cytochrome $b_{558}$ from human phagocytes is a heme containing integral membrane protein found in secretory granules, specific granules, and plasma membranes of human neutrophils and macrophages (60-62). The protein functions as the central redox component for the multi-protein enzyme system known as NADPH oxidase (63). It is responsible for transferring electrons across the membrane to molecular oxygen to form superoxide, the high energy electron source for the generation of a number of microbicidal toxic oxygen compounds (64).

The increase in oxygen consumption by phagocytes exposed to opsonized bacteria is known as the 'respiratory burst'. When this 'respiratory burst' was first observed in 1933 it was thought to involve mitochondrial respiratory components (65). However, in 1959 it was shown that inhibitors of the reduction-oxidation centers in the mitochrondrial system, such as azide and cyanide, were ineffective at disrupting the consumption of oxygen by activated neutrophils (66). The cyanide-insensitive 'respiratory burst' has been

shown to be a critical component of the host defensive arsenal of vertebrates (67) and abscence of the 'respiratory burst' in humans inflicted with the genetic disorder chronic granulomatous disease, or CGD, results in chronic, recurrent, life-threatening infections for these individuals (68).

Further research found that the substrate for the enzyme involved in the reduction of oxygen to superoxide for production of the 'respiratory burst' was either NADH or NADPH (63). After this discovery, the enzyme involved in the reduction of molecular oxygen at the expense of NADPH was known as NADPH oxidase. The chemistry of this reaction is summerized by:

$$NADPH + 2\ O_2 \cdot \rightarrow NADP^+ + H^+ + 2\ O_2^{\cdot-}$$

Prior to the discovery of the NADPH oxidase system in neutrophils, a b-type cytochrome was found in the cell membranes and specific granules of these cells (69). Spectral studies of this protein showed that it had a room temperature Soret band at 414 nm in the oxidized form and a reduced minus oxidized absorbance spectrum with a Soret band at 426 nm and α- and β- bands at 558 nm and 528 nm, respectively (69). Data collected on this protein suggested that this b-type cytochrome was part of the NADPH oxidase. For example, the protein had a low midpoint redox potential of -245 mV, lower than any other mammalian cytochrome b (70) and low enough to participate in the electron transport chain between NADPH and molecular oxygen. In addition, the kinetics of superoxide production mirrored the steady-state reduction kinetics of cytochrome $b_{558}$ in neutrophil membranes (70). However, some of the most convincing data suggesting that the protein was indeed involved in the production of superoxide was the fact that its

spectral activity could not be found in patients having CGD (71). The connection between the genetic disorder CGD and the protein product cytochrome $b_{558}$ was finally proven when cDNA was cloned and sequenced (72) and antisera made against fusion protein of the gene product were shown to recognize one of the subunits of the purified protein from neutrophils (73). Thus cytochrome $b_{558}$ from the membranes of human neutrophils was found to be the obligate electron transferase involved in shuttling high energy electrons from NADPH to molecular oxygen to form superoxide, and the abscence of cytochrome $b_{558}$ leads to CGD.

Characteristics of Human Cytochrome $b_{558}$

Cytochrome $b_{558}$ is a heterodimeric integral membrane protein found in neutrophils at approximately 7 nmol/cell. To purify the protein from membranes, detergents such as Triton X-100 and octylglucoside must be used to produce a monomeric distribution of protein. Also, prudent use of protease inhibitors are required during purification to avoid degradation of the protein by the abundant endogenous proteases found in neutrophils. Isolation of membranes involves the collection of fresh whole blood from normal human donors followed by separation of the neutrophils. These cells are then disrupted and membranes are isolated by centrifugation.

Parkos et al. were the first to purify cytochrome $b_{558}$ from neutrophil membranes (74). The authors demonstrated that the protein is a heterodimer consisting of a glycosylated large subunit (a.k.a. **gp**91-*phox* referring to **glyco**protein 91 kDa m.w.-*ph*agocyte *ox*idase) and a non-glycosylated small subunit (a.k.a. p22-*phox*) (74). Huang et

al. later confirmed that the stoichiometry of the subunits is 1:1 (75). When the purified protein is observed by SDS-PAGE, the large subunit is seen as a broad or 'fuzzy' band between 72-110 kDa while the small subunit runs as a narrow sharp band at 22 kDa (74,76,77). Sequencing of the genes for each subunit indicates that the large subunit is comprised of 570 amino acids with a total molecular weight of 65,291 Da, while the small subunit is comprised of 195 amino acids with a total molecular weight of 20,957 Da (78). When the protein is deglycosylated by treatment with *N*-glycosidase F and analyzed using SDS-PAGE, the large subunit shifts from the broad band at $M_r$= 72-110kDa to a single band at approximately $M_r$= 57 kDa while the band for the small subunit does not change. When the protein is treated with 0.1 N NaOH to remove any O-linked oligosaccharide, no change in the mass of the large subunit, nor the small subunit, is observed. Therefore it has been inferred the large subunit contains only N-linked sites of glycosylation at asparigine residues and that neither the large or the small subunit contains O-linked sites of glycosylation at serine or threonine residues (74,79). Recently, Wallach et al. have advocated that the sites of glycosylation on the large subunit are asparagines 131, 148, and 239 (80). However, this hypothesis was formed from results obtained using incompletely processed large subunit expressed in canine membranes, not whole human cells. Thus the location of the glycosylation sites in the purified protein has yet to be determined.

The reduced form of the protein displays weak CO binding as evident by the decrease in the absorbance of the Soret band and the α and β bands in the presence of CO (70,81). The absorbance spectrum of the protein is sensitive to excess pyridine, and is

completely lost by the addition of 1 M NaCl, or denaturing reagents, thus indicating that the hemes are non-covalently bound (74,81). Extinction coefficients for the oxidized and reduced bands of cytochrome $b_{558}$ have been calculated using the pyridine hemochrome assay (81,82). Values for the reduced minus oxidized $\Delta\epsilon$@ 426 nm range from 106-161 $mM^{-1}$ $cm^{-1}$ while the values for $\Delta\epsilon$@ 558 nm range from 21.7-29.3 $mM^{-1}$ $cm^{-1}$.

The specific heme content of purified cytochrome $b_{558}$, calculated using the extinction coefficients quoted above, is 20-30 nmol/mg of protein (74). The theoretical value for a 1:1 protein to heme ratio would result in only 8.9 nmol of heme per milligram of protein. This observation suggests that there is more than one heme in the molecule. Optical absorbance studies on cytochrome $b_{558}$ done *in situ* by Iizuka et al., found that at 77 K the $\alpha$ band at 558 nm splits into two distinct peaks when cells are stimulated under reducing conditions (83). Work by Cross et al. showed that there are indeed two non-identical hemes present in the molecule as evident from the deviations in the redox titration curves of normal and mutated forms of cytochrome $b_{558}$. The mid-point potentials for the two hemes were determined to be at -225 and -265 mV (84).

Topology of Cytochrome $b_{558}$

No X-ray crystal structure for cytochrome $b_{558}$ exists at this time due to difficulties in purifying large amounts of the protein. Additionally, since it is an integral membrane protein it must be kept in detergent to keep it from aggregating and thus is most likely difficult to crystallize. Consequently, only low-resolution information on the orientation of the protein in the membrane is available. Hydropathy analysis of the cytochrome $b_{558}$

suggests that there are five, possibly six, hydrophobic transmembrane spanning regions on gp91-*phox* and three transmembrane regions on p22-*phox*. Extracellular regions on the large subunit include $^{150}$SYLNFARKRIKNPEGGLYL$^{172}$ and $^{246}$KISEWGKIKEC$^{256}$ as determined by FACS analysis (85)(Barnidge, unpublished results). Intracellular regions on the large subunit include $^{86}$ STRVRRQL$^{93}$, $^{450}$FEWFADLLQLL$^{457}$, $^{490}$ FAVHHDEEKDVITG$^{503}$ , and $^{554}$ESGPRGVHFIF$^{464}$ as determined by the inhibition of the interaction between the cytosolic protein p47 *phox* with cytochrome $b_{558}$ by peptides mimicing these regions (61,86). Small subunit intracellular regions include $^{148}$KQPPSNPPRPPPAE$^{161}$ and $^{175}$AGGPPGGPQVNPIPVTDEVV$^{194}$ that were also found to be binding regions of p47 *phox* (86-88). In addition, the region between $^{181}$GGPQVNI$^{188}$ was found to be intracellular by FACS analysis after identification of this region as the binding site for a small subunit monoclonal antibody (89). There also is evidence that suggests that this anti-small subunit antibody recognizes not only the region $^{181}$GGPQVNI$^{188}$ but also $^{27}$ATAGRF$^{32}$ as part of a 'split-epitope' (Burritt, unpublished results).

The amino acid sequence of the pg91-*phox* and p22-*phox* is listed on the next page taken from the Swiss-Prot protein database.

**Table 1**

**Amino Acid Sequence of Large Subunit Human Cytochrome $b_{558}$**

**SEQUENCE** amino acids - 569; molecular weight - 65,204 Da; SWISS-PROT #: P04839

[1]GNWAVNEGLS IFVILVWLGL NVFLFVWYYR VYDIPPKFFY TRKLLGSALA LARAPAACLN

[61]FNCMLILLPV CRNLLSFLRG SSACCSTRVR RQLDRNLTFH KMVAWMIALH SAIHTIAHLF

[121]NVEWCVNARV NNSDPYSVAL SELGDRQNES YLNFARKRIK NPEGGLYLAV TLLAGITGVV

[181]ITLCLILIIT SSTKTIRRSY FEVFWYTHHL FVIFFIGLAI HGAERIVRGQ TAESLAVHNI

[241]TVCEQKISEW GKIKECPIPQ FAGNPPMTWK WIVGPMFLYL CERLVRFWRS QQKVVITKVV

[301]THPFKTIELQ MKKKGFKMEV GQYIFVKCPK VSKLEWHPFT LTSAPEEDFF SIHIRIVGDW

[361]TEGLFNACGC DKQEFQDAWK LPKIAVDGPF GTASEDVFSY EVVMLVGAGI GVTPFASILK

[421]SVWYKYCNNA TNLKLKKIYF YWLCRDTHAF EWFADLLQLL ESQMQERNNA

[471]GFLSYNIYLT GWDESQANHF AVHHDEEKDV ITGLKQKTLY GRPNWDNEFK TIASQHPNTR

[531]IGVFLCGPEA LAETLSKQSI SNSESGPRGV HFIFNKENF

**Potential Transmembrane Residues**

TRANSMEM $^{8}$L to $^{29}$Y TRANSMEM $^{98}$T to $^{121}$N TRANSMEM $^{166}$L to $^{190}$T

TRANSMEM $^{204}$F to $^{223}$A TRANSMEM $^{265}$N to $^{285}$V

**Potential FAD and NADPH Binding Domains**

FAD $^{406}$V to $^{447}$T NADPH $^{503}$G to $^{512}$R and $^{531}$I to $^{569}$F

**Know Mutations found in X-linked CGD Patients**

VARIANT $^{100}$H -> R (IN X-CGD); VARIANT $^{155}$A -> T (IN X-CGD)

VARIANT $^{208}$H -> Y (IN X-CGD); VARIANT $^{243}$C -> S (IN X-CGD)

VARIANT $^{338}$P -> H (IN X-CGD); VARIANT $^{388}$G -> A (IN X-CGD)

VARIANT $^{414}$P -> H (IN X-CGD); VARIANT $^{499}$D -> G (IN X-CGD)

**Table 2**

**Amino Acid Sequence of Small Subunit Human Cytochrome $b_{558}$**

**SEQUENCE** amino acids - 194; molecular weight - 20,827 Da; SWISS-PROT#: P13498

[1]GQIEWAMWAN EQALASGLIL ITGGIVATAG RFTQWYFGAY SIVAGVFVCL LEYPRGKRKK

[61]GSTMERWGQK HMTAVVKLFG PFTRNYYVRA VLHLLLSVPA GFLLATILGT ACLAIASGIY

[121]LLAAVRGEQW TPIEPKPRER PQIGGTIKQP PSNPPPRPPA EARKKPSEEE AAAAAGGPPG

[181]GPQVNPIPVT DEVV

**Potential Transmembrane Residues**

TRANSMEM [5]W to [28]T TRANSMEM [36]Y to [54]P TRANSMEM [90]A to [110]T

**Know Mutations found in Autosomal Recessive CGD Patients**

VARIANT [89]R -> Q (IN AR-CGD); VARIANT [93]H -> R (IN AR-CGD);

VARIANT [117]S -> R (IN AR-CGD); VARIANT [155]P -> Q (IN AR-CGD)

The shaded regions in the amino acid sequences listed for gp91-*phox* and p22-*phox* denote the potential transmembrane regions for the subunits deduced from hydropathy analysis. The residues involved in these proposed transmembrane domains are also listed. Proposed sites of glycosylation are designated by bold, double underlined, asparagine residues (**N**). All histidines in both gp91-*phox* and p22-*phox* are shown in bold (**H**). The residues implicated in the FAD binding domain, as well as the residues of the proposed NADPH binding sites are listed below the amino acid sequence for gp91-*phox*(90-92).

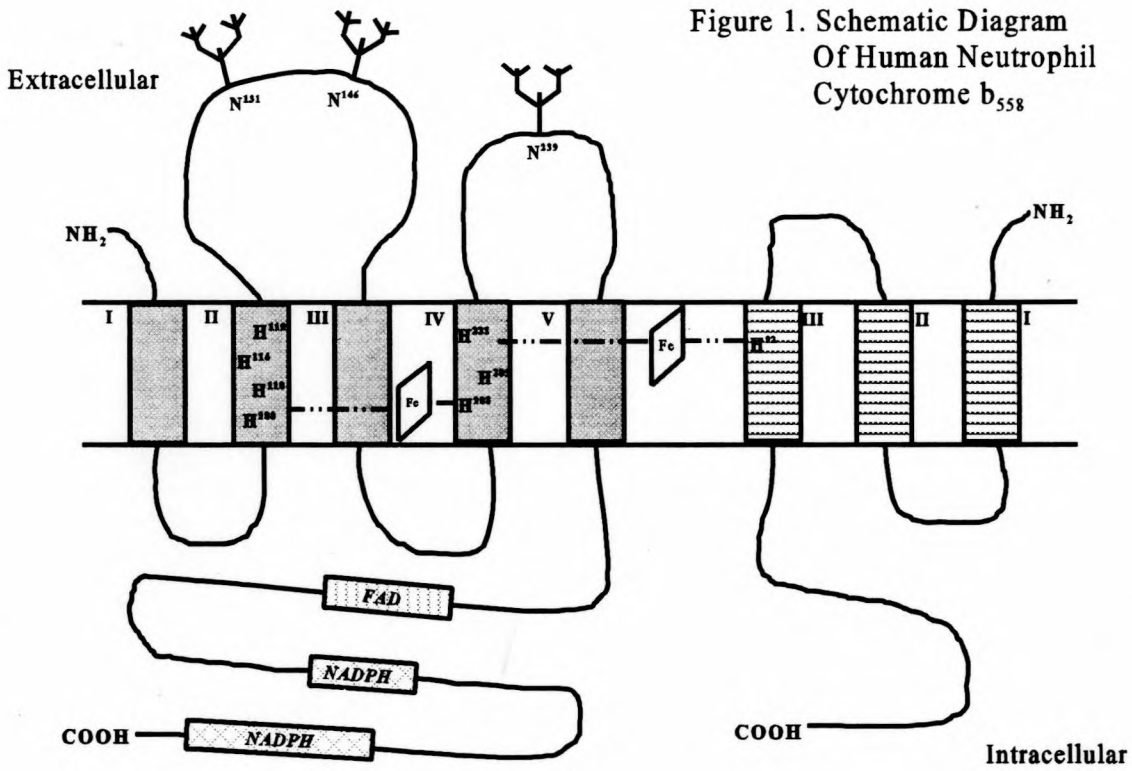


Figure 1. Schematic Diagram Of Human Neutrophil Cytochrome $b_{558}$

A schematic diagram of human cytochrome $b_{558}$ based on hydropathy analysis is shown in Figure 1 (60). Figure 1 serves to portray the topology of the protein in the membrane based on a recently proposed model of cytochrome $b_{558}$ topology by Parkos et. al (93). The figure also shows the proposed FAD and NADPH binding domains (90,91). In addition the proposed sites of glycosylation are shown by 'glyco-trees' at their respective asparagine residues as determined by Wallach et al. (80). The histindines that are labeled along with the icons representing heme and their arrangement in the membrane will be discussed below.

Location of the Hemes in Cytochrome $b_{558}$

The exact location of the residues that coordinate the hemes in cytochrome $b_{558}$ is not known. There is no clear homology between known heme bearing proteins and cytochrome $b_{558}$ making the assignment of a heme binding domain from sequence data difficult. Identity profiles indicate that there is a 31 residue region within the small subunit that is 39% identical with the known heme bearing region of polypeptide I from mitochondrial cytochrome c oxidase (78). There is also evidence from hydropathy analysis that this same region is similar to the heme binding region of myoglobin (78). FRE 1 ferric reductase from the yeast *Saccharomyces cerevisiae* has been shown to share some homology with the large subunit of cytochrome $b_{588}$ relative to their histidine containing hydrophobic regions (94,95). The protein has a reduced minus oxidized spectrum similar to b-type cytochromes, however it is a monomeric protein. One key point that aids in narrowing the location of the hemes is that the energetics of the electron transfer function of the protein preclude the existence of a heme center in a water accessible environment, suggesting that the sites of heme ligation must lie within the membrane (60). This deduction is supported by the insensitivity of the absorbance spectrum neutrophil membranes subjected to partial digestion (96).

Electron spin resonance experiments performed on purified cytochrome $b_{558}$ and cytochrome $b_{558}$ in membranes have suggested that the hemes are bound to the protein through low spin bis-histidine ligation (90,97-103). Radiation inactivation experiments carried out on cytochrome $b_{558}$ in purified membranes have also suggested a target size of ~ 21 kDa, implicating the small subunit in the binding of the hemes (104). Another

experiment aimed at purifiying the heme containing moiety of cytochrome $b_{558}$ resulted in the isolation of a single protein component at a molecular weight of ~ 20 kDa (105). This protein purified separate from the large subunit of cytochrome $b_{558}$ and displayed the same absorbance spectrum as the intact protein. Partial digestion experiments done by Quinn et al. showed that purified cytochrome $b_{558}$ solubilized in Triton X-100 did not lose spectral activity after digestion with V8 even though the subunits were clearly degraded into smaller fragments (96). The products of the digestion were separated by LDS-PAGE at 4°C and stained with tetramethylbenzidine (TMBZ) to determine the location of heme in the gel. Their findings clearly showed that an immunoreactive fragment exhibiting heme staining activity was present at ~ 20 kDa. TMBZ staining of undigested cytochrome $b_{558}$ separated by LDS-PAGE showed that both the large and small subunits contained heme. These results indicated that both the large and small subunits of cytochrome $b_{558}$ are involved in heme binding.

The histidines that are marked in Figure 1 represent the possible hydrophobic locations for the bis-histidinal coordination of the hemes in cytochrome $b_{558}$ based on the model by Parkos et al. (93). The histidines found in transmembrane regions II and IV at positions 100 and 208 (shown with heme attached) have been implicated in the binding of heme in porcine neutrophil cytochrome $b_{558}$ as determined by Fujii et al. (100). The position of the other heme in the figure serves to show another possible coordination site. To date there has been no evidence to completely rule out the possibility of the small subunit sharing a heme with the large subunit. Yet it is known that the small subunit is not capable of coordinating the heme by itself as determined by DNA sequencing of the small

subunit which displays a polymorphism at H 71 (106). Therefore. The model shown in Figure 1 functions as a reference in this thesis regarding the possible heme binding domains of cytochrome $b_{558}$.

Goals of This Dissertation Research: Isolation and Identification of Spectrally Active Heme Binding Domains in Human Neutrophil Cytochrome $b_{558}$

Cytochrome $b_{558}$ is the terminal component in the NADPH oxidase system responsible for the production of superoxide in neutrophils, and thus it plays an essential role in the function of these cells as guardians against host infection (60-62). Without knowing the complete structure of the cytochrome $b_{558}$, it is difficult to design approaches aimed at manipulating the inflammatory response by altering the function of the protein. Knowing the location of hemes in cytochrome $b_{558}$ would be particularly useful, since these prosthetic groups are ultimately responsible for the redox chemistry of the enzyme.

Therefore, the goal of the second part of this thesis was to develop methods aimed at isolating spectrally active heme binding domains from partially digested cytochrome $b_{558}$. Experiments were designed to facilitate the accurate mass determination of the heme bearing fragments obtained by partial digestion to allow for identification from the known sequence of the protein. Specific proteases combined with the accurate mass data, along with specific immunological probes, would facilitate localization of the heme binding domain. This appoach can provide direct biochemical evidence as to the primary structures of the heme binding domain of human neutrophil cytochrome $b_{558}$.

## References


1. Fenn, J. B., J. Rosell, T. Nohmi, S. Shen, and F. J. Banks,Jr. 1996. Biochemical and biotechnological applications of electrospray ionization mass spectrometry. A. P. Snyder, editor. ACS Symposium Series; American Chemical Society, Washington, D.C. 60-80.

2. Burlingame, A. L., R. K. Boyd, and S. J. Gaskell. 1996. Mass spectrometry. *Anal. Chem.* 68:599R-651R.

3. Stults, J. T. 1995. Matrix-assisted laser desorption/ionization mass spectrometry (MALDI-MS). *Curr. Opin. Struct. Biol.* 5:691-698.

4. Burlingame, A. L., and S. A. Carr. 1996. Mass spectrometry in the biological sciences. Humana Press, Totowa, NJ.

5. Carr, S. A., M. E. Hemling, M. F. Bean, and G. D. Roberts. 1991. Integration of mass spectrometry in analytical biotechnology. *Anal. Chem.* 63:2802-2824.

6. Chait, B. T. and S. B. Kent. 1992. Weighing naked proteins: practical, high-accuracy mass measurement of peptides and proteins. *Science* 257:1885-1894.

7. Wang, R. and B. T. Chait. 1994. High-accuracy mass measurement as a tool for studying proteins. *Curr. Opin. Biotechnol.* 5:77-84.

8. Sunner, J. 1993. Ionization in liquid secondary ion mass spectrometry (LSIMS). *J. Org. Mass Spectrom.* 28:805-823.

9. Whitehouse, C. M., R. N. Dreyer, M. Yamashita, and J. B. Fenn. 1985. Electrospray interface for liquid chromatographs and mass spectrometers. *Anal. Chem.* 57:675-679.

10. Kebarle, P. and L. Tang. 1993. Ions from solution to ions in the gas phase: the mechanism of electrospray ionization. *Anal. Chem.* 65:972A-986A.

11. Loo, J. A., R. R. Loo, H. R. Udseth, C. G. Edmonds, and R. D. Smith. 1991. Solvent-induced conformational changes of polypeptides probed by electrospray-ionization mass spectrometry. *Rapid. Commun. Mass. Spectrom.* 5:101-105.

12. Zhang, Z. and D. L. Smith. 1993. Determination of amide hydrogen exchange by mass spectrometry: a new tool for protein structure elucidation. *Protein Sci.* 2:522-531.

13. Yost, R. A. and R. K. Boyd. 1990. Tandem mass spectrometry: quadrupole and hybrid instruments. *Methods Enzymol.* 193:154-200.

14. Burlingame, A. L., R. K. Boyd, and S. J. Gaskell. 1994. Mass spectrometry. *Anal. Chem.* 66:634R-683R.

15. Smith, J. B., G. Thevenon-Emeric, D. L. Smith, and B. Green. 1991. Elucidation of the primary structures of proteins by mass spectrometry. *Anal. Biochem.* 193:118-124.

16. Smith, R. D., J. A. Loo, C. G. Edmonds, C. J. Barinaga, and H. R. Udseth. 1990. New developments in biochemical mass spectrometry: electrospray ionization. *Anal. Chem.* 62:882-899.

17. Arnott, D., J. Shabanowitz, and D. F. Hunt. 1993. Mass spectrometry of proteins and peptides: sensitive and accurate mass measurement and sequence analysis. *Clin. Chem.* 39:2005-2010.

18. Takemoto, L. J., T. Emmons, D. Granstrom, P. R. Griffin, J. Shabanowitz, and D. F. Hunt. 1990. Analysis of tryptic peptides from the C-terminal region of alpha-crystallin from cataractous and normal human lenses. *Exp. Eye Res.* 50:695-702.

19. Hunt, D. F., 3. d. Yates JR, J. Shabanowitz, S. Winston, and C. R. Hauer. 1986. Protein sequencing by tandem mass spectrometry. *Proc. Natl. Acad. Sci. U. S. A.* 83:6233-6237.

20. Fenselau, C., M. M. Vestling, and R. J. Cotter. 1993. Mass spectrometric analysis of proteins. *Curr. Opin. Biotechnol.* 4:14-19.

21. McCormack, A. L., D. M. Schieltz, B. Goode, S. Yang, G. Barnes, D. Drubin, and J. R. Yates,3rd. 1997. Direct analysis and identification of proteins in mixtures by LC/MS/MS and database searching at the low-femtomole level. *Anal. Chem.* 69:767-776.

22. Nuwaysir, L. M. and J. T. Stults. 1993. Electrospray ionization mass spectrometry of phosphopeptides isolated by on-line immobilized metal-ion affinity chromatography. *J. Am. Soc. Mass Spectrom.* 4:662-669.

23. Huddleston, M. J., R. S. Annan, and M. F. Bean. 1993. Selective detection of phosphopeptides in complex mixtures by electrospray liquid chromatography / mass spectrometry. *J. Am. Soc. Mass Spectrom.* 4:710-717.

24. Watts, J. D., M. Affolter, D. L. Krebs, R. L. Wange, L. E. Samelson, and R. Aebersold. 1994. Identification by electrospray ionization mass spectrometry of the sites of tyrosine phosphorylation induced in activated Jurkat T cells on the protein tyrosine kinase ZAP-70. *J. Biol. Chem.* 269:29520-29529.

25. Schindler, P. A., C. A. Settineri, X. Collet, C. J. Fielding, and A. L. Burlingame. 1995. Site-specific detection and structural characterization of the glycosylation of human plasma proteins lecithin:cholesterol acyltransferase and apolipoprotein D using HPLC/electrospray mass spectrometry and sequential glycosidase digestion. *Protein Sci.* 4:791-803.

26. Burlingame, A. L. 1996. Characterization of protein glycosylation by mass spectrometry. *Curr. Opin. Biotechnol.* 7:4-10.

27. Hunter, A. P. and D. E. Games. 1995. Evaluation of glycosylation site heterogeneity and selective identification of glycopeptides in proteolytic digests of bovine alpha 1-acid glycoprotein by mass spectrometry. *Rapid. Commun. Mass. Spectrom.* 9:42-56.

28. Mann, M. and G. Talbo. 1996. Developments in matrix-assisted laser desorption/ionization peptide mass spectrometry. *Curr. Opin. Biotechnol.* 7:11-19.

29. Zaluzec, E. J., D. A. Gage, and J. T. Watson. 1995. Matrix-assisted laser desorption ionization mass spectrometry: applications in peptide and protein characterization. *Protein Expr. Purif.* 6:109-123.

30. Beavis, R. C. and B. T. Chait. 1990. Rapid, sensitive analysis of protein mixtures by mass spectrometry. *Proc. Natl. Acad. Sci. U. S. A.* 87:6873-6877.

31. Hillenkamp, F., M. Karas, R. C. Beavis, and B. T. Chait. 1991. Matrix-assisted laser desorption/ionization mass spectrometry of biopolymers. *Anal. Chem.* 63:1193A-1203A.

32. Hillenkamp, F. and M. Karas. 1990. Mass spectrometry of peptides and proteins by matrix-assisted ultraviolet laser desorption/ionization. *Methods Enzymol.* 193:280-295.

33. Karas, M. and F. Hillenkamp. 1988. Laser desorption ionization of proteins with molecular masses exceeding 10,000 daltons. *Anal. Chem.* 60:2299-2301.

34. Spengler, B. and R. J. Cotter. 1990. Ultraviolet laser desorption/ionization mass spectrometry of proteins above 100,000 daltons by pulsed ion extraction time-of-flight analysis. *Anal. Chem.* 62:793-796.

35. Salehpour, M., I. Perera, J. Kjellberg, A. Hedin, M. A. Islamian, P. H akansson, and B. U. Sundqvist. 1989. Laser-induced desorption of proteins. *Rapid. Commun. Mass. Spectrom.* 3:259-263.

36. Beavis, R. C. 1992. MALDI matrices. *Org. Mass Spectrom.* 60:2299-2301.

37. Beavis, R. C. and B. T. Chait. 1989. Cinnamic acid derivatives as matrices for ultraviolet laser desorption mass spectrometry of proteins. *Rapid. Commun. Mass. Spectrom.* 3:432-435.

38. Sunner, J., E. Dratz, and Y. C. Chen. 1995. Graphite surface-assisted laser desorption/ionization time-of-flight mass spectrometry of peptides and proteins from liquid solutions. *Anal. Chem.* 67:4335-4342.

39. Juhasz, P., M. T. Roskey, I. P. Smirnov, L. A. Haff, M. L. Vestal, and S. A. Martin. 1996. Applications of delayed extraction matrix-assisted laser desorption ionization time-of-flight mass spectrometry to oligonucleotide analysis. *Anal. Chem.* 68:941-946.

40. Beavis, R. C. and B. T. Chait. 1990. High-accuracy molecular mass determination of proteins using matrix-assisted laser desorption mass spectrometry. *Anal. Chem.* 62:1836-1840.

41. Yang, Y. and R. Orlando. 1996. Identifying the glycosylation sites and site-specific carbohydrate heterogeneity of glycoproteins by matrix-assisted laser desorption/ ionization mass spectrometry. *Rapid. Commun. Mass. Spectrom.* 10:932-936.

42. Harmon, B. J., X. Gu, and D. I. Wang. 1996. Rapid monitoring of site-specific glycosylation microheterogeneity of recombinant human interferon-gamma. *Anal. Chem.* 68:1465-1473.

43. Barnidge, D. R., E. A. Dratz, J. Sunner, and A. J. Jesaitis. 1997. Identification of transmembrane tryptic peptides of rhodopsin using matrix-assisted laser desorption/ionization time-of-flight mass spectrometry. *Protein Sci.* 6:816-824.

44. Kanda, F., S. Yoshida, T. Okumura, and T. Takamatsu. 1995. Asparaginyl endopeptidase mapping of proteins with subsequent matrix-assisted laser desorption/ionization mass spectrometry. *Rapid. Commun. Mass. Spectrom.* 9:1095-1100.

45. Mortz, E., O. Vorm, M. Mann, and P. Roepstorff. 1994. Identification of proteins in polyacrylamide gels by mass spectrometric peptide mapping combined with database search. *Biol. Mass. Spectrom.* 23:249-261.

46. Boss, H. J., M. F. Rohde, and R. S. Rush. 1995. Multiple sequential fraction collection of peptides and glycopeptides by high-performance capillary electrophoresis. *Anal. Biochem.* 230:123-129.

47. Laidler, P., D. A. Cowan, R. C. Hider, A. Keane, and A. T. Kicman. 1995. Tryptic mapping of human chorionic gonadotropin by matrix-assisted laser desorption/ionization mass spectrometry. *Rapid. Commun. Mass. Spectrom.* 9:1021-1026.

48. Billeci, T. M. and J. T. Stults. 1993. Tryptic mapping of recombinant proteins by matrix-assisted laser desorption/ionization mass spectrometry. *Anal. Chem.* 65:1709-1716.

49. Schindler, P. A., A. Van Dorsselaer, and A. M. Falick. 1993. Analysis of hydrophobic proteins and peptides by electrospray ionization mass spectrometry. *Anal. Biochem.* 213:256-263.

50. le Maire, E. L., S. Deschamps, J. V. Moller, J. P. le Caer, and J. Rossier. 1993. Electrospray ionization mass spectrometry on hydrophobic peptides electroeluted from sodium dodecyl sulfate-polyacrylamide gel electrophoresis application to the topology of the sarcoplasmic reticulum Ca2+ ATPase. *Anal. Biochem.* 50-57.

51. Hufnagel, P., U. Schweiger, C. Eckerskorn, and D. Oesterhelt. 1996. Electrospray Ionization Mass Spectrometry of Genetically and Chemically Modified Bacteriorhodopsins. *Anal. Biochem.* 243:46-54.

52. Schey, K. L., D. I. Papac, D. R. Knapp, and R. K. Crouch. 1992. Matrix-assisted laser desorption mass spectrometry of rhodopsin and bacteriorhodopsin. *Biophys. J.* 63:1240-1243.

53. Rosinke, B., K. Strupat, F. Hillenkamp, J. Rosenbusch, N. Dencher, U. Kruger, and H. J. Galla. 1996. Matrix-Assisted Laser Desorption/Ionization Mass Spectrometry (MALDI-MS) of Membrane Proteins and Non-covalent Complexes. *Journal of Mass Spectrometry* 30:1462-1468.

54. Poulter, L., J. P. Earnest, R. M. Stroud, and A. L. Burlingame. 1989. Structure, oligosaccharide structures, and posttranslationally modified sites of the nicotinic acetylcholine receptor. *Proc. Natl. Acad. Sci. U. S. A.* 86:6645-6649.

55. Moore, C. R., J. R. Yates III, P. R. Griffin, J. Shabanowitz, P. A. Martino, D. F. Hunt, and D. S. Cafiso. 1989. Proteolytic fragments of the nicotinic acetylcholine receptor identified by mass spectrometry: implications for receptor topography. *Biochemistry* 28:9184-9191.

56. Orlando, R., P. T. M. Kenny, C. Moquin-Pattey, K. A. Lerro, and K. Nakanishi. 1993. Sequencing membrane proteins by tandem mass spectrometry. *Org. Mass Spectrom.* 28:1395-1402.

57. Machold, J., Y. Utkin, D. Kirsch, R. Kaufmann, V. Tsetlin, and F. Hucho. 1995. Photolabeling reveals the proximity of the alpha-neurotoxin binding site to the M2 helix of the ion channel in the nicotinic acetylcholine receptor. *Proc. Natl. Acad. Sci. U. S. A.* 92:7282-7286.

58. Baiwei, L. Ph.D. Thesis. 1992. Ion transport by vicous gas flow through capillaries and electrospray mass spectrometry of proteins. Montana State Unversity. Bozeman, MT. USA.

59. Long, J. M. Ph.D. Thesis. 1993. Electrospray ionization mass spectrometry and its environmental applications. Montana State Unversity. Bozeman, MT. USA.

60. Jesaitis, A. J. 1995. Structure of human phagocyte cytochrome b and its relationship to microbicidal superoxide production. *J. Immunol.* 155:3286-3288.

61. Kleinberg, M. E., D. Mital, D. Rotrosen, and H. L. Malech. 1992. Characterization of a phagocyte cytochrome b558 91-kilodalton subunit functional domain: identification of peptide sequence and amino acids essential for activity. *Biochemistry* 31:2686-2690.

62. Dinauer, M. C. and S. H. Orkin. 1988. Molecular genetics of chronic granulomatous disease. *Immunodefic. Rev.* 1:55-69.

63. Rossi, F. 1986. The O2- -forming NADPH oxidase of the phagocytes: nature, mechanisms of activation and function. *Biochim. Biophys. Acta* 853:65-89.

64. Rotrosen, D. 1992. The respiratory burst oxidase. In Inflammation: basic principles and clinical correlates. Second edition. J. I. Gallin, I. M. Goldstein, and R. Snyderman, editors. Raven Press, Ltd. New York. 589-601.

65. Baldridge, C. W. and R. W. Gerard. 1933. The extra respiration of phagocytosis. *Am. J. Physiol.* 10:235-236.

66. Sbarra, A. J. and M. L. Karnovsky. 1959. The biochemical basis of phagocytosis. *J. Biol. Chem.* 234:1355-1362.

67. Morgenstern, D. E., M. Gifford, L. Li, C. M. Doerschuk, and M. C. Dinauer. 1997. Absence of respiratory burst in X-linked chronic granulomatous disease mice leads to abnormalities in both host defense and inflammatory response to *Aspergillus fumigatus*. *J. Exp. Med.* 185:207-218.

68. Holmes, B., A. R. Page, and R. A. Good. 1967. Studies of the metabolic activity of leukocytes from patients with a genetic abnormality of phagocyte function. *J. Clin. Invest.* 46:1422-1432.

69. Segal, A. W. and O. T. Jones. 1978. Novel cytochrome b system in phagocytic vacuoles of human granulocytes. *Nature (London)* 276:515-517.

70. Cross, A. R., O. T. Jones, A. M. Harper, and A. W. Segal. 1981. Oxidation-reduction properties of the cytochrome b found in the plasma-membrane fraction of human neutrophils. A possible oxidase in the respiratory burst. *Biochem. J.* 194:599-606.

71. Segal, A. W., A. R. Cross, R. C. Garcia, N. Borregaard, N. H. Valerius, J. F. Soothill, and O. T. Jones. 1983. Absence of cytochrome $b_{-245}$ in chronic granulomatous disease: a multicenter European evaluation of its incidence and relevance. *N. Engl. J. Med.* 308:245-251.

72. Royer-Pokora, B., L. M. Kunkel, A. P. Monaco, S. C. Goff, R. L. Newburger, R. L. Baehner, F. S. Cole, J. T. Curnutte, and S. H. Orkin. 1986. Cloning of the gene for an inherited human disorder-chronic granulomatous disease- on the basis of its chromosomal location. *Nature* 322:32-38.

73. Dinauer, M. C., S. H. Orkin, R. Brown, A. J. Jesaitis, and C. A. Parkos. 1987. The glycoprotein encoded by the X-linked chronic granulomatous disease locus is a component of the neutrophil cytochrome b complex. *Nature* 327:717-720.

74. Parkos, C. A., R. A. Allen, C. G. Cochrane, and A. J. Jesaitis. 1987. Purified cytochrome b from human granulocyte plasma membrane is comprised of two polypeptides with relative molecular weights of 91,000 and 22,000. *J. Clin. Invest.* 80:732-742.

75. Huang, J., N. D. Hitt, and M. E. Kleinberg. 1995. Stoichiometry of p22-phox and gp91-phox in phagocyte cytochrome b558. *Biochemistry* 34:16753-16757.

76. Harper, A. M., M. J. Dunne, and A. W. Segal. 1984. Purification of cytochrome $b_{-245}$ from human neutrophils. *Biochem. J.* 219:519-527.

77. Harper, A. M., M. F. Chaplin, and A. W. Segal. 1985. Cytochrome $b_{-245}$ from human neutrophils is a glycoprotein. *Biochem. J.* 227:783-788.

78. Parkos, C. A., M. C. Dinauer, L. E. Walker, R. A. Allen, A. J. Jesaitis, and S. H. Orkin. 1988. Primary structure and unique expression of the 22-kilodalton light chain of human neutrophil cytochrome *b*. *Proc. Natl. Acad. Sci. U. S. A.* 85:3319-3323.

79. Kleinberg, M. E., D. Rotrosen, and H. L. Malech. 1989. Asparigine-linked glycosylation of cytochrome $b_{558}$ large subunit varies in different human phagocytic cells. *J. Immunol.* 143:4152-4157.

80. Wallach, T. M. and A. Segal. 1997. Analysis of glycosylation sites on gp91phox, the flavocytochrome of the NADPH oxidase, by site-directed mutagenesis and translation *in vitro*. *Biochem. J.* 321:583-585.

81. Lutter, R., M. L. J. van Schaik, R. V. van Zwieten, R. Wever, D. Roos, and M. N. Hamers. 1985. Purification and partial characterization of the *b*-type cytochrome from human polymorphonuclear leukocytes. *J. Biol. Chem.* 260:2237-2244.

82. Cross, A. R., F. K. Higson, O. T. Jones, A. M. Harper, and A. W. Segal. 1982. The enzymic reduction and kinetics of oxidation of cytochrome b-245 of neutrophils. *Biochem. J.* 204:479-485.

83. Iizuka, T., S. Kanegasaki, R. Makino, T. Tanaka, and Y. Ishimura. 1985. Studies on neutrophil *b*-type cytochrome *in situ* by low tempurature absorption spectroscopy. *J. Biol. Chem.* 260:12049-12053.

84. Cross, A. R., J. Rae, and J. T. Curnutte. 1995. Cytochrome b-245 of the neutrophil superoxide-generating system contains two nonidentical hemes. Potentiometric studies of a mutant form of gp91phox. *J. Biol. Chem.* 270:17075-17077.

85. Imajoh Ohmi, S., K. Tokita, H. Ochiai, M. Nakamura, and S. Kanegasaki. 1992. Topology of cytochrome b558 in neutrophil membrane analyzed by anti-peptide antibodies and proteolysis. *J. Biol. Chem.* 267:180-184.

86. DeLeo, F. R., L. Yu, J. B. Burritt, L. R. Loetterle, C. W. Bond, A. J. Jesaitis, and M. T. Quinn. 1995. Mapping sites of interaction of p47-phox and flavocytochrome b with random-sequence peptide phage display libraries. *Proc. Natl. Acad. Sci. U. S. A.* 92:7110-7114.

87. Leto, T. L., A. G. Adams, and I. de Mendez. 1994. Assembly of the phagocyte NADPH oxidase: binding of Src homology 3 domains to proline-rich targets. *Proc. Natl. Acad. Sci. U. S. A.* 91:10650-10654.

88. Leusen, J. H., M. de Boer, B. G. Bolscher, P. M. Hilarius, R. S. Weening, H. D. Ochs, D. Roos, and A. J. Verhoeven. 1994. A point mutation in gp91-phox of cytochrome b558 of the human NADPH oxidase leading to defective translocation of the cytosolic proteins p47-phox and p67-phox. *J. Clin. Invest.* 93:2120-2126.

89. Burritt, J. B., M. T. Quinn, M. A. Jutila, C. W. Bond, and A. J. Jesaitis. 1995. Topological mapping of neutrophil cytochrome b epitopes with phage-display libraries. *J. Biol. Chem.* 270:16974-16980.

90. Segal, A. W., I. West, F. Wientjes, J. H. Nugent, A. J. Chavan, B. Haley, R. C. Garcia, H. Rosen, and G. Scrace. 1992. Cytochrome b-245 is a flavocytochrome containing FAD and the NADPH-binding site of the microbicidal oxidase of phagocytes. *Biochem. J.* 284P781-8:781-788.

91. Rotrosen, D., C. L. Yeung, T. L. Leto, H. L. Malech, and C. H. Kwong. 1992. Cytochrome b558: the flavin-binding component of the phagocyte NADPH oxidase. *Science* 256:1459-1462.

92. Sumimoto, H., N. Sakamoto, M. Nozaki, Y. Sakaki, K. Takeshige, and S. Minakami. 1992. Cytochrome b558, a component of the phagocyte NADPH oxidase, is a flavoprotein. *Biochem. Biophys. Res. Commun.* 186:1368-1375.

93. Parkos, C. A., M. T. Quinn, and A. J. Jesaitis. 1992. Molecular basis of oxidative damage by leukocytes. A. J. Jesaitis and E. A. Dratz, editors. CRC Press, Boca Raton,FL.

94. Shatwell, K. P., A. Dancis, A. R. Cross, R. D. Klausner, and A. W. Segal. 1996. The FRE1 ferric reductase of Saccharomyces cerevisiae is a cytochrome b similar to that of NADPH oxidase. *J. Biol. Chem.* 271:14240-14244.

95. Finegold, A. A., K. P. Shatwell, A. W. Segal, R. D. Klausner, and A. Dancis. 1996. Intramembrane bis-heme motif for transmembrane electron transport conserved in a yeast iron reductase and the human NADPH oxidase. *J. Biol. Chem.* 271:31021-31024.

96. Quinn, M. T., M. L. Mullen, and A. J. Jesaitis. 1992. Human neutrophil cytochrome b contains multiple hemes;
evidence for heme associated with both subunits. *J. Biol. Chem.* 267:7303-7309.

97. Miki, T., H. Fujii, and K. Kakinuma. 1992. EPR signals of cytochrome b558 purified from porcine neutrophils. *J. Biol. Chem.* 267:19673-19675.

98. Hurst, J. K., T. M. Loehr, J. T. Curnutte, and H. Rosen. 1991. Resonance Raman and electron paramagnetic resonance structural investigations of neutrophil cytochrome b558. *J. Biol. Chem.* 266:1627-1634.

99. Doussiere, J., J. Gaillard, and P. V. Vignais. 1996. Electron transfer across the O2-generating flavocytochrome b of neutrophils. Evidence for a transition from a low-spin state to a high-spin state of the heme iron component. *Biochemistry* 35:13400-13410.

100. Fujii, H., M. G. Finnegan, T. Miki, B. R. Crouse, K. Kakinuma, and M. K. Johnson. 1995. Spectroscopic identification of the heme axial ligation of cytochrome b558 in the NADPH oxidase of porcine neutrophils. *FEBS Lett.* 377:345-348.

101. Ueno, I., S. Fujii, H. Ohya Nishiguchi, T. Iizuka, and S. Kanegasaki. 1991. Characterization of neutrophil b-type cytochrome in situ by electron paramagnetic resonance spectroscopy. *FEBS Lett.* 281:130-132.

102. Isogai, Y., Y. Shiro, A. Nasuda-Kouyama, and T. Iizuka. 1991. Superoxide production by cytochrome b558 purified from neutrophils in a reconstituted system with an exogenous reductase. *J. Biol. Chem.* 266:13481-13484.

103. Fujii, H., M. K. Johnson, M. G. Finnegan, T. Miki, L. S. Yoshida, and K. Kakinuma. 1995. Electron spin resonance studies on neutrophil cytochrome b558. Evidence that low-spin heme iron is essential for O2-. generating activity. *J. Biol. Chem.* 270:12685-12689.

104. Nugent, J. H., W. Gratzer, and A. W. Segal. 1989. Identification of the haem-binding subunit of cytochrome $b_{-245}$. *Biochem. J.* 264:921-924.

105. Yamaguchi, T., T. Hayakawa, M. Kaneda, K. Kakinuma, and A. Yoshikawa. 1989. Purification and some spectral properties of the small subunit of cytochrome b558 from human neutrophils. *J. Biol. Chem.* 264:112-118.

106. Dinauer, M. C., E. A. Pierce, R. W. Erickson, T. J. Muhlebach, H. Messner, S. H. Orkin, R. A. Seger, and J. T. Curnutte. 1991. Point mutation in the cytoplasmic domain of the neutrophil p22-phox cytochrome b subunit is associated with a nonfunctional NADPH oxidase and chronic granulomatous disease. *Proc. Natl. Acad. Sci. U. S. A.* 88:11231-11235.

# Chapter 2

## A PHASE-SEPARATION TECHNIQUE FOR THE ANALYSIS OF DETERGENT SOLUBILIZED BACTERIORHODOPSIN BY ELECTROSPRAY IONIZATION MASS SPECTROMETRY

### Introduction

The use of mass spectrometry for the accurate mass determination of integral membrane proteins has been reported in a number of articles (1-6) with bacteriorhodopsin, or BR, being one of the most studied integral membrane proteins. BR is commonly used since it is readily available from purple membrane of the bacterium *Halobacterium halobium* in high concentrations (7) and in addition, the protein is extremely stable and has a known seven-transmembrane helical structure (8). These characteristics make it an ideal model in methods development designed to make the accurate mass determination of

intact integral membrane proteins a less arduous task.

In most mass spectrometric analyses BR is prepared directly from native membranes of *Halobacterium halobium* by solubilizing the protein in solvents such as hexafluoroisopropanol, tri-fluoroacetic acid (TFA), and formic acid prior to ionization by MALDI or ESI. Because BR is present in native membranes at a high concentration purification is not needed, however, most integral membrane proteins are obtainable in low concentrations and as part of a complex mixture when taken from native membranes. Therefore, integral membrane proteins are typically solubilized in detergent, then isolated using standard purification methods such as ion exchange chromatography, gel filtration chromatography, and affinity chromatography (9). Since detergent is used in most, if not all, purification schemes involving integral membrane proteins, a method that would tolerate the presence of detergent in the sample is essential for routine use of mass spectrometry in the analysis of this class of proteins.

Examples of studies incorporating detergent include the works by Rosinke et al., Hufnagel et al. and Le Maire, where detergent solubilized purple membranes were analyzed by MALDI and ESI respectively (1,2,5). In the case of Rosinke et al., detergent solubilized BR was directly mixed with matrix solution and analyzed using MALDI. Hufnagel et al. precipitated the protein from detergent solution, washed the precipitant with hexane to remove lipid, then solubilized the dried pellet in chloroform/methanol/water formic acid preceding analysis by ESI. The analysis done by Le Maire et al., obtained accurate mass on BR separated by SDS-PAGE, where the band containing the BR was excised from the gel, and electroeluted into solution. The SDS was

removed from the electroelution solution by cold acetone precipitation, then the BR was solubilized in acetonitrile/water/formic acid and finally analyzed by ESI-MS. Of the three preceding examples, only the study by Rosinke et al. shows the effect of various detergents on the quality of the mass spectrum using MALDI MS. To date no comparison has been made on the quality of ESI MS mass spectra of BR using different detergents.

BR in an aqueous detergent solution cannot be analyzed using standard electrospray solvents and detergent concentrations (3). In this paper we present an approach to the analysis of bacteriorhodopsin solubilized in the detergents, cetyltrimethylammonium bromide (CTAB), octyl glucoside (OG), and CHAPSO. This method utilizes the isolation of BR from detergent solution into a chloroform rich phase produced when the aqueous detergent solution of BR is combined with a tertiary mixture of chloroform/methanol/water 1% acetic acid. This 'phase separation' technique allows for the isolation of the protein in a solvent that can be easily electrosprayed, thus avoiding the trouble of generating a stable electrospray from an aqueous detergent solution.

The findings presented here show that the phase separation technique can be used to obtain the accurate mass of bacterioopsin or BO, (M.W. 26,784) solubilized in the detergents cetyltrimethylammonium bromide (CTAB), octyl glucoside (OG) and CHAPSO. Additionally, the phase separation technique was successful at providing the means for analyzing a synthetic hydrophobic peptide. This peptide was synthesized to model the transmambrane region of an integral membrane protein and consisted of the sequence KKAA$(FAA)_7$AKK. This peptide was found to consist of a mixture of peptides differing by the mass of one alanine when analyzed by ESI-MS using the phase separation

technique. This finding was confirmed by comparing MALDI MS spectra with ESI-MS spectra.

## Materials and Methods

### Sample preparation

Bacteriorhodopsin used in this study was obtained from purple membranes isolated from *Halobacterium halobium* and further purified by sucrose gradient centrifugation. The final suspension of membranes contained 30% sucrose in water. A 100 $\mu$l volume of the membrane suspension containing a 370 pmol of bacteriorhodopsin (determined photometrically) was mixed with 100 $\mu$l of a 1% stock detergent solution of either CTAB, OG, or CHAPSO. The BR in aqueous detergent solution was combined with 800 $\mu$l of a 2:5:2 v/v/v chloroform/methanol/water 1% acetic acid solution and agitated for 10 seconds in a vortex mixer to create an emulsion. The emulsion was then centrifuged at 10,000 X g for 5 minutes, generating two phases. The lower chloroform rich phase was then injected into the electrospray source via a Rheodyne HPLC injector.

The lyophilized synthetic peptide having the proposed sequence KKAA(FAA)$_7$AKK was subjected to the same phase separation process described above. All solvents and detergents used for the analysis were obtained from commercial sources and were of analytical grade.

Mass spectrometry

ESI mass spectra were collected on a VG TRIO-2 (VG, Manchester, UK) with a mass range of 2,000 Da and a home-built capillary ESI interface (10). Spectra were collected by scanning from *m/z* 1000 to 2200 in 5 s with each spectra representing the average of 10 scans. The scanning rate for the synthetic peptide was 5s over a range of *m/z* 200 to 1500 Da with 10 scans averaged for the spectrum. External calibration was done using myoglobin (M.W. 16,951 Da). The electrospray carrier solvent was the same as that used by Schindler et al. (3) consisting of chloroform/methanol/water 1% acetic acid at a ratio of 2:5:2 v/v/v. The flow rate for the electrospray solvent was 1 $\mu$l / min sustained by a syringe pump. The volume of sample injected for each spectra shown was 10 $\mu$l. The sample was introduced to the source via a non-coated fused silica capillary tubing having the dimensions 50 $\mu$m I.D. x 150 $\mu$m O.D. and a length of 50 cm. The MALDI data for the synthetic peptide was collected on a PerSeptive Biosystems Voyager benchtop model time-of-flight mass spectrometer. The synthetic peptide sample was solubilized in 1,1,1,3,3,3 hexafluoroisopropanol then mixed 1:1 with a saturated solution of the matrix α-cyano-4-hydroxycinnamic acid (ACHCA). The sample was spotted on a sample tray and allowed to air dry before analysis.

## Results

A summary of the structures and physical properties of the detergents used in this study is given in Table 3. The non-ionic detergent octyl-β-glucoside is a non-denaturing detergent with a hydrophobic tail of n-octane and a hydrophilic head of β-D-glucoside. It

is commonly used for assays where purified protein is reconstituted into phospholipid membranes or vesicles.

**Figure 2**

Detergents used for solubilization of Bacteriorhodopsin.

| Detegent | Structural Formula | | CMC | Micelle $M_r$ |
|---|---|---|---|---|
| octyl-β-glucoside | 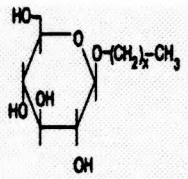 | x=7<br>292.4 Da | 25 mM<br>(0.73% w/v) | 8,000 |
| CTAB | 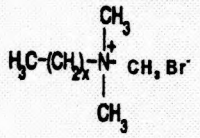 | x=11<br>364.5 Da | 1 mM<br>(0.36% w/v) | 62,000 |
| CHAPSO | 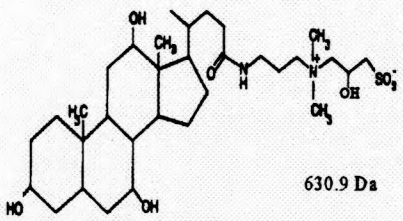 | 630.9 Da | 8 mM<br>(0.49% w/v) | 6,150 |

This detergent has the benefit of a high CMC and a low micellar average molecular weight making it ideal for studies where the sample needs to be concentrated without raising the detergent concentration. The detergent CHAPSO is a zwitterionic detergent with a bile salt moiety for the hydrophobic region and a sulfobetaine hydrophilic group. It

is less denaturing than ionic detergents and also has the benefit of reducing non-specific interactions between hydrophobic proteins once they are solubilized from the membrane. The ionic detergent CTAB used for this study is a quaternary ammonium salt that has properties similar to that of the commonly used anionic detergent sodium dodecyl sulfate (SDS), accordingly it has a propensity to denature proteins.

Mass spectra of detergent solubilized BR acquired from the chloroform layer after the phase separation technique, using the detergents described above, are shown in Figures 3, 4 and 5. Figure 3 shows the spectrum of BR that was solubilized in the detergent CTAB and analyzed by ESI-MS. The additional peaks at higher mass, that are not resolved, are thought to represent the precursor forms of mature BR where the leader sequence is incompletely cleaved prior to transport to the membrane (11).

The ESI mass spectrum of BR that was solubilized in octyl-β-glucoside prior to phase separation is shown in Figure 4. The series of peaks labeled ◊ can be seen slightly higher in mass than BO. These peaks represent either BO with the leader sequence GVS- incompletely removed or possibly BO with retinal attached. The peaks higher in mass than the peaks labeled ◊ are better resolved relative to BR run in CTAB and are again likely due to BR with an incompletely cleaved leader sequence, however, a proper centroid cannot be assigned to these peaks.

The best resolution was achieved when BR was solubilized in CHAPSO as shown in Figure 5. Peaks labeled ◊ are well resolved as are the peaks labeled ***a*** and ***b***. Again, the peaks labeled ◊ represents either BO with the leader sequence GVS- incompletely removed or possibly BO with retinal attached. Based on the mass assignment for these

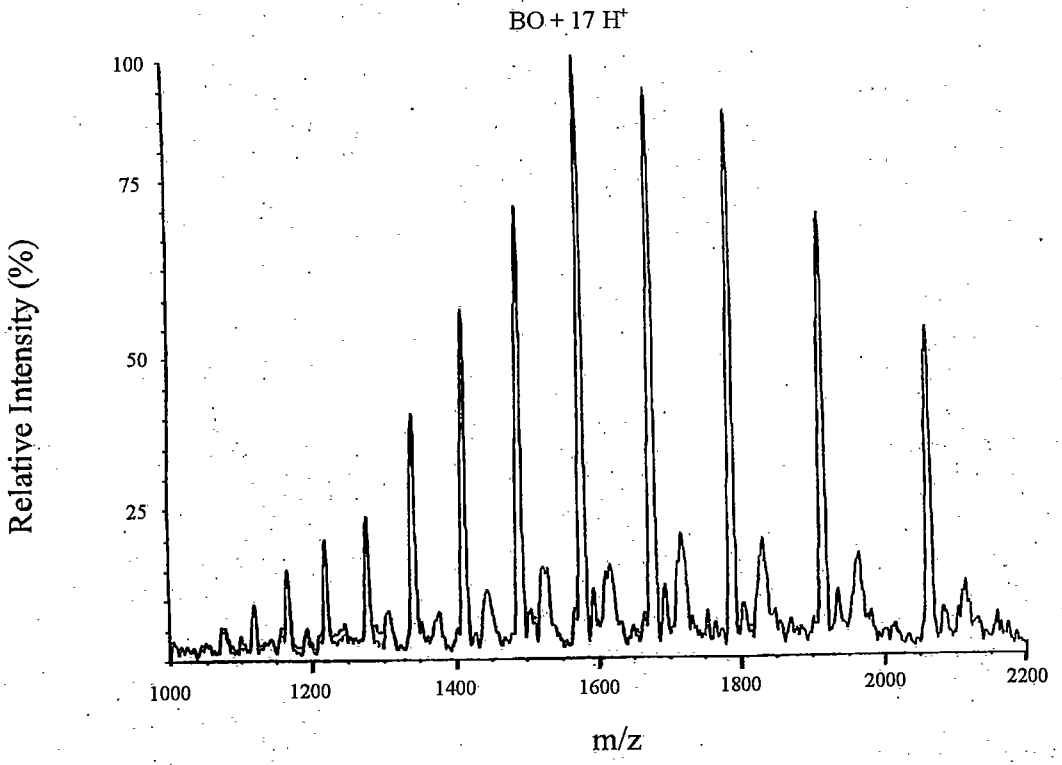


**Figure 3.** ESI mass spectrum of bacteriorhodopsin (BR) from purple membranes solubilized in cetyltrimethylammonium bromide (CTAB). The spectrum represents the average of 10 scans and approximately 110 pmol of protein. The sample was derived from the chloroform phase using the phase separation technique described in the text. The major peaks in the spectrum are from bacterioopsin (BO) while the smaller unresolved peaks are presumably due to BR with an incompletely cleaved leader sequence.

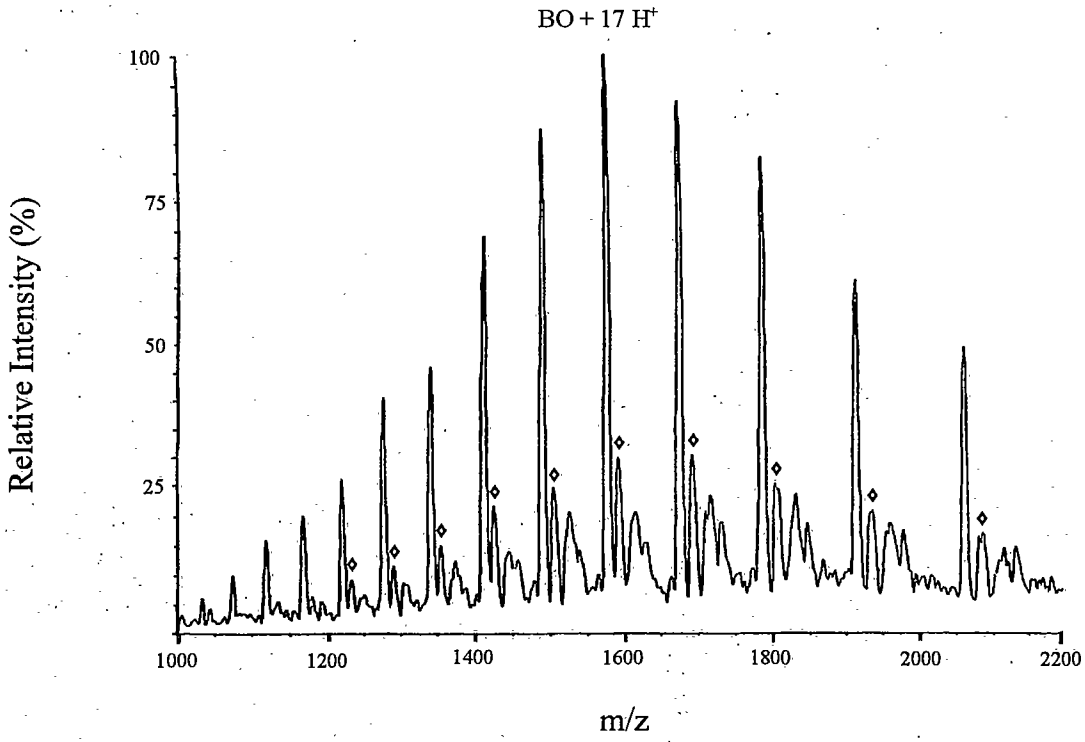


**Figure 4.** ESI mass spectrum of bacteriorhodopsin (BR) from purple membranes solubilized in octyl-β-glucoside (OG). The spectrum represents the average of 10 scans and approximately 110 pmol of protein. The sample was derived from the chloroform phase using the phase separation techniqued described in the text. The series of peaks labeled ◊ are either from BR or BO with the incompletely cleaved leader sequence GVS-. The unlabled peaks are also presumably due to incompletely processed forms of BR.

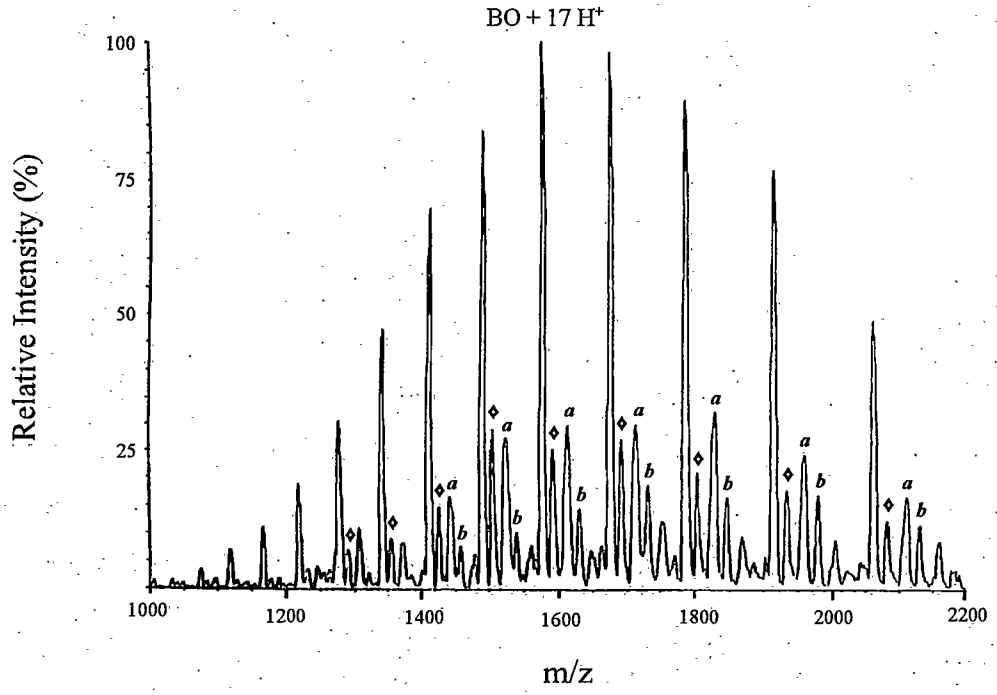


**Figure 5.** ESI mass spectrum of bacteriorhodopsin (BR) from purple membranes solubilized in CHAPSO. The spectrum represents the average of 10 scans and approximately 110 pmol of protein. The sample was derived from the chloroform phase using the phase separation technique described in the text. The series of peaks labeled by ◊ represent either BR with the retinal attached, or BO with with the incompletely cleaved leader sequence GVS-. The peaks labeled ***a*** and ***b*** originate from incompletely processed precursor forms of BR (see Table 2).

## Table 3

Calculated and experimental masses found for bacterioopsin, bacteriorhodopsin and precursor forms solubilized in detergent

| | Observed Masses | | |
|---|---|---|---|
| **SAMPLE** | **1% CTAB** | **1% OG** | **1% CHAPSO** |
| Bacterio**opsin** m.w. 26,784 Da | 26,800 Da error - 0.06% | 26,793 Da error - 0.04% | 26,795 Da error - 0.04% |
| Bacterio-**rhodopsin** m.w. 27,068 Da | n/a | 27,062 Da error - 0.01% | 27,065 Da error - 0.01% |
| Bacterio**opsin** precursor GVS- m.w. 27,044 Da | n/a | 27,062 Da error - 0.06 % | 27,065 Da error - 0.07 % |
| Bacterio**opsin** precursor TAVEGVS- m.w. 27,444 Da | n/a | n/a | 27,424 Da error - 0.07% |
| Bacterio**opsin** precursor LPTAVEGVSQ- m.w. 27,729 Da | n/a | n/a | 27,692 Da error - 0.13% |

peaks, it appears that BR remains intact when solubilized in CHAPSO. However, BO with the leader sequence GVS- incompletely removed has been described by Hufnagel et al. using ESI-MS and the mass difference between BR and BO with the leader sequence GVS- is only 24 Da. The other peaks labeled ***a*** and ***b*** are due to the precursors described by Miercke et al. and recently characterized by Hufnagel et al. (1,11). The peaks labeled ***a*** in Figure 5 are within 0.07% of the mass determined for the incompletely processed form of BO having the leader sequence TAVEGVS-. The peaks labeled ***b*** in Figure 5 are within 0.13% of the mass determined for the incompletely processed form of BO having the leader sequence LPTAVEGVS-. Table 4 lists the calculated masses and observed masses for BO and BR. It also includes the calculated and observed masses for the incompletely cleaved protein.

The spectra in Figure 6 represents the results from solubilizing BR in the electrospray solvent containing 2:5:2 chloroform:methanol:water 1% acetic acid prior to analysis by ESI-MS. Clearly the spectra is of lesser quality than those obtained with BR solubilized in detergent preceding analysis. This was also the case for spectra obtained with BR solubilized in 100% formic acid (data not shown). The 50 $\mu$m I.D. capillary used for the experiments became blocked after a short time (~30 s) disrupting the electrospray when chloroform:methanol:water or 100% formic acid was used to solubilize BR. This is in contrast to BR solubilized in detergent followed by isolation using the phase separation technique which did not result in any blockage of the capillary.

The ESI-MS spectrum in Figure 7 represents the heterogeneous mixture of synthetic peptides produced from the synthesis of the transmembrane peptide mimic

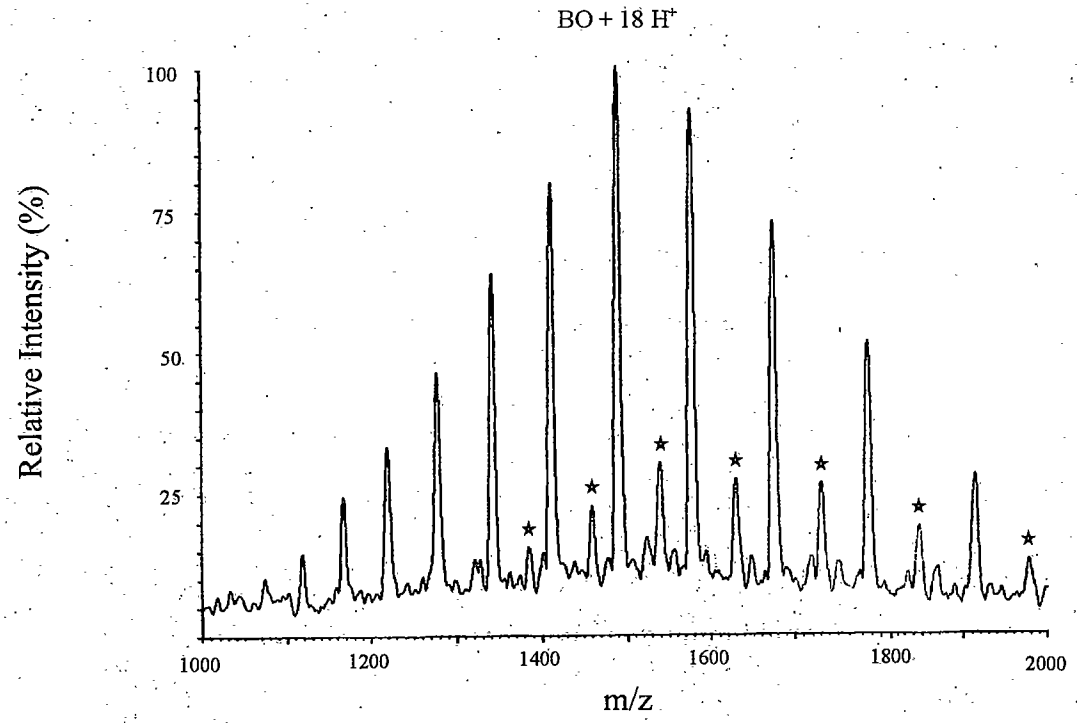


**Figure 6 .** ESI mass spectrum of bacterioopsin (BO) from purple membranes in water without detergent, isolated by the phase separation method. The sample was derived from the chloroform layer using the phase separation method described in the text. The spectrum represents the average of 10 scans and approximately 110 pmol of protein. The presence of the peaks labeled with a ⋆, higher in mass than BO, match the mass of the peaks labeled with ***b*** in Figure 3. These peaks are due to a precursor form of BR with the precursor leader sequence LPTAVEGVS- attached to mature BR .

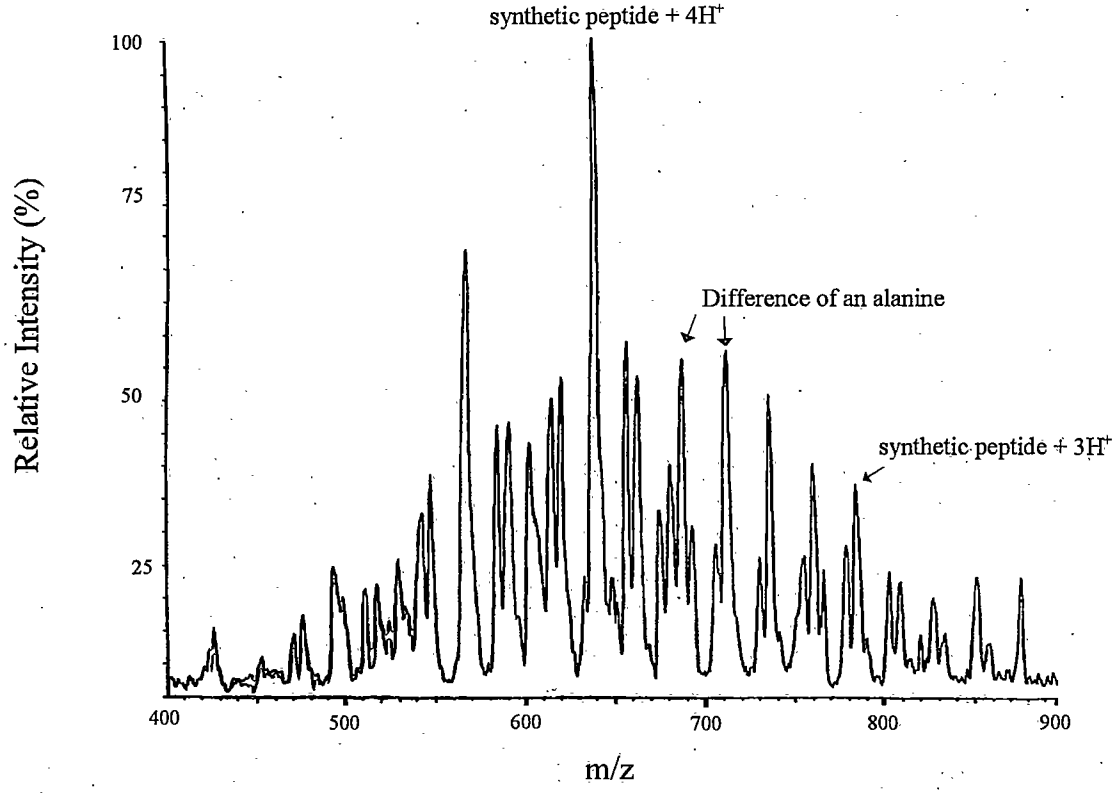


**Figure 7.** ESI mass spectrum of the synthetic peptide KKAA(FAA)$_7$AKK solubilized in CTAB. The sample was derived from the chloroform phase using the phase separation technique described in the text. Isoforms representing varying numbers of alanine residues are clearly visible and two such isoforms are labeled by arrows in the figure.

KKAA$(FAA)_7$AKK having a mass of 2,769 Da. The peptide was not soluble in typical electrospray solvents and could not be solubilized in straight formic acid. In addition, standard acetonitrile/water gradients in reverse-phase HPLC could not be used to determine the purity of the lyophilized product so the phase separation technique was employed to examine the components of the peptide sample. The lyopholized peptide mixture was solubilized in a 1% aqueous solution of CTAB and isolated into the chloroform layer after mixing with the 2:5:2 chloroform/methanol/water 1% acetic acid electrospray solvent. The amount of heterogeneity in the synthesis is clear from the spectrum, with the most prevalent isoforms having a mass difference of one alanine. MALDI MS was performed on the same lyopholized peptide by combining the sample with 1,1,1,3,3,3-hexafluoro-2-isopropanol and the matrix ACHCA. The spectrum can be seen in Figure 8 and the resolved ions differ by the mass of an alanine. On comparison of Figure 7 vs. Figure 8 it is clear that the isoforms are better resolved using ESI with the phase separation technique.

## Discussion

Evidence for the presence of gas phase ions of intact BR (with the retinal attached) is based upon the mass assignments for the peaks labeled ◊ in Figures 4 and 5. There is the distinct possibility that these peaks are due to another incompletely cleaved form of BO where the leader sequence GVS- is not cleaved. This form of BO has been described previously by Hufnagel et al. and differs in mass by 24 Da compared to the mass of BR. BR is an extremely stable protein functioning under extreme conditions of salt and

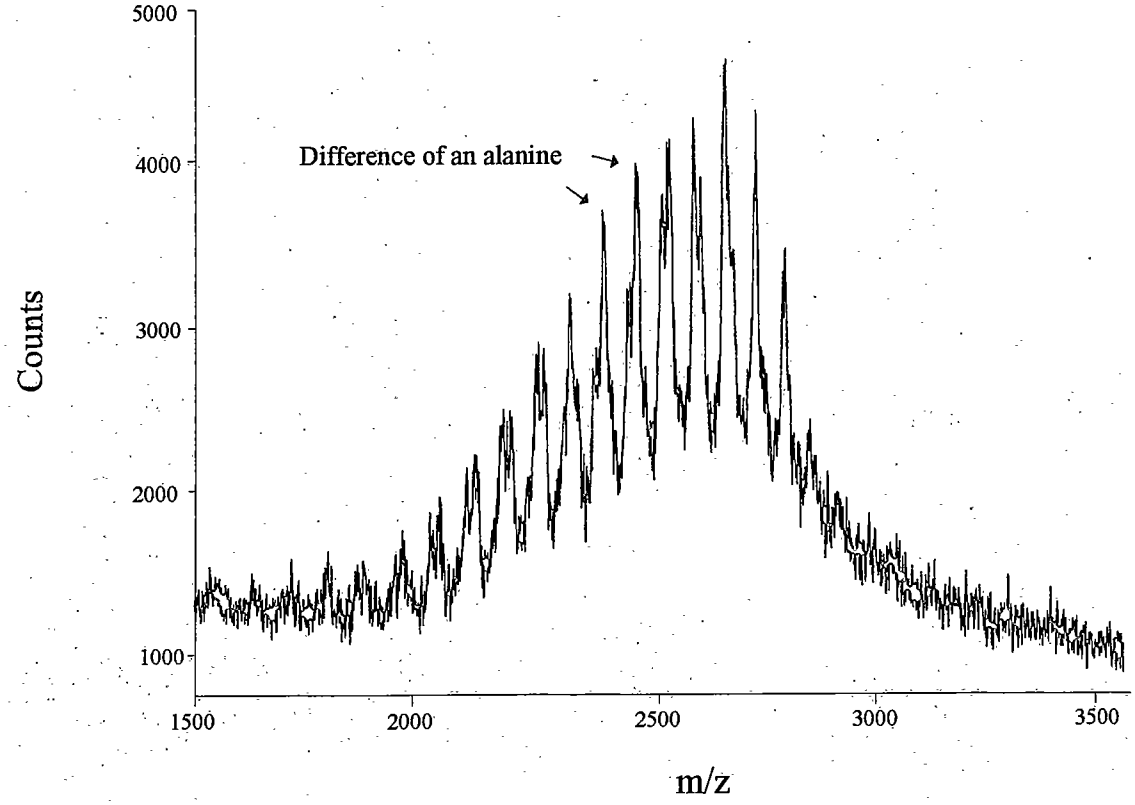


**Figure 8**. The transmembrane mimic peptide KKAA(FAA)$_7$AKK analyzed by MALDI-MS using the matrix α-cyano-4-hydroxycinnamic acid (ACHCA). Isoforms representing varying numbers of alanine residues are clearly visible and two such isoforms are labeled by arrows in the figure.

temperature. Thus it is possible that the protein retains the retinal even after exchange from detergent solution into a non-polar acidic solvent during the phase separation step. However, with the resolution obtained using our instrument, it is not possible to unequivocally assign the origin of the peaks labeled ◊ in Figures 4 and 5. Yet, it is interesting to note that the denaturing detergent CTAB (Figure 3) has little if any peaks at the mass of the peaks labeled ◊ in the Figures 4 and 5, where the less denaturing detergents OG and CHAPSO were used. This difference suggests that the tertiary structure of BR within OG and CHAPSO detergent micelles is maintained while it is disrupted in the presence of CTAB. However, it is difficult to conclude if this is a result of the denaturing effect of the detergent, or the effect of the detergent on the electrospray since the other precursors are of lower intensity. The difference in resolution between the different detergents is quite obvious. The reason for the improvement when using CHAPSO is not known, however, all the spectra from the three detergents were collected on the same day using the same BR stock, the same instrument settings for the mass spectrometer, and new fused silica capillary tubing for each detergent.

The amount of sample used for each spectrum over the ten scans averaged is equal to 110 pmol of BR. It is not surprising that the spectra have good signal to noise for this amount of protein, however, signal is lost after 60 seconds. The reason for this is not known, yet BR has been shown to be present in SDS-PAGE gels performed on the remaining analyte in the capillary. The interaction of the detergent, protein, and lipid existing in the capillary is not completely understood and attempts to spray the chloroform layer directly from a syringe, with only a short piece of capillary tubing, have not been

successful. Currently we are pursuing approaches to describe the elution profile of the detergent relative to the elution pattern of the analyte. In addition, samples of purple membranes solubilized and sprayed using the 2:5:2 ESI carrier solvent alone, as previously described (3), had signal loss after ~30 seconds (Figure 6). This suggests that incompletely solubilized lipids play a role in the loss of signal.

One objective of this technique has been to obtain accurate mass determination of mammalian G-protein coupled receptors, such as bovine rhodopsin, and the spectra of BR represent a good starting point. Efforts to acquire accurate mass data on rhodopsin directly from ROS have so far failed using this technique. The large difference in the ratio of lipid to protein in purple membranes of *Halobacterium halobium* vs. bovine ROS (3/1 vs 20/1) is apparently one obstacle. When the phase separation technique is applied to rhodopsin in ROS, a precipitate like emulsion is formed between the chloroform layer and the aqueous layer. This result differs significantly from purple membranes where the boundary is well-defined. Currently we are trying to remove lipid by solubilizing rhodopsin from ROS in OG then isolating the protein from a HPLC gel filtration column.

The ability to generate ions using ESI from a sample containing detergent has proven to be a difficult task. While MALDI has shown to be tolerant of many reagents commonly used in protein purification including buffers, salts, and even detergent (2,12, 13,14) ESI has had a tendency to be intolerant of these same reagents. The process in which an analyte ion in solution becomes an ion in the gas phase is fundamentally linked to the number of total ions in the solution. Thus it becomes difficult to produce a stable electrospray when the concentration of ions in solution is above roughly $10^{-3}$M (15). When

detergents are used to solubilize an integral membrane protein, the amount of detergent used is dependent upon the critical micelle concentration or CMC. Since most ionic detergents such as SDS and CTAB, have CMCs in the low millimolar range, the resulting ions are at a concentration in solution high enough to disrupt the electrospray. However, for zwitter ionic detergents and non-ionic detergents this is not the case. Yet, the presence of zwitterionic detergents and non-ionic detergents creates an unstable electrospray in samples that are otherwise easily ionized (16). Therefore, the loss of analyte signal in the presence of detergent is most likely due to modification of the solution (i.e. surface tension) and/or competition of the detergent for the electrospray current.

With this in mind a phase separation technique described here was designed to help eliminate the amount of detergent present in a sample without losing the sample due to aggregation. The phase separation technique does not involve excessive sample handling and results in a quick approach to alleviating the disruptive effects of detergent in a sample to be analyzed by ESI-MS. Since the majority of integral membrane proteins are found in low abundance, they must first be solubilized in detergent prior to purification. Hence a technique designed to tolerate detergent solubilized protein has significant value and should thus prove useful for analysis of other hydrophobic integral membrane proteins.

## References


1. Hufnagel, P., U. Schweiger, C. Eckerskorn, and D. Oesterhelt. 1996. Electrospray Ionization Mass Spectrometry of Genetically and Chemically Modified Bacteriorhodopsins. *Anal. Biochem.* 243:46-54.

2. Rosinke, B., K. Strupat, F. Hillenkamp, J. Rosenbusch, N. Dencher, U. Kruger, and H. J. Galla. 1996. Matrix-Assisted Laser Desorption/Ionization Mass Spectrometry (MALDI-MS) of Membrane Proteins and Non-covalent Complexes. *Journal of Mass Spectrometry* 30:1462-1468.

3. Schindler, P. A., A. Van Dorsselaer, and A. M. Falick. 1993. Analysis of hydrophobic proteins and peptides by electrospray ionization mass spectrometry. *Anal. Biochem.* 213:256-263.

4. Schey, K. L., D. I. Papac, D. R. Knapp, and R. K. Crouch. 1992. Matrix-assisted laser desorption mass spectrometry of rhodopsin and bacteriorhodopsin. *Biophys. J.* 63:1240-1243.

5. le Maire, E. L., S. Deschamps, J. V. Moller, J. P. le Caer, and J. Rossier. 1993. Electrospray ionization mass spectrometry on hydrophobic peptides electroeluted from sodium dodecyl sulfate-polyacrylamide gel electrophoresis application to the topology of the sarcoplasmic reticulum Ca2+ ATPase. *Anal. Biochem.* 50-57.

6. Chait, B. T. and S. B. Kent. 1992. Weighing naked proteins: practical, high-accuracy mass measurement of peptides and proteins. *Science* 257:1885-1894.

7. Oesterhelt, D. and W. Stoeckenius. 1974. Isolation of the cell membrane of *Halobacterium halobium* and its fractionation into red and purple membranes. *Methods Enzymol.* 31:667-678.

8. Grigorieff, N., T. A. Ceska, K. H. Downing, J. M. Baldwin, and R. Henderson. 1996. Electron-crystallographic refinement of the structure of bacteriorhodopsin. *J. Mol. Biol.* 259:393-421.

9. Jennings, D. N. 1989. Methods for the structural analysis of membrane proteins. *Annu. Rev. Biochem.* 58:999-1027.

10. Bai-Wei, L. 1992. Thesis. Ion transport by viscous gas flow through capillaries and electrospray mass spectrometry of proteins. Montana State University, Bozeman, MT., USA.

11. Miercke, L. J. W., P. E. Ross, R. M. Stroud, and E. A. Dratz. 1989. Purification of bacteriorhodopsin and characterization of mature and partially processed forms. *J. B. C.* 264:7531-7535.

12. Beavis, R. C. and B. T. Chait. 1990. High-accuracy molecular mass determination of proteins using matrix-assisted laser desorption mass spectrometry. *Anal. Chem.* 62:1836-1840.

13. Beavis, R. C. and B. T. Chait. 1990. Rapid, sensitive analysis of protein mixtures by mass spectrometry. *Proc. Natl. Acad. Sci. U. S. A.* 87:6873-6877.

14. Hillenkamp, F., M. Karas, R. C. Beavis, and B. T. Chait. 1991. Matrix-assisted laser desorption/ionization mass spectrometry of biopolymers. *Anal. Chem.* 63:1193A-1203A.

15. Kebarle, P. and L. Tang. 1993. Ions from solution to ions in the gas phase: the mechanism of electrospray ionization. *Anal. Chem.* 65:972A-986A.

16. Loo, R. R., N. Dales, and P. C. Andrews. 1994. Surfactant effects on protein structure examined by electrospray ionization mass spectrometry. *Protein Sci.* 3:1975-1983.

# Chapter 3

## IDENTIFICATION OF TRANSMEMBRANE TRYPTIC PEPTIDES OF RHODOPSIN USING MATRIX ASSISTED LASER DESORPTION/IONIZATION TIME-of-FLIGHT MASS SPECTROMETRY

### Introduction

Integral membrane proteins play central roles in a variety of cell functions, such as signal transduction, cellular homeostasis, cell-cell recognition, and host defense. These proteins are deeply imbedded in oily cell membranes and have properties that make structural analysis considerably more difficult than for water soluble proteins. The 3-D structures of a small number of integral membrane proteins have been successfully determined through the use of X-ray crystallography (1-3). Low resolution structures have been obtained for bacteriorhodopsin (4) and rhodopsin (5-7) by electron crystallography and electron microscopy. However, detailed structural information is not available for the vast majority of integral membrane proteins. Typically, structural features of integral membrane proteins are inferred from their amino acid sequences or studies employing low resolution biochemical methods such as in-situ proteolysis, chemical

modification, and epitope mapping (8,9). Covalent affinity labeling studies have provided structural and binding site information on water soluble proteins (10-12) to a lesser extent, in membrane proteins (13,14). The information obtained in covalent labeling studies of integral membrane proteins has been limited by the difficulty in identifying the hydrophobic amino acid sequence containing the modified residues.

Sites of covalent labeling in proteins can be identified using mass spectrometry by determining the change in mass of peptide fragments after labeling and by sequencing of the modified peptides in the mass spectrometer. However, transmembrane cleavage fragments from integral membrane proteins present problems for the ionization methods used in mass spectrometry. This is due to the hydrophobicity of the peptides and to interference from the detergents employed for solubilization of these peptides. Still, progress has been reported on characterizing both hydrophilic and hydrophobic peptide fragments from a few integral membrane proteins. For example, peptide fragments of the nicotinic acetylcholine receptor have been identified using mass spectrometry in a number of studies that focussed on the topography of the subunits (15), the sites of post-translational modifications (16), and the site of α-neurotoxin binding (17). In addition, chymotryptic peptides from the digestion of the recombinant hepatitis B surface antigen integral membrane protein have been identified using mass spectrometry (18). Studies identifying peptides containing complete transmembrane regions include the analysis of cyanogen bromide digests of apobacteriorhodopsin by fast atom bombardment (FAB) mass spectrometry (19). Nine of the ten expected cyanogen bromide cleavage fragments from apoBR were identified directly from the digest mixture. FAB MS/MS was

successful in providing amino acid sequence information on six of the nine peptide fragments. The remaining peptides were too large ( > 3,000 Da) for sequencing using FAB MS/MS. A chymotryptic digest of aporhodopsin was also analyzed in the same study, but only 5 of the 55 peptides expected (all with masses below 1,500 Da) were identified and confirmed by sequencing using FAB MS/MS (19). Larger proteolytic peptides (9,428 Da to 11,860 Da) from sarcoplasmic reticulum $Ca^{+2}$ ATPase, obtained by digestion in membranes by V8 protease, have been identified by mass spectrometry. The peptide fragments were isolated by SDS-PAGE, electroeluted into solution, and analyzed by electrospray ionization mass spectrometry (20). These peptides contained complete putative transmembrane regions from $Ca^{+2}$ ATPase.

In this study, we have used MALDI mass spectrometry to identify transmembrane tryptic peptides of bovine rhodopsin. Rhodopsin is an archetype of the large superfamily of G protein-coupled receptors and serves as a useful test case. Bovine rhodopsin was reduced, alkylated and digested with trypsin, both in situ in ROS membranes and after affinity purification in the detergent octyl-β-glucoside (OG). The detergent OG was retained through the subsequent RP-HPLC and MALDI MS procedures. This approach allowed for the mass-based identification of four of the six transmembrane tryptic fragments of rhodopsin by MALDI MS. The identities of the peptides were confirmed by Edman sequencing since the peptides were too large for sequencing by post-source decay in the time-of-flight (TOF) mass spectrometer. The heterogeneity in the glycosylation of the N-terminal tryptic peptide of rhodopsin was characterized by MALDI MS, without modifying the carbohydrate prior to analysis. In summary, we have shown that, by the

appropriate use of detergent, transmembrane peptides derived from integral membrane proteins can be analyzed by MALDI MS.

## Materials and Methods

### Reagents

Chemicals and solvents used in the study were either analytical grade or HPLC grade. Sequencing grade trypsin (Type XI) and PNGaseF were obtained from Boehringer Mannheim GmbH, Germany. Melittin, concanavalin A-agarose Type V-B, and methyl-$\alpha$-mannoside were obtained from Sigma Chemical Company. SDS was obtained from Bio-Rad. Octyl-β-glucoside (OG) and lauryldimethylamine oxide (LDAO) were obtained from Calbiochem. Formic acid was obtained from Fluka (p.a.; 98%). Bovine retinal rod outer segments were prepared from bovine retinas and were kindly provided by Professor Heidi Hamm.

### Preparation of Washed ROS Membranes

ROS were washed by suspending them in a deionized water solution containing 1 μM EDTA and 0.02 % sodium azide. The suspension was centrifuged at 80,000 g for 30 min. The supernatant was removed and the pellet resuspended by mild sonication in fresh wash solution and centrifuged again. The membranes were washed and centrifuged a third time to prepare a pellet of washed ROS membranes.

Preparation of Concanavalin-A Affinity Purified Rhodopsin

All steps in the preparation of rhodopsin were carried out in dim red light to avoid bleaching of rhodopsin. The washed ROS membrane pellet was solubilized in 3 % OG in 20 mM PIPES. Rhodopsin was purified by affinity chromatography on concanavalin-A bound to agarose beads (32). The OG concentration in the purified rhodopsin fractions was decreased to 0.7 % (w/v) using a 10,000 Da cut-off Centricon concentrator (Amicon). This procedure also reduced the concentrations of methyl-α-mannoside and buffer used in the elution step. Rhodopsin concentrations throughout the procedure were determined by measuring the absorbance at 500 nm in 3 % LDAO. Purity was estimated to be >95 % by SDS-PAGE.

Tryptic Digest

Samples were removed from Centricon filters and made 4 M in urea to partially denature rhodopsin. Samples were then reduced and alkylated unless stated otherwise. The samples were reduced with DTE then alkylated with iodoacetamide (33). The samples were diluted 2 fold to lower the urea concentration to 2 M and were digested for 24 hours at 37°C with sequencing grade trypsin at an enzyme to substrate ratio of 1:25 w/w. The digestion was carried out at pH 8.5 in microcentrifuge tubes and stopped by freezing the samples. Each sample digested contained approximately 100 μg of protein. A 50 μg sample of melittin was used as a positive control for the digest. The complete loss of intact melittin was confirmed with RP-HPLC. The efficiency of the rhodopsin digestion was followed by SDS-PAGE and by HPLC gel filtration chromatography.

Reverse Phase HPLC

Chromatography was carried out on a Hitachi Model L-2500 HPLC system with a variable wavelength UV detector set at 220 nm (Hitachi Instruments Inc., San Jose, CA). SDS and formic acid were added to the digest to a final concentration of 20 mM and 2 % v/v, respectively, to reduce aggregation of peptide fragments prior to RP-HPLC separation. The sample was sonicated briefly and centrifuged at 10,000 g for 3 minutes before injection. The injection volume was 100 µl and contained approximately 30 µg (~700 pool) of digested rhodopsin. Separation of tryptic peptides was performed on a Vydac $C_4$ 25 x 4.6 mm reverse phase column (The Separations Group, Hesperia, CA) maintained at 55°C with a column heater. A binary solvent system for the separation of hydrophobic peptides was used (34). The solvent system was comprised of mobile phase A) 0.1 % v/v TFA, 0.08 % v/v morpholine and 0.1 % w/v octyl-β-glucoside in water and mobile phase B) 0.1 % v/v TFA, 0.08 % v/v morpholine and 0.1 % w/v octyl-β-glucoside in 2:2:1 v/v/v acetonitrile:1-propanol:water. The gradient started at 100 % A, ramped linearly over 50 minutes to 100 % B, and was then held at 100 % B for 15 minutes. The flow rate was 0.8 ml/min throughout the run. Fractions were collected into 2.0 ml polyethylene microcentrifuge tubes, concentrated 40-120 fold using a SpeedVac to a final volume of approximately 10 µl, and stored at 4 °C. In order to reduce the possibility of carry-over of any poorly solubilized material from run to run, the HPLC column was washed between injections using 98 % formic acid. Blank gradients were run prior to injecting a sample to ensure that carry-over was not contributing to the detected fractions.

Mass Spectrometry

MALDI mass spectra were obtained on a PerSeptive Biosystems/Vestec Voyager RP TOF mass spectrometer (PerSeptive Biosystems, Framingham, MA). The instrument has a 1.3 m linear flight tube, a 4 ns pulsed 337 nm nitrogen laser, a dual stage source, and a single stage reflector. All samples were run in linear mode with 28 kV accelerating voltage, 16.8 kV secondary grid voltage, and 84 V guide wire voltage. Three matrices were tried, 2,5-dihydroxybenzoic acid, sinapinic acid, and *alpha*-cyano-4-hydroxycinnamic acid. Of these three, *alpha*-cyano-4-hydroxycinnamic acid gave superior results and was used in all MALDI experiments presented. The matrix was prepared as a saturated solution in 2:1 v/v water:acetonitrile. It was observed that larger crystals were formed, and MALDI mass spectra were improved, when a volume of the concentrated peptide solution was first diluted with an equal volume of a 1:1 v/v mixture of water:acetonitrile with 0.1 % TFA. A 0.3 µl aliquot of the resulting solution was then mixed with an equal volume of the saturated matrix solution in a sample well and allowed to air-dry before analysis. Melittin was used as an external standard (2,847 Da) for mass calibration.

Amino Terminal Peptide Sequence Analysis

Sequencing was carried out at the Harvard Microchemistry Facility (Cambridge, MA). Concentrated sample fractions from the RP-HPLC, described above, were applied to the biphasic column of a Hewlett Packard G1005A sequenator (Palo Alto, CA) and subjected to automated Edman sequencing, using the manufacturer's recommended chemistry and protocols (Hewlett Packard Routine 3.0).

# Results

## MALDI MS Used to Identify Transmembrane Tryptic Peptides of Rhodopsin.

Figure 9 shows a model of the transmembrane organization of bovine rhodopsin, based upon the consensus of a large number of G protein-coupled receptor sequences (4,21). The most hydrophobic amino acids are colored dark green, and the less hydrophobic amino acids are colored light green. Arrows indicate trypsin cleavage sites. Sites of covalent post-translational palmitoylation on C322 and C323 are indicated by bold zig-zag lines, and the glycosylated sites at residues N2 and N15 are indicated by chains of small open circles. The inset to Figure 9 shows the peptides that were identified by MALDI mass spectrometry and confirmed by Edman microsequencing (black) as well as the glycosylated N-terminus identified by MALDI mass spectrometry (grey). The high hydrophobicity of the peptides shown in black in the inset can be seen in Figure 9 by the abundance of dark green hydrophobic residues for the same regions in the color model.

Tryptic digestion of reduced and alkylated rhodopsin was carried out in room light on two different types of preparations: affinity purified rhodopsin in OG and rhodopsin in washed ROS membranes. Peptides generated from the digestions of these different rhodopsin preparations were separated by RP-HPLC. Figure 10 shows RP-HPLC chromatograms of a tryptic digest of concanavalin A purified rhodopsin while Figure 11 is a tryptic digest of rhodopsin in washed ROS membranes. Figure 12 is a blank trypsin digestion. Fractions were collected for every peak in the chromatogram, and each fraction was analyzed by MALDI MS. Rhodopsin peptides were shown to be present in the

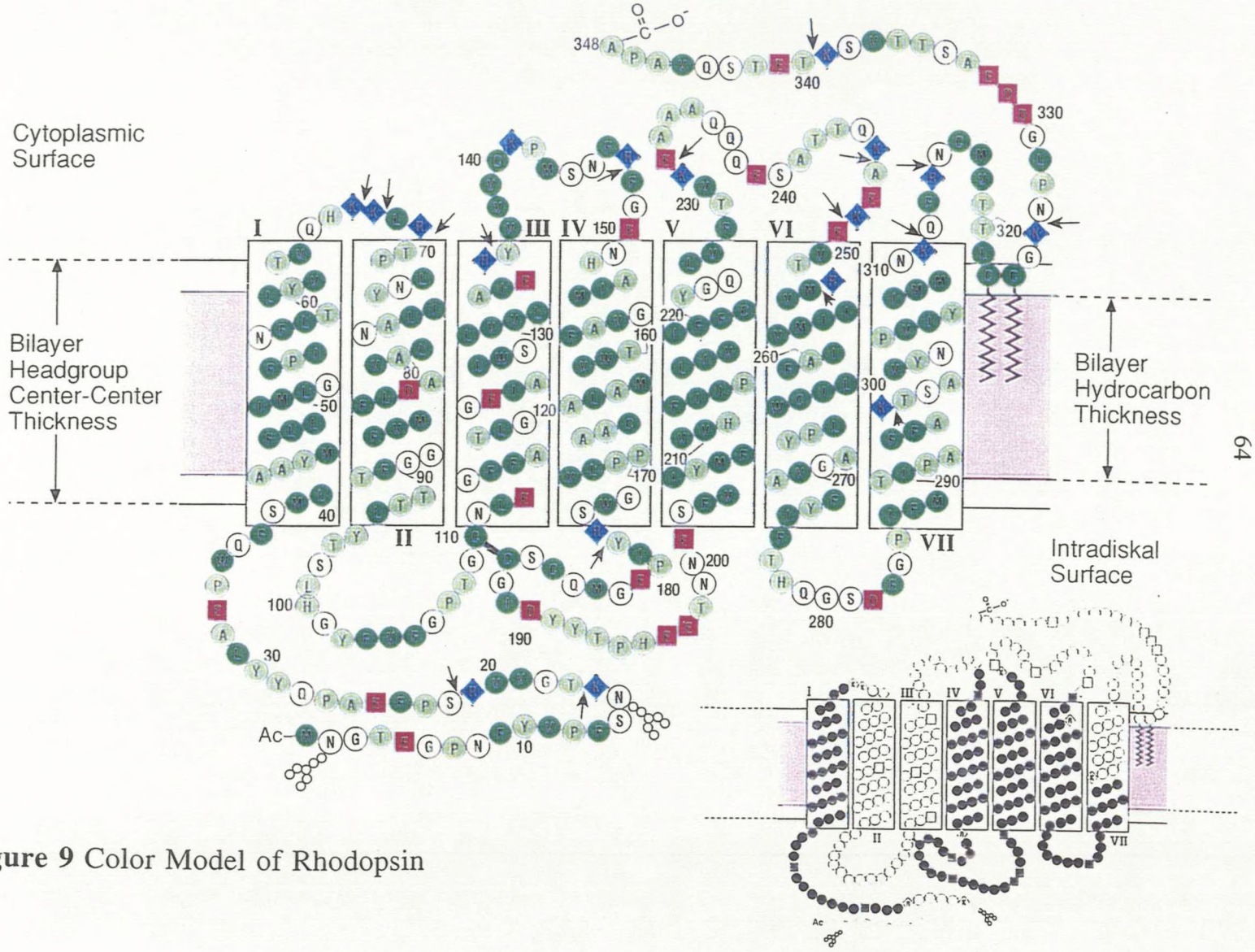


**Figure 9** Color Model of Rhodopsin

**Table 4**

**Hydrophobic tryptic peptides from the transmembrane regions of rhodopsin**

| Position of tryptic peptide in sequence amount [c] | | Retention time (RP-HPLC) | Hydrophobicity Index (Bull&Breese) | Calculated Mass[b] | Mass Obs. by MALDI MS | N-terminal sequence / |
|---|---|---|---|---|---|---|
| #1 | 22-66 | 48.6 min. | -22,490 | 5,331 Da | 5,330 Da | SPFEA-- |
| #2 | 70-135 | N/A | -26,080 | 7,233 Da | N/A | N/A |
| #3 | 148-177 | 37.3 min. | -4,160 | 3,260 Da | 3,264 Da | FGENH-- |
| #4 | 178-231 | 50.6 min. | -22,620 | 6,528 Da | 6,536 Da | YIPEG-- |
| #5 | 253-296 | N/A | -23,320 | 5,329 Da | N/A | N/A |
| #5*[a] | 249-296 | 50.6 min. | -22,580 | 5,531 Da | 5,536 Da | EVTRM-- |

[a] This peptide includes the tetra peptide EVTR that was not cleaved at R 252

[b] All masses listed include the alkylation of available cysteines

[c] Amount refers to the amount of sample estimated by Edman microsequencing data

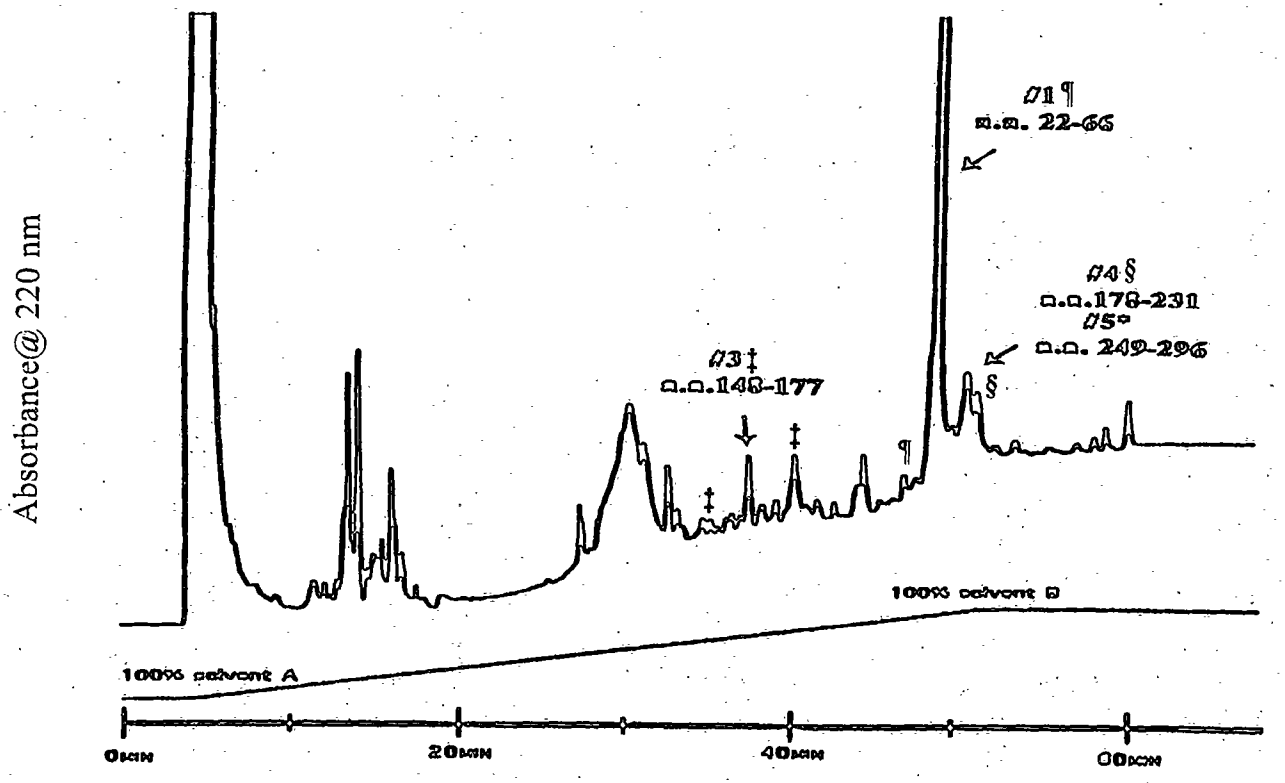


**Figure 10.** Chromatogram of a tryptic digest of concanavalin A purified rhodopsin. The peaks labeled with an arrow contain the peptides characterized by MALDI MS and Edman sequencing. Symbols above peaks denote fractions that contained transmembrane peptides that were identified by MALDI MS only

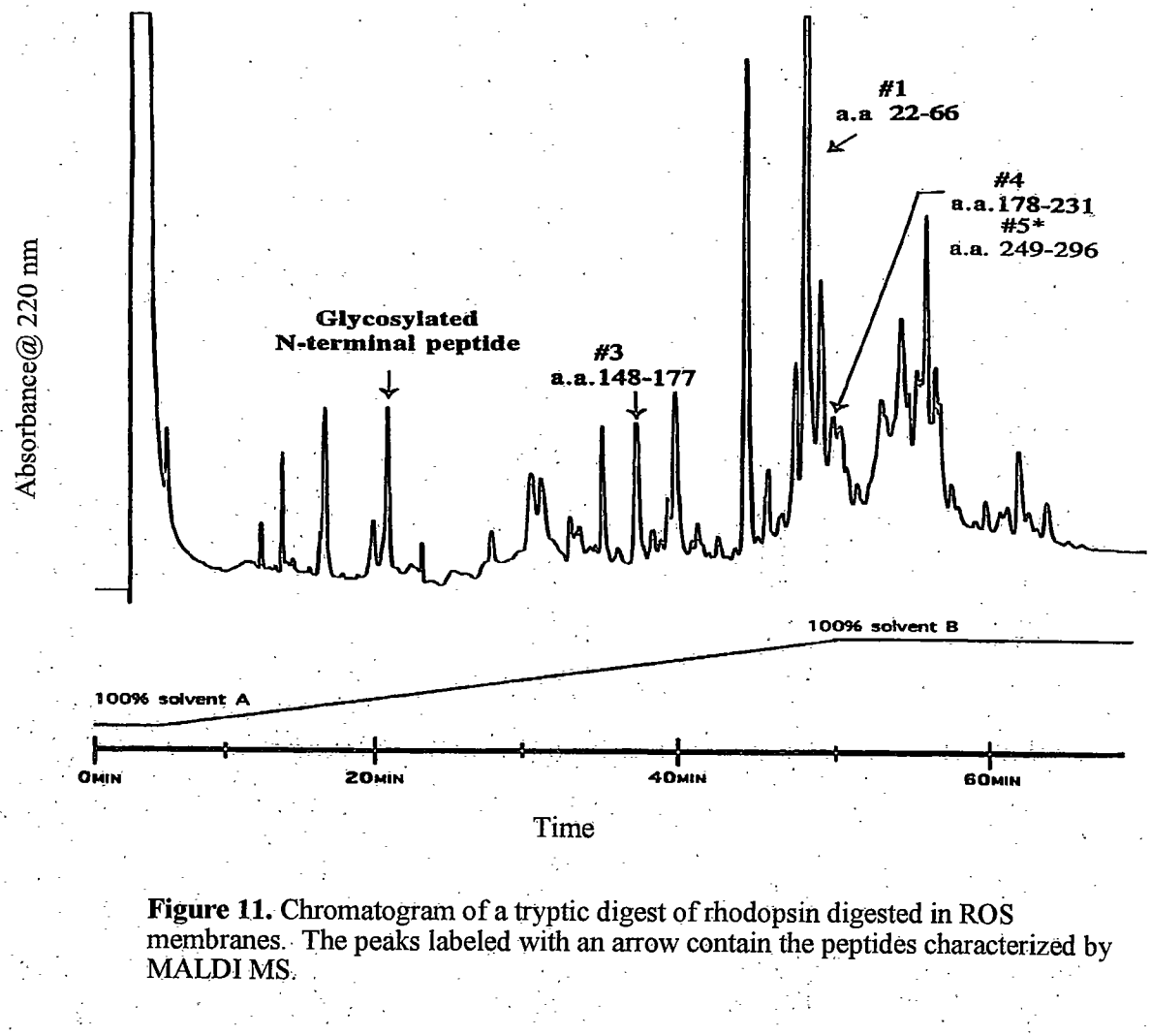


**Figure 11.** Chromatogram of a tryptic digest of rhodopsin digested in ROS membranes. The peaks labeled with an arrow contain the peptides characterized by MALDI MS.

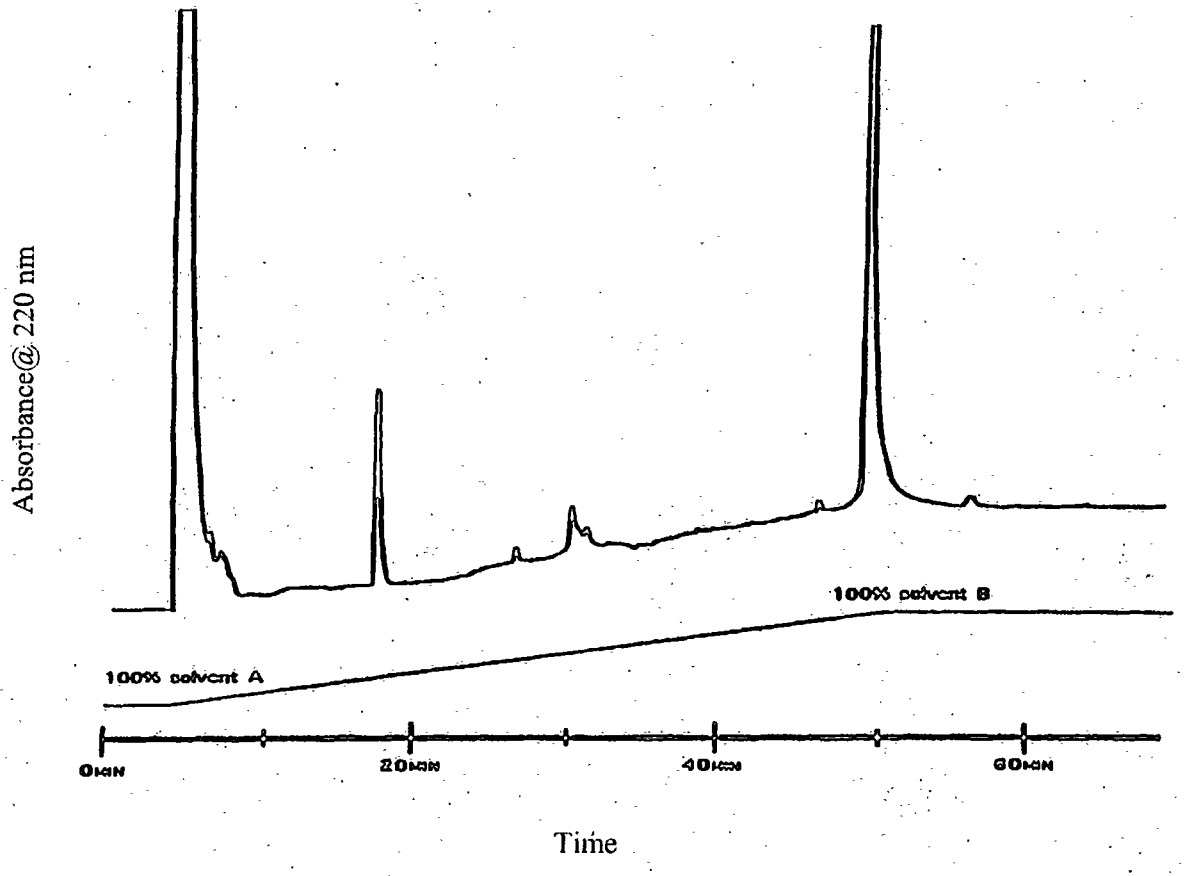


**Figure 12.** Chromatogram of a blank tryptic digest of rhodopsin digest. The large peak at approximately 50 minutes is due to the detergent octyl-β-glucoside in the mobile phases.

majority of the HPLC fractions collected between 35 and 55 minutes in chromatograms A) and B). To assist in the discussion of these results, properties of the transmembrane tryptic peptides of rhodopsin are listed in Table 5. The table gives the position of the peptides in the sequence of rhodopsin, RP-HPLC retention times obtained in this work, hydrophobicity index (22), calculated molecular weight (after alkylation of cysteine residues), observed mass by MALDI MS, and the N-terminal sequence identified by Edman microsequencing. We will first discuss the MALDI results for four HPLC peaks in chromatogram A), selected on the basis of the quality of the mass spectra. We will proceed from left to right in the color model, shown in Figure 9.

Figure 13 shows the MALDI mass spectrum obtained from the HPLC fraction that eluted at 48.6 minutes in Figure 10. Mass peaks are observed at m/z 5,330 Da (***a***) and 5,458 Da (***b***). The lower mass is within 0.02 % of the calculated mass of peptide #1 in Table 5. This peptide, amino acids 22-66, includes transmembrane helix I of rhodopsin (Figure 9). The peak labeled ***b*** has a mass corresponding to peak ***a*** plus an additional lysine (amino acids 22-67). When there are two consecutive lysines, as in K66 and K67 in rhodopsin, it is not unusual for trypsin to skip a cleavage site. This results in two peptides that have the same N-terminus but differ in their carboxy terminus by one lysine, and this pattern adds confidence to the mass spectral interpretation. The identity of this peptide was confirmed by Edman sequencing as discussed below.

Figure 14 shows the MALDI mass spectrum of the HPLC fraction that eluted at 37.3 minutes in Figure 10. The mass of the larger peak at m/z 3,264 is within 0.1 % of the calculated mass of peptide #3 in Table 5. As seen in Figure 9, this peptide (amino acids

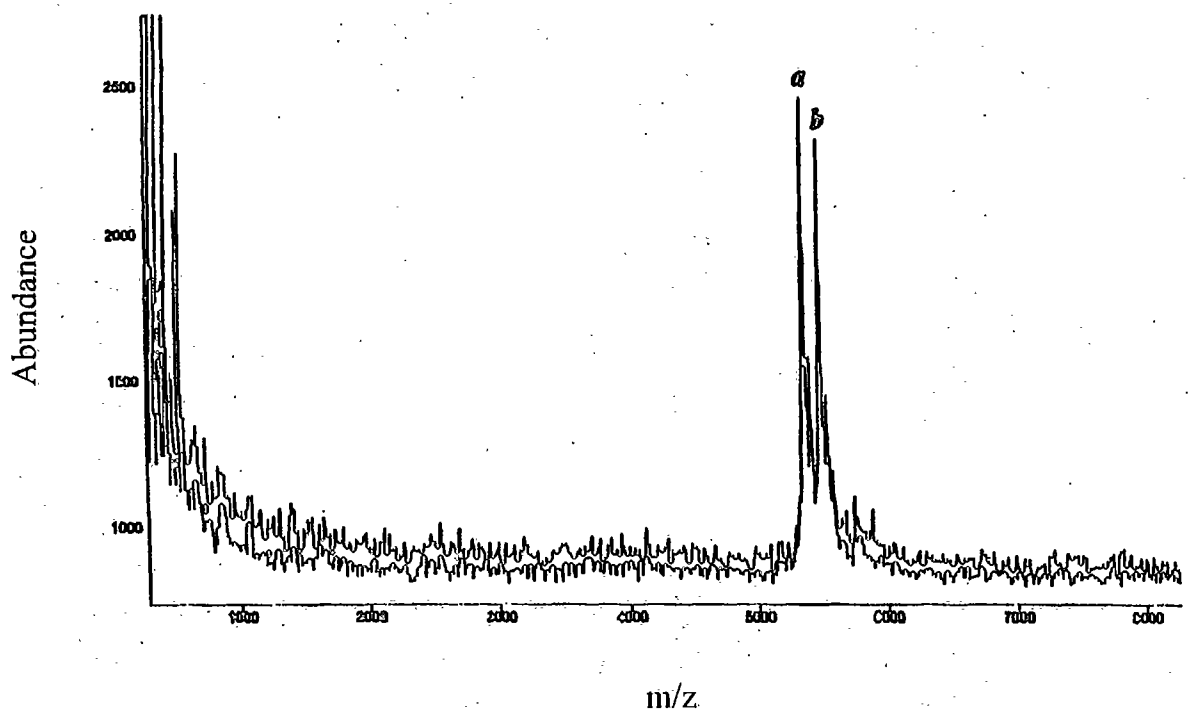


**Figure 13**. MALDI mass spectrum of hydrophobic tryptic peptide #1, described in Table 2, isolated from affinity purified rhodopsin. The sample is from the RP-HPLC fraction eluting at 48.6 minutes and contains transmembrane helix 1 (shown in Figure 10). The peak labeled *a* contains amino acids 22-66 while the peak labeled *b* contains amino acids 22-67 indicating incomplete trypsin cleavage. The spectrum is the average of 78 laser shots.

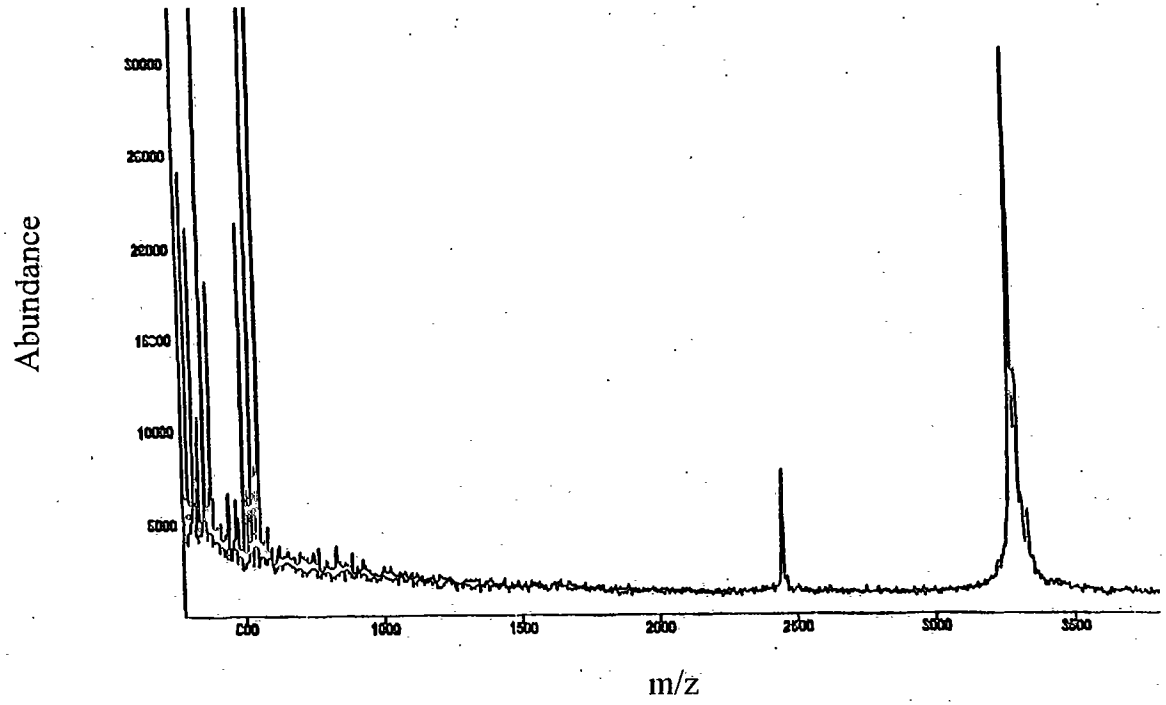


**Figure 14**. MALDI mass spectrum of hydrophobic tryptic peptide #3 described in Table 2 isolated from affinity purified rhodopsin. The sample is from the RP-HPLC fraction eluting at 37.3 minutes. The peak at *m/z* 3,264 represents the mass of amino acids 148-177 and includes transmembrane helix IV (shown in Figure 10). The spectrum is the average of 26 laser shots.

148-177) includes transmembrane helix IV of rhodopsin. The peak at m/z 3,264 is seen to have two distinct shoulder peaks, at 16 and 32 Da higher mass. These are likely to be the result of oxidation of methionines to sulfoxides (+16) and/or sulfones (+32). The smaller peak at mass m/z 2,442 in Figure 14 has not been identified.

The MALDI mass spectrum of the HPLC fraction that eluted at 50.6 minutes in Figure 10 is shown in Figure 15. The higher mass peak (***b***) was identified with peptide #4, since the measured mass was within 0.1 % of the calculated mass as shown in Table 5. Peptide #4 consists of amino acids 178-231 and includes transmembrane helix V (Figure 9). The measured mass for the peak labeled ***a*** in Figure 15 was 5,536 Da. This mass is not close to the calculated mass of any peptide that would result from the complete tryptic cleavage of rhodopsin. However, it is within 0.1 % of the mass calculated for amino acids 249-296. This peptide would result from incomplete cleavage by trypsin at R252. As seen in Figure 9, this peptide includes transmembrane helix VI and part of helix VII and is labeled #5* in Table 5. The mass-based identification of this peptide was confirmed by Edman sequencing, as discussed next.

<u>The Identities of Rhodopsin Tryptic Peptides were Confirmed by Edman Microsequencing</u>

The mass-based identification of peptides #1, #3, #4, and #5* outlined above is quite convincing. However, with a mass accuracy of 0.1 %, sequence information is required for unequivocal identification of the peptides. For this reason, Edman sequencing of the first five amino acids was performed on the samples used to obtain the MALDI

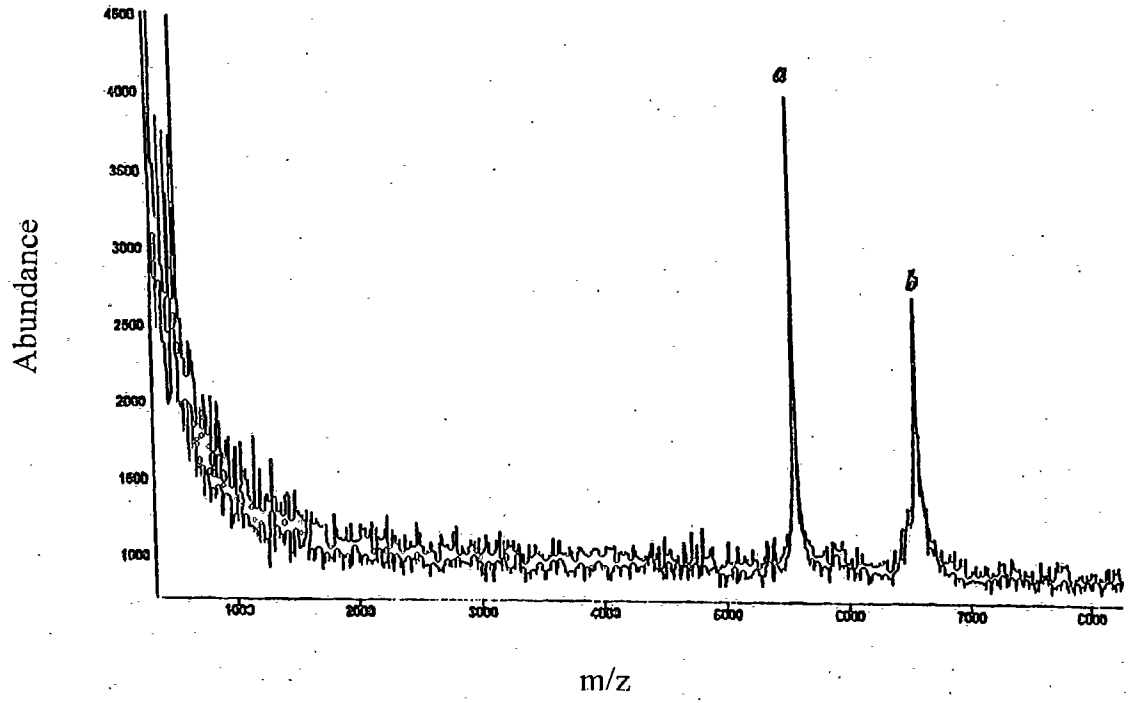


**Figure 15.** MALDI mass spectrum of hydrophobic tryptic peptides #4 and #5*, described in Table 2 isolated from affinity purified rhodopsin. The sample is from the RP-HPLC fraction eluting at 50.6 minutes. The peak labeled ***a*** at *m/z* 6,536 represents the mass of amino acids 178-231 (peptide #4) and includes transmembrane helix V (shown in Figure 10). The peak labeled ***b*** at *m/z* 5,535 represents the mass of amino acids 249-296 (peptide #5*) and includes transmembrane helix VI and a portion of helix VII (shown in Figure 1). The spectrum is the average of 28 laser shots.

mass spectra in Figures 13 to 15. All five N-terminal residues were correctly identified for all of the peptides #1, #3, and #4 in their respective fractions. Hydrophobic tryptic peptide #5* was identified as a minor sequence from the HPLC fraction at 50.6 minutes in Figure 10. In this case the amino acid assignments were made with reference to the sequence of rhodopsin. Two additional minor sequences were read from the HPLC fractions discussed above. The sequence for the tryptic peptide making up the C-terminal half of the seventh transmembrane region, starting at threonine 297 (Figure 9), was read from a fraction that also contained peptide #1. The sequence for the tryptic peptide starting at asparagine 315, that contains the sites of palmitoylation at cysteines 322 and 323, was read from a fraction that also contained peptide #3 and from a second fraction that also contained peptides #4 and #5*. Both of these minor sequence peptides are hydrophobic, as shown by a large negative Bull and Breese hydrophobicity value (- 5,190) for the peptide starting at threonine 297 and due to the addition of palmitoyl groups in the case of the peptide starting at asparagine 315. No mass peaks were found in the MALDI spectra that could correspond to possible tryptic peptides starting with these sequences.

Positive identification of the transmembrane tryptic peptide #2 was not achieved, either by MALDI MS or by Edman sequencing. The peptide must have been produced in the digestion, since peptides on either side were positively identified. However, since peptide #2 is the largest and also the most hydrophobic (Table 5), the recovery of this peptide may be considerably lower than for the other peptides. The small hydrophilic peptides (<1,000 Da) from the loop regions of rhodopsin and the C-terminus were not detected by MALDI MS. This study focussed on hydrophobic peptides, and it is likely

that under the RP-HPLC conditions used, these small hydrophilic peptides were not retained by the column but were eluted in the void fraction which was not studied by MALDI MS. However, the N-terminal glycopeptide was isolated by RP-HPLC, both with OG and without OG (data not shown). The signal intensities of this peptide in both HPLC chromatograms and in MALDI spectra were similar. Therefore, for this particular hydrophilic peptide, OG did not significantly effect HPLC recovery or MALDI ionization.

Some of the mass spectra of the fractions from the RP-HPLC of the concanavalin A purified rhodopsin digest, Figure 10 contained mass peaks that could not be identified (data not shown). Their masses did not match those of the tryptic peptides of rhodopsin or concanavalin A. The possibility of chymotryptic activity by autolyzed trypsin on rhodopsin or concanavalin A, was investigated; however, no matches were found. The unidentified mass peaks did not originate from trypsin autolysis since they did not appear in the mass spectra of the HPLC fractions collected in the blank digest, Figure 12.

Tryptic Digestion of Rhodopsin in Washed ROS Membranes

Figure 11 shows the RP-HPLC chromatogram of the tryptic digest of rhodopsin in washed ROS membranes. Peptides that were identified by MALDI MS are listed next to each corresponding HPLC peak, using the numbering in Table 5. It is noteworthy that exactly the same peptides were identified from HPLC fractions at essentially the same retention times as for the concanavalin-A purified rhodopsin. The additional large peaks between 51 and 58 minutes in Figure 11 are due primarily to membrane phospholipids as identified by mass (600-800 Da) and mass 28 ($-CH_2-CH_2-$) periodicity using MALDI MS.

When a sample of concanavalin-A purified rhodopsin digest was injected after a run of a digest of rhodopsin in washed ROS membranes and a routine formic acid column wash, no phospholipids were detected by MALDI in the HPLC fractions from 51 to 58 minutes. Thus, no carry-over of phospholipids was observed.

In addition to trypsin, the more specific protease Lys-C (which cleaves at lysine only) was used to digest washed ROS membranes. In this digest, the hydrophobic transmembrane peptide labeled #1 in Table 5 with three additional amino acids, amino acids 17-20, was positively identified by MALDI MS and Edman sequencing (data not shown). This peptide appeared at essentially the same retention time as did peptide #1 in Figures 10 and 11. The similarity in the results using different sources for rhodopsin and different proteases demonstrates the reliability of the technique.

Heterogeneity in the Glycosylation of Rhodopsin Assessed by MALDI MS

The MALDI mass spectrum of the HPLC fraction eluting at 19.8 minutes, Figure 10, displayed a number of mass peaks between m/z 4,000 and 5,200. A mass spectrum with the same mass peaks, but of superior quality, was obtained at a similar HPLC retention time from a tryptic digest of rhodopsin in washed ROS membranes without reduction and alkylation. This mass spectrum is shown in Figure 16. The most intense mass peak appears at m/z 4,036. It has been shown that mannose and *N*-acetylglucosamine monosaccharides are the primary components of the carbohydrate portions of rhodopsin (23). More recent work has shown that the glycopeptide from the N-terminal portion of rhodopsin contains 3 mannoses and 3 *N*-acetylglucosamines

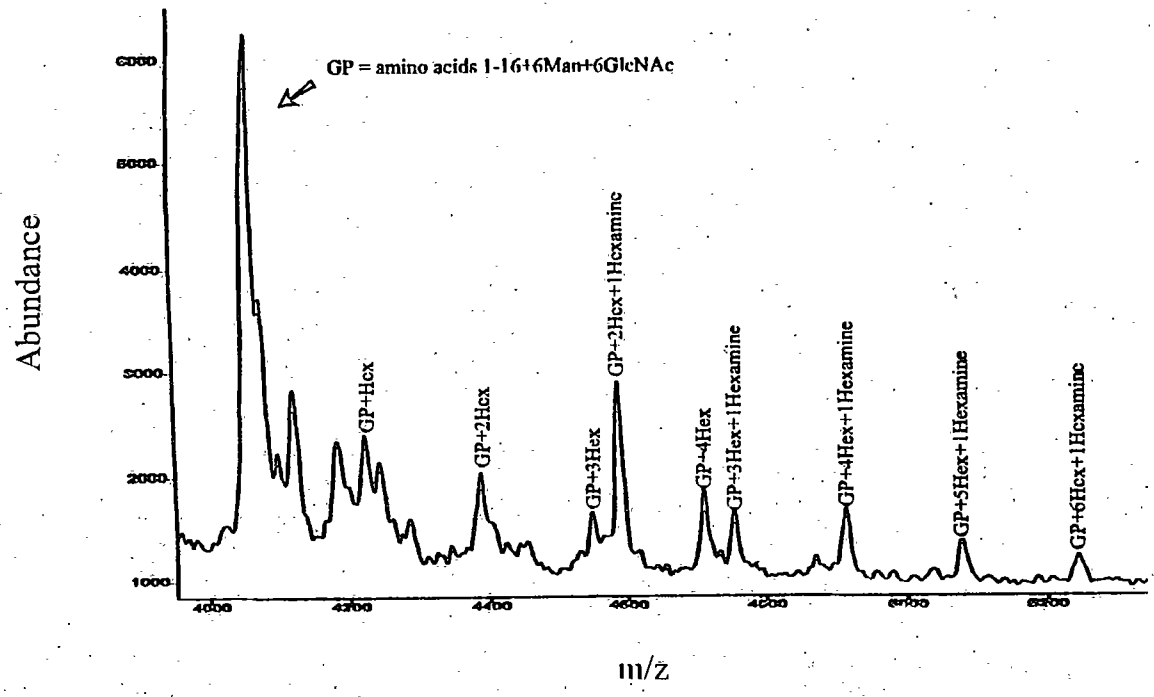


**Figure 16.** MALDI mass spectrum of the N-terminal tryptic peptide (amino acids 1-16) of rhodopsin digested in washed ROS membranes. The peak labeled GP (glycopeptide) at *m/z* 4,036 represents the predominant glycosylated peptide containing the glycosylation sites at N2 and N15 with each site having an oligosaccharide comprised of 3 mannoses and 3 *N*-acetylglucoseamines. Peaks at higher *m/z* represent oligosaccharide heterogeneity and are labeled by the number of additional hexose (Hex) and *N*-acetylhexosamine (Hexamine) monomers added to the GP peak, as determined by the mass differences between peaks.

attached to each glycosylation site; N2 and N15 (24). Indeed, the 4,036 Da mass in Figure 16 matches the calculated mass of the tryptic peptide containing amino acids 1-16 with the addition of 6 mannoses and 6 *N*-acetylglucosamine monomers. Additional verification that our sample was the glycosylated N-terminus of rhodopsin was achieved by treating the sample with the glycosidase PNGase F. The glycosidase reaction was monitored by MALDI MS. A gradual shift to lower mass peaks was observed, and after complete digestion a single peak with the expected mass of the non-glycosylated peptide was observed at m/z 1,844 (data not shown).

Most of the higher mass peaks in Figure 16 match the mass of the 4,036 Da primary glycopeptide with the addition of varying numbers of hexoses and *N*-acetylhexosamines. Other higher mass peaks were not identified and may be due to modifications to the carbohydrate or alternatively to substitutions with other monosaccharides having different molecular weights. Without carbohydrate sequencing studies, the exact structures of these glycoforms cannot be determined. However, the MALDI mass spectrum reveals that there are many more rhodopsin glycoforms than had previously been shown to exist (24-27). This demonstrates that MALDI mass spectrometry is a simple and powerful approach for assessing the heterogeneity of glycosylation in membrane proteins without derivatization of the carbohydrate.

## Discussion

The use of the non-ionic detergent octyl-β-glucoside in the RP-HPLC mobile phase as well as during the subsequent sample handling procedures was critical to the

success of identifying transmembrane tryptic peptides of rhodopsin in this work. In similar experiments, done without detergent, hydrophobic peptides could not be isolated and identified by MALDI-MS. The detergent kept the hydrophobic peptides solubilized during the sample concentration and MALDI matrix crystal formation. On the other hand, the presence of detergents generally results in degradation of MALDI mass spectra with loss of sensitivity and mass resolution. The choice of octyl-β-glucoside was therefore important because this particular detergent was shown to be well tolerated by MALDI even at the relatively high concentrations used. This is in agreement with recent work that showed that, while many detergents are incompatible with the MALDI MS analysis of intact membrane proteins, octyl-β-glucoside resulted in only a minor degradation of the MALDI mass spectra (28).

Peptides that contain transmembrane stretches of integral membrane proteins can often be produced using trypsin since the cleavage sites, arginine and lysine, are typically found outside of the hydrophobic membrane regions (1-3,29). In this work, the efficiency of digestion was followed by SDS-PAGE and HPLC gel filtration chromatography. It was found that in order to obtain adequate tryptic digestion of rhodopsin, it was necessary to partially unfold the protein with 4M urea and to reduce and alkylate cysteine residues. Still, approximately 50 % of the total rhodopsin remained intact after 24 hours of digestion. In contrast, digests performed without the use of urea and without reduction and alkylation did not generate detectable hydrophobic peptides.

The detection of the hydrophobic peptide #5* described in Table 5 shows that under the conditions used for denaturation (4M urea and exposure to room light) lysine

296 is accessible to trypsin. This may seem surprising, because lysine 296 is thought to be located in the middle of transmembrane helix VII in native rhodopsin, see Figure 9. Lysine 296, however, serves as the Schiff base linkage site for the highly hydrophobic retinal in dark-adapted rhodopsin (30). The retinal Schiff base linkage is hydrolyzed after exposure to light, and this results in the formation of the retinal-free form of rhodopsin, or opsin. The loss of retinal generates a hydrophilic lysine in the middle of the hydrophobic region of helix VII, and this may well be a factor in the increased sensitivity of opsin to denaturation and unfolding as compared to rhodopsin (31). Thus, the conditions of the digests may explain both the observed cleavage at lysine 296 and the observation that only retinal-free peptide #5* was observed in the MALDI mass spectra.

Aggregation of peptides in the RP-HPLC is a concern since this causes inefficient separation. As already mentioned, the presence of octyl-β-glucoside in the mobile phase served to inhibit aggregation during the chromatography. However, immediately after the injection onto the RP-HPLC column, the total concentration of peptides is the highest. The addition of SDS and formic acid to the sample prior to injection was designed to limit the aggregation of hydrophobic peptides at this point. Despite these precautions, however, each of the peptides identified were found in at least two HPLC fractions. Therefore, it is clear that non-covalent peptide aggregation was still a problem during the RP-HPLC separation. Peptide aggregates were not identified by MALDI MS. Clearly, the aggregates dissociated into their peptide components, either during the sample handling preceding the MALDI analysis or during the MALDI process itself. Whether peptides that were originally associated in the protein remained associated throughout the

digestion and the chromatography, or whether detergent solubilized peptides re-associated, is not known. However, some interesting patterns in the combinations of peptides that co-eluted were observed. Most noteworthy is that peptides #4 and #5* co-eluted in all cases. The possibility of a non-covalent complex between these peptides is appealing because they are thought to be associated with each other in native rhodopsin (7,29).

Of the 700 pmol of rhodopsin that was submitted to digestion roughly 350 pool was actually digested as determined by SDS-PAGE and gel filtration chromatography. Estimates for the amount of peptide recovered from fractions analyzed by Edman microsequencing range from 25 to 100 pool. The low yield can be partially explained by the fact that peptide aggregation caused the same peptide to elute under two or more HPLC peaks, see above.

When concentrating HPLC fractions in a SpeedVac prior to MALDI analysis, the mobile phase evaporated, and the detergent concentration increased to 5 to 10 % w/v, well above the critical micellar concentration. At the same time, the peptide concentration increased 40 to 100 fold. It is remarkable that high-quality MALDI mass spectra were obtained despite the relatively high detergent concentration in these samples. This circumstance was also fortunate because the high detergent concentration presumably prevented extensive aggregation of the concentrated hydrophobic peptides, or these would not have been detected by MALDI MS. There is evidence that suppression of ion signals in MALDI was a problem since several peptides were identified by Edman sequencing but not detected by MALDI MS. Yet, for the peptides that were identified, the MALDI mass

peaks were of good intensity for the amount of peptide deposited on the sample stage (approximately 1-5 pmol).

It is widely recognized that sample handling and separation of hydrophobic peptides from integral membrane proteins is difficult. Attempts at analyzing tryptic digests of rhodopsin by MALDI MS without prior separation of the cleavage products were unsuccessful. However, by employing a RP-HPLC method designed to separate hydrophobic peptides, we were able to isolate the tryptic peptides of rhodopsin to a level that allowed for accurate determination of their masses by MALDI MS. Still, there is room for improvement in the chromatographic conditions by further inhibiting peptide aggregation. If peptides could be completely separated their detection and structural characterization by MALDI would be facilitated.

A long term goal of this work is to establish reliable methods to identify specific sites of covalent modification of rhodopsin and other integral membrane proteins. The present work represents a step towards achieving this goal, and our report is the first to apply mass spectrometry to identify hydrophobic peptides from the putative transmembrane regions of a G-protein-coupled receptor. We anticipate that these methods will open the way to more detailed interpretation of affinity labeling studies, to allow identification of important binding sites, and to provide structural information on integral membrane proteins.

## References


1. Deisenhofer, J. and H. Michel. 1989. The photosynthetic reaction centre from the purple bacterium Rhodopseudomonas viridis [published erratum appears in Biosci Rep 1989 Dec;9(6):763]. *Biosci. Rep.* 9:383-419.

2. Wilmanns, M., P. Lappalainen, M. Kelly, E. Sauer-Eriksson, and M. Saraste. 1995. Crystal structure of the membrane-exposed domain from a respiratory quinol oxidase complex with an engineered dinuclear copper center. *Proc. Natl. Acad. Sci. U. S. A.* 92:11955-11959.

3. Tsukihara, T., H. Aoyama, E. Yamashita, T. Tomizaki, H. Yamaguchi, K. Shinzawa-Itoh, R. Nakashima, R. Yaono, and S. Yoshikawa. 1996. The whole structure of the 13-subunit oxidized cytochrome c oxidase at 2.8 A [see comments]. *Science* 272:1136-1144.

4. Grigorieff, N., T. A. Ceska, K. H. Downing, J. M. Baldwin, and R. Henderson. 1996. Electron-crystallographic refinement of the structure of bacteriorhodopsin. *J. Mol. Biol.* 259:393-421.

5. Schertler, G. F., C. Villa, and R. Henderson. 1993. Projection structure of rhodopsin. *Nature* 362:770-772.

6. Schertler, G. F. and P. A. Hargrave. 1995. Projection structure of frog rhodopsin in two crystal forms. *Proc. Natl. Acad. Sci. U. S. A.* 92:11578-11582.

7. Unger, V. M. and G. F. Schertler. 1995. Low resolution structure of bovine rhodopsin determined by electron cryo-microscopy. *Biophys. J.* 68:1776-1786.

8. Jennings, D. N. 1989. Methods for the structural analysis of membrane proteins. *Annu. Rev. Biochem.* 58:999-1027.

9. Burritt, J. B., M. T. Quinn, M. A. Jutila, C. W. Bond, and A. J. Jesaitis. 1995. Topological mapping of neutrophil cytochrome b epitopes with phage-display libraries. *J. Biol. Chem.* 270:16974-16980.

10. Shoelson, S. E., J. Lee, C. S. Lynch, J. M. Backer, and P. F. Pilch. 1993. BpaB25 insulins. Photoactivatable analogues that quantitatively cross-link, radiolabel, and activate the insulin receptor. *J. Biol. Chem.* 268:4085-4091.

11. Williams, K. P. and S. E. Shoelson. 1993. A photoaffinity scan maps regions of the p85 SH2 domain involved in phosphoprotein binding. *J. Biol. Chem.* 268:5361-5364.

12. Dorman, G. and G. D. Prestwich. 1994. Benzophenone photophores in biochemistry. *Biochemistry* 33:5661-5673.

13. Nakanishi, K., H. Zhang, K. A. Lerro, S. Takekuma, T. Yamamoto, T. H. Lien, L. Sastry, D. J. Baek, C. Moquin-Pattey, and M. F. Boehm. 1995. Photoaffinity labeling of rhodopsin and bacteriorhodopsin. *Biophys. Chem.* 56:13-22.

14. Nakayama, T. A. and H. G. Khorana. 1990. Orientation of retinal in bovine rhodopsin determined by cross-linking using a photoactivatable analog of 11-cis-retinal. *J. Biol. Chem.* 265:15762-15769.

15. Moore, C. R., J. R. Yates,3d, P. R. Griffin, J. Shabanowitz, P. A. Martino, D. F. Hunt, and D. S. Cafiso. 1989. Proteolytic fragments of the nicotinic acetylcholine receptor identified by mass spectrometry: implications for receptor topography. *Biochemistry* 28:9184-9191.

16. Poulter, L., J. P. Earnest, R. M. Stroud, and A. L. Burlingame. 1989. Structure, oligosaccharide structures, and posttranslationally modified sites of the nicotinic acetylcholine receptor. *Proc. Natl. Acad. Sci. U. S. A.* 86:6645-6649.

17. Machold, J., Y. Utkin, D. Kirsch, R. Kaufmann, V. Tsetlin, and F. Hucho. 1995. Photolabeling reveals the proximity of the alpha-neurotoxin binding site to the M2 helix of the ion channel in the nicotinic acetylcholine receptor. *Proc. Natl. Acad. Sci. U. S. A.* 92:7282-7286.

18. Hemling, M. E., S. A. Carr, C. Capiau, and J. Petre. 1988. Structural characterization of recombinant hepatitis B surface antigen protein by mass spectrometry. *Biochemistry* 27:699-705.

19. Orlando, R., P. T. M. Kenny, C. Moquin-Pattey, K. A. Lerro, and K. Nakanishi. 1993. Sequencing membrane proteins by tandem mass spectrometry. *Org. Mass Spectrom.* 28:1395-1402.

20. le Maire, E. L., S. Deschamps, J. V. Moller, J. P. le Caer, and J. Rossier. 1993. Electrospray ionization mass spectrometry on hydrophobic peptides electroeluted from sodium dodecyl sulfate-polyacrylamide gel electrophoresis application to the topology of the sarcoplasmic reticulum Ca2+ ATPase. *Anal. Biochem.* 50-57.

21. Baldwin, J. M. 1993. The probable arrangement of the helices in G protein-coupled receptors. *EMBO J.* 12:1693-1703.

22. Bull, H. B. and K. Breese. 1974. Hydrophobicity estimates for proteins and peptides. *Arch. Biochem. Biophys.* 161:665

23. Plantner, J. J. and E. L. Kean. 1976. Carbohydrate composition of bovine rhodopsin. *J. Biol. Chem.* 251:1548-1552.

24. Liang, C. J., K. Yamashita, C. G. Muellenberg, H. Shichi, and A. Kobata. 1979. Structure of the carbohydrate moieties of bovine rhodopsin. *J. Biol. Chem.* 254:6414-6418.

25. Plantner, J. J., M. L. Le, and E. L. Kean. 1991. Enzymatic deglycosylation of bovine rhodopsin. *Exp. Eye Res.* 53:269-274.

26. Hargrave, P. A., J. H. McDowell, D. R. Curtis, J. K. Wang, E. Juszczak, S. L. Fong, J. K. Rao, and P. Argos. 1983. The structure of bovine rhodopsin. *Biophys. Struct. Mech.* 9:235-244.

27. Kean, E. L., S. Hara, A. Mizoguchi, A. Matsumoto, and A. Kobata. 1983. The enzymatic cleavage of rhodopsin by the retinal pigment epithelium. II. The carbohydrate composition of the glycopeptide cleavage product. *Exp. Eye Res.* 36:817-825.

28. Rosinke, B., K. Strupat, F. Hillenkamp, J. Rosenbusch, N. Dencher, U. Kruger, and H. J. Galla. 1996. Matrix-Assisted Laser Desorption/Ionization Mass Spectrometry (MALDI-MS) of Membrane Proteins and Non-covalent Complexes. *Journal of Mass Spectrometry* 30:1462-1468.(Abstr.)

29. Baldwin, J. M. 1994. Structure and function of receptors coupled to G proteins. *Curr. Opin. Cell Biol.* 6:180-190.

30. Wang, J. K., J. H. McDowell, and P. A. Hargrave. 1980. Site of attachment of 11-cis-retinal in bovine rhodopsin. *Biochemistry* 19:5111-5117.

31. Miljanich, G. P., M. F. Brown, S. Mabrey-Gaud, E. A. Dratz, and J. M. Sturtevant. 1985. Thermotropic behavior of retinal rod membranes and dispersions of extracted phospholipids. *J. Membr. Biol.* 85:79-86.

32. DeGrip, W. J. 1982. Purification of bovine rhodopsin over concanavalin A-sepharose. In Methos in Enzymology. L. Packer, editor. Academic Press, New York. 197-207.

33. Stone, K. L., M. Lo Presti, J. Crawford, R. DeAngelis, and K. Williams. 1989. Enzymatic digestion of proteins and HPLC peptide isolation. In A practical guide to protein and peptide purification for microsequencing. P. T. Matsudaira, editor. Academic Press, San Diego. 31-47.

34. Tomich, J. M., L. W. Carson, K. J. Kanes, N. J. Vogelaar, M. R. Emerling, and J. H. Richards. 1988. Prevention of aggregation of synthetic membrane-spanning peptides by addition of detergent. *Anal. Biochem.* 174:197-203.

# Chapter 4

## CHARACTERIZATION OF RABBIT POLYCLONAL ANTIBODIES α-ARK AND α-KIS: SPECIFICITY FOR EXTRACELLULAR DOMAINS of HUMAN CYTOCHROME $b_{558}$

### Introduction

Western blot analysis is a technique by which a specific protein from a polyacrylamide gel can be identified using antibodies. When a protein is separated by sodium dodecyl sulfate-polyacrylamide gel electrophoresis (SDS-PAGE) and electro-transferred onto a solid support, antibodies specific for the protein of interest are able to bind the immobilized protein (1). Primary antibodies which bind the immobilized protein can in turn be labeled by a secondary antibody. This approach provides detection amplification due to multiple secondary antibodies binding to sites on the primary antibody. The visualization can be performed using a number of strategies including

autoradiography, colloidal gold, biotinylation, or more commonly, enzyme conjugated secondaries. Enzymes such as horseradish peroxidase or alkaline phosphatase coupled to the secondary generate a color change on the electrotransferred band, containing the specific protein, by reacting with substrates that produce an insoluble chromogenic product (2). This technique is most commonly utilized to determine the presence of an intact protein from a mixture that cannot be unambiguously identified by SDS-PAGE alone. It can also be used to identify fragments of the protein that contain the epitope specifically recognized (or bound) by the antibody.

An antibody specific for a certain epitope on a protein, may or may not recognize the epitope when the protein is in a cell, since the epitope may be hidden due to steric considerations or protein tertiary structure. However, in Western blot analysis an immobilized protein is probed after exposure to the denaturing detergent SDS. This technique generally does not give information of tertiary structure since the protein is unfolded. When an antibody is found to be specific for an epitope on a protein using Western blot analysis the results can be compared with flow cytometry data. If the antibody no longer recognizes the epitope within a cell, it can be assumed that the epitope is no longer accessible to the antibody. This approach is often used when examining the topology of integral membrane proteins in cells (3).

This chapter describes the preparation and use of the antibodies designed to provide information about the cellular topology of human neutrophil cytochrome $b_{558}$. Western blot analysis is routinely used in our laboratory to identify both the large (gp91-*phox*) and the small (p22 *phox*) subunits of cytochrome $b_{558}$. Most of the antibodies

used in these analyses are specific for the carboxy-terminal portion of gp91-*phox* and p22-*phox*. Additional antibodies were needed for gp91-*phox* to aid in mapping the topology of this domain using immunofluorescence, and to aid in the identify of proteolytic fragments of the molecule.

Using the previously published primary structure of gp91-*phox* (4) efforts were focused on synthetic peptides emulating regions of the large subunit of human neutrophil cytochrome $b_{558}$ having the sequences $^{155}$ARKRIKNPEGG$^{165}$ and $^{246}$KISEWGKIKEC$^{256}$. These sequences are thought to be extracellular and flank the predicted heme binding domain in the large subunit (5,6). Rabbits were immunized with peptide haptens having the two sequences shown above (referred to as ARK and KIS). To facilitate the generation of highly specific rabbit polyclonal antibodies, pure peptide preparations are needed and often require additional purification of the crude product from the original peptide synthesis. Both ARK and KIS were subjected to HPLC and eluting fractions were subsequently identified by accurate mass analysis using MALDI-TOF mass spectrometry. Purified peptides were cross-linked to keyhole limpet hemocyanin and injected into rabbits. Antibodies were affinity purified using purified peptide coupled to CNBr activated sepharose beads. The specificity of the antibodies produced was evaluated both by Western blot and FACS analyses.

# Materials and Methods

## Peptide Purification

Crude lyophilized peptide was solubilized in water/0.1%TFA v/v to a concentration of 2-5 mg/ml. This solution was subjected to RP-HPLC using a standard water/acetonitrile gradient starting at 96% water/4% acetonitrile/0.1%TFA and ending at 100% acetonitrile/0.1% TFA ramped over a period of 30 minutes. The column used initially for ARK peptide purification was a preparative size $C_{18}$ column run using a steeper gradient from 96% water/4% acetonitrile/0.1%TFA and ending at 100% acetonitrile/0.1% TFA over a period of 15 minutes with a flow rate of 1.5 ml/min. This column was changed to a Whatman partisil 5 analytical size $C_{18}$ column for purification of the KIS peptide and the final purification of the ARK peptide. All RP-HPLC was carried out on a Hitachi Model L-2500 HPLC system with a variable wavelength detector set at 230 nm. Injection volumes were 500 $\mu$l and the flow rate was set at 0.8 ml/min. Fractions were collected manually for major eluted peaks and analyzed by MALDI MS.

## Mass Spectrometry

Samples for MALDI were taken from HPLC fractions diluted in 50:50 water:acetonitrile to within a range of 10-100 pmol/$\mu$l, estimated by peak area, or taken from a stock derived from lyophilized fractions. A microliter of each fraction was then spotted onto a sample well along with one microliter of matrix solution and mixed thoroughly. The matrix was a saturated solution of $\alpha$-cyano-4-hydroxycinnamic acid in 2:1 v/v water:acetonitrile 0.1% TFA. MALDI mass spectra were obtained on a PerSeptive

Biosystems Voyager RP-TOF mass spectrometer as described in Chapter 2. Bradykinin (Sigma Chemical Co., St. Louis, MO) was used as an external standard for mass calibration of the instrument. Fractions having the correct molecular weight for the peptide of interest were lyopholized and stored at -20°C for later use.

Antibody Production

RP-HPLC purified peptide fractions were crosslinked to keyhole limpet hemocyanin (KLH) using gluteraldehyde followed by dialysis of excess reagents with PBS. An emulsified mixture containing 250 $\mu$g of KLH crosslinked peptide antigen in 200 $\mu$l of phosphate buffered saline (PBS), 750 $\mu$l Incomplete Freund's Adjuvant, and 550 $\mu$l of PBS, was used for the immunogen (7,8). Rabbits were bled prior to being immunized for use in control experiments. Rabbits were then injected with immunogen following an established Animal Research Center (ARC) protocol schedule. Serum from prebleeds and post-inoculation bleeds were prepared and frozen at -80°C for rabbits injected with the ARK peptide at Scripp's Research Institute (La Jolla, CA). Sera from prebleeds and post-inoculation bleeds from rabbits immunized with the KIS peptide were stored at 4°C. Specificity of antisera against the two peptides were evaluated by Western blots analysis. For each procedure the gp91-*phox* antigen was present from 2% OG solubilized neutrophil membranes prepared by the procedure of Jesaitis et al. (9). Sera containing antibodies that displayed staining for the large subunit of cytochrome $b_{558}$ were selected for further purification.

Antibody Purification Using Immobilized Peptides Coupled to CNBr Activated Sepharose

To immunopurify anti-ARK and anti-KIS peptide antibodies from serum, approximately 2 mg of peptide was immobilized onto 1 ml swollen CNBr activated Sepharose beads using the protocols provided by the manufacturer (Pharmacia Biotech, Uppsala Sweden). A volume of 10 ml of serum was cleared of excess lipid using Seroclear and allowed to mix with the peptide coupled beads for either 12 hrs at 4°C or 4 hrs. at room temperature. The beads were cleared of non-specific antibodies by washing with 10 column volumes of PBS containing 300 mM high salt. Antibodies specific for the ARK bound peptide were eluted with either 2 M Glycine pH 2.5 containing 300 mM NaCl and 4 M urea or 0.5 M TRIS pH 11 containing 300 mM NaCl and 4 M urea. The pH of the eluate buffer was adjusted to pH 8.0 by adding 1 M Tris and diluted 1:1 with glycerol to preserve the activity of the antibody. Antibodies specific for the KIS bound peptide were eluted in the same fashion except that the eluate buffer was dialyzed against PBS. The total yield for amount of antibody recovered was estimated by observing the absorbance at 280 nm and applying the standard ratio of 1 AU being equivalent to approximately 750 $\mu$g of antibody. The yield of affinity purified anti-ARK antibodies from 10 ml of serum from rabbits immunized with the ARK peptide coupled to KLH was roughly 500 $\mu$g while the yield of affinity purified anti-KIS antibodies from 10 mls of serum was on the order of 1.5 mg.

Specificity of Antibodies Assayed by Western Blot analyses

To evaluate the specificity of the antibodies for gp91-*phox*, Western blots were

performed using 10 pmol (~1 $\mu$g) of cytochrome $b_{558}$ from crude detergent extract of solubilized neutrophil membranes and partially purified cytochrome $b_{558}$. Detergent solubilized proteins were denatured in sample buffer containing 2% SDS and separated on a 7-18% gradient SDS-PAGE gel then transferred onto nitrocellulose (1). The nitrocellulose with the electrotransferred proteins was blocked using 5% non fat dry milk and 0.2% Tween 20 in PBS pH 7.4, overnight at 4°C or for 3 hours at 37°C to prevent non-specific adherence of antibodies. Affinity purified anti-ARK and anti-KIS antibodies were applied to the blots in antibody diluting buffer consisting of 3% normal goat serum, 1% BSA and 0.2% Tween. The dilution used for the anti-ARK antibody was 1:50 while the anti-KIS antibodies were used at a dilution of 1:150. These antibodies were incubated for 3 hours at room temperature. Non-specifically bound primary was rinsed off 5 times at 5 minute intervals using wash buffer containing 250 mM NaCl, 10 mM HEPES pH 7.4, and 0.2% Tween. The secondary antibody, an alkaline phosphotase conjugated goat anti-rabbit IgG, was applied at a dilution of 1:1,000 v/v in diluting buffer and incubated for 1 hour at room temperature. After rinsing with a total of 4 washes, a fifth wash was carried out using alkaline Tris-buffered saline pH 8.0 for development with BCIP and NBT reagents allowing for a visible precipitate at the sites of alkaline phosphatase-conjugated IgG. The reaction was halted by rinsing with distilled water. Specificity of the binding was examined by measuring the loss of staining when the primary antibody was mixed with 500 $\mu$M of the synthetic peptide used for the immunization of the rabbits. Controls were performed using 500 $\mu$M of the non-specific peptide bradykinin.

FACS Analysis of Neutrophil Labeling Using Affinity Purified Anti-peptide Antibodies

FACS analysis was carried out by a previously published procedure (8) using gelatin prepared neutrophils from normal human donors (7). Cells were treated on ice with the serine protease inhibitor di-isopropylfluorophosphate (DFP) prior to blocking of $F_c$ receptors and incubation with primary antibodies. Cells were washed by centrifugation to remove excess DFP, isolated by centrifugation, and then resuspended in Dulbecco's PBS (DPBS) containing 3 % normal goat serum (NGS) for 30 minutes to block $F_c$ receptors and non-specific binding sites on the cell surface. $5 \times 10^5$ cells per sample were then incubated with either the anti-peptide antibody ARK or KIS in DPBS for 1 hour at 1:50 and 1:150 dilutions, respectively. Unbound primary antibodies were removed from the cell suspension by washing with PBS followed by centrifugation. Bound primary antibodies were then labeled on ice for 30 minutes with fluorescein isothiocyanate (FITC)-conjugated goat anti-rabbit secondary antibody. Permeabilized cells were treated in the same manner except 0.1% saponin was present in each to step to ensure that the cells remained permeabilized. The extent of cell labeling was assessed by comparison of cells incubated with prebleed IgG antibodies at the same concentration. The prebleed antibodies were isolated from prebleed serum using a Protein A column following the manufacture's protocols (Pharmacia Biotech, Uppsala Sweden). The difference in staining between permeabilized and non-permeabilized cells was also evaluated in order to determine whether binding was intracellular or extracellular. All experiments were run on a Becton Dickinson FACScan type flow cytometer analyzer equipped with a 15-milliwatt argon

laser. Data was acquired using CONSORT 30 and analyzed using LYSYS software according to the manufacturer's protocols.

## Results

### Purification of Peptide Antigen for Production of Affinity Purified Antibodies

The preparation of rabbit anti-sera against the synthetic peptide ARKRIKNPEGGC was carried out by C. Parkos and A. Jesaitis at the Scripp's Research Institute as described by Jesaitis et al. (9). The titer of the anti-peptide antibody in the serum was low and thus its utility in Western blot analysis was limited. Therefore, to prepare highly specific affinity purified antibodies, the peptide was repurified for derivitization on a new affinity matrix. Figure 17 shows a RP-HPLC chromatogram obtained from 5 mg of crude lyophilized peptide dissolved in deionized water. The sample was run on a high capacity $C_{18}$ column used for clean-up of sythesized peptides at the Peptide Synthesis Laboratory located at MSU. A total of 28 mg of crude peptide was injected onto the column in 4 consecutive runs. The peak labeled ARKRIKNPEGGC-peptide in Figure 18 is a lyopholized pooled fraction from each of the 4 runs with a final recovery of 8 mg or 28%. Because the resolving capability of the preparative column is less than an analytical size RP-HPLC column, the lyophilized peptide was rechromatographed on an analytical column with a shallower gradient. The chromatogram from this experiment is shown in Figure 18. It is clear that the majority of peptide elutes as a single peak labeled ARKRIKNPEGGC-peptide. This peak was analyzed by MALDI MS and the resulting mass spectrum is shown in Figure 19. The base peak in the spectrum

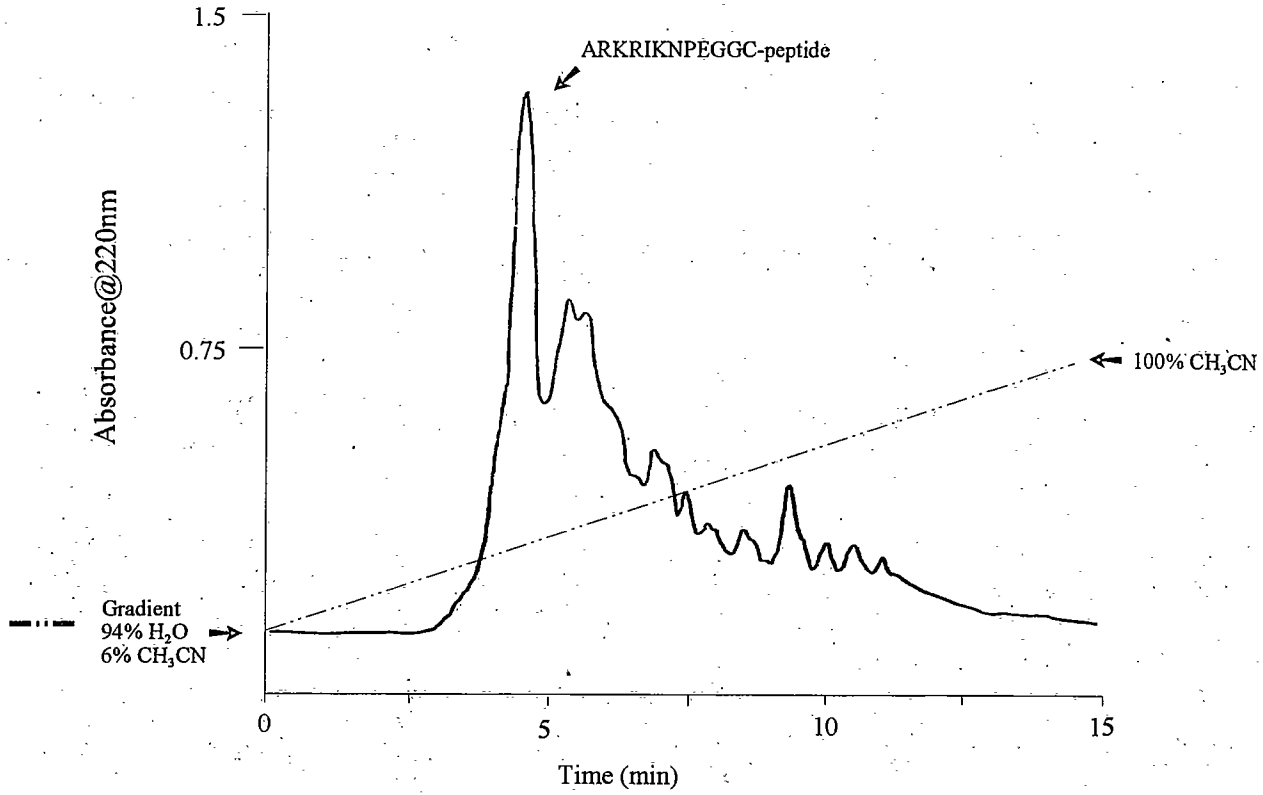


**Figure 17**. HPLC chromatogram from the purification of the ARK peptide. The chromatogram represents 5 mg of the crude peptide injected onto a preparative column. The peak labeled ARKRIKNPEGGC-peptide was collected and rerun on a HPLC column for further purification.

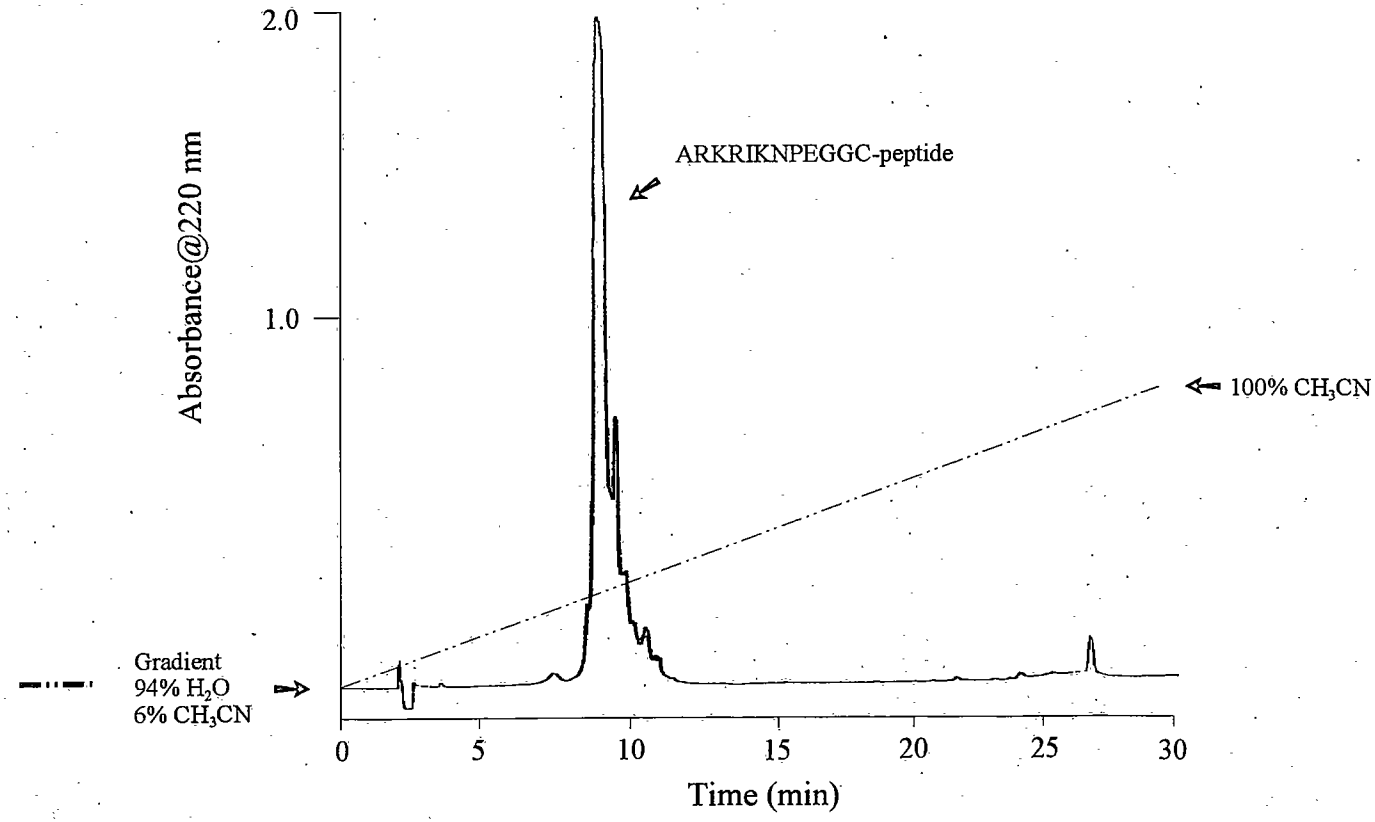


**Figure 18**. HPLC chromatogram from the purification of the ARK peptide. The chromatogram represents the labeled peak in Figure 19 lyopholized and rechromatographed on an analytical grade reverse-phase HPLC column. Approximately 2 mg of the crude peptide injected onto the analytical column. The peak labeled ARKRIKNPEGGC-peptide was collected and analyzed by MALDI MS to find the mass of the desired peptide.

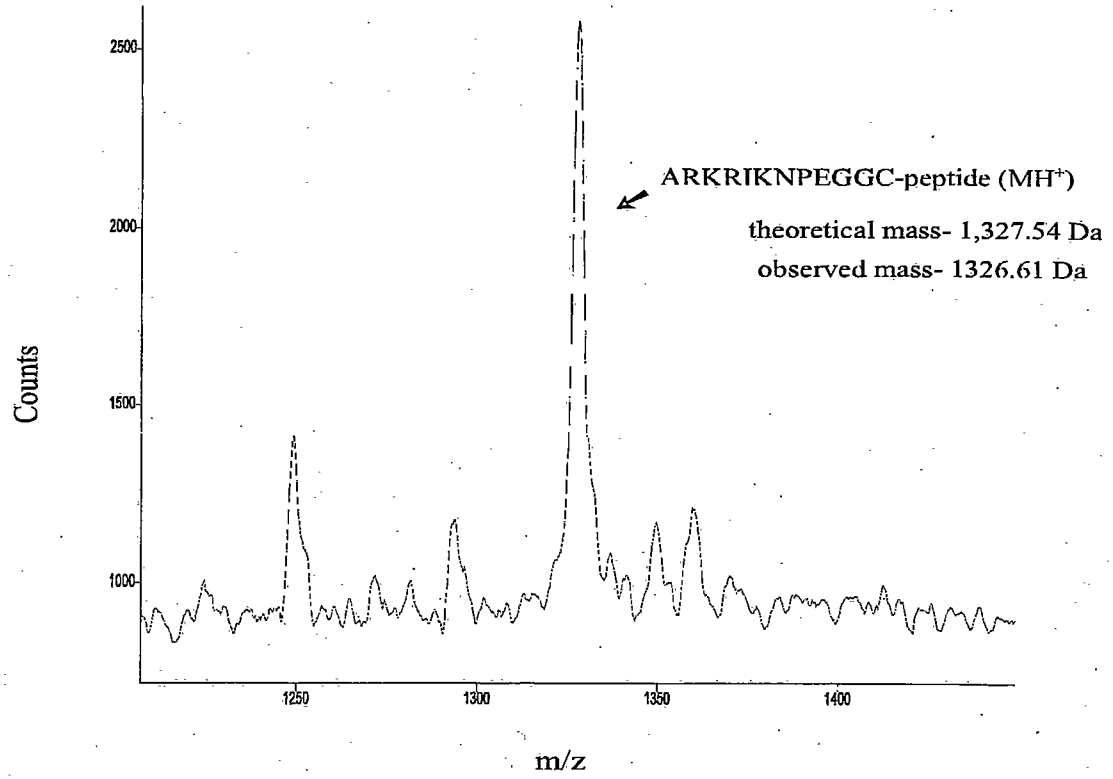


**Figure 19**. MALDI mass spectrum of HPLC purified peptide used to immunopurify the anti-peptide antibody ARK. The sample was derived from the lyopholized fraction labeled in Figure 2. This fraction was coupled to CNBr activated sepharose beads to purify rabbit polyclonal antibodies from serum.

(above 500 Da) is labeled $M_2H^+$, while the next largest peak is labeled ARKRIKNPEGGC-peptide ($MH^+$). These two peaks were the only major ions generated from the sample and represent the singly charged monomer ($MH^+$) and the singly charged dimer ($M_2H^+$) of ARKRIKNPEGGC. The observed mass of the peptide was 1,329.77 Da which is 2.23 Da higher than the calculated mass. The prevalence of the dimer is most likely due to a cysteine that was added to the carboxy terminus of the peptide when synthesized. Although it is possible that the cyteines formed disulfide bonds linking the two peptides into a dimer, it is unlikely that the monomer and dimer would have eluted at the same time from the RP-HPLC column. The presence of dimers in the mass spectrum was not a concern since the method of peptide coupling to Sepharose beads did not require the presence of free sulfhydryl.

The peptide KISEWGKIKEC was synthesized at MSU in the Peptide Synthesis Laboratory on a Millipore Model 9050 peptide synthesizer. The synthetic peptide above was purified following the same procedures described for the peptide ARKRIKNPEGGC however, the RP-HPLC was carried out entirely on a Whatman Partisil 5 analytical size $C_{18}$ column. Figure 20 shows a HPLC chromatogram from the injection of 2 mg crude peptide (one of four injections) utilizing the analytical column's maximum capacity. A total of 6 mg of crude peptide was applied to the column over 3 runs and a total of 4 mg was recovered as determined by weighing the lyophilized fractions from the main peak in each run. This peak is labeled KISEWGKIKEC-peptide in Figure 20. Fractions of this peak from consecutive runs were pooled, lyophilized, then analyzed by MALDI MS. A mass spectrum of the pooled samples used for making the immunoaffinity matrix is shown

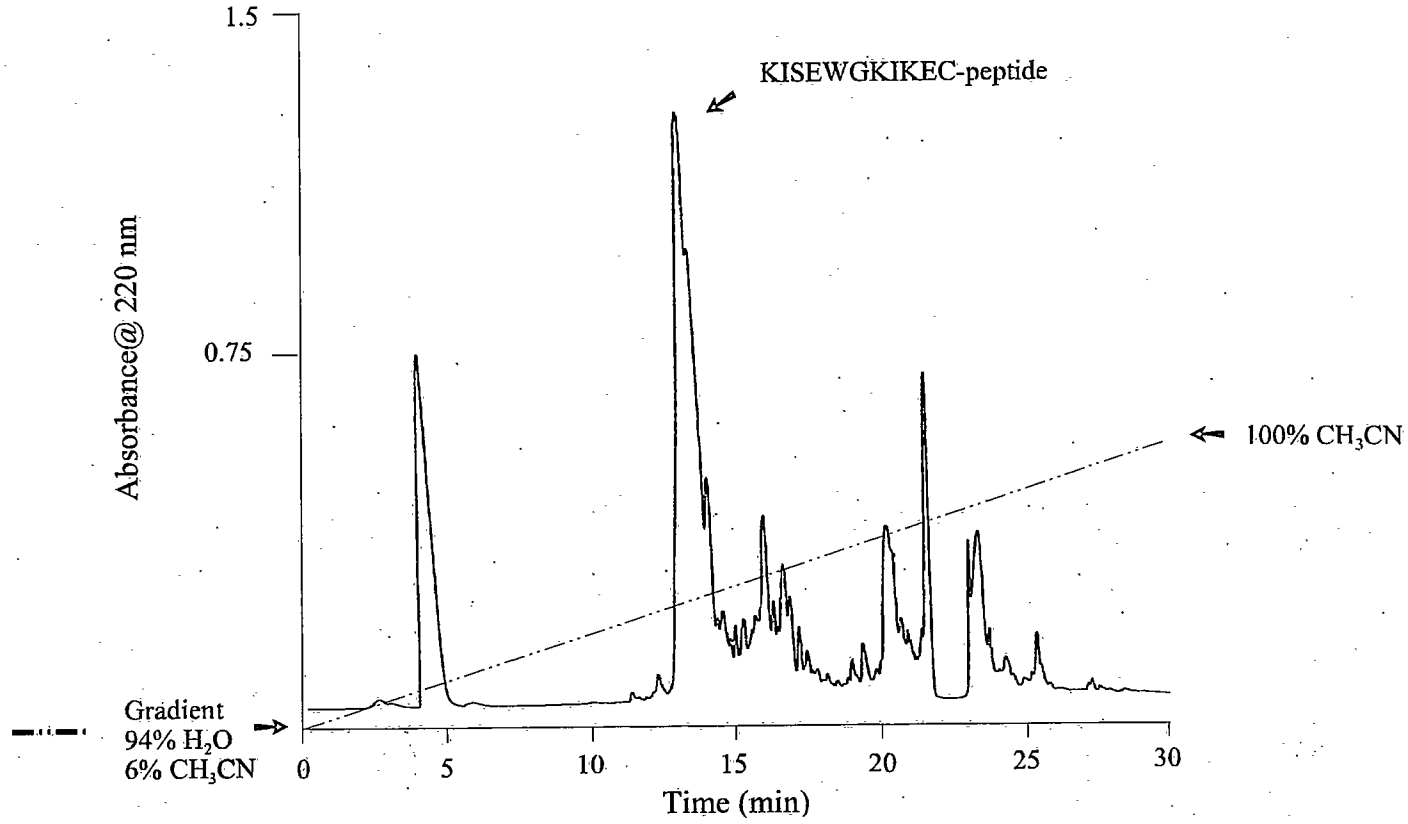


**Figure 20**. HPLC chromatogram from the purification of the KIS peptide. The chromatogram represents 4mg of the crude peptide injected onto an analytical column. The peak labeled KISEWGKIKEC-peptide was collected, lyopholized, and mass analyzed by MALDI MS.

in Figure 21. The observed mass of the purified peptide was 1,321.87 Da which is 2.31 Da higher than the calculated mass. The spectrum also shows a significant peak at 1,195 Da resulting from the loss of a lysine from the peptide. It is not known if the lysine was lost from the peptide during ionization or while the peptide was being sythesized. The peptide KISEWGKIKEC also has a cysteine at the carboxy terminus and the dimer ($M_2H^+$) was also detectable in this mass spectrum (data not shown). The ratio of monomer and dimer (~1:1) was similar to that in the mass spectrum of the peptide ARKRIKNPEGGC.

Rabbits were immunized with the purified peptide cross-linked to keyhole limpet hemocyanin by glutaldehyde as described previously (9) and the serum was examined for specificity in the recognition of gp91-*phox*. The serum containing anti-ARK antibodies was first screened for specificity using 2% OG solubilized human neutrophil membranes by ELISA assays and Western blots (9). After six weeks and 5 immunizations, the titer for both the anti-ARK and anti-KIS antibodies was low but detectable. These results indicated that immuno-purification of the specific antibodies present was needed in order to obtain better staining. It should be noted that serum from rabbits given an additional boost, 2 months after the original immunization schedule, have yet to be screened and may have an even higher titer.

Immunoaffinity columns were made by coupling free amino groups of the peptides ARKRIKNPEGGC and KISEWGKIKEC to CNBr activated Sepharose with a final bead volume of 1ml. A volume of 10 ml of rabbit serum pre-cleared of lipids by treating the sample with SeroClear® followed by incubation with the beads for 2 hours at room temperature. The column matrix was washed with 300 mM NaCl in PBS and eluted with

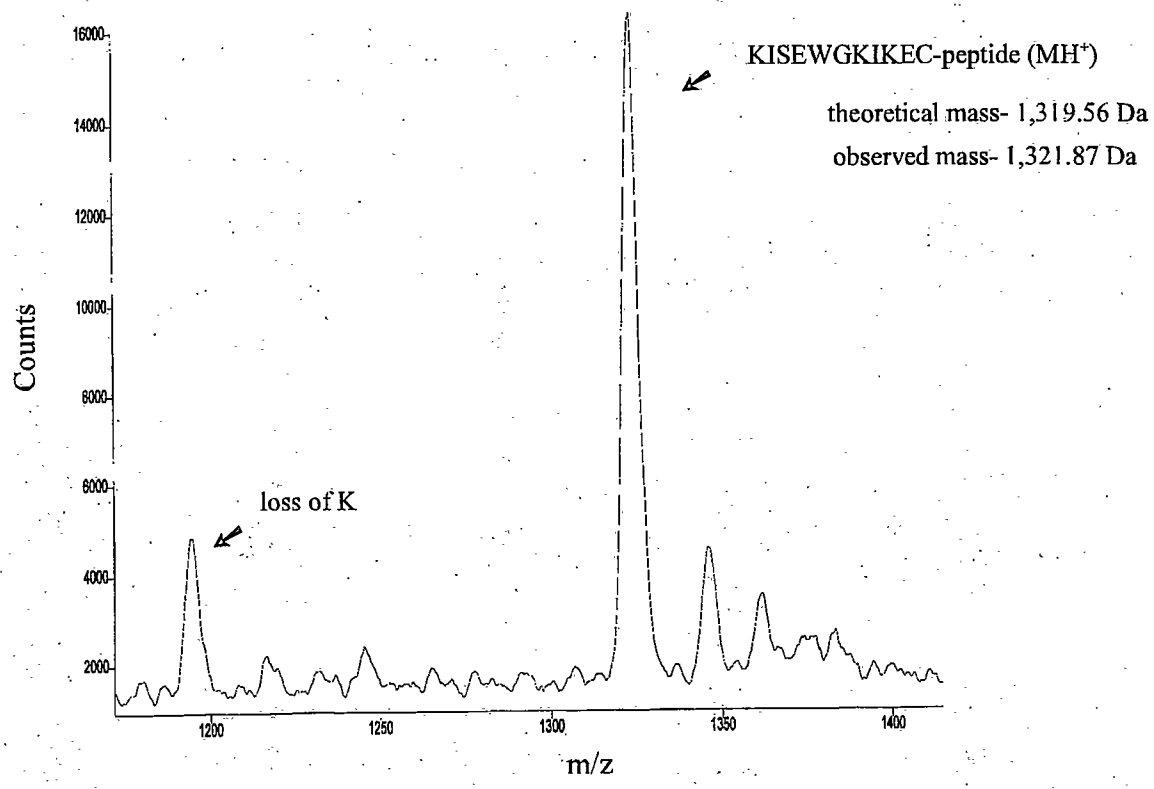


**Figure 21**. MALDI mass spectrum of HPLC purified peptide used to immunopurify the anti-peptide antibody KIS. The sample was derived from the lyopholized fraction identically labeled in Figure 21. This fraction was coupled to CNBr activated sepharose beads to purify rabbit polyclonal antibodies from serum.

either high or low pH buffers containing 300 mM NaCl and 4 M urea. The pH of the samples was immediately adjusted to 8.0 using 1 M Tris and diluted 1:1 with glycerol.

Figure 22 shows a MALDI mass spectrum of anti-ARK peptide rabbit polyclonal antibodies eluted from the immunoaffinity column using low pH. Roughly 4 pmol of antibodies were spotted on the sample try in this experiment. The mass spectrum showed no signs of contamination from other components. The average mass of the intact antibodies was found to be 142,900 Da using bovine serum albumin as an external standard. Figure 23 is a MALDI mass spectrum of the same anti-ARK antibodies after reduction and alkylation. This experiment was done to evaluate the heterogeneity of the antibodies in the preparation. The base peak in the spectrum is the light chain which on closer inspection clearly shows the presence of three smaller peaks that are unresolved. This result suggests that there are at least three species of antibody in the immunopurified antibody preparation that may have been derived from different B cell clones. Mass spectral analysis has yet to be performed on the anti-KIS antibodies or a control of mouse monoclonal antibodies where there should be a single mass for the heavy and light chains upon reduction and alkylation.

To evaluate the ability of the immunopurified antibodies to specifically recognize gp91-*phox*, Western blotting analyses were carried out on human neutrophil membranes solubilized in 2% OG. The amount of staining was compared for samples containing only purified antibodies vs. samples 500 $\mu$M in either peptide ARKRIKNPEGGC or KISEWGKIKEC added along with the antibodies. If the antibody binds to the peptide, then the antibody is inhibited from binding to the immobilized protein and the specificity of

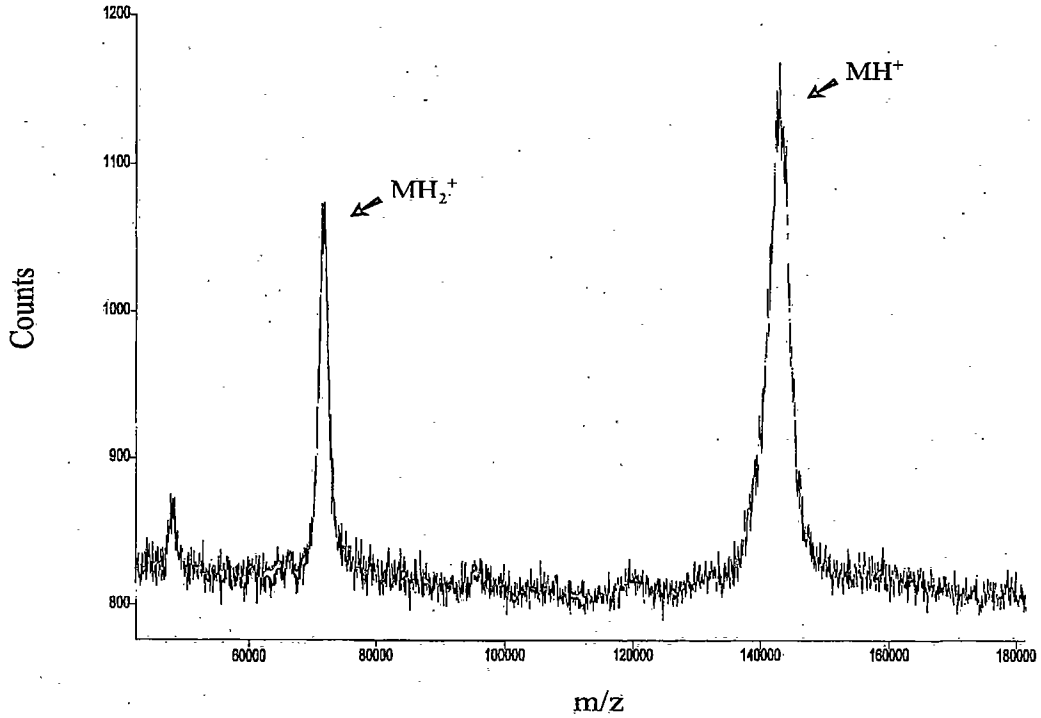


**Figure 22**. MALDI mass spectrum of the immunopurified anti-peptide antibody ARK. The sample was eluted from CNBr activated sepharose beads containing the purified peptide used to immunize the rabbit for polyclonal antibody production.

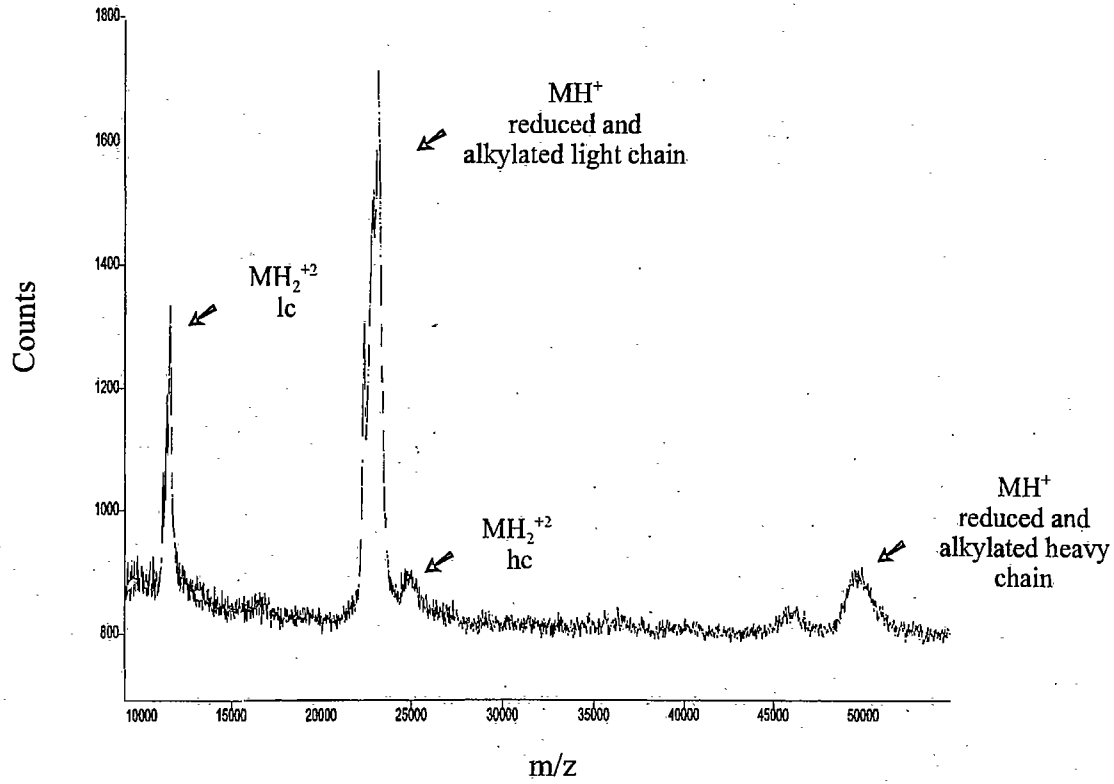


**Figure 23**. MALDI mass spectrum of reduced and alkylated immunopurified anti-peptide antibody ARK. The sample was derived from elute off CNBr activated sepharose beads containing the purified peptide used to immunize the rabbit for polyclonal antibody production then reduced and alkylated in order to observe heterogeneity in the polyclonal antibodies.

the antibodies is confirmed.

Figure 24 is a Western blot evaluating the anti-ARK antibodies using 2% OG solubilized neutrophil membranes. This blot clearly illustrates the difference in staining between lane 1, where no peptide is added, and lane 2 where 500 $\mu$M ARKRIKNPEGGC was added. Lane 3 contains 500 $\mu$M bradykinin as an irrelevant peptide that contains no similarity to ARKRIKNPEGGC where the staining is of the same order as the control in lane 1. Lane 4 in Figure 24 shows intense staining for purified cytochrome $b_{558}$ indicating that the anti-ARK antibodies can detect 10 pmol (or 1 $\mu$g) of the purified protein. In addition there is a clear difference in the staining pattern in Lane 1 (crude membranes) vs. Lane 4 (purified cytochrome $b_{558}$).

Anti-KIS peptide antibodies evaluated in the same fashion are shown in Figure 25. This Western blot shows the staining of purified cytochrome $b_{558}$ in relation to the presence of the KIS peptide. In Figure 25, Lane 1 with no peptide added exhibits intense staining as opposed to lane 2 containing 500 $\mu$M KISEWGKIKEC where little or no staining exists. Lane 3 includes 500 $\mu$M bradykinin as the control peptide and no reduction in staining intensity is observed. The pattern of staining is much different than that found with immunopurified anti-ARK antibodies. The staining has a somewhat more broad but clearly bimodal distribution, yet once again the staining for purified cytochrome $b_{558}$ is intense for the region between 67.5 kDa and 103 kDa. The reasoning for the variability in staining may be attributable to a number of factors discussed below, nonetheless, inhibition of this staining indicates that the binding is specific.

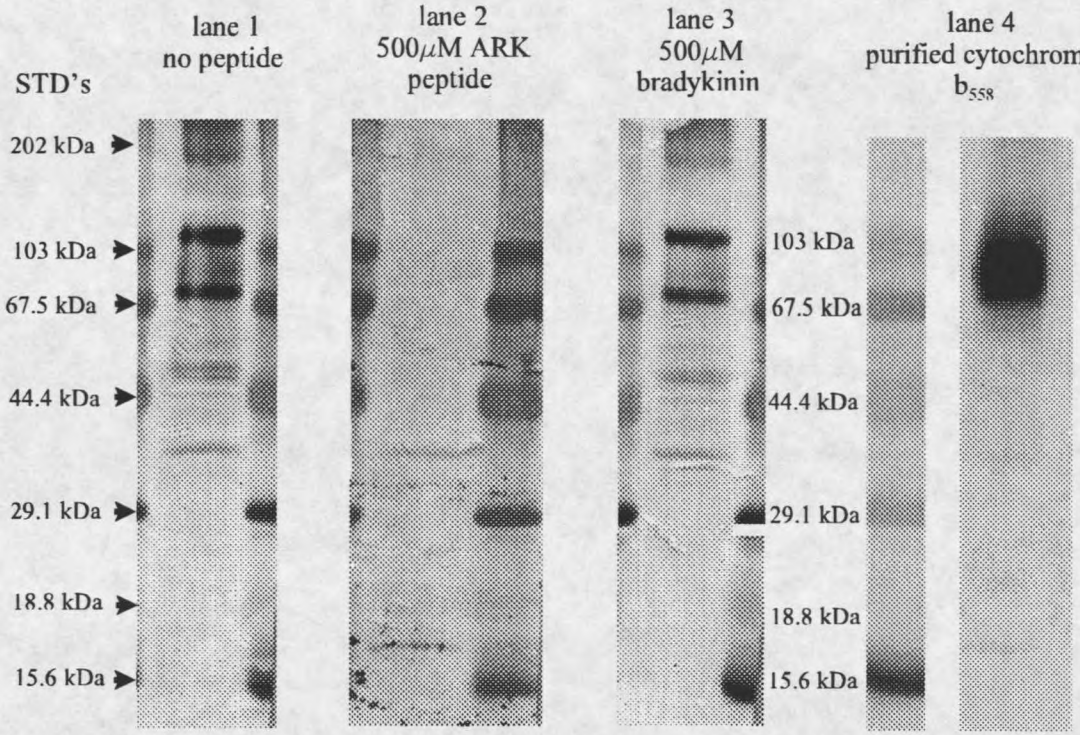


**Figure 24**. Western blot showing binding inhibition due to the peptide ARKRIKNPEGGC. Lanes 1-3 contain 10 pmol of cytochrome $b_{558}$ from 2% OG solubilized neutrophil membranes. Lane 4 contains 10 pmol of purified cytochrome $b_{558}$. Lane 2 containing the ARK peptide clearly inhibits binding of immunopurified antibodies. Primary antibodydilutions were1:50 v/v for each blot.

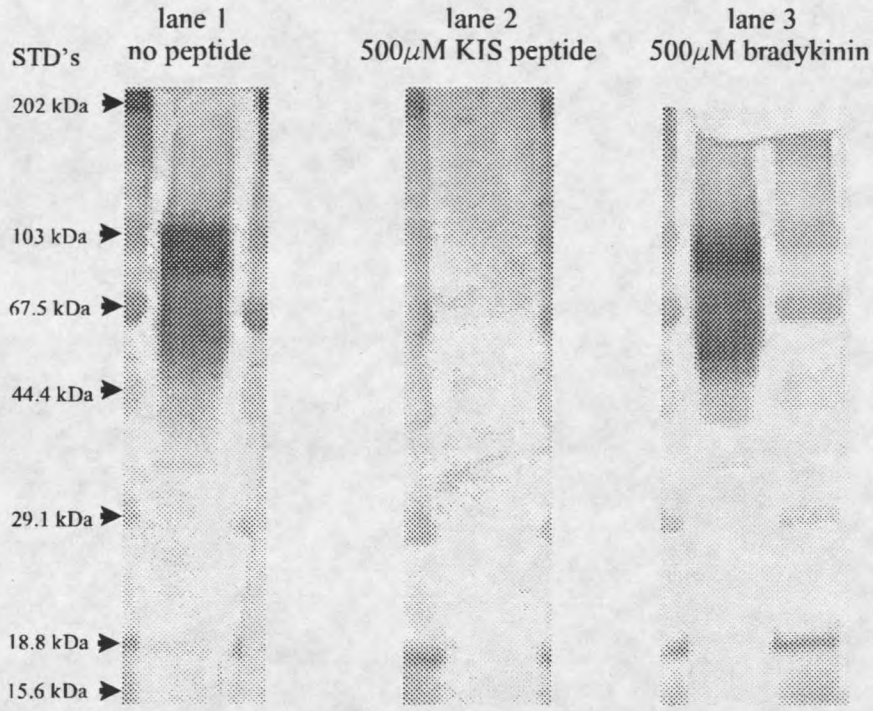


**Figure 25**. Western blot showing binding inhibition due to the peptide KISEWGKIKEC. Lanes 1-3 contain 10 pmol of cytochrome $b_{558}$ from 2% OG solubilized neutrophil membranes. Lane 2 clearly shows inhibition of antibody binding due to the peptide KISEWGKIKEC. Primary antibodies were diluted 1:100 v/v.

FACS Analysis for Peptide Epitope Location on Intact gp91-*phox*

To determine the extracellular vs. intracellular topology of the epitopes $^{155}$ARKRIKNPEGG$^{165}$ and $^{246}$KISEWGKIKEC$^{256}$ on gp91- *phox* in permeabilized and intact human neutrophils, the immunopurified anti-ARK and anti-KIS epitope polyclonal antibodies were used to label cells that were then analyzed by FACS analysis. These antibodies were shown to be specific for gp91-*phox* by Western blot analysis, which does not address the accessibility of the antibodies to the same epitopes on intact cells since Western blot analysis is performed on samples that are denatured during SDS-PAGE separation.

Figure 26 shows the results of FACS analysis on intact fixed neutrophils labeled with anti-ARK and anti-KIS antibodies. The outlined, or open peaks in Figure 26, show the amount of staining observed when the cells are incubated with purified prebleed IgG antibodies. The shaded peaks represent staining observed with affinity IgG anti-peptide antibodies. The upper histogram clearly shows a 25 fold increase in fluorescence intensity using the anti-ARK antibodies. The lower histogram shows a 12.5 fold increase in fluorescence intensity of the anti-KIS antibodies as compared to the prebleed IgG antibodies. It is worth noting that there is a slight increase in the staining between the cells labeled with prebleed IgG antibodies from the rabbits injected with the peptide ARKRIKNPEGG vs. the prebleed IgG antibodies from the rabbits injected with the KISEWGKIKEC peptide. It is not known whether this increase is due to specific binding of IgG antibodies that were present in the rabbits injected with the KISEWGKIKEC peptide prior to immunization, or if non-specifically bound antibodies were incompletely

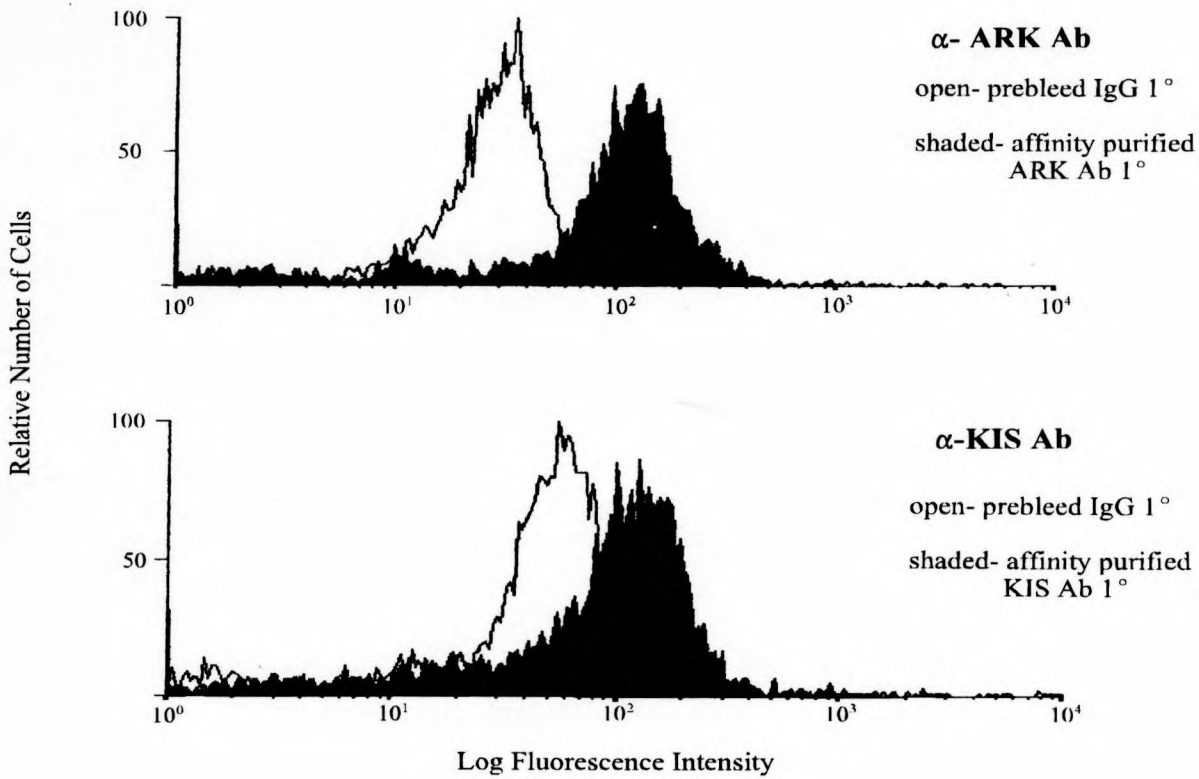


**Figure 26.** FACS analysis of neutrophils stained with α-ARK and α-KIS affinity purified antibodies. The α-ARK antibody was diluted 1:50 while the α-KIS antibody was diluted 1:100. Each experiment contained $1x10^6$ cells.

removed during the staining procedure.

To examine whether the labeling observed in intact cells was increased with cells that were permeabilized, the detergent saponin was used to treat the fixed cells prior to labeling with affinity purified antibodies. Figure 27 shows the histograms from the same experiment where anti-ARK antibodies (upper histogram) and anti-KIS antibodies (lower histogram) were incubated with permeabilized cells. The modest increase in fluorescence intensity from permeabilized cells is most likely due to incomplete removal of secondary antibodies from the permeabilized cells.

This evidence supports the assumption that the epitopes $^{155}$ARKRIKNPEGG$^{165}$ and $^{246}$KISEWGKIKEC$^{256}$ on gp91-*phox* are external since exposing the interior of the cell by treatment with saponin did not appreciably strengthen the fluorescence intensity. Figure 28 and Figure 29 depict the amount of fluorescence from the two different unpermeabilized cell types present in the preparations when stained with anti-ARK and anti-KIS antibodies, respectively. The scatter plot at the bottom of Figure 28 and Figure 29 each have two outlined regions representing neutrophils (region 1) and lymphocytes (region 2), as established by their forward scattering and side scattering values. The top of both figures shows the fluorescence intensity for each of these regions. The difference in fluorescence intensity between region 1 and region 2 plainly demonstrates that neutrophils display the binding domains ARKRIKNPEGG and KISEWGKIKEC but lymphocytes do not, in agreement with the low level of cytochrome $b_{558}$ expression in lymphocytes (10). This evidence supports the specificity of anti-ARK and anti-KIS antibodies for an extracellular region on gp91-*phox*. It also shows that

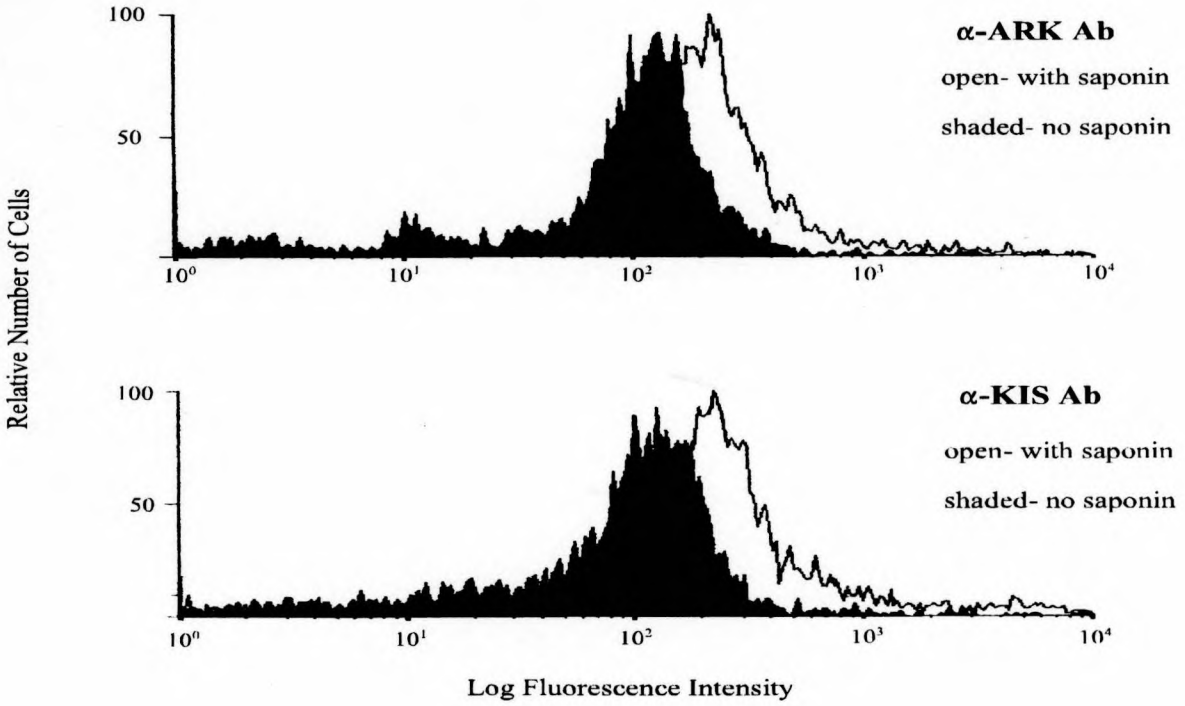


**Figure 27.** FACS analysis comparing saponin permeabilized and unpermeabilized neutrophils stained with α-ARK and α-KIS affinity purified antibodies. The α-ARK antibody was diluted 1:50 while the α-KIS antibody was diluted 1:100. Each experiment contained $1x10^6$ cells.

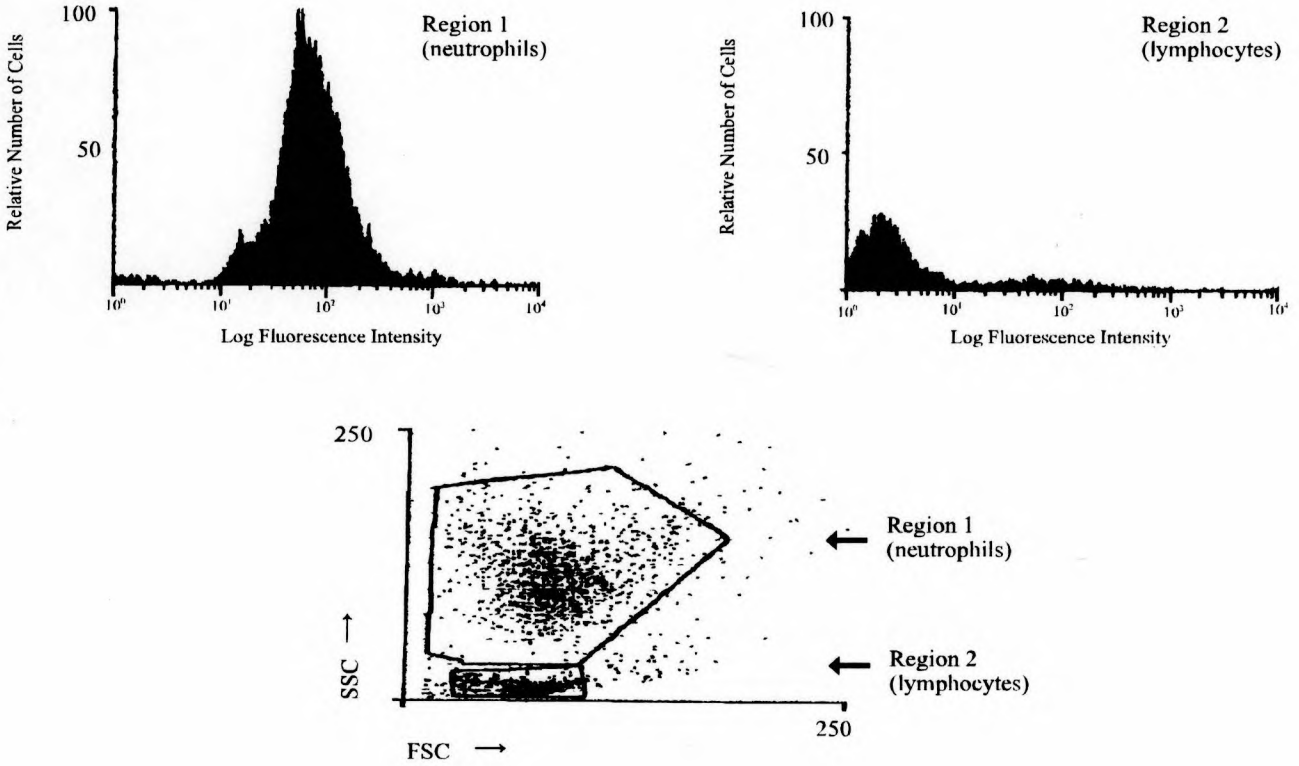


**Figure 28.** FACS analysis of unpermeabilized neutrophils and lymphocytes stained with ARK antibodies. The comparison of the staining between the two cell types shows that the α-ARK antibody is specific for an antigen expressed on the surface on neutrophils only (i.e. cytochrome $b_{558}$).

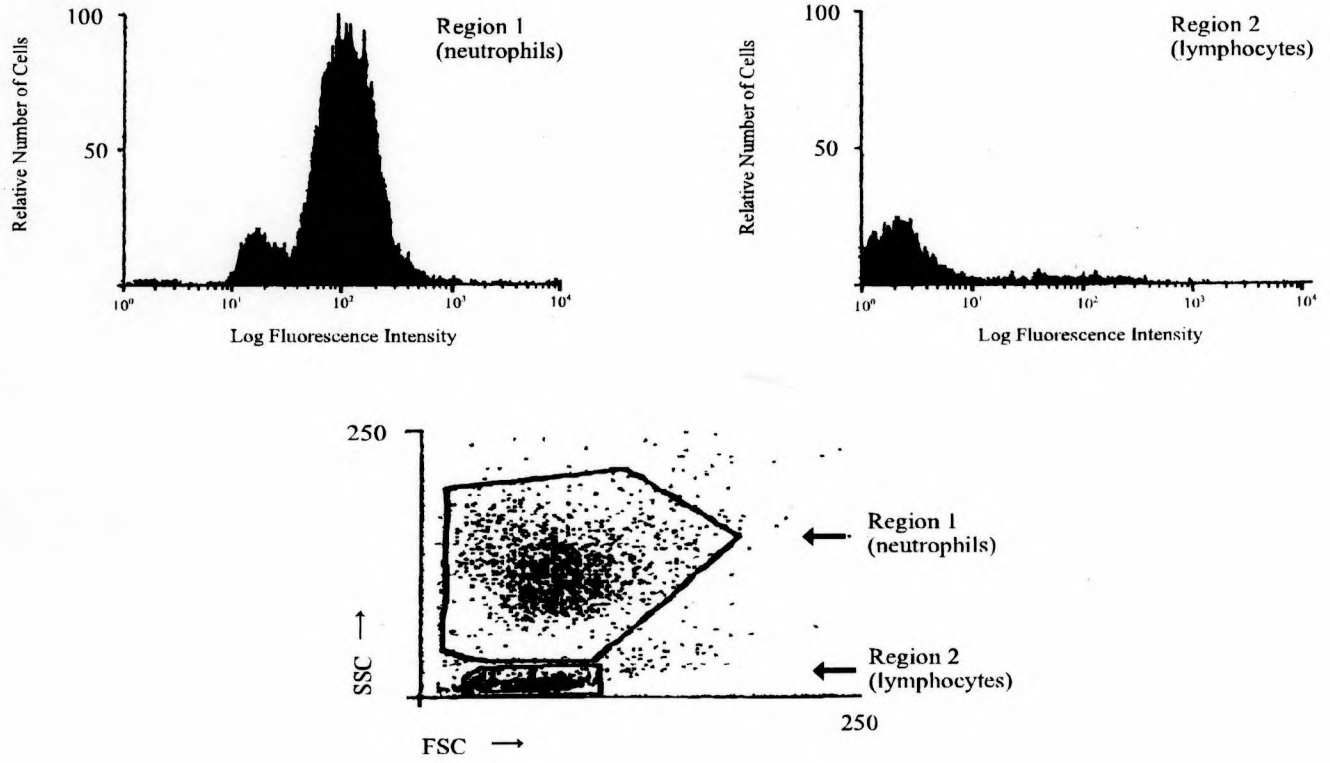


**Figure 29.** FACS analysis of unpermeabilized neutrophils and lymphocytes stained with KIS antibodies. The comparison of the staining between the two cell types shows that the α-KIS antibody is specific for an antigen expressed on the surface of neutrophils only (i.e. cytochrome $b_{558}$).

membrane proteins common to each cell type are not contributing to the non-specific staining.

## Discussion

The capability of antibodies to identify proteins in complex mixtures is a property that is utilized in Western blot analysis as well as other immunological methods. The former technique has been exploited in situations where limits on the amount of material, sample purity, or a combination of both, preclude determination by amino acid sequencing. A goal of this thesis was to identify the heme binding domain in cytochrome $b_{558}$ after partial proteolytic digestion. Partial tryptic or V8 digestion of Triton X-100 solubilized cytochrome $b_{558}$ generates spectrally active fragments ranging in mass from ~ 9 to 20 kDa as determined by SDS-PAGE and MALDI MS. Since the masses determined by MALDI MS are not accurate enough to unequivocally identify these fragments, and because glycosylation may confound the mass determination, an additional approach was employed to aid in the identification. This approach involved the production of anti-peptide polyclonal antibodies for both the large and small subnits of cytochrome $b_{558}$ that might aid in recognizing the epitope in the vicinity of the proposed heme binding domain.

Aside from needing additional antibodies to identify fragments of gp91-*phox*, there was also a need to map other regions of the protein. Several earlier studies have provided structural information on the carboxyl region of the large subunit of cytochrome $b_{558}$ and its interaction with cytosolic components. Kleinberg et al. (11) discovered that a synthetic peptide from the carboxy terminus of the large subunit, $^{559}$RGVHFIF$^{565}$, inhibited the

production of superoxide by NADPH oxidase. By substituting alanine for each amino acid along the peptide, they found that each residue was needed for inhibition except for the glycine and the histidine. The disruption in the superoxide generating capacity of cytochrome $b_{558}$ was attributed to the inhibitory effect of the peptide on the assembly of gp 91-*phox* with other cytosolic components. Analyses by DeLeo et al., using phage-display, reproduced the findings of Kleinberg, and showed that the peptide shown to inhibit superoxide production was indeed a binding site on gp91-*phox* for the cytosolic component of the NADPH oxidase system, termed p47*phox*. Additional p47 *phox* binding regions on gp91-*phox* were found in this study and include the epitopes $^{86}$STRVRRQL$^{93}$ and $^{450}$FEWFADLL$^{457}$ (12). Synthetic peptides mimicking these regions were shown to inhibit the superoxide generating activity of the oxidase.

Together these results suggest that the carboxyl-terminal portion of gp91-*phox* is located on the cytosolic side of the membrane. Phage-display analysis has been shown by Burritt et al. to be useful in mapping the topology of gp91-*phox* (8). The sites of interaction for mouse monoclonal antibodies against gp91-*phox*, were determined using the phage-display technique. A consensus found in phage selected for immobilized anti-gp91-*phox* antibodies, strongly indicated a region in the middle of the protein containing the epitope $^{382}$PKIAVDGP$^{389}$. Attempts to decipher whether this epitope was intra- or extra- cellular using FACS scan analysis were inconclusive because the epitope recognized by the antibody was not accessible in either permeabilized or unpermeabilized cells.

The approach to producing antibodies whose epitopes are known involves the generation of antibodies to a peptide antigen mimicking an epitope on the mature protein.

Anti-peptide polyclonal antibodies have been shown to be beneficial in establishing the topography of gp91-*phox* in human neutrophil membranes. Rabbit anti-peptide polyclonal antibodies to the epitope $^{547}$KQSISNSESGPRG$^{559}$ were shown not to be surface accessible as examined by electron microscopy and immunostaining by Jesaitis et al. (10). These results were later confirmed by the observations of Imajoh-Ohmi et al. using rabbit polyclonal anti-peptide antibodies against the peptide emulating the region $^{550}$ISNSESGPRGVHFIFNKENF$^{569}$ on gp91-*phox*. FACS scan analysis using antibodies against this peptide showed that only upon freeze permeabilization of the cell, did an increase in fluorescence intensity occur (13). This group tested additional rabbit polyclonal anti-peptide antibodies against the epitope $^{150}$SYLNFARKRIKNPEGGLYLAVTL$^{172}$ on gp91-*phox* in close proximity to the potential glycosylation sites at N 131 and N 148. The antibodies produced against this epitope were found to be extracellular when analyzed by FACS scan since the fluorescence intensity did not increase upon freeze fracturing of the cell.

At present, the antibodies mentioned above constitute the full extent of topologically relevant antibodies described in the literature. Other monoclonal and polyclonal antibodies have been used to identify cytochrome $b_{558}$ both by Western blot analysis and by immunological staining of neutrophils (14-16). However, these studies have not determined the exact amino acid sequences of the epitopes on gp91-*phox* or p22-*phox* where these various antibodies bind. The FACS scan analysis discussed in this chapter for the rabbit polyclonal antibodies raised against the

epitopes $^{155}$ARKRIKNPEGG$^{165}$ and $^{246}$KISEWGKIKEC$^{256}$ on gp91-*phox*, clearly shows the external aspect of these two sequences. The extracellular location of these epitopes is not surprising since there are a number of potential glycosylation sites nearby at N131, N149, and N239, that have recently been shown to be glycosylated by mutated cDNA's expressed in *E. coli.* (17). Furthermore, the finding that the epitope $^{155}$ARKRIKNPEGG$^{165}$ is extracellular confirms the work done by Imajoh-Ohmi (13). In addition, these antibodies were shown to specifically stain cytochrome $b_{558}$ by Western blot analysis.

The FACS analysis performed using the anti-peptide antibodies ARK and KIS with permeabilized and unpermeabilized neutrophils suggest that the epitopes recognized by these antibodies are extracellular. In addition, the epitopes were found to be absent from cells that have low levels of expression of gp91-*phox* . Immunohistological examination of neutrophils probed with the antibody KIS show distinct staining for the membranes of cells immobilized on coverslips (K. Billings-Sandoval, unpublished results). This antibody may prove to be beneficial for characterization of cytochrome $b_{558}$ in situ.

These data in combination with previously published results suggest; 1) There is a transmembrane region between the intracellular p47-phox binding site at $^{86}$STRVRRQL$^{93}$ and the extracellular epitope $^{155}$ARKRIKNPEGG$^{165}$ recognized by anti-ARK antibodies and 2) There must be two transmembrane regions between the $^{155}$ARKRIKNPEGG$^{165}$ and $^{246}$KISEWGKIKEC$^{256}$ epitopes if the histidines in the primary sequence between these two regions are indeed involved in the coordination of heme. These results also support the hypothesis that within the first 170 residues of gp91-*phox* there are three sites of

glycosylation, three transmembrane regions, and a number of histidines within transmembrane regions capable of heme coordination. There is the implication that a transmembrane domain exists between the epitope $^{246}$KISEWGKIKEC$^{256}$ (found to be extracellular) and the epitope at $^{450}$FEWFADLL$^{457}$ (found to be intracellular). Imajoh-Ohmi et al. found that cytochrome $b_{558}$ in unpermeabilized cells, proteolyzed by papain treatment, resulted in the loss of an ~18 kDa fragment from the carboxy-terminus (13). The authors speculated that the site of cleavage was an extracellular epitope containing residues 369-398. However, this region has been implicated as being adjacent to an intracellular flavin binding region by homology to other flavin-binding proteins (18,19). Due to the ambiguity of the sidedness (intra- or extra- cellular) of the monoclonal antibody 54.1 (binding site $^{328}$PKIAVDGP$^{389}$), and the incompatibility of the Imajoh-Ohmi finding of an extracellular papain cleavage site in a predicted FAD binding region, the location of the transmembrane region between the projected extracellular epitope $^{246}$KISEWGKIKEC$^{256}$ and the intracellular epitope $^{450}$FEWFADLL$^{457}$ can only be interpreted through hydropathy analysis (20, 21).

In conclusion, the anti-peptide polyclonal antibodies raised against gp91-*phox* have reinforced our current model of the topology of the protein (see Figure 1) (22) and have added new insights. Their use in interpreting results from the isolation of a homogenous isoform of cytochrome $b_{558}$, and in identifying fragments from partial digests of the protein, will be discussed in the upcoming chapters.

## References


1. Towbin, H., T. Staehelin, and J. Gordon. 1979. Electrophoretic transfer of proteins from polyacrylamide gels to nitrocellulose sheets: Procedure and some applications. *Proc. Natl. Acad. Sci.* 76:4350-4354.

2. Blake, M. S., K. H. Johnston, G. J. Russell-Jones, and E. C. Gotschlich. 1984. A rapid, sensitive method for detection of alkaline phosphatase-conjugated antiantibody on Western blots. *Anal. Biochem.* 136:175-179.

3. Gilman-Sachs, A. 1994. Flow cytometry. *Anal. Biochem.* 66:700A-707A.

4. Dinauer, M. C., S. H. Orkin, R. Brown, A. J. Jesaitis, and C. A. Parkos. 1987. The glycoprotein encoded by the X-linked chronic granulomatous disease locus is a component of the neutrophil cytochrome b complex. *Nature* 327:717-720.

5. Shatwell, K. P., A. Dancis, A. R. Cross, R. D. Klausner, and A. W. Segal. 1996. The FRE1 ferric reductase of Saccharomyces cerevisiae is a cytochrome b similar to that of NADPH oxidase. *J. Biol. Chem.* 271:14240-14244.

6. Quinn, M. T., M. L. Mullen, and A. J. Jesaitis. 1992. Human neutrophil cytochrome b contains multiple hemes: evidence for heme associated with both subunits. *J. Biol. Chem.* 267:7303-7309.

7. Parkos, C. A., A. A. Allen, C. G. Cochrane, and A. J. Jesaitis. 1987. Purified cytochrome b from human granulocyte plasma membrane is comprised of two polypeptides with relative molecular weights of 91,000 and 22,000. *J. Clin. Invest.* 80:732-742.

8. Burritt, J. B., M. T. Quinn, M. A. Jutila, C. W. Bond, and A. J. Jesaitis. 1995. Topological mapping of neutrophil cytochrome b epitopes with phage-display libraries. *J. Biol. Chem.* 270:16974-16980.

9. Jesaitis, A. J., E. S. Buescher, D. Harrison, M. T. Quinn, C. A. Parkos, S. Livesey, and J. G. Linner. 1990. Ultrastructural localization of cytochrome b in the membranes of resting and phagocytosing human granulocytes. *J. Biol. Chem.* 3:321-335.

10. Pick, E. and R. Gadba. 1988. Certain lymphoid cells contain the membrane-associated component of the phagocyte-specific NADPH oxidase. *J. Immunol.* 140:1611-1617.

11. Kleinberg, M. E., D. Mital, D. Rotrosen, and H. L. Malech. 1992. Characterization of a phagocyte cytochrome b558 91-kilodalton subunit functional domain: identification of peptide sequence and amino acids essential for activity. *Biochemistry* 31:2686-2690.

12. DeLeo, F.R., Nauseef, W.M., Jesaitis, A.J., Burritt, J.B., Clark, R.A., and Quinn, M.T. 1995. A domain of p47phox that interacts with human neutrophil flavocytochrome $b_{558}$. *J.Biol.Chem.* 270:26246-26251.

13. Imajoh-Ohmi, S., K. Tokita, H. Ochiai, M. Nakamura, and S. Kanegasaki. 1992. Topology of cytochrome b558 in neutrophil membranes analyzed by anti-peptide antibodies and proteolysis. *J. Biol. Chem.* 267:180-184.

14. Nakamura, M., M. Murakami, T. Koga, Y. Tanaka, and S. Minakami. 1987. Monoclonal Antibody 7D5 Raised to Cytochrome b558 of Human Neutrophils: immunochemical detection of the antigen in peripheral phagocytes of normal subjects, patients with chronic granulomatous disease, and their carrier mothers. *Blood* 69:1404-1408.

15. Nakamura, M., S. Sendo, R. van Zwieten, T. Koga, D. Roos, and S. Kanegasaki. 1988. Immunocytochemical discovery of the 22- to 23-Kd subunit of cytochrome b558 at the surface of human peripheral phagocytes. *Blood* 5:1550-1552.

16. Ginsel, L. A., J. J. Onderwater, J. A. Fransen, A. J. Verhoeven, and D. Roos. 1990. Localization of the low-Mr subunit of cytochrome b558 in human blood phagocytes by immunoelectron microscopy. *Blood* 76:2105-2116.

17. Wallach, T. M. and A. Segal. 1997. Analysis of glycosylation sites on gp91phox, the flavocytochrome of the NADPH oxidase, by site-directed mutagenesis and translation *in vitro*. *Biochem. J.* 321:583-585.

18. Rotrosen, D., C. L. Yeung, T. L. Leto, H. L. Malech, and C. H. Kwong. 1992. Cytochrome b558: the flavin-binding components of the phagocyte NADPH oxidase. *Science* 256:1459-1462.

19. Taylor, W. R., D. T. Jones, and A. W. Segal. 1993. A structural model for the nucleotide binding domains of the flavocytochrome $b_{-245}$ β-chain. *Protein Science* 2:1675-1685.

20. Parkos, C. A., M. C. Dinauer, L. E. Walker, R. A. Allen, A. J. Jesaitis, and S. H. Orkin. 1988. Primary structure and unique expression of the 22-kilodalton light chain of human neutrophil cytochrome b. *Proc. Natl. Acad. Sci. U. S. A.* 85:3319-3323.

21. Royer-Pokora, B., L. M. Kunkel, A. P. Monaco, S. C. Goff, R. L. Newburger, R. L. Baehner, F. S. Cole, J. T. Curnutte, and S. H. Orkin. 1986. Cloning the gene for an inherited disorder-chronic granulomatous disease-on the basis of its chromosomal location. *Nature* 322:32-38.

22. Parkos, C. A., M. T. Quinn, S. Sheets, and A. J. Jesaitis. 1992 The structure of human neutrophil b-type cytochrome involved in superoxide production. In: Molecular basis of oxidative damage by leukocytes. A. J. Jesaitis and E. A. Dratz, eds. CRC Press, Boca Raton, FL, p. 45-55.

# Chapter 5

## CHARACTERIZATION OF A CYTOCHROME $b_{558}$ ISOFORM IN HUMAN NEUTROPHILS

### Introduction

Cytochrome $b_{558}$ is a glycosylated, heterodimeric, integral membrane protein found in the plasma lemma and specific granule membranes of human neutrophils. The protein consists of two polypeptides, the large glycosylated polypeptide ( 569 residues; M.W.= 65,160 Da) and the small nonglycosylated polypeptide (194 residues; M.W.= 20,956 Da). The large subunit also known as gp91-*phox* (**g**lyco**p**rotein -m.w. **91** kDa ***ph****agocyte* ***ox****idase*), contains all the sites of heterogeneous *N*-linked glycosylation and does not contain any apparent O-linked glycosylation (1). The first published reports of the partially purified protein suggested different molecular weights for gp91-*phox* which may have been due in part to the heterogeneous nature of the glycosylation (1-6).

The function of the glycosylation on gp91-*phox* is unknown. However, if the carbohydrate is removed, the deglycosylated protein is still functional, though partially

impaired(7). The carbohydrate may participate in cellular communication, localization or targeting, protein binding, and protection from proteolysis (8-10). Though the function of the carbohydrate on gp91-*phox* is not known, it has been utilized in purification and labeling procedures. The gp91-*phox* gene has been cloned and sequenced (11,12), yet little has been done to determine the exact location of the sites of glycosylation on the protein and the extent of glycosylation at each site.

The first work that was done to determine the type of carbohydrate linkage (O-glycosylation refers to carbohydrate bound to a serine or threonine residue vs. N-glycosylation that refers to carbohydrate bound to an asparagine residue) found that the glycosylation was N-linked and was localized to the large subunit of cytochrome $b_{558}$ (1). The sites of glycosylation were then projected to be on asparagine residues that were part of the known N-glycosylation motifs -Asn-Xaa-Ser, -Asn-Xaa-Thr and -Asn-Xaa-Cys. Recent work has shown that in a model system expressing the large subunit of cytochrome $b_{558}$, incorporating truncated forms of carbohydrate, three out of a total of six asparagines, N131, N148, and N239, are possible sites for carbohydrate linkage (13).

Carbohydrate binding proteins, such as wheat-germ agglutinin, can be used as an affinity purification matrix for glycosylated proteins. This approach was first described by Cuatrecasas and co-workers and has been applied towards the purification of cytochrome $b_{558}$ (14). It has been used subsequently in the Jesaitis laboratory for routine purification of cytochrome $b_{558}$ from neutrophil membranes (1,15). Additional steps in this purification procedure include the use of a cation exchange based interaction of cytochrome $b_{558}$ with heparin. Heparin is a sulfonated glycosaminoglycan immobilized on agarose beads. The

negative charge on the sulfonate group attached to the six-membered ring of the carbohydrate introduces a cation binding property that allows for the additional purification of the cytochrome $b_{558}$ from components retained by the wheat-germ agglutinin. By passing the glycosylated protein mixture over the heparin column, only the constituents having a positive charge at the pH being used will be retained. The retained material can then be eluted using a salt gradient that further purifies the cytochrome $b_{558}$ from the other proteins in the preparation by taking advantage of the different degrees of interaction of the proteins attached to the heparin. The combination of two orthogonal approaches to purification, lectin affinity and ion exchange, enables a nine fold enrichment in cytochrome $b_{558}$ relative to 2% octylglucoside solubilized membranes.

Although this purification scheme has been used successfully for ten years, the advent of HPLC columns that drastically reduce the amount of time and materials involved in protein purification, spawned an attempt at a new approach to the purification of cytochrome $b_{558}$. Tandem anion exchange followed by gel filtration was performed isocratically with a buffered mobile phase containing detergent and a volatile salt. This HPLC system enabled the continuous monitoring of the absorbance at 414 nm (the peak absorbance wavelength for the Soret band of the molecule) along with online tryptophan fluorescence detection for total protein detection. Initial experiments were designed to determine whether or not an acceptable purification factor could be obtained along with sufficient recovery. The rational for running an anion exchange column was to retain components of the detergent solubilized membranes that did not interact with the heparin column using the conventional purification scheme since the heparin is a cation exchanger.

The cytochrome $b_{558}$ theoretically should not interact with the anion exchanger and would be further purified by size on the following gel filtration column. Also, the use of a detergent containing mobile phase at physiological pH would facilitate the retention of the non-covalently bound heme in the protein. Analysis of the HPLC fractions included, Western blotting, MALDI MS, and LC MS/MS sequencing of proteolytic peptides derived from an in-gel digest of proteins isolated by SDS-PAGE. The results of these experiments suggested that a homogeneous form of gp 91-phox, along with the heterogeneously glycosylated forms, was present in neutrophil membranes in amounts that varied with individual donors. Western blot analysis showed that an immunoreactive isoform of cytochrome $b_{558}$ was present at 82 kDa and silver stained SDS-PAGE gels indicated that this isoform was a single component at that molecular weight. MALDI-TOF experiments supported this evidence resulting in an accurate mass of 82,054 Da for the isoform.

## Materials and Methods

### Detergent Solubilization of Cytochrome $b_{558}$

Solubilization of membranes derived from the neutrophils of normal human donors followed the procedure of Parkos et al. (1). Membranes, frozen at -80°C, were thawed on ice and salt washed by making the suspension 1 M in NaCl in order to disrupt most ionic interactions of peripherally-bound membrane proteins. The suspension was vortexed to ensure mixing of the salt with the membranes, then centrifuged at 100,000 g for 45 minutes at 4°C. The clear, green-yellow colored supernatant was removed and the salt

washing step was repeated to more thoroughly extract any peripherally-bound proteins, primarily myeloperoxidase which is a heme-bearing component of azurophil granules (16). The tan-colored pellet was suspended in membrane resuspension buffer (MRB) consisting of relax buffer pH 7.4 with 1 mM EDTA, 0.1 mM DTT, 1 mM PMSF, and 10 $\mu$g/ml chymostatin and 2% octylglucoside. Sonication was used to disrupt the membranes and complete solubilization was accomplished by allowing the solution to mix at 4°C on ice for 1 hour. The detergent solubilized membranes were then centrifuged at 100,000 g for 45 minutes and the amount of cytochrome $b_{558}$ present was determined by reduced-oxidized spectra using an extinction coefficient of 29.3 $mM^{-1}$ $cm^{-1}$ for the alpha band at 558 nm or 131 $mM^{-1}$ $cm^{-1}$ for the oxidized Soret band (1,3). The supernatant from the centrifugation was used for subsequent anion exchange / gel filtration chromatography.

Anion Exchange / Gel Filtration HPLC

All chromatography was performed on a Hitachi Model L-2500 HPLC system with a Model L-4200 UV/VIS variable wavelength detector set at 414 nm. A Hitachi Model F-1050 on-line fluorescence spectrophotometer was also used to monitor tryptophan fluorescence with excitation at 280 nm and emission monitored at 340 nm. The columns utilized for the chromatography consisted of a Synchropak AX 500 4mm x 25 cm anion exchange column (Synchrome Inc.) and a TosoHaas model TSK G3000SW 75mm x 60 cm gel filtration column run in tandem. The buffers used for the runs were; Buffer A:1% octylglucoside, 5 mM HEPES pH 7.4, 0.02% $NaN_3$ and Buffer B:1 M ammonium acetate, 5 mM HEPES pH 7.4, 0.02% $NaN_3$. The runs were isocratic having 94% Buffer A and

6% Buffer B injection volumes of 2% OG solubilized membranes were 1ml unless stated otherwise. The flow rate for Figures 1,2, 8, 20, and 23 was a gradient flow rate starting at 0.4 ml/min and ending with 1 ml/min over a period of 30 minutes. The chromatogram in Figure 30 shows a typical HPLC run with a constant flow rate of 0.8 ml/min.

SDS-PAGE Electrophoresis

SDS-PAGE was performed using slab gels 1.5 mm x 8 cm x 20 cm having an acrylamide gradient of 7-18% and containing 0.1% SDS. Samples were mixed 1:1 v/v with sample buffer consisting of 1 part 10% SDS, 1 part 0.5 M Tris base pH 6.8, 1 part glycerol, and 500 mM 2-mercaptoethanol. Samples were then placed on the gel without boiling and run with standards using 15 or 28 lane combs. Gels were silver stained under acidic conditions or analyzed by Western blot analysis.

Western Blot Analysis

Proteins bands in SDS-PAGE gels were electrophoretically transferred to nitrocellulose according the procedure described by Towbin (17). The nitrocellulose containing the blotted proteins was blocked with blocking buffer, consisting of 5% non fat dry milk and 0.2% Tween 20 in PBS pH 7.4, overnight at 4°C or for 3 hours at 37°C. Primary antibodies were applied to the blots in antibody diluting buffer consisting of 3% normal goat serum, 1% BSA and 0.2% Tween at the various dilutions listed in Table 6. Primary antibodies were incubated for 3 hours at room temperature. Non-specifically bound primary was rinsed off the blot using wash buffer containing 250 mM NaCl, 10 mM

HEPES pH 7.4, and 0.2% Tween with a total of 5 washes at 5 minute intervals. The secondary antibody (either an alkaline phosphatase conjugated goat anti-mouse or goat anti-rabbit IgG) was applied at a dilution of 1:1,000 v/v in diluting buffer and incubated for 1 hour at room temperature. After rinsing with a total of 4 washes, a fifth wash was done using alkaline TBS pH 8.0 for subsequent development with alkaline phosphatase conjugated IgG. The reaction was halted by rinsing with distilled water.

Deglycosylation Experiments

Removal of *N*-linked glycosylation was performed using *N*-glycosidase F, Boehringer Mannheim, using the manufacture's protocols. Samples were boiled in 0.5% SDS for 5 minutes, then incubated with enzyme for 12 hours. Samples were then analyzed using SDS-PAGE and silver staining and Western blot analysis.

Mass Spectrometry

MALDI mass spectra were obtained on a PerSeptive Biosystems / Vestec Voyager RP TOF mass spectrometer (PerSeptive Biosystems, Framingham, MA) as described in Chapter 2. Samples were run in linear mode with +28 kV accelerating voltage, +16.8 kV secondary grid voltage, and +84 V guide wire voltage. Sinapinic acid was used in all MALDI experiments presented. The matrix was prepared as a saturated solution in 1:1 v/v water:acetonitrile with 0.1% TFA. All samples were concentrated using a microcon 50 concentrator (Amicon) and diluted 1:1 with purified water to dilute the detergent and salt concentrations. Samples were typically concentrated approximately 5-10 fold prior to

analysis using centrifugation through a membrane having a 30 kDa molecular weight limit. A microliter of the protein concentrate was mixed 1:1 with water: acetonitrile:0.1% TFA before adding to the matrix. However, larger crystals were formed and MALDI mass spectra were improved, when a volume of the protein solution was first diluted with an equal volume of a 1:1 v/v mixture of water:acetonitrile with 0.1 % TFA prior to mixing with the sinapinic acid matrix.

UV / VIS Absorbance Measurements

All absorbance measurements on detergent extracts and on isolated fractions of partially purified protein were carried out using a Hewlett Packard Model 8452A diode array spectrophotometer. The cuvette used had a 1 cm pathlength and a minimum of 150 $\mu$l sample capacity. Reduced-oxidized spectra were obtained by adding 4 $\mu$l of a freshly made 1 M stock of sodium dithionite to the oxidized solution to fully reduce the sample. All concentrations were determined by using the extinction coefficients of 131 $mM^{-1}$ $cm^{-1}$ for the oxidized Soret band at 414 nm, 161 $mM^{-1}$ $cm^{-1}$ for the reduced-minus oxidized band at 426 nm, and 29.3 $mM^{-1}$ $cm^{-1}$ for the reduced-minus oxidized band at 558 nm (1,3)

## Results

Tandem Anion Exchange / Gel Filtration System

Although cytochrome $b_{558}$ from human neutrophils can be partially purified to a reasonable recovery (~50%) by serial lectin (wheat germ-agglutanin) and cation exchange (heparin) chromatography, the possibility remains that isoforms exist that are not retained

using these techniques. To examine this possibility, and to evaluate atlternative approaches to purification, tandem anion exchange / gel filtration chromatography was applied to the purification of crude extracts of solubilized neutrophil membranes. The first runs using the tandem anion exchange / gel filtration chromatographic configuration produced chromatograms containing a number of components with different sizes, but each having absorbance at 414 nm. Only some of these fractions had reduced minus oxidized spectra characteristic of cytochrome $b_{558}$, and blotted for intact large and small subunits by Western blot analysis.

The most intriguing observations from these initial experiments were found when the anion exchange / gel filtration columns were cleared by the injection of high salt. The fractions that eluted early from the column had absorbance at 414 nm and also immuno-blotted very strongly with anti-large and anti-small subunit antibodies. The band staining with the large subunit antibody was not only extremely intense, but it also had a homogeneous electrophoretic migration pattern when analyzed by SDS-PAGE, with a molecular weight of approximately 82 kDa. This result was surprising since the typical band for the large subunit of cytochrome $b_{558}$ is a smeared band at molecular weights ranging from 80 to 100 kDa.

This unique observation sparked interest to further characterize this isolated protein. Since the protein was most likely being differentially retained by the anion exchange column, this potential cytochrome $b_{558}$ isoform may have different glycosylation properties relative to conventionally purified cytochrome $b_{558}$. Since the pI of the large subunit is 8.6 without carbohydrate, the glycosylation must account for the retention by

the anion exchange column relative to the conventionally purified form. Thus, it was anticipated that this form of the protein could provide new information on the glycosylation of cytochrome $b_{558}$.

The chromatogram shown in Figure 30 illustrates the absorbance profile obtained at 414 nm for 2% OG solubilized membranes injected onto the tandem anion exchange / gel filtration columns. The chromatogram typifies one of three runs made in sequence each run containing approximately 12 $\mu$g of cytochrome as estimated by reduced-oxidized absorbance spectra. Western blot analysis of the peaks at 28.2 minutes and 29.9 minutes using the antibodies α-KQS and 44.1 respectively, revealed bands at the correct molecular weight for the large subunit and the small subunit of cytochrome $b_{558}$. The peak at 28.2 minutes had the most intense staining while the staining for the peak at 29.9 minutes was much less intense. An example of a Western blot from the peak at 28.2 minutes can be found in the inset to Figure 30. The peak at 33.6 minutes had the highest absorbance at 414 nm of the components injected from the detergent solubilized membranes. However, the fraction from this peak did not blot for the large subunit when probed with the anti-large subunit antibody KQS but did blot for the small subunit using the anti-small subunit antibody 44.1. There exists the possibility that the fraction contained cytochrome $b_{558}$ from the preceding peak at 29.9 minutes since the peaks were not fully resolved. Silver staining of fractions separated by SDS-PAGE, revealed that the 33. 6 minute fraction was a composite of a number of discrete proteins since the stained bands did not have the characteristic dispersed appearance indicative of a glycosylated protein.

After completing three consecutive injections of 2% OG solubilized membranes

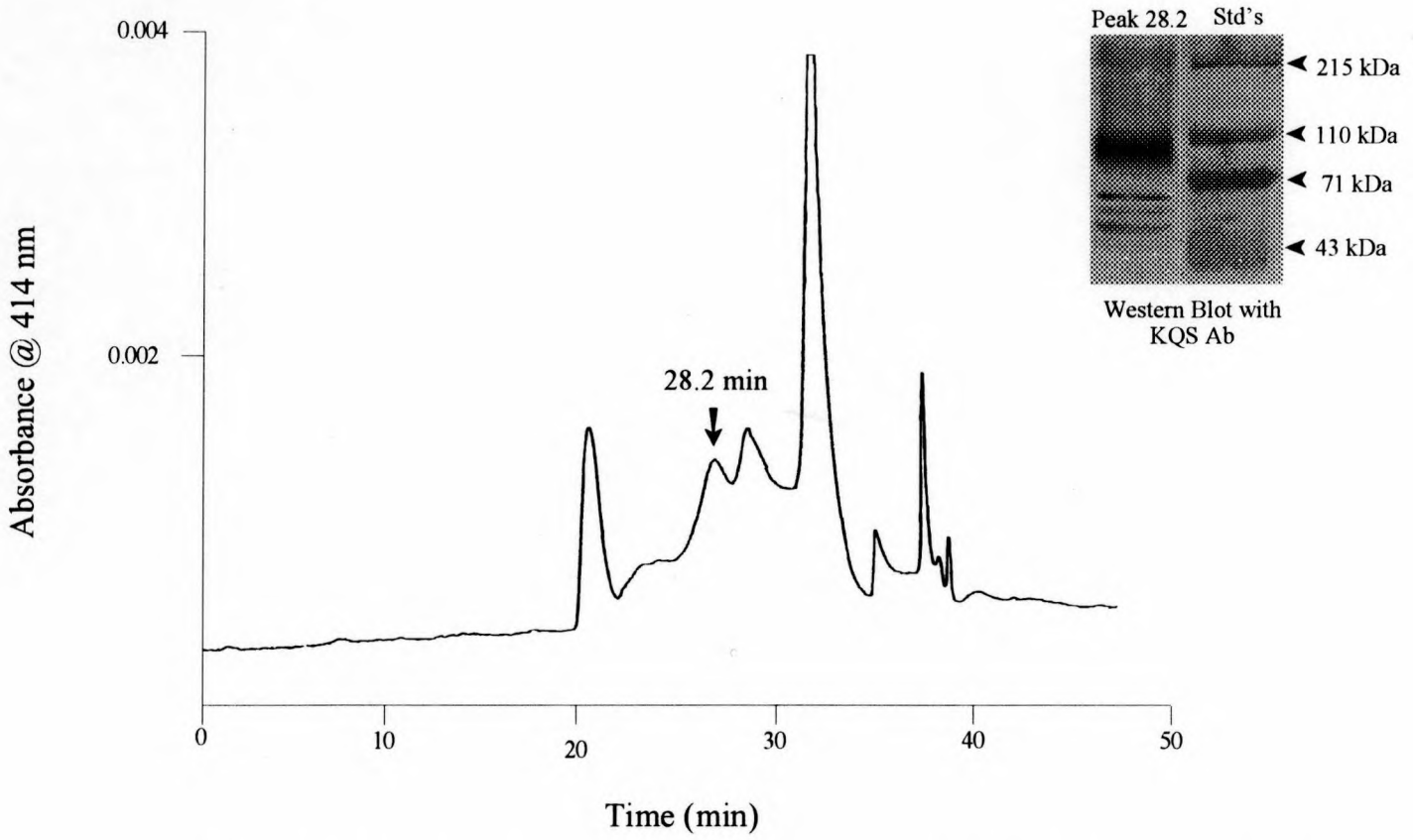


**Figure 30**. Chromatogram showing the profile of components eluted off the anion exchange / gel filtration column after injection of 2% OG solubilized membranes from two donors. This profile is from the original experiment where the isoform of cytochrome $b_{558}$ was first discovered. Labeled peak was found to stain specificly with antibodies KQS and 44.1.

(45 $\mu$g each), the column was flushed with three bed volumes of column buffer before an injection of 300 $\mu$l of 5M NaCl to clear the anion exchange column of any retained proteins. Components eluted by the injection of NaCl were monitored both for absorbance at 414 nm and for tryptophan fluorescence. The chromatogram representing this elution is shown in Figure 31. The fractions labeled at 23.5 min and 25.8 min stained intensely by Western blot analysis using the immunopurified anti-peptide antibody α-ARK, described in Chapter 3, made against a peptide mimicking residues $^{155}$ARKRIKNPEGGC$^{165}$ of the large subunit. Figure 32 shows the blot of the peaks at 23.5 and 25.8 min along with a silver stained SDS-PAGE gel of the same samples. The blot clearly shows a single band at approximately 82 kDa and the silver stain shows that this protein is the primary component at that molecular weight. Western blots of these same fractions with antibodies α-KQS and 44.1 are shown in Figure 33. The antibodies recognized the large and small subunits in these fractions without the presence of cytochrome $b_{558}$ at any other molecular weight in the gel. The fact the small subunit was present and the only other band in the gel having large subunit staining was at 82 kDa, suggested that the two were associated. Also, having two separate antibodies blotting at the same molecular weight was good evidence that the band at 82 kDa was indeed from the large subunit.

To compare the α-ARK antibody recognition of both heparin purified cytochrome $b_{558}$ and the salt elution peak at 23.5 min, a Western blot was performed with the two samples side-by-side as shown in Figure 34. The ability of the antibody to blot both samples is clear and the molecular weight of the protein at 82 kDa is well within the molecular weight range typically observed for purified cytochrome $b_{558}$. In addition, there

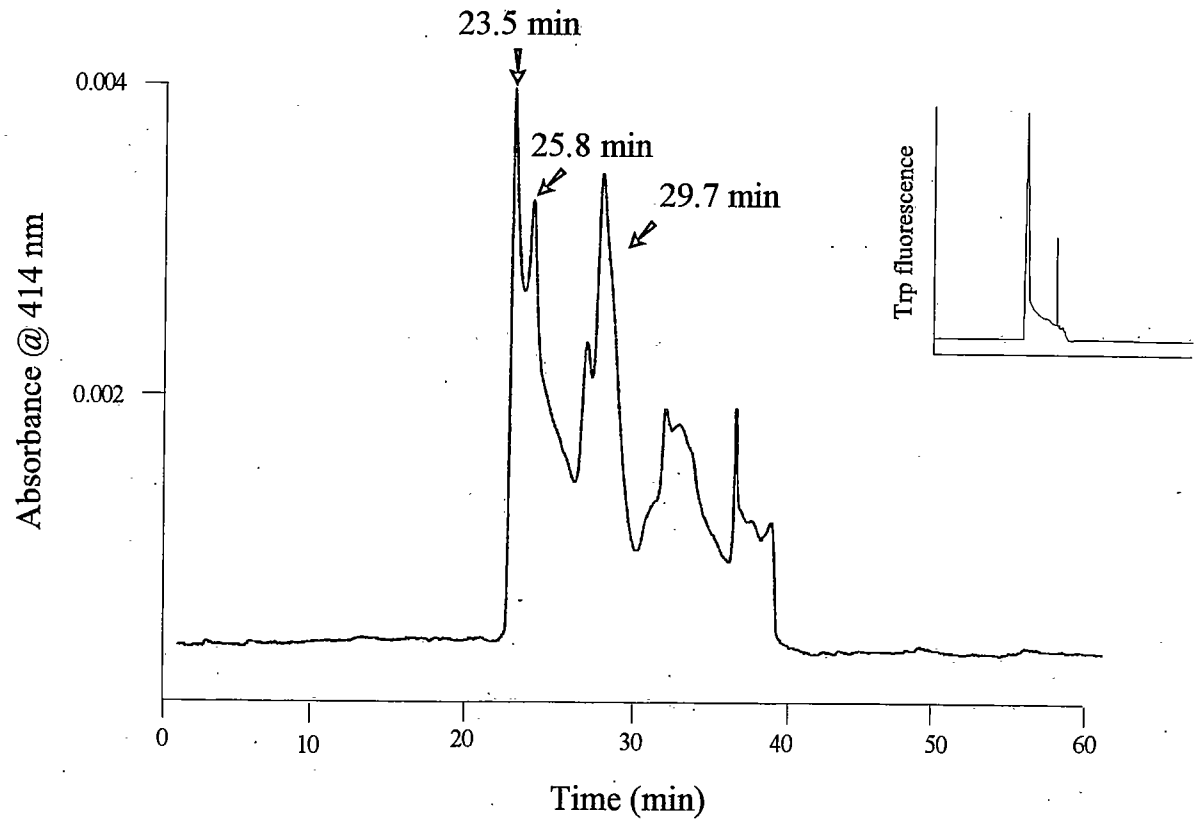


**Figure 31**. Chromatogram showing the profile of components eluted off the anion exchange / gel filtration column after injection of 300 $\mu$l of 5M NaCl from the first isolation of the cytochrome $b_{558}$ isoform. The material was retained on the column from three prior injections, each 45$\mu$g of 2% OG solubilized membranes . Labeled peaks at 23.5 min and 25.8 min gave intense staining with ARK, KQS, and 44.1 antibodies.

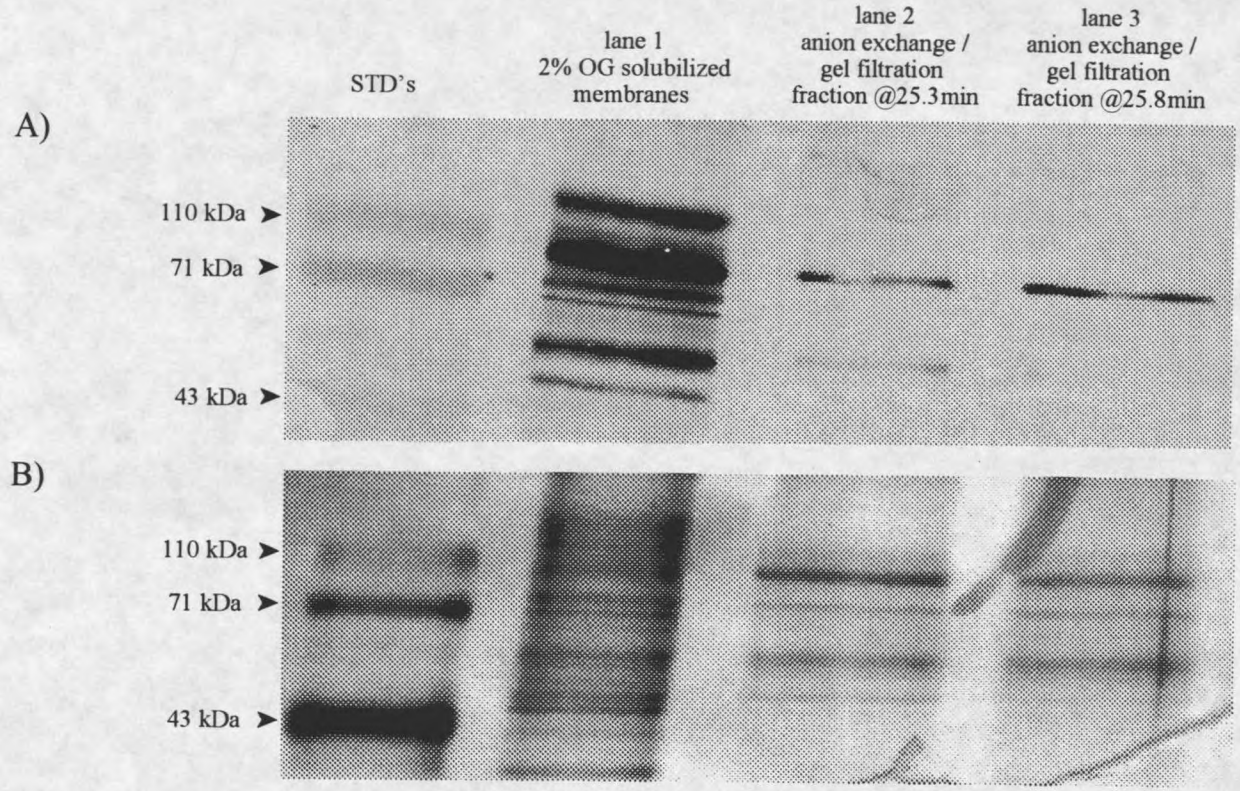


**Figure 32**. Comparison of fractions from tandem anion exchange / gel filtration chromatography eluted with high salt following the injection of 2% OG solubilized membranes. Fractions at 23.5 and 25.8 minutes represent early eluting peaks having absorbance at 414 nm in Figure 32. A) Western blot using anti-ARK antibodies diluted 1:50. B) Silver stain.

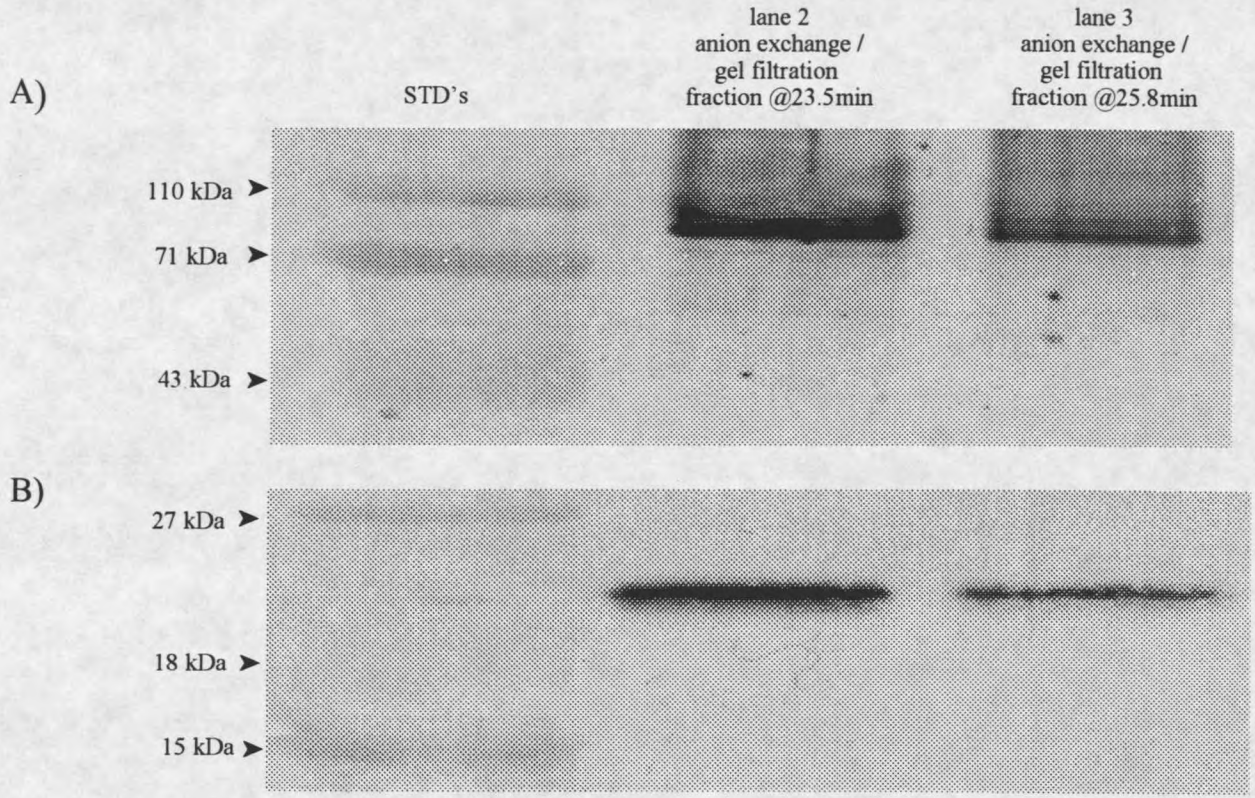


**Figure 33**. Comparison of fractions from tandem anion exchange / gel filtration chromatography eluted with high salt after injection of 2% OG solubilized membranes. Fractions at 23.5 and 25.8 minutes represent peaks having absorbance at 414 nm in Figure 32. A) Western blot using rabbit polyclonal anti-KQS antibodies diluted 1:1,000 B) Western blot using mAb 44.1 diluted 1:1,000.

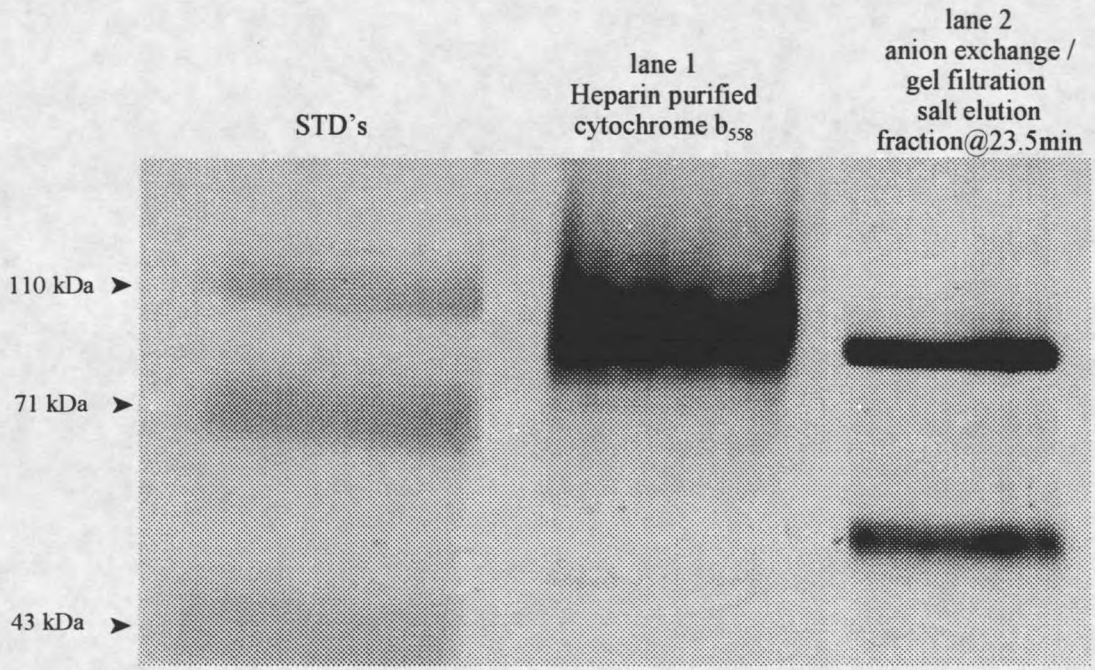


**Figure 34**. Comparison of Western blots using affinity purified anti-ARK antibodies diluted 1:50 Lane 1 contains 10 pmol of heparin purified cytochrome $b_{558}$. Lane 2 is the fraction eluting at 23.5 minutes from tandem anion exchange / gel filtration chromatography eluted with high salt after injection of 2% OG solubilized membranes in Figure 32.

was a peak at approximately 65kDa that was not observed in the heparin purified cytochrome $b_{558}$ but was present in the membranes used for both preparations. This protein is presumed to be either a fragment, or non-glycosylated precursor of the protein at 82 kDa, but could also represent an unrelated protein with a similar epitope recognized by the anti-ARK antibody not isolated in the heparin purification. The peak labeled at 28.4 min was not characterized by SDS-PAGE or Western blotting in this experiment.

MALDI MS analysis of the peaks at 23.5 and 25.8 min in Figure 31 confirmed the molecular weight findings from the silver stain and Western blot analyses. Indeed, the immunoreactive band at $M_r$ = 82,000 Da was found to have an accurate mass of 82,054 Da by MALDI MS and the sample was ionizable in an amount readily detected by MALDI TOF mass spectrometry. Figure 35 shows the MALDI mass spectrum from the peak at 25.8 min in Figure 31. The peak labeled ***a*** at m/z 82,054 Da may represent the isoform of the large subunit that was seen to stain at 82 kDa in Figure 33 and 34. The mass of the doubly charged ion of the isoform is seen at m/z 41,200 Da and is labeled $a_2$. The peak at ~m/z 20,000 Da has an accurate mass of 20,064 Da which is significantly less than the calculated mass of the amino acid sequence for the small subunit (20,957 Da) (12). The mass of the 20kDA peak is also much lower than the calculated masses for the possible contaminating G proteins such as Rap-1A (20,987 Da) and Rac 2 (21,429 Da) (18,19). However, the presence of the small subunit in the sample by Western blot analysis does not necessarily mean that the protein would ionize and be detected by MALDI MS. The origin of the peak at m/z 25,482 Da will be discussed in more detail in Chapter 6.

A common contaminant of 2% OG solubilized membrane preparations is the

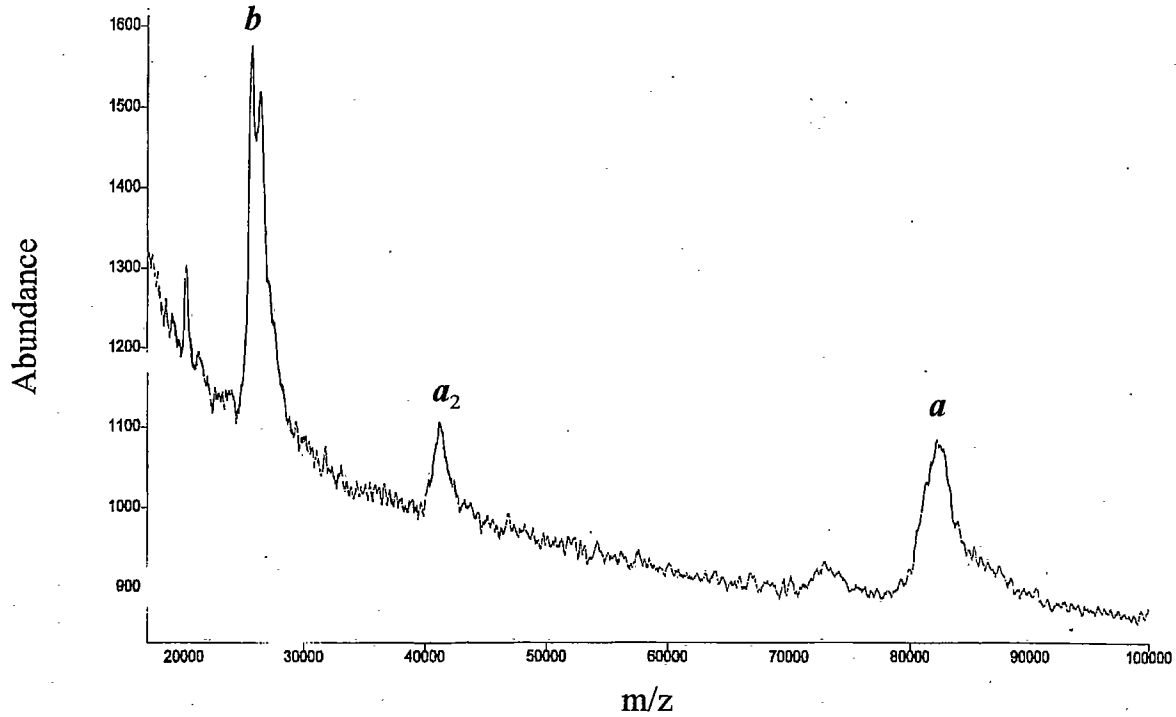


**Figure 35**. MALDI TOF mass spectrum of the cytochrome $b_{558}$ isoform from the original isolation shown in Figure 32. The sample represents the peak at 25.8 min from the salt elution off the anion exchange / gel filtration column. The fraction was concentrated in a Centricon 50 concentrator then mixing 1:1 v/v with acetonitrile:water:0.1% TFA before being combined with ACHCA matrix. The peak labeled ***a*** signifies the isoform with an accurate mass value of 82,054 Da. The peak labeled $a_2$ represents the doubly charged ion of the isoform. The peak labeled ***b*** is a 26 kDa polypeptide that will be discussed in more detail in Chapter 6. A peak at the accurate mass for the small subunit (20,957 Da) is not present in the mass spectrum.

heterodimeric adhesion protein CD11b/CD18. CD18 has a $M_r$ = 96,000 Da, is glycosylated, and by mass consideration alone can easily be mistaken for the large subunit of cytochrome $b_{558}$. To rule out the possibility that the 82 kDa protein was an unknown form of CD18, rabbit anti-peptide antibodies against the carboxy tail of CD 18 (kindly provided by Dr. Charles Parkos) were used in Western blot analysis to see if they would recognize the immobilized protein. Figure 36 shows the results of a Western blot comparing 2% OG solubilized membranes with the peak labeled 25.8 min in Figure 31. Only marginal staining can be seen in the lane containing the peak at 25.8 minutes as compared to the 2% OG solubilized membranes where CD18 is clearly present at 110 kDa.

Reproducibility of the Preparation

In order to reproduce the anion exchange / gel filtration chromatography, membranes from three separate donors were pooled and solubilized in detergent following the procedures from the first experiment. Membranes from a total of 2 x $10^9$ cells were solubilized in 10 ml of detergent solution and 220 $\mu$g of cytochrome $b_{558}$ were recovered as determined by reduced-oxidized spectra. Figure 37 shows the chromatogram from the injection of 1 ml of the solubilized membranes (22 $\mu$g of cytochrome $b_{558}$) injected onto the tandem anion exchange / gel filtration system. The chromatogram has a much larger peak at ~28 minutes as compared to the chromatogram in Figure 31. However, intact cytochrome $b_{558}$ is found at 28-30 minutes as determined by oxidized spectra and Western blot analysis using the anti-large subunit antibody 54.1 similar to the results from the

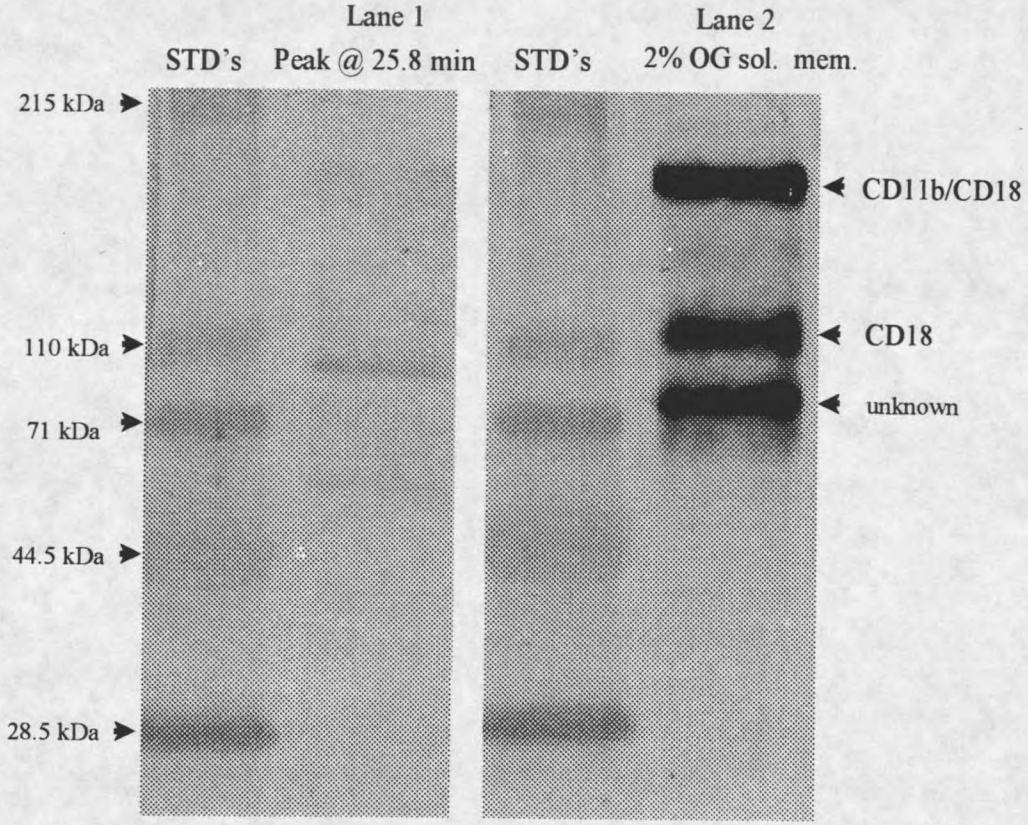


**Figure 36**. Western blot using the rabbit polyclonal anti-peptide antibody R7928E that recognizes an epitope on the carboxy-tail of CD18 (kindly provided by Dr. Charles Parkos). Lane 1 contains the peak that eluted at 25.8 min in Figure 32 that contained the 82 kDa protein recognized by the large subunit antibodies KQS and ARK. Only slight staining can be seen in Lane 1 at 82 kDa. Lane 2 contains 2% OG solubilized membranes. CD18 is clearly visible at 110 kDa.

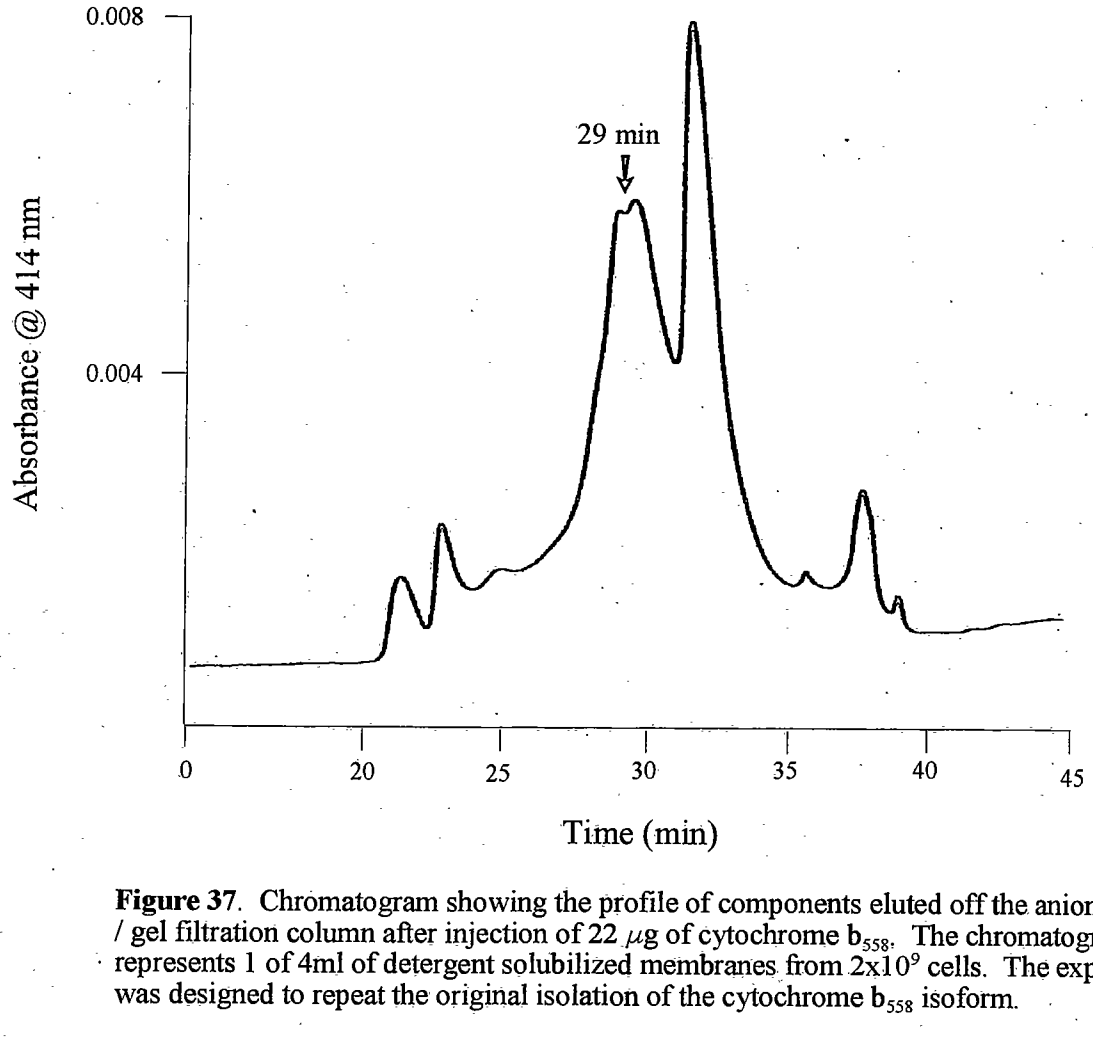


**Figure 37**. Chromatogram showing the profile of components eluted off the anion exchange / gel filtration column after injection of 22 $\mu$g of cytochrome $b_{558}$. The chromatogram represents 1 of 4ml of detergent solubilized membranes from $2x10^9$ cells. The experiment was designed to repeat the original isolation of the cytochrome $b_{558}$ isoform.

chromatogram shown in Figure 31. Silver stains of fractions containing the cytochrome $b_{558}$ were considerably enriched in both the large and small subunits and the recovery of the cytochrome as estimated by oxidized spectra was approximately 50%.

The salt elution carried out done after the injection of solubilized membranes is shown in Figure 38. This chromatogram shows significant differences to the first salt elution chromatogram shown in Figure 31. The retention times and the tryptophan fluorescence profiles (see inset) are analogous, however, the signal intensities of the peaks were not proportional to the previous run. Nevertheless, the Western blots and silver stains gave results consistent with the first experiment. Figure 39 illustrates the intense staining that is found when corresponding salt elution fractions are blotted with the α-ARK antibody. It is evident from the solubilized membranes in Lane 3 that the labeled band at 82 kDa is inclusive of the sample after the membranes are solubilized. The cytochrome $b_{558}$ that elutes from the anion exchange / gel filtration, without salt addition, after the injection of 2% OG solubilized membranes, does not display staining for the 82 kDa isoform when probed with the anti-ARK antibody. Yet it it is clear that α-ARK recognizes the 82 kDa protein prior to injection. This result suggests that the 82 kDa isoform is preferentially retained by the anion exchange / gel filtration system. Figures 40, 41, and 42 give the results of Western blots on the fractions at 17.6 and 25.2 minutes in Figure 38 using antibodies 54.1, KQS, and 44.1 respectively. The silver stain for the two fractions is shown in Figure 43. A control for the presence of CD18 in the fractions from the peaks at 17.6 and 25.2 minutes was also carried out by blotting with the anti-peptide antibodies to CD18. Once again, there was no staining at the molecular weight for the 82

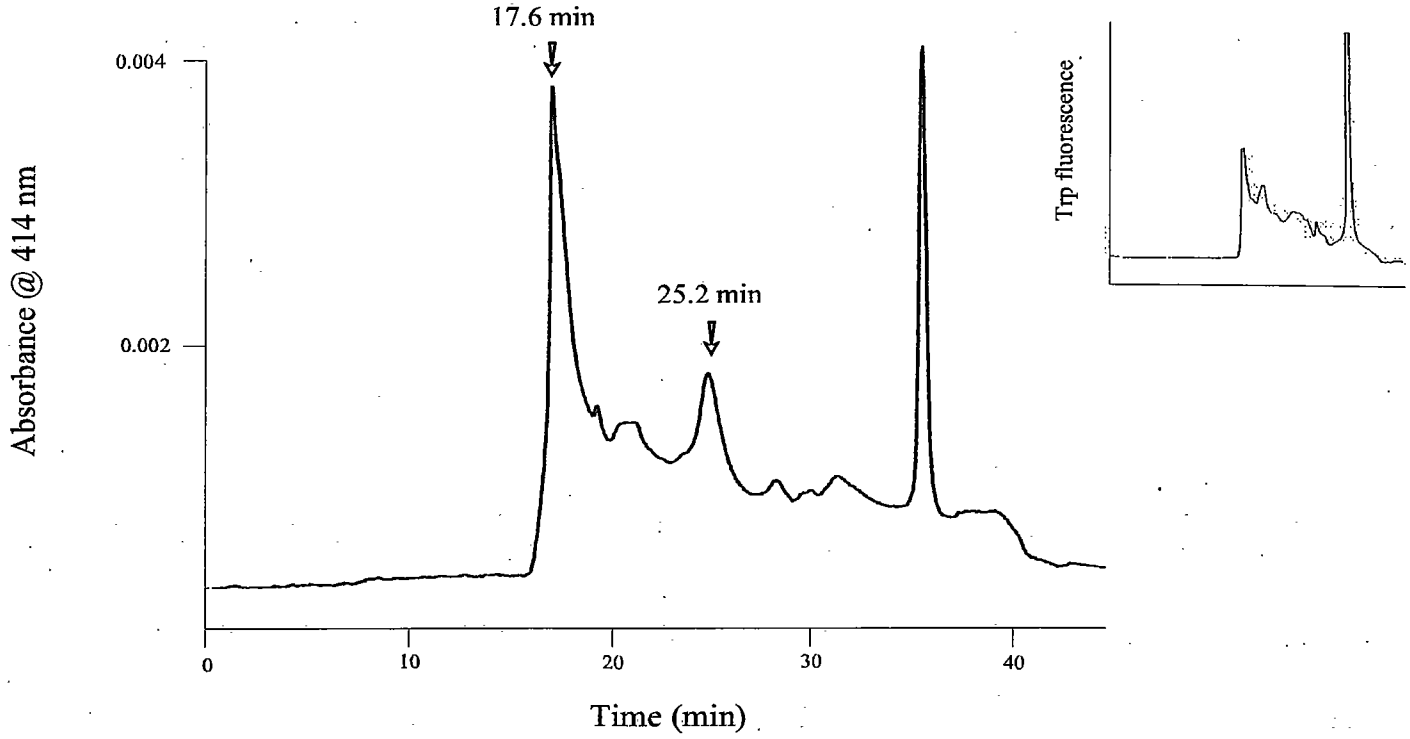


**Figure 38**. Chromatogram showing the profile of components eluted off the anion exchange / gel filtration column after injection of 300$\mu$l of 5 M NaCl following an injection of 2% OG solubilized membranes from multiple donors. Labeled peaks were found to stain specificly with antibodies 54.1, 44.1, KQS, and ARK by Western blot analysis.

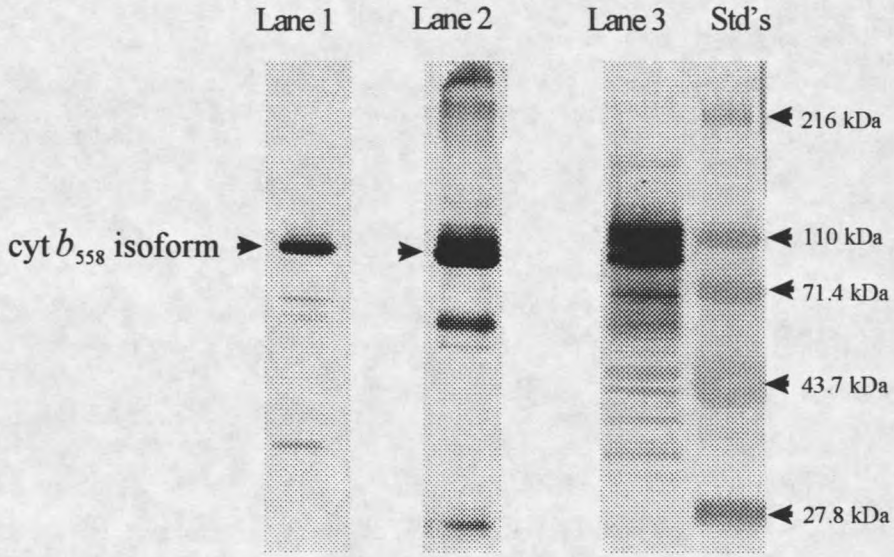


**Figure 39**. Western blot using the anti-peptide antibody α-ARK on the fractions from the peaks eluting at 17.6 and 25.2 minutes in Figure 39. The immunopurified antibodies were used at a 1:50 dilution. Lane 1 contains the fraction from the peak at 25.2 minutes with approximately 10 pmol of sample. Lane 2 contains the fraction from the peak at 17.6 minutes with approximately 20 pmol of sample. Lane 3 contains 10 pmol of the detergent solubilized membranes used for the experiment.

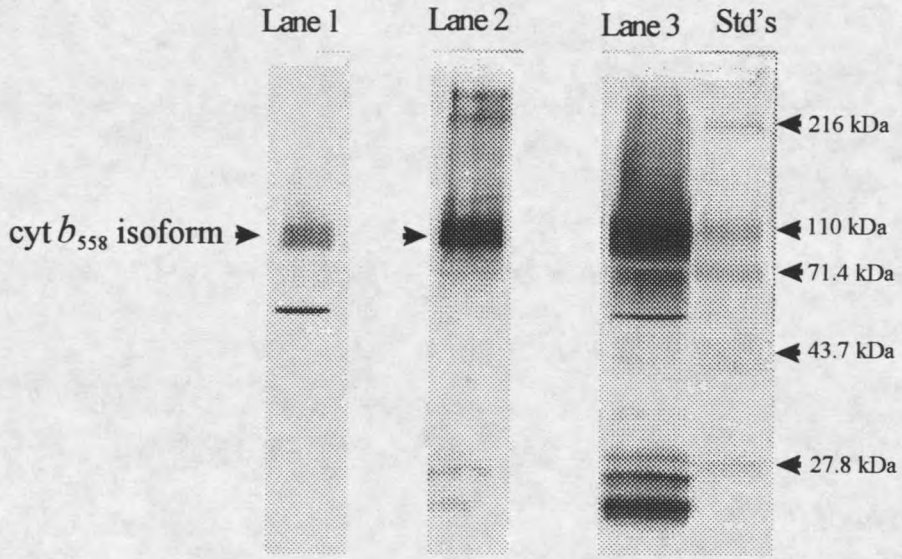


**Figure 40**. Western blot using the monoclonal antibody 54.1on the fractions from the peaks eluting at 17.6 and 25.2 minutes in Figure 39. The immunopurified antibodies were used at a 1:50 dilution. Lane 1 contains the fraction from the peak at 25.2 minutes with approximately 10 pmol of sample. Lane 2 contains the fraction from the peak at 17.6 minutes with approximately 20 pmol of sample. Lane 3 contains 10 pmol of the detergent solubilized membranes used for the experiment.

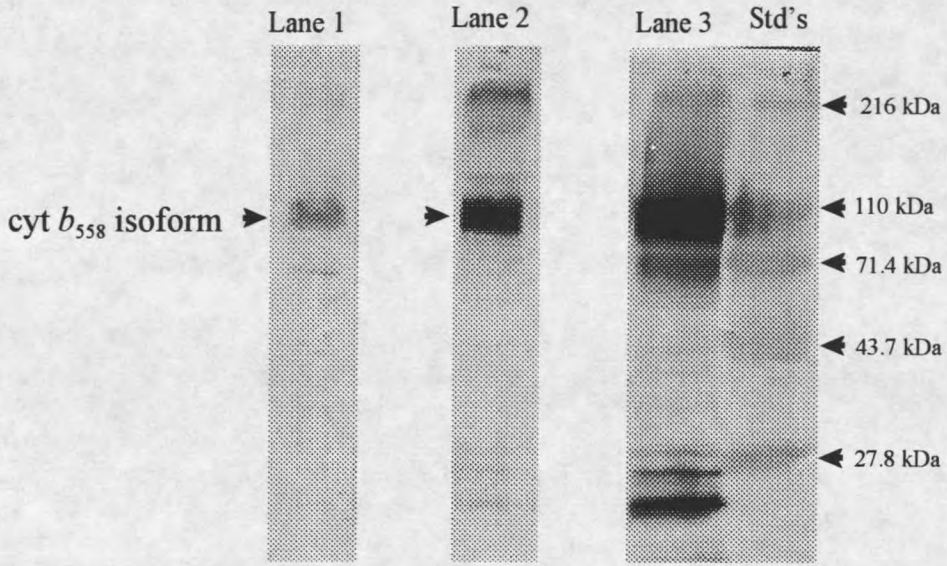


**Figure 41**. Western blot using the anti-peptide antibody KQS on the fractions from the peaks eluting at 17.6 and 25.2 minutes in Figure 39. The antibodies were used at a 1:1,000 dilution. Lane 1 contains the fraction from the peak at 25.2 minutes with approximately 10 pmol of sample. Lane 2 contains the fraction from the peak at 17.6 minutes with approximately 20 pmol of sample. Lane 3 contains 10 pmol of the detergent solubilized membranes used for the experiment

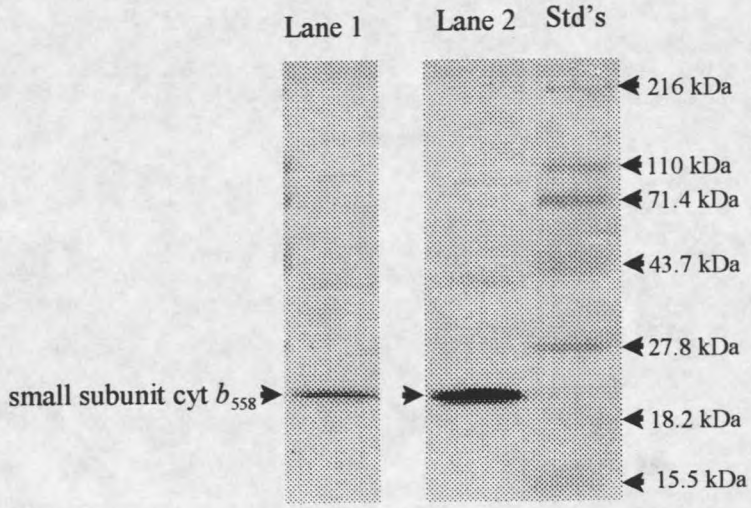


**Figure 42**. Western blot using the monoclonal antibody 44.1 on the fractions from the peaks eluting at 17.6 and 25.2 minutes in Figure 39. The antibodies were used at a 1:1,000 dilution. Lane 1 contains the fraction from the peak at 25.2 minutes with approximately 10 pmol of sample. Lane 2 contains the fraction from the peak at 17.6 minutes with approximately 20 pmol of sample.

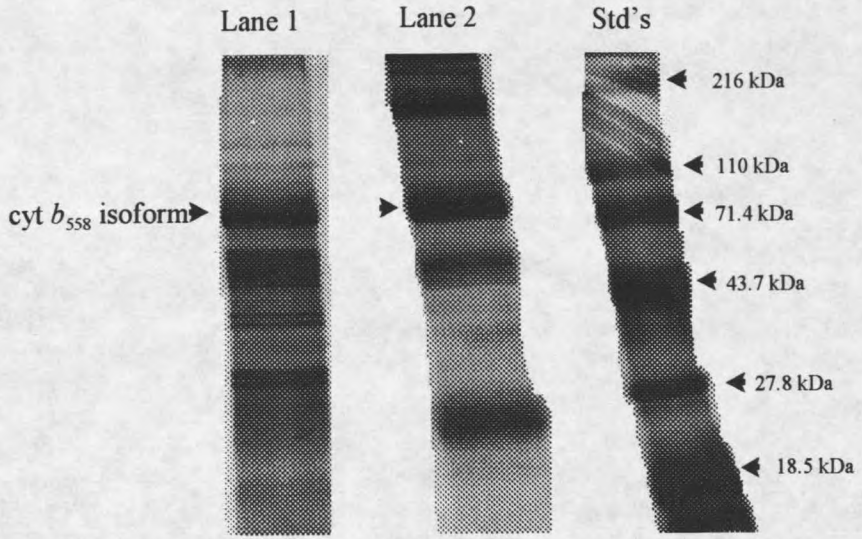


**Figure 43**. Silver stain of the fractions from the peaks eluting at 17.6 and 25.2 minutes in Figure 39. Lane 1 contains the fraction from the peak at 25.2 minutes with approximately 10 pmol of sample. Lane 2 contains the fraction from the peak at 17.6 minutes with approximately 20 pmol of sample.

kDa isoform.

Western blots of the peaks eluting at 17.6 and 25.2 minutes support the assumption that the fractions contain cytochrome $b_{558}$. The different retention times may be explained by a number of hypothesis, including aggregation, donor variability, or heterogeneous glycosylation, as seen in the silver stain in Figure 43 where there is a band at 210 kDa in the 17.6 minute fraction that is not seen in the 25.2 minute fraction. In addition, the retention time for the peak at 17.6 minutes is very close to the void volume and the highest resolvable mass of over 500,000 Da, while the retention time of 25.2 minutes is close to the retention time of ordinary cytochrome $b_{558}$ at a mass of 112,000 plus the bound detegent (10,000-20,000 Da). The difference in the retention times for the peaks having 414 nm absorbance in Figure 31 vs. Figure 38 may also be explained by the fact that the flow rate for the chromatogram in Figure 38 was a constant 0.8 ml/min instead of a ramped flow from 0.4 ml/min to 1 ml/min over 30 minutes.

The MALDI MS analysis for the fraction at 25.2 minutes is shown in Figure 44. The mass of the band with the intense staining found by Western blot analysis for the intact large subunit was again estimated to be 82 kDa by SDS-PAGE. The mass assigned to the peak using MALDI MS was found to be 82,003 Da. The mass agreement is very good when a comparison is made between mass found in the original experiment for the isoform (82,054 Da) as opposed to the mass from the second experiment (82,003 Da). The close correspondence of the MALDI MS data at ~ 82,000 Da suggests that the presence of an ion from the possible contaminant CD18 is unlikely since the mass of the primary amino acid sequence alone is for CD18 is 84,790 Da and the mass of the

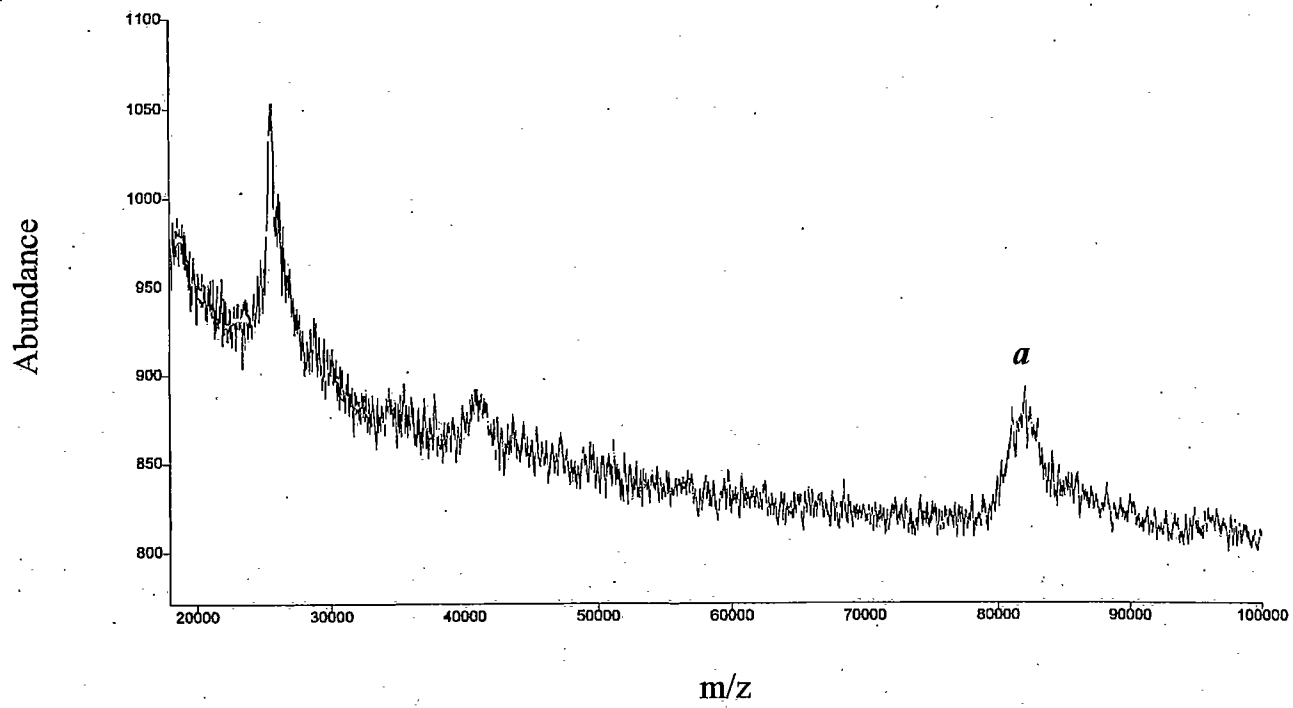


**Figure 44.** MALDI TOF mass spectrum of the cytochrome $b_{558}$ isoform from the preparation reproducing the original results. The sample was from the salt elution fraction off the anion exchange / gel filtration column representing the peak at 25.2 minutes in Figure 39. The fraction was concentrated in a Centricon 50 concentrator then mixed 1:1 v/v with acetonitrile:water:0.1% TFA before being combined with matrix. The peak labeled ***a*** signifies the isoform found in Figure 36 with an accurate mass of 82,056 Da. The difference in mass as compared to Figure 36 can be attributed to the difficulty in assigning a centroid due to less signal intensity. The spectrum represents the average of 93 laser shots.

glycosylated form of the protein is estimated to be 96,000 Da. This would require that a homogeneous fragment of at least 14,000 Da would have to be cleaved from CD18. Although this is possible, a fragment of this type has not been reported in the literature.

The absorbance spectra for the peaks at 17.6 and 25.2 minutes from this preparation were difficult to interpret. The absorbance intensity at 414 nm from the detector attached to the HPLC was well within the range for detection after concentrating the samples and rerunning them to obtain a complete absorbance spectrum. This assertion was made by comparing values observed with controls such as myoglobin, hemoglobin, and heparin purified cytochrome $b_{558}$ analyzed using the same chromatographic arrangement. However, examination of the absorbance spectra from the salt elution fractions after concentration in Centricon 50 concentrators indicated that recovery was low (~ 20% estimated by peak heights at 414 nm). This finding was interpreted to mean that the protein was no longer retaining the heme in a stable form and was thus probably unstable in the HPLC elution buffer. The stability of cytochrome $b_{558}$ in the detergent OG will be discussed further in Chapter 6.

An additional experiment performed on heparin purified cytochrome $b_{558}$, using the gel filtration column only, clearly showed a bimodal distribution for the 414 nm absorbance eluting of the gel filtration column (data not shown). These analyses indicated that a form of cytochrome $b_{558}$ was preferrentially separated from the rest of the cytochrome by the gel filtration column. The silvered stained SDS-PAGE gel and Western blot analysis using monoclonal antibodies against the large subunit (54.1) and the small subunit (44.1) blotted for the fraction that eluted at a later time while MALDI MS analysis

of the fraction resulted in a mass peak at 83,578 Da (data not shown). These findings were consistent with the masses determined for the 82 kDa protein isolated using the anion exchange / gel filtration system.

Donor Variability in the 82 kDa Isoform

Membranes from neutrophils of two individual blood donors (referred to as 'Donor X' and 'Donor Y') used in the original separation shown in Figures 31 were prepared on separate days, one week apart, using the same reagents. The membranes were solubilized at the same time and compared using Western blot analysis. Figure 45 shows the results of 2% OG solubilized membranes from each donor compared side-by-side using the antipeptide antibody α-ARK. It is clear from the blot that Donor X has the isoform present in solubilized membranes as compared to the same amount of material from Donor Y. Solubilized membranes from Donor X were applied to the anion exchange / gel filtration columns (with a 0.8 ml/min flow rate) and the separation and elution profiles were similar to those shown in Figures 37 and 38. The salt elution of the columns is shown in Figure 46 with the peaks at 17.6 and 25.3 minutes clearly evident. The reduced and the oxidized absorbance spectrum of the fraction at 25.3 minutes is shown in Figure 47 along with the reduced-oxidized spectrum shown in the inset. The shift in the Soret band at 414 nm in the oxidized spectrum to 426 nm in the reduced spectrum coupled with the appearance of the α band at 558 nm, were convincing evidence that cytochrome $b_{558}$ was present in the fraction. The reduced and oxidized spectra for the peak at 17.6 minutes also suggested the presence of cytochrome $b_{558}$ as in the fraction at 25.3

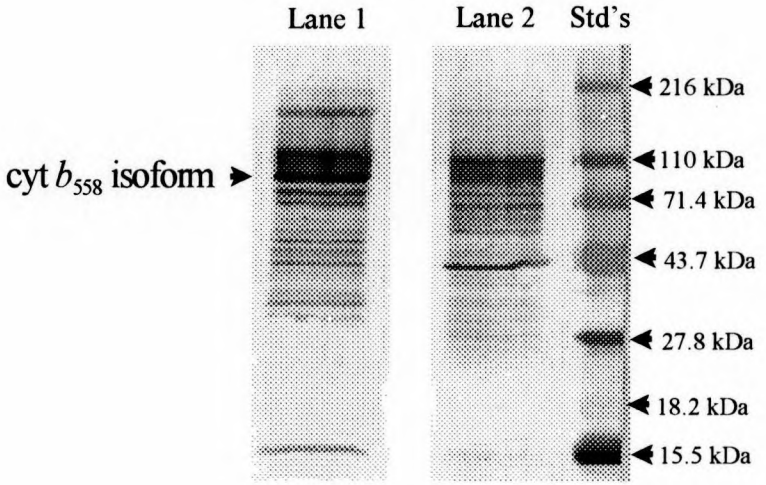


**Figure 45.** Western blot using the anti-peptide antibody ARK on detergent solubilized membranes taken separately from each of the two donors from the original cytochrome $b_{558}$ isoform preparation. The immunopurified antibodies were used at a 1:50 dilution. Lane 1 contains solubilized membranes from Donor X. Lane 2 contains solubilized membranes from Donor Y. Each lane contains an equal number of cell equivalents of membrane extract.

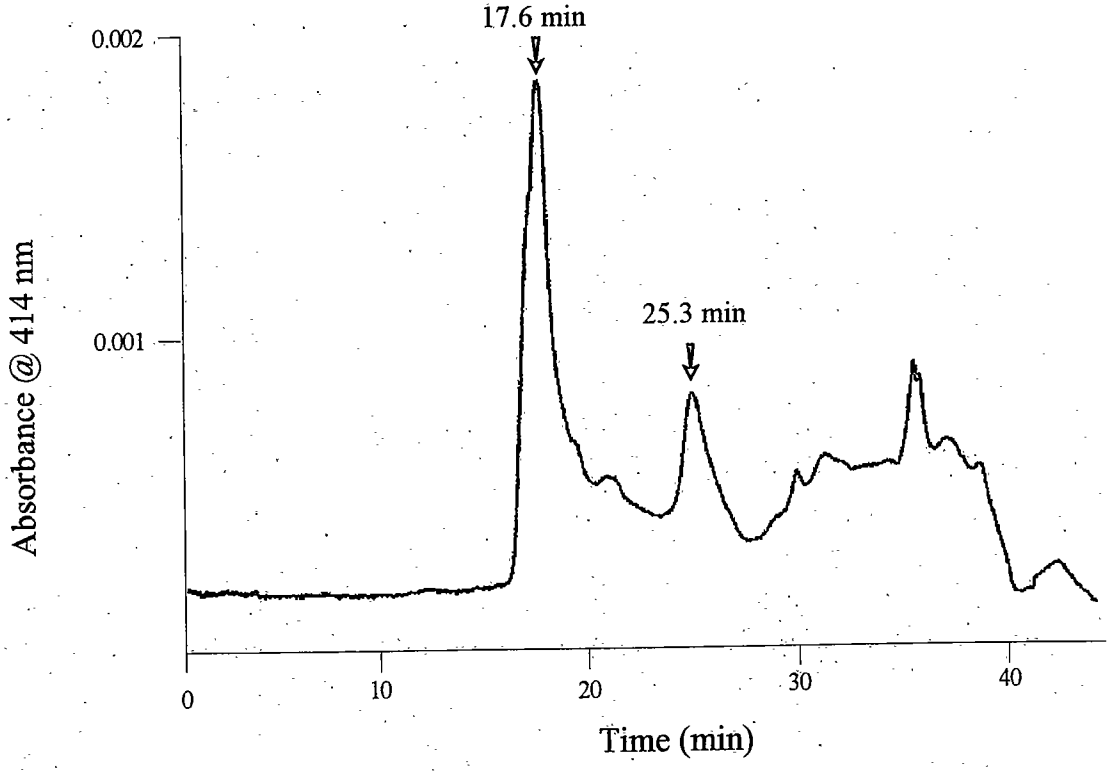


**Figure 46**. Chromatogram showing the profile of components eluted off the anion exchange / gel filtration column after injection of 300 $\mu$l of 5M NaCl following the injection of solubilized membranes from Donor X.

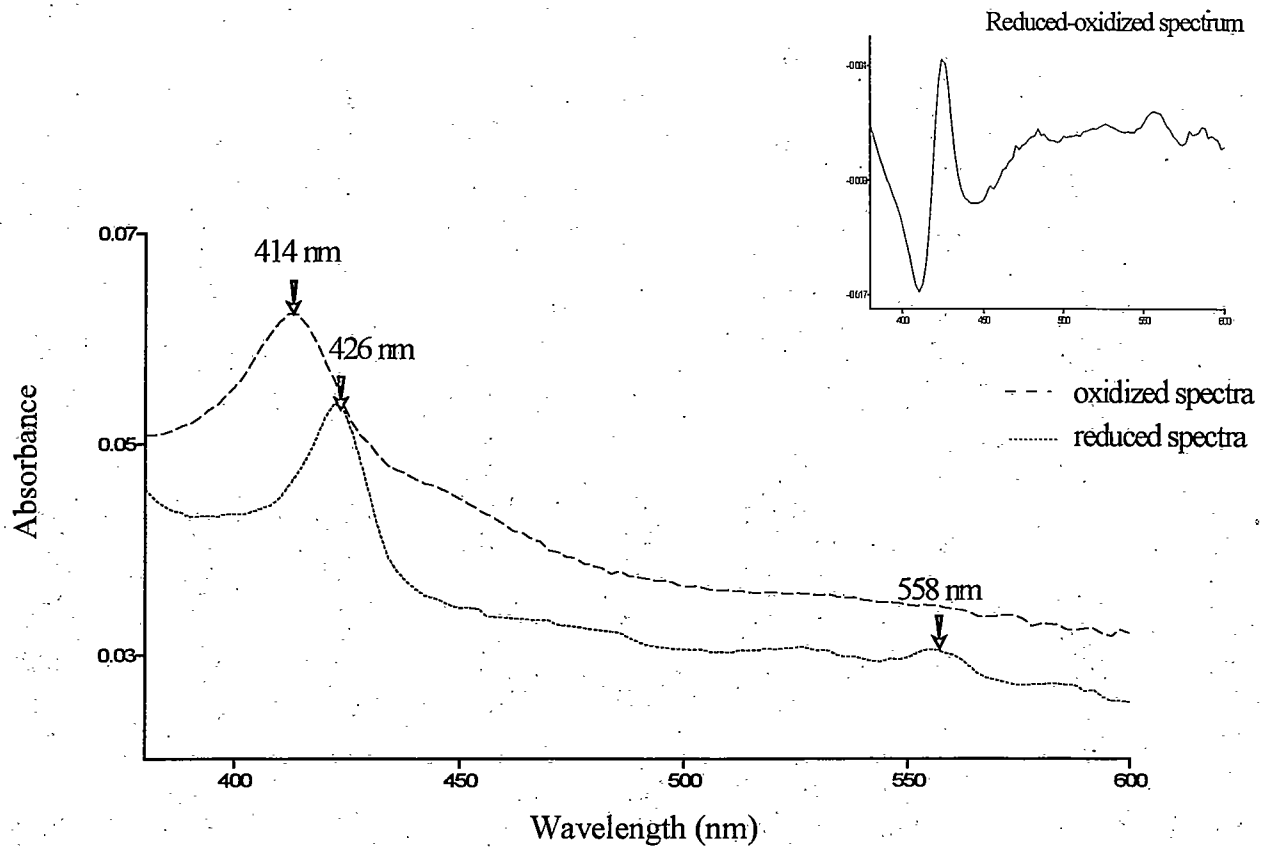


**Figure 47**. Reduced and oxidized absorbance spectra of the peak at 25.3 minutes from the salt elution off the anion exchange / gel filtration columns after the application of detergent solubilized membranes from Donor X in Figure 47. The inset shows the reduced-oxidized spectrum of the fraction with a marked decrease in the baseline at 450 nm indicating the possible presence of flavin in the sample.

minutes. However, the presence of a shoulder between 430-480 nm in Figure 47, that is lost upon reduction, is suggestive of a second component, possibly a flavin or flavoprotein. Flavins typically display absorbance spectra maxima at 450 nm and are 'bleached' to the colorless leukoform upon reduction. Since the protein is associated with the non-salt elution fraction peak at 17.6 minutes there may some non-specific interaction between the cytochrome $b_{558}$ isoform and this as yet uncharacterized component.

Due to the limited amount of sample recovered (< 40 pmol), only a small fraction (5%) was analyzed by MALDI MS and mass spectrum showed no peaks above 20 kDa. Attempts at sequencing the remaining protein by *in situ* digestion of a band excised from a SDS-PAGE gel were unsuccessful because of the presence of contaminants and insufficient yields.

Deglycosylation of the Isoform

Since the mass of the 82 kDa protein was greater than the mass of unglycosylated gp 91phox (65,204 Da), additional experiments were carried out to confirm that polypeptide of the isoform was indeed that of the large subunit. Attempts to deglycosylate the 82 kDa isoform with PNGaseF were inconclusive due to significant aggregation at $M_r$>100 kDa. Nevertheless, Western blot analysis of a deglycosylated fraction of the isoform using the antipeptide antibody KQS did indicate the presence of a band at $M_r$=57 kDa as shown in Figure 48. The molecular weight of the deglycosylated form of gp91 phox has been previously described as having a Mr≅57 kDa by SDS-PAGE 23) and further indicated the presence of cytochrome $b_{558}$ in the fraction at 17.6 minutes.

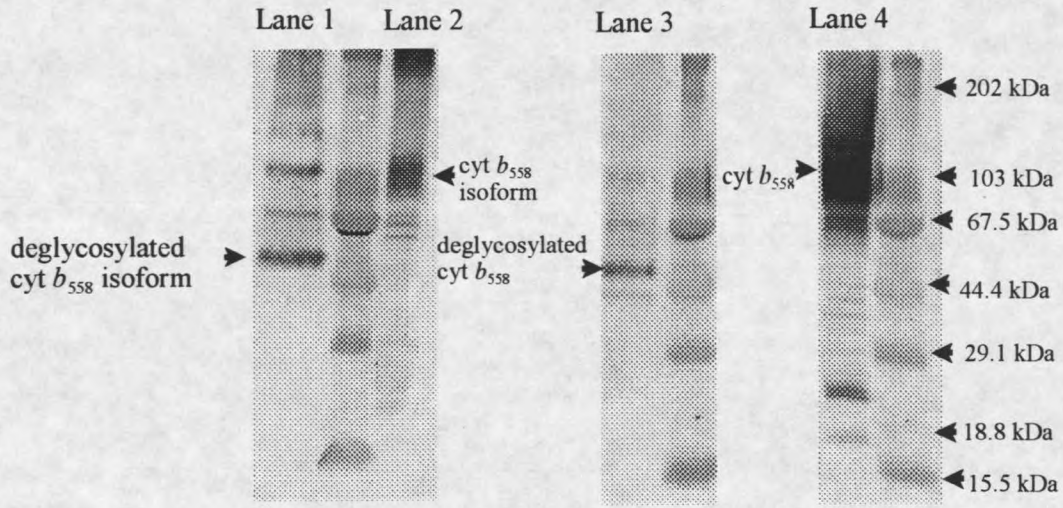


**Figure 48**. Western blot using the anti-peptide antibody α-KQS on deglycosylated 2% OG solubilized membranes from Donor X and the fraction eluting at 17.6 minutes in Figure 47. The antibody was used at a 1:500 dilution. Lane 1 contains the fraction from the peak at 17.6 minutes after deglycosylation. Lane 2 contains the fraction from the peak at 17.6 before deglycosylation. Lane 3 contains the detergent solubilized membranes after deglycosylation while Lane 4 contains the detergent solubilized membranes before deglycosylation.

## Discussion

To find alternative approaches to the purification of cytochrome $b_{558}$ the use of HPLC tandem anion exchange / gel filtration was examined. The method was designed to reduce preparation time post-solubilization which reduces the amount of denatured or partially digested end product. This is an important consideration when purifying proteins found in neutrophils since this cell type contains large amounts proportion of endogenous proteases. The effects of protease activity are mitigated by the use of protease inhibitors before and after cell disruption, yet the protease content is so high (>10% of cellular proteins) that inhibitors often do not completely inhibit their activity. The use of a method that decreases the amount of time involved in purifying a protein can aid in offsetting the effects of residual protease activity. High performance liquid chromatography has been used in many cases for the purification of detergent solubilized membrane proteins (20-22). The time that is saved in using HPLC (typically on the order of hours for purification times vs. days for standard techniques) can result in a purified sample that contains fewer proteolytic fragments.

The approach described in this chapter of obtaining purified cytochrome $b_{558}$ by HPLC tandem anion exchange / gel filtration chromatography resulted in the identification of a novel species of protein with an accurate mass of 82,054 Da as determined by MALDI MS. This protein exhibited spectral properties similar to cytochrome $b_{558}$ along with blotting activity by Western blot analysis. An accurate mass of the intact large subunit of cytochrome $b_{558}$, using mass spectrometry, has never been published and this approach suggested a method for obtaining an accurate mass of an isoform of cytochrome $b_{558}$. The

existence of a stable homogeneously glycosylated form of cytochrome $b_{558}$ has also never been reported and could have important implications for the function of NADPH oxidase in the host.

The data acquired from Western blot analyses implied that the 82 kDa protein contained the epitopes specific for the antibodies used to probe the samples. However, it was later found although the anti-ARK peptide antibody specifically recognized gp91-*phox*, it was also shown to cross react with purified CD18 (data not shown). In spite of this ambiguity, the identity of this isoform was confirmed by alternative methods as shown in Figures 39-41 where this isoform was clearly labeled by three different α-gp91-*phox* antibodies. Since MALDI MS spectra along with the silver stained SDS-PAGE gels indicate that there is only one component in the molecular weight range of the 82 kDa protein in this isolation, the results strongly suggest that the 82 kDa protein is an isoform of cytochrome $b_{558}$.

As mentioned in the introduction to this chapter, the molecular weight of the large subunit of cytochrome $b_{558}$ exhibits heterogeneity in the glycosylation. This heterogeneity produces a 'fuzzy' band when the protein is stained in an SDS-PAGE gel or analyzed by Western blot analysis. However, purification strategies published by other authors have shown the existence of a band at approximately 82 kDa when probed by Western blot analysis, similar to the isoform discussed in this chapter. Most striking is the prevalence of the homogeneous band at 82 kDa seen in CGD patients that possess mutated forms of cytochrome $b_{558}$ in the membranes of their neutrophils described by Cross et al. (23). In this study the CGD patient displayed a missense mutation in the large subunit resulting in

arginine 54 being changed to a serine. This mutation creates a situation in the protein where the FAD bound to the large subunit is reduced by accepting electrons from NADPH, but the electron is not transferred to $O_2$ via heme to generate superoxide. The other CGD patient described had a mutation where proline 415 is changed to a histidine and the electron from NADPH is never accepted by FAD. Although neither mutation involved potential glycosylation sites, both of these patients possessed a protein that showed staining centered on a molecular weight of roughly 82 kDa when detergent solubilized membranes were probed with an affinity purified rabbit polyclonal anti-peptide antibody. Detergent solubilized membranes from typical X-linked CGD patients showed no staining in this region when probed with the same antibody.

In an experiment by Segal et al., membranes from the patient with the missense mutation in the large subunit were examined after being exposed to $P^{32}$ labeled NADPH. In this experiment a band at 82 kDa was clearly present after development of the gel containing the labeled cytochrome $b_{558}$ from this patient (24). These studies suggest that numerous examples exist in which cytochrome $b_{558}$ displays an 'anomalous' $M_r$. under appropriate conditions the $M_r$ observed by SDS-PAGE.

Additional experiments must be performed to prove that the 82 kDa protein is an isoform of cytochrome $b_{558}$ that is present in certain individuals. The quickest, most promising approach incorporates mass spectrometric analysis of deglycosylated 82 kDa protein and deglycosylated large subunit of "conventional" cytochrome $b_{558}$. The benefits of refining an experiment of this type are several. First, if the masses of the deglycosylated forms of both the 82 kDa protein and the large subunit of cytochrome b558 were identical,

this would prove that they were from the same polypeptide chain. Second, an accurate mass of the deglycosylated protein defined using MALDI or ESI MS could be used to evaluate the presence of post-translational modifications within the protein and possibly even the presence of polymorphisms in purified cytochrome $b_{558}$ from single donors. Thirdly, deglycosylated protein would also be an ideal starting point for peptide mapping studies. The ability to identify unknown proteins from a gel slice using the accurate mass of proteolytic peptides found using mass spectrometry, is a powerful technique for protein characterization. However, if the protein contains multiple sites of glycosylation, it is difficult to compare the masses of the glycosylated peptides with the known amino acid sequence since the masses will be different. Therefore, it is easier to generate a peptide map from a deglycosylated protein.

Lastly, it would be useful to screen an extensive number of donors individually to repeat the findings found in Figure 45. This screen would serve to give a broader view of the distribution of this protein (i.e. sex, age) and could possibly identify changes in mass associated with atypical glycosylation of the protein. A preliminary experiment using membranes from normal donors and a CGD patient, probed with the anti-large subunit antibodies KQS and ARK, indicated that the 82 kDa fragment was present in the normal donors but not in the CGD patient.

To conclude, the identity of the 82 kDa protein has not been unequivocally established. The data presented in this chapter strongly favor this protein being an isoform of cytochrome $b_{558}$, nonetheless, without sequence data the identity of this protein remains unproven.

## References


1. Parkos, C. A., A. A. Allen, C. G. Cochrane, and A. J. Jesaitis. 1987. Purified cytochrome b from human granulocyte plasma membrane is comprised of two polypeptides with relative molecular weights of 91,000 and 22,000. *J. Clin. Invest.* 80:732-742.

2. Green, T. R. and K. L. Pratt. 1988. Purification of the solubilized NADPH:$O_2$ oxidoreductase of human neutrophils. Isolation of its catalytically inactive cytochrome b and flavoprotein redox centers. *J. Biol. Chem.* 263:5617-5623.

3. Lutter, R., M. L. J. van Schaik, R. V. van Zwieten, R. Wever, D. Roos, and M. N. Hamers. 1985. Purification and partial characterization of the *b*-type cytochrome from human polymorphonuclear leukocytes. *J. Biol. Chem.* 260:2237-2244.

4. Markert, M., G. A. Glass, and B. M. Babior. 1985. Respiratory burst oxidase from human neutrophils: Purification and some properties. *Proc. Natl. Acad. Sci. U. S. A.* 82:3144-3148.

5. Huang, J., N. D. Hitt, and M. E. Kleinberg. 1995. Stoichiometry of p22-phox and gp91-phox in phagocyte cytochrome b558. *Biochemistry* 34:16753-16757.

6. Segal, A. W. 1987. Absence of both cytochrome $b_{245}$ subunits from neutrophils in X-linked chronic granulomatous disease. *Nature* 326:88-91.

7. Kleinberg, M.E., Rotrosen, D., and Malech, H.L. 1989. Asparigine-linked glycosylation of cytochrome $b_{558}$ large subunit varies in different human phagocytic cells. *J.Immunol.* 143:4152-4157.

8. O'Connor, S. E. and B. Imperiali. 1996. Modulation of protein structure and function by asparagine-linked glycosylation. *Chem. Biol.* 3:803-812.

9. Kobata, A. 1992. Structures and functions of the sugar chains of glycoproteins. *Eur. J. Biochem.* 209:483-501.

10. Wyss, D. F. and G. Wagner. 1996. The structural role of sugars in glycoproteins. *Curr. Opin. Biotechnol.* 7:409-416.

11. Dinauer, M. C., S. H. Orkin, R. Brown, A. J. Jesaitis, and C. A. Parkos. 1987. The glycoprotein encoded by the X-linked chronic granulomatous disease locus is a component of the neutrophil cytochrome b complex. *Nature* 327:717-720.

12. Parkos, C. A., M. C. Dinauer, L. E. walker, R. A. Allen, A. J. Jesaitis, and S. H. Orkin. 1988. Primary structure and unique expression of the 22-kilodalton light chain of human neutrophil cytochrome *b*. *Proc. Natl. Acad. Sci. U. S. A.* 85:3319-3323.

13. Wallach, T. M. and A. Segal. 1997. Analysis of glycosylation sites on gp91phox, the flavocytochrome of the NADPH oxidase, by site-directed mutagenesis and translation *in vitro*. *Biochem. J.* 321:583-585.

14. LeBon, T.R., Jacobs, S., Cuatrecasas, P., Kathuria, S., and Y. Fujita-Yamaguchi. 1986. Purification of insulin-like growth factor I receptor from human placental membranes. *J.Biol.Chem.* 261:7685-7689.

15. Quinn, M. T., C. A. Parkos, and A. J. Jesaitis. 1995. Purification of human neutrophil NADPH oxidase cytochrome b-558 and association with Rap 1A. *Methods Enzymol.* 255:476-487.

16. Nauseef, W.M., Olsson, I., and K. Arnljots. 1988. Biosynthesis and processing of myeloperoxidase--a marker for myeloid cell differentiation. *Eur.J.Haematol.* 40:97-110.

17. Towbin, H., T. Staehelin, and J. Gordon. 1979. Electrophoretic transfer of proteins from polyacrylamide gels to nitrocellulose sheets: Procedure and some applications. *Proc. Natl. Acad. Sci.* 76:4350-4354.

18. Bokoch, G. M., L. A. Quilliam, B. P. Bohl, A. J. Jesaitis, and M. T. Quinn. 1991. Inhibition of Rap1A binding to cytochrome b558 of NADPH oxidase by phosphorylation of Rap1A. *Science* 254:1794-1796.

19. Quinn, M.T., Parkos, C.A., and A. J. Jesaitis. 1995. Purification of human neutrophil NADPH oxidase cytochrome b-558 and association with Rap 1A. *Methods Enzymol.* 255:476-487.

20. Miyasaki, K. T., M. E. Wilson, E. Cohen, P. C. Jones, and R. J. Genco. 1986. Evidence for and partial characterization of three major and three minor chromatographic forms of human neutrophil myeloperoxidase. *Arch. Biochem. Biophys.* 751-764.

21. Wearsch, P.A. and C. V. Nicchitta. 1996. Purification and partial molecular characterization of GRP94, an ER resident chaperone. *Protein Expr.Purif.* 1:114-121.

22. Kumar, V., Heinemann, F.S., and J. Ozols. 1995. Purification and characterization of hepatic oligosaccharyltransferase. *Biochem.Mol.Biol.Int.* 36:817-826.

23. Cross, A. R., P. G. Heyworth, J. Rae, and J. T. Curnutte. 1995. A variant X-linked chronic granulomatous disease patient ($X91^+$) with partially functional cytochrome b. *J. Biol. Chem.* 270:8194-8200.

24. Segal, A. W., I. West, F. Wientjes, J. H. Nugent, A. J. Chavan, B. Haley, R. C. Garcia, H. Rosen, and G. Scrace. 1992. Cytochrome b-245 is a flavocytochrome containing FAD and the NADPH-binding site of the microbicidal oxidase of phagocytes. *Biochem. J.* 284P781-8:781-788.

# Chapter 6

## STUDIES ON THE ISOLATION and CHARACTERIZATION OF HEME CONTAINING FRAGMENTS FROM PARTIALLY DIGESTED HUMAN NEUTROPHIL CYTOCHROME $b_{558}$

### Introduction

Cytochrome $b_{558}$ is an integral membrane protein found in the membranes of phagocytic leukocytes and is part of an enzymatic system known as NADPH oxidase. The oxidase consists of several different proteins that form a complex that ultimately transfers electrons from NADPH to molecular oxygen (1). The transfer of electrons to molecular oxygen results in the production of the potent microbicide superoxide ($O_2^-$). This molecule must be present for neutrophils to perform their task of protecting the host from invading pathogens, most notably bacteria and fungi. As its name suggests, the protein contains

heme involved in the transfer of electrons from intracellular NADPH to oxygen in phagosomes or extracelluarly. Cytochrome $b_{558}$ functions as an electron transferase (2,3) shuttling high energy electrons across the lipid bilayer as part of the reaction;

$$NADPH + 2O_2 \rightarrow NADP^+ + H^+ + 2O_2^-$$

Structural characterization of human neutrophil cytochrome $b_{558}$ has been hampered by several problems. Since it is an integral membrane protein it requires detergent for isolation and purification. Integral membrane proteins have been exceedingly difficult to crystallize in detergents thus generation of an x-ray crystal structure for cytochrome b558 is not feasible at this time. Protease sensitivity of the protein during purification has also been a problem because of the high concentration of endogenous proteases in neutrophils. Although these proteases are responsible for degradation of engulfed microbes, they degrade endogenous proteins once the cell is disrupted (1). The choice of detergent is critical if the protein is to retain its native conformation once it is solubilized from the cell membrane. If cytochrome $b_{558}$ is solubilized in a detergent that destabilizes the protein, the absorbance spectrum degrades indicating that the protein is no longer in a functional state. Thus, any inferences about the tertiary structure from such a preparation become difficult to make. These factors have combined to significantly hinder structural studies of cytochrome $b_{558}$.

The name given to cytochrome $b_{558}$ is derived from the reduced minus oxidized alpha absorbance spectrum at 558.5 nm, characteristic of plasma membrane b-type cytochromes (4-6). However, the protein has also been called cytochrome $b_{559}$, neutrophil cytochrome b, and cytochrome $b_{-245}$ in reference to its low midpoint potential of -245 mV,

which is the lowest reported for any known mammalian cytochrome (7,8). Recently the name flavocytochrome b has been adopted because it binds FAD, has activity when reconstituted in liposomes with FAD, and shares homology with other flavoproteins (9-11). A variety of molecular weights for the intact protein, ranging from 11,000 to 127,000 Da, were reported from initial attempts at purifying the protein (6,12-14). Finally, purification by Parkos et al. yielded a pure ( >90 %) heterodimer consisting of a glycosylated large subunit, named gp 91-phox, with $M_r$= 91,000 Da and a non-glycosylated small subunit, named p 22-phox, with $M_r$= 22,000 Da (5). Purification of cytochrome $b_{558}$ permitted identification of the large subunit as the X-linked gene product that is missing or defective in chronic granulomatous disease or CGD. Neutrophils from persons inflicted with certain X-linked and autosomal recessive forms of this disease do not produce superoxide. In addition, detergent solubilized membranes from neutrophils of these persons do not exhibit the absorbance spectrum indicative of cytochrome $b_{558}$. An experiment performed using antibodies against sequence specific synthetic peptides and fusion proteins found that the antibodies recognized both purified gp 91-phox and cDNA derived material (2,15). The absence of the small subunit in CGD was later shown to result in the autosomal recessive form of the disease where mutations in the gene locus on chromosome 16 encoding p 22-phox results in nonfunctional cytochrome $b_{558}$ (16). These results, and others, led to the conclusion that cytochrome $b_{558}$ was indeed the electron transferase ultimately responsible for transferring electrons from NADPH to molecular oxygen (17,18).

Until recently, the stoichiometry of the heme prosthetic groups that reside in cytochrome $b_{558}$ was unknown. Early work by Iizuka et al. found spectral evidence for two hemes in different environments determined by the splitting of the α band in PMA stimulated porcine neutrophils (19). Later, Parkos et al. calculated a stoichiometry of at least 2:1 heme:protein in purified cytochrome $b_{558}$ by comparing the amount of purified protein with the extinction coefficient for the heme determined by the pyridine hemochrome assay (5,12). Additional work by Quinn et al. confirmed that there were at least two hemes present in cytochrome $b_{558}$ (20). The authors found that heme remained associated with both the large and small subunits when separated by LDS-PAGE carried out at 0°C followed by tetramethylbenzidine (TMBZ/$H_2O_2$) staining of heme present in the gel. Recently a study by Cross et al. supported the existence of two non-identical hemes in cytochrome $b_{558}$ by studying the redox titration curve from a patient having $X^+$ CGD (21). The protein this patient expressed had an absorbance spectrum similar to normal cytochrome $b_{558}$. However, the protein did not produce superoxide due to a $Arg^{54}$→ Ser mutation (22). Redox titrations were followed by the change in absorbance at 559 nm vs. the half-cell potential relative to a saturated calomel reference electrode. Comparison of theoretical Nernst titration curves for a single component redox center with the observed curves from the patient's cytochrome $b_{558}$ clearly showed that the curves were a composite of two non-identical hemes. Results from the same study also showed that cytochrome $b_{558}$ from normal donors exhibited titration curves indicative of two redox centers.

In spite of the importance of this protein and the intense activity focused on it, the locations of the hemes within this heterodimeric protein are still unknown. Several research groups have tried to evaluate the location of the heme prosthetic groups in cytochrome $b_{558}$ by using electron paramagnetic resonance spectroscopy (EPR) (11,23-30), resonance Raman spectroscopy (RR) (25,28), and near-infrared magnetic circular dichroism spectroscopy (NIR-MCD) (28). Hurst et al. were the first to publish EPR and resonance Raman spectra of cytochrome $b_{558}$ from human neutrophils. Their work suggested that multiple, closely-spaced hemes were present in the oxidase bound through bis-histidinyl ligation (25). Recent studies by Fujii et al. have maintained that only histidines are involved in axial ligation of the heme prosthetic groups in purified cytochrome $b_{558}$ from pig (porcine) neutrophils (28-30). The authors also contend that the iron in the heme is in a low-spin state as determined by electron paramagnetic resonance spectroscopy. These results are in accordance with other studies using EPR and RR to probe the structure of porcine cytochrome $b_{558}$, but their addition of NIR-MCD spectral data provided more evidence for bis-histidine ligation of the hemes due to the strong charge transfer bands at wavelengths similar to molecules with known bis-histidine ligation (28).

Work by Segal et al., Hurst et al., and Doussiere et al. (11,25,26) are the only published studies examining the EPR spectrum of purified human cytochrome $b_{558}$. Data from the investigations of Hurst et al. and Segal et al. suggested that the hemes are coordinated in the molecule by low-spin bis-histidine ligation. However, Doussiere et al. report the finding of a transient high-spin pentcoordinated form after addition of

arachidonic acid. The published EPR spectra for porcine (Fujii et al.) and human cytochrome $b_{558}$ (Hurst et al. and Segal et al.) are difficult to compare. For example, the experiments performed by Hurst et al. used much less material than the experiments done by Fujii et al. Therefore the signal obtained by Hurst and coworkers is weaker and the published spectrum does not resemble published spectra of porcine cytochrome $b_{558}$. Nonetheless, resonance Raman spectra from the Hurst publication does appear to be similar to that of porcine cytochrome $b_{558}$. EPR spectral data published by Segal et al., using more material that Hurst and coworkers, does not show a complete EPR spectrum, yet the region that is published is somewhat similar to the EPR spectra of porcine cytochrome $b_{558}$.

It is likely that the spectral data using porcine cytochrome $b_{558}$ is valid for human cytochrome $b_{558}$ since the amino acid sequences are quite similar (e.g. the large subunit has 92.1% identity between species while the small subunit has 83% identity). Since blood from pigs is much easier to obtain than blood from humans, it is not surprising that this source of cytochrome $b_{558}$ has been used extensively. However, all the data concerning mutations in the protein, along with a majority of the data pertaining to interactions of cytochrome $b_{558}$ with cytosolic components, involve human sources (1). Thus, any unequivocal structural information regarding the location of the hemes within human cytochrome $b_{558}$ should come from human protein.

In terms of sequence homology with other non-human heme containing proteins, there is some evidence for the large subunit of cytochrome $b_{558}$ being a part of the reductase family of proteins, especially with a FRE 1 ferric reductase found in the

membranes of *Saccharomyces cerevisiae* (31,32). In spite of this similarity, there is still no clear role for the small subunit in relation to heme-binding, even though it has some homology to heme-binding proteins such as myoglobin, polypeptide I from cytochrome $b_5$ from endoplasmic reticulum, and plant mitochondrial b-type cytochromes (18,33). In addition, the only study to date that has evaluated the location of the hemes in human cytochrome $b_{558}$, by actually identifying fragments of the protein having heme associated with them, is the work by Quinn et al. (20).

With the location of the heme-binding domains in cytochrome $b_{558}$ still uncertain, experiments were designed with two objectives in mind; 1) confirm the small subunit involvement in the heme-binding and 2) determine the heme-binding domains of the large subunit. This chapter describes experiments leading to the isolation of heme-binding domains from partially purified human neutrophil cytochrome $b_{558}$.

## Materials and Methods

### Detergent Solubilization of Cytochrome $b_{558}$

Neutrophils membranes used for this study were from normal human donors and were prepared following the procedure of Parkos et al. Membranes frozen at -80°C were thawed on ice and salt washed by making the suspension 1 M in NaCl in order to disrupt most ionic interactions of non-membrane components with the membranes. The suspension was thoroughly mixed with a vortex mixer, to ensure mixing of the salt with the membranes, and then centrifuged at 100,000 g for 45 minutes at 4°C. The clear green-yellow colored supernatant was removed and the salt washing step was repeated to more

thoroughly extract any non-membrane bound proteins, primarily myeloperoxidase, which is another heme-bearing component of neutrophils (34). The tan colored pellet was suspended in membrane resuspension buffer (MRB) consisting of relax buffer pH 7.4 with 1 mM EDTA, 0.1 mM DTT, 1 mM phenylmethylsulfanofluoride (PMSF), and 10 $\mu$g/ml chymostatin and 2% octylglucoside. Sonication was used to disrupt the membranes and complete solubilization was accomplished by allowing the solution to mix at 4°C on ice for 1 hour. The detergent solubilized membranes were then centrifuged at 100,000 g for 45 minutes and the amount of cytochrome $b_{558}$ present was determined by absorbance spectroscopy, using an extinction coefficient of 29.3 $mM^{-1}$ $cm^{-1}$ for the reduced minus oxidized alpha band at 558 nm or 131 $mM^{-1}$ $cm^{-1}$ for the oxidized Soret band.

Purification of Cytochrome $b_{558}$

Cytochrome $b_{558}$ was purified from detergent solubilized neutrophil membranes by the method of Parkos et al. using wheat germ agglutinin-conjugated Sepharose affinity chromatography and heparin ion exchange chromatography (5). In order to make the preparation more amenable to accurate mass analysis by MALDI MS, some of the preparations contained octylglucoside in all buffers used throughout the purification process. Other purification preparations, using OG solubilized membranes as the starting material, later switched to Triton X-100 as the solubilizing detergent during the purification procedure according to the same method.

Partial Digestion of Intact Cytochrome $b_{558}$

Heparin fractions containing purified cytochrome $b_{558}$ solubilized in either octylglucoside or Triton X-100 in relax buffer pH 7.4, were subjected to partial digestion with sequencing grade *S. aureus* protease V8 or trypsin from Boehringer Mannheim, Germany. The heparin column eluate fractions were pooled and then incubated with protease at various enzyme to substrate ratios ranging from 1:50 to 1:12 w/w. Protease inhibitors were not used in the heparin column elution buffer in order to avoid inactivation of the protease. In addition, samples containing greater than 600 mM NaCl were diluted and concentrated with heparin column elution buffer to give a NaCl concentration of 500 to 600 mM. Digestions were carried out for 60 minutes at 37°C and absorbance spectra were taken at 5 to 10 minute intervals during the digestion. Samples were treated with 1 mM PMSF to inactivate the residual protease, then centrifuged at 10,000 g for 5 minutes to remove any insoluble material before being subjected to gel filtration chromatography.

Gel Filtration Chromatography

All chromatography was performed on a Hitachi Model L-2500 HPLC system with a Model L-4200 UV/VIS variable wavelength detector set at 414 nm. A Hitachi Model F-1050 on-line fluorescence spectrophotometer was also used to monitor tryptophan fluorescence with excitation at 300 nm and emission monitored at 360 nm. A TosoHaas model TSK G3000SW 75mm x 60 cm gel filtration column was used to separate the proteolytic fragments. The buffers used for the runs were; Buffer A:1% octylglucoside, 5 mM HEPES pH 7.4, 0.02% $NaN_3$ and Buffer B:1 M ammonium acetate, 5 mM HEPES

pH 7.4, 0.02% $NaN_3$. The runs were isocratic containing 90% Buffer A and 10% Buffer B and a flow rate of 0.8 ml/min. Fractions were collected at 1 minute intervals.

UV / VIS Absorbance Measurements

All absorbance measurements were performed on a Hewlett Packard Model 8452A diode array spectrophotometer. The cuvette used had a 1 cm pathlength and required a minimum of 140 $\mu$l sample. Reduced minus oxidized spectra were obtained by adding 4 $\mu$l of a freshly made 1 M stock of sodium dithionite to the oxidized solution to fully reduce the heme. Fractions having absorbance at 414 nm, as determined by the chromatogram from the gel filtration run, were concentrated ~6 fold in a Centricon 10 with a 10 kDa molecular weight cut-off prior to analysis. All concentrations were determined by using the extinction coefficients of 131 $mM^{-1}$ $cm^{-1}$ for the oxidized Soret band at 414 nm, 161 $mM^{-1}$ $cm^{-1}$ for the reduced-minus oxidized band at 426 nm, and 29.3 $mM^{-1}$ $cm^{-1}$ for the reduced-minus oxidized band at 558 nm (12).

SDS-PAGE Electrophoresis

SDS-PAGE was performed using slab gels 1.5 mm x 8 cm x 20 cm having an acrylamide gradient of 7-18% and containing 0.1% SDS. Fractions from the gel filtration column were mixed 1:1 v/v with sample buffer consisting of 1 part 10% SDS, 1 part 0.5 M Tris base pH 6.8, 1 part glycerol, and 500 mM 2-mercaptoethanol. Samples were then placed on the gel without boiling and run with standards using 15 or 28 lane combs. Gels were then silver stained under acidic conditions or analyzed by Western blot analysis.

Western Blot Analysis

Proteins bands in SDS-PAGE gels were electrophoretically transferred to nitrocellulose according to the procedure described by Towbin (35). Nitrocellulose retaining the blotted proteins was blocked with blocking buffer, consisting of 5% non fat dry milk and 0.2% Tween 20 in PBS pH 7.4, overnight at 4°C or for 3 hours at 37°C. Primary antibodies were applied to the blots in antibody diluting buffer consisting of 3% normal goat serum, 1% BSA and 0.2% Tween at various dilutions.

Primary antibodies were incubated for 3 hours at room temperature. Non-specifically bound primary was rinsed off the blot using wash buffer containing 250 mM NaCl, 10 mM HEPES pH 7.4, and 0.2% Tween with a total of 5 washes at 5 minute intervals. The secondary antibodies were alkaline phosphatase-conjugated goat anti-mouse or goat anti-rabbit IgG, applied at a dilution of 1:1,000 v/v in diluting buffer, and incubated for 1 hour at room temperature. After rinsing with a total of 4 washes, a fifth wash was performed using alkaline Tris-buffered saline at pH 8.0. Development was performed using BCIP/NBT as substrates. The reaction was halted by rinsing with distilled water.

Affinity Labeling Using Wheat Germ Agglutinin-Conjugated Cascade Blue

Proteins bands in SDS-PAGE gels were electrophoretically transferred to nitrocellulose according to the procedure described by Towbin (32). Immobilized samples were then blocked with 4% BSA in phosphate buffered saline solution for 2 hours at room temperature. The samples were then incubated with 200$\mu$g of wheat germ agglutinin conjugated-Cascade Blue fluorescent probe (Molecular Probes, Eugene, OR) for 2 hours

in the dark at room temperature. The nitrocellulose blot was then washed with wash buffer containing 250 mM NaCl, 10 mM HEPES pH 7.4, and 0.2% Tween with a total of 5 washes at 5 minute intervals. Fluorescently labeled WGA was viewed by illuminating blots with UV light and then recorded by photographing the blot with a Polaroid camera using ASA 700 Polaroid film.

Mass Spectrometry

MALDI mass spectra were obtained on a PerSeptive Biosystems / Vestec Voyager RP TOF mass spectrometer (PerSeptive Biosystems, Framingham, MA) as described in Chapter 2. The spectra were obtained in linear mode with +28 kV accelerating voltage, +16.8 kV secondary grid voltage, and -84 V guide wire voltage. Sinapinic acid was used in all MALDI experiments. The matrix was prepared as a saturated solution in 1:1 v/v water:acetonitrile with 0.1% TFA. All samples solubilized in TX-100 were concentrated using a microcon 50 concentrator (Amicon) and mixed 1:1 with purified water to dilute the detergent and salt concentrations. These samples were concentrated roughly 10 fold over the samples used for spectrophotometric analysis in order to get adequate signal in the mass spectrometer. Samples solubilized in OG were used at the same concentration as those used for spectrophotometric analysis. A microliter of the concentrated protein solution was mixed with one microliter of a water:acetonitrile solution before one microliter of the matrix. It was observed that larger crystals were formed, and MALDI mass spectra were improved, when the protein solution was first diluted as described above prior to mixing with the sinapinic acid matrix solution. External calibration was

performed using apo-myoglobin (m.w. 16,950.5 Da) as the standard solubilized in gel filtration column buffer. Analysis of the mass data was performed using the computer program GPMAW, Lighthouse Data, Odense Denmark.

## Results

The experiments performed on partially purified cytochrome $b_{558}$ were intended to confirm the involvement of the small subunit in heme-binding and to determine the heme-binding domains within the large subunit. To facilitate a clearer understanding of the detergent dependence of the partial digestion of cytochrome $b_{558}$, results from the partial tryptic digestion of cytochrome $b_{558}$ solubilized in OG will be presented first. This will be followed by the presentation of results from the partial tryptic and V8 digestions of cytochrome $b_{558}$ solubilized in TX-100.

### Partial Tryptic Digestion of Cytochrome $b_{558}$ Solubilized in Octylglucoside

Initial MALDI MS experiments with cytochrome $b_{558}$ solubilized in Triton X-100 were unsuccessful in determining accurate mass of the analytes due to interference from the detergent. A previous study by our group, where MALDI MS was used to identify transmembrane peptide fragments of rhodopsin, showed that OG is compatible with MALDI (36). Therefore, to facilitate MALDI ionization of proteolytic fragments of cytochrome $b_{558}$, the protein was first purified and digested in the detergent OG.

Figure 50 shows the change in the oxidized absorbance spectra at 10 min intervals for 150 $\mu$g of OG solubilized, heparin purified, cytochrome $b_{558}$ digested with trypsin

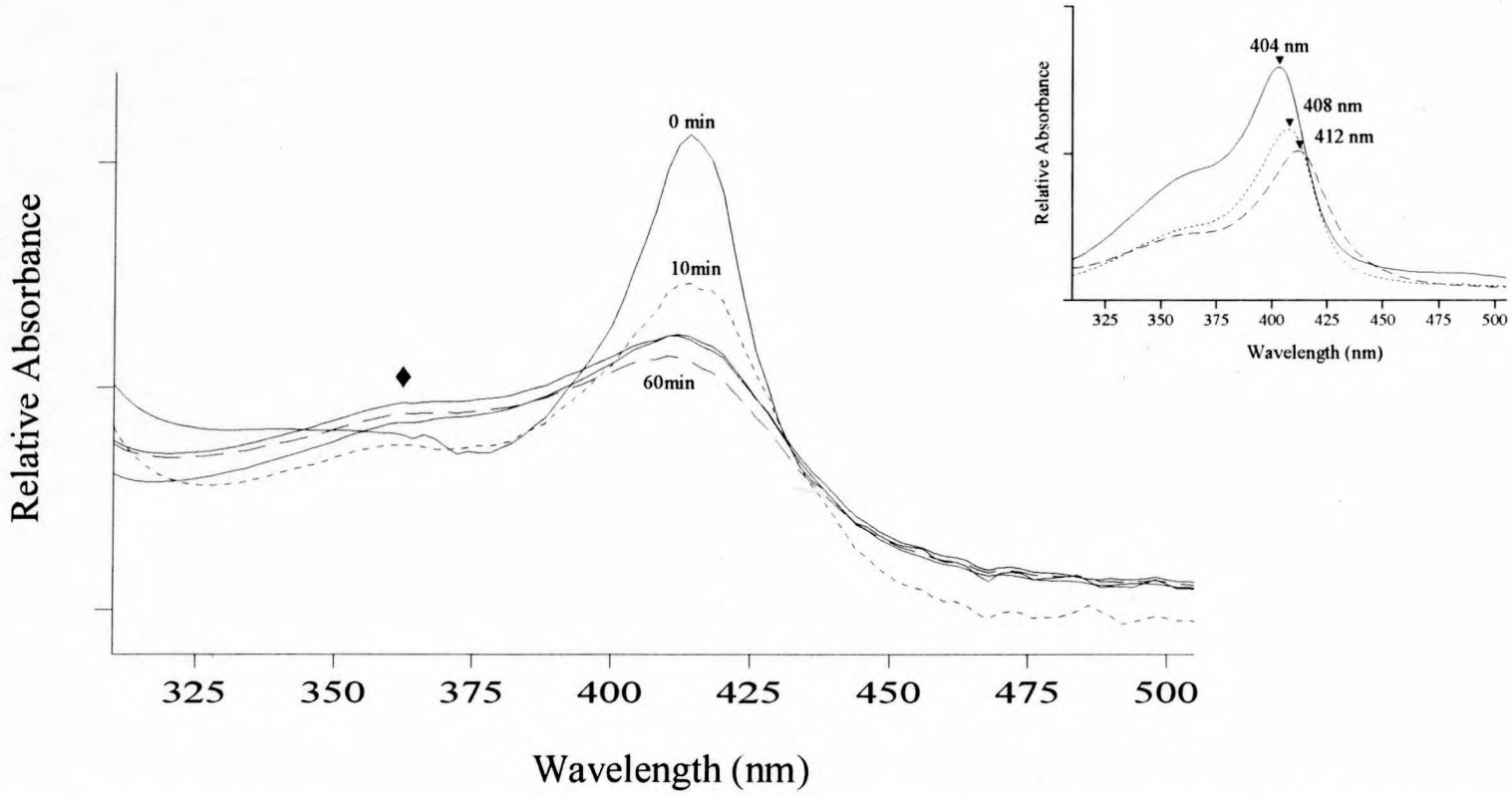


**Figure 50.** Oxidized absorbance spectra of the partial tryptic digest of purified cytochrome $b_{558}$ solubilized in OG showing the change in the absorbance profile with time. The solid line labeled 0 min is the spectrum of the starting material with an absorbance maximum at 414 nm. The dotted line is the profile after 10 min of digestion with a maximum at 412 nm and the dashed line is the profile after 60 min of partial digestion with an absorbance maximum at 408 nm. The shoulder peak labeled (♦) has a maximum at 364 nm. The inset shows the absorbance spectra for oxidized hemin (solid line), myoglobin (dotted line), and hemoglobin (dashed line). The results clearly show that after 60min of digestion the heme binding regions of the protein are no longer stabile.

(enzyme to substrate ratio of 1:100). These spectra clearly show that the heme- binding domains within the protein are no longer stable after 60 min. In addition, it appears that the environment for the heme is somewhere between free hemin (see inset) and coordinated heme, as evident from the shift in the Soret band from 414 nm to 412 nm and the appearance of a peak at 364 nm. The inset to Figure 50 also shows these spectra of myoglobin, hemoglobin, and hemin all solubilized in the same buffer used for digestion. It is evident from the spectra that hemin, myoglobin, and hemoglobin each have a shoulder peak at ~365 nm. Although the intensity of the absorbance at 412 nm for the partially digested cytochrome $b_{558}$ is roughly half that of the peak at 414 nm for the undigested material, the total area under the peaks from 412 nm to 364 nm is equal to that of the single peak at 414 nm in the undigested protein. Evidently the heme-binding domains are unstable in OG when subjected to partial digestion with trypsin since the study by Quinn et al. clearly showed that even after 4 hours, the absorbance spectrum of cytochrome $b_{558}$ in purified neutrophil membranes was stable to proteolysis by trypsin (20).

Figure 51 shows a 7%-18% gradient SDS-PAGE gel that illustrates the change in the purified cytochrome $b_{558}$ before and after digestion. It is clear that the high molecular weight components of the sample (large subunit of cytochrome $b_{558}$ and CD11b) are substantially degraded upon partial digestion, as is the small subunit. Bands that appear after digestion can be seen at ~29 kDa and 15.5 kDa while bands that apparently do not change after digestion can be seen at 45 kDa and 17 kDa. It is not known if these bands represent new material that was shifted to that molecular weight after digestion or if the material at that molecular weight is resistant to proteolysis. Control digests clearly showed

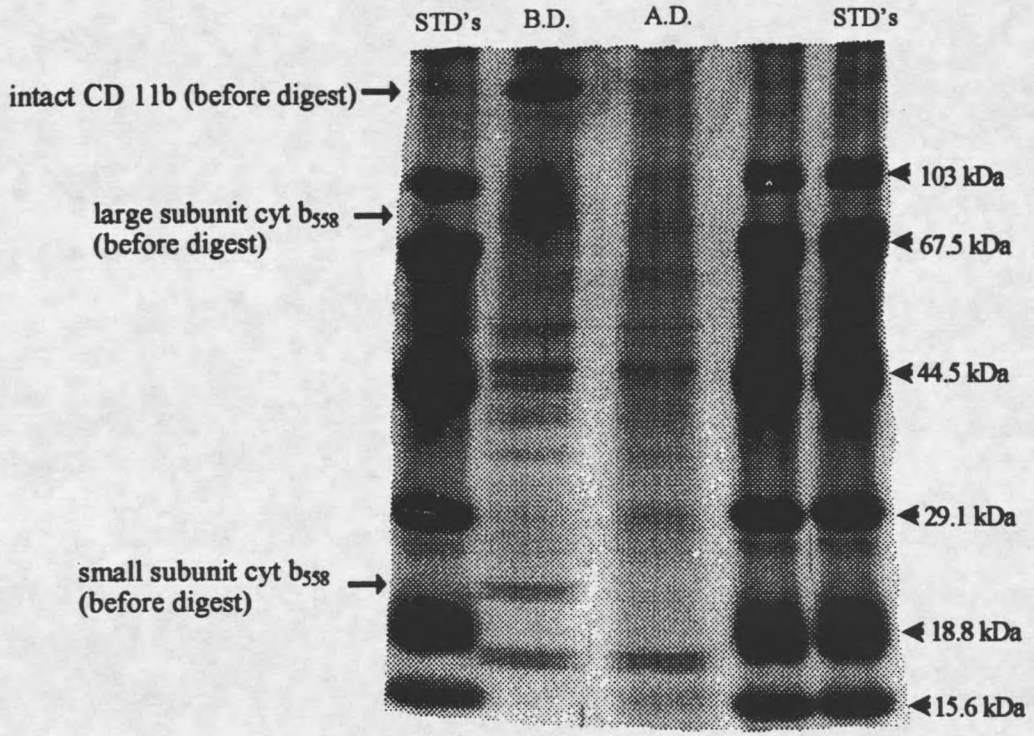


**Figure 51**. Silver stained SDS-PAGE gel of heparin purified cytochrome $b_{558}$ before (B D.) and after (A.D.) partial tryptic digestion. The reduction in staining for the large subunit of cytochrome $b_{558}$ due to digestion is clearly visible between the 103 kDa and 67.5 kDa standards while a complete loss of staining for the small subunit is seen just above the 18.8 kDa molecular weight standard. In addition, digestion of the co-purified protein CD11b is plainly seen by the reduction in staining of the band at 150 kDa. Bands that appear after digestion are seen near the 29.1 kDa standard and near the 15.6 kDa standard. Bands that do not change before and after digestion can be seen at 44.5 kDa and 17 kDa. Each lane contains equivalent amounts of sample. The gel illustrates the reduction in staining after partial proteolysis in the regions indicative of the large and small subunits.

that trypsin (m.w. 23,310 Da) is below the level of detection by silver staining, relative to the amount of cytochrome $b_{558}$ present. The presence of the integrin CD11b in the purified cytochrome $b_{558}$ fractions could be problematic. However, control digests using purified CD11b/CD18 (kindly provided by Dr. Charles Parkos) and the same amount of trypsin revealed that CD11b/CD18 is cleaved into fragments smaller than the lowest molecular weight standard (data not shown).

Separation of Tryptic Fragments from OG Solubilized Cytochrome $b_{558}$ Using Gel Filtration Chromatography

To separate proteolytic fragments and to isolate heme-coordinating peptides, gel filtration chromatography was carried out in the non-denaturing detergent, octyl-β-glucoside (OG). The gel filtration column effluent was monitored for absorbance at 414 nm and fractions were collected every minute. The chromatogram from the injection of partially digested cytochrome $b_{558}$ onto the gel filtration column is shown in Figure 52. The predominant peak at 13.9 minutes elutes at a retention time similar to the standard thyroglobulin at a molecular weight of 670 kDa, while the small peak at 25.8 minutes elutes at a retention time similar to that of myoglobin at a molecular weight of 17.6 kDa. Both standards were run under the same column conditions. The inset to Figure 52 shows the tryptophan fluorescence profile for the digest. Two tryptophan containing peaks are seen to elute at the same time as the peaks having absorbance at 414 nm. The peak at 14 minutes is a single peak. However, the attenuation on the detector was set at a level that would allow for the peak at 25 minutes to be seen easily. The gel filtration chromatogram

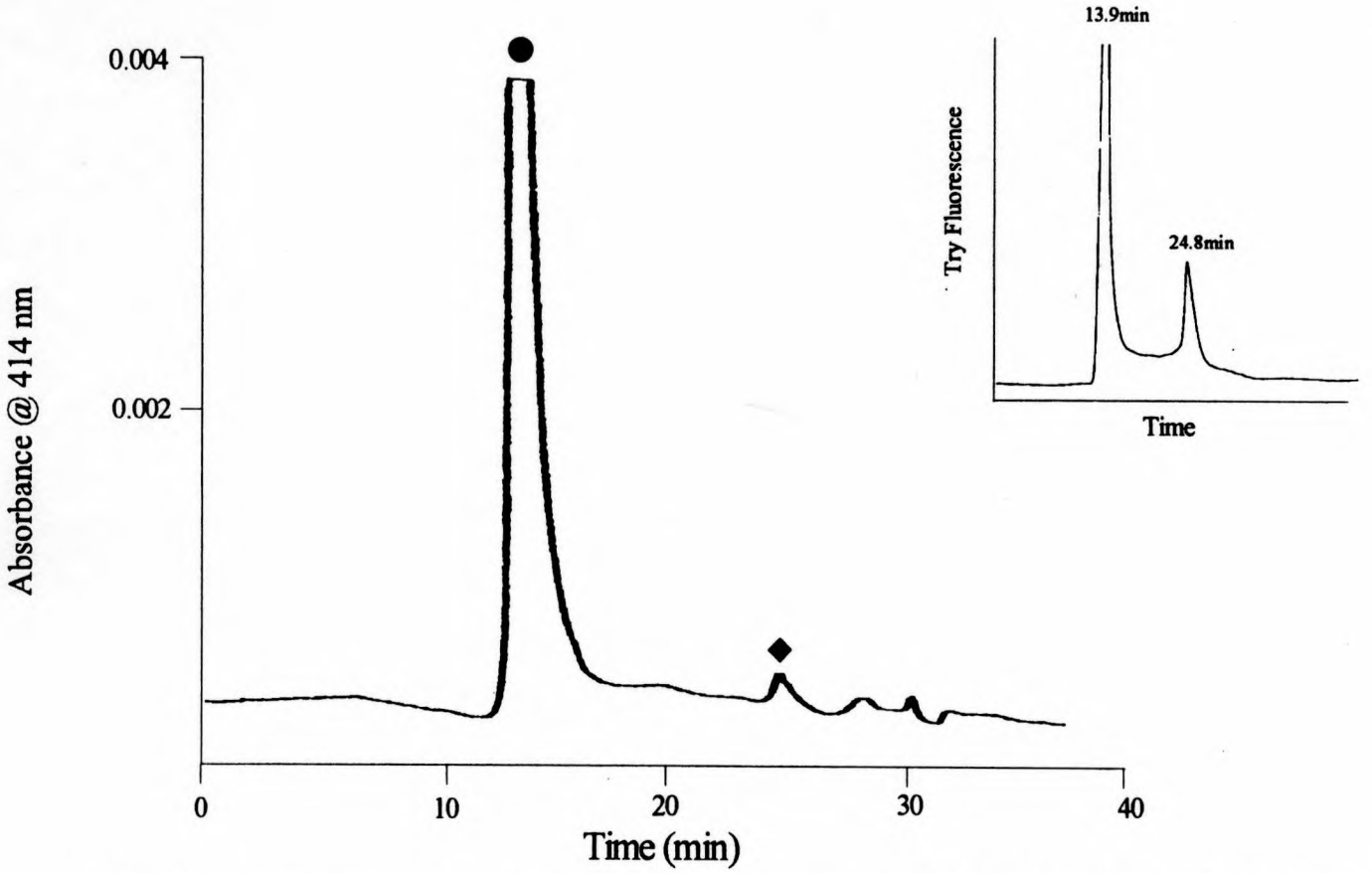


**Figure 52**. Chromatogram of the gel filtration run of cytochrome $b_{558}$ solubilized in OG and partially digested with trypsin. The labeled peaks represent aggregated (peak labeled ● at 14 min) and unaggregated (peak labeled ◆ 25 min) fragments having 414 nm absorbance. The inset shows the fluorescence emission profile set for tryptophan residues. The chromatogram clearly shows that a majority of the heme containing fragments eluted as part of an aggregate.

for the absorbance at 414 nm clearly shows that a majority of the heme containing material eluted as an aggregate.

After the gel filtration run was complete, aliquots were taken from each fraction and analyzed by SDS-PAGE. The 7-18% gradient SDS-PAGE gel showing the fractions eluted from the gel filtration column is seen in Figure 53. The figure shows that the peak eluting at 14 minutes contains a number of fragments that would not elute at that retention time unless they were part of an aggregate. This aggregation is evident by looking at lanes 13 and 14 where a broad smear of bands ranging from molecular weight ~15 kDa to ~30 kDa can be seen. Above a molecular weight of 30 kDa it becomes difficult to interpret the $M_r$ of the fragments due to increased smearing in the gel. Diffuse bands are typical of glycosylated proteins but this phenomenon may also be due to incomplete dissociation of the proteolytic fragments, even in sample buffer containing reducing agent and SDS.

Tryptic fragments produced were, however, very evident at different gel filtration column elution times. The band at 15.5 kDa in Figure 53, that was produced upon digestion, can easily be seen in fractions 13 and 14. It is also present, at a lower concentration, in fractions 26 and 27 as indicated by the arrow. The band at 29 kDa can be seen in gel filtration fractions 25-27 along with the prominent band at 17 kDa. The molecular weights of the components in fractions 24 through 26, as determined by SDS-PAGE, suggest that they were being separated by size in the gel filtration column since their elution times vary inversely with their SDS-PAGE $M_r$. The bands between 44.5 and 67.5 kDa in fractions 24-27 are from keratin-like proteins. These contaminants can also be seen in fraction 12 where no protein eluted from the gel filtration column.

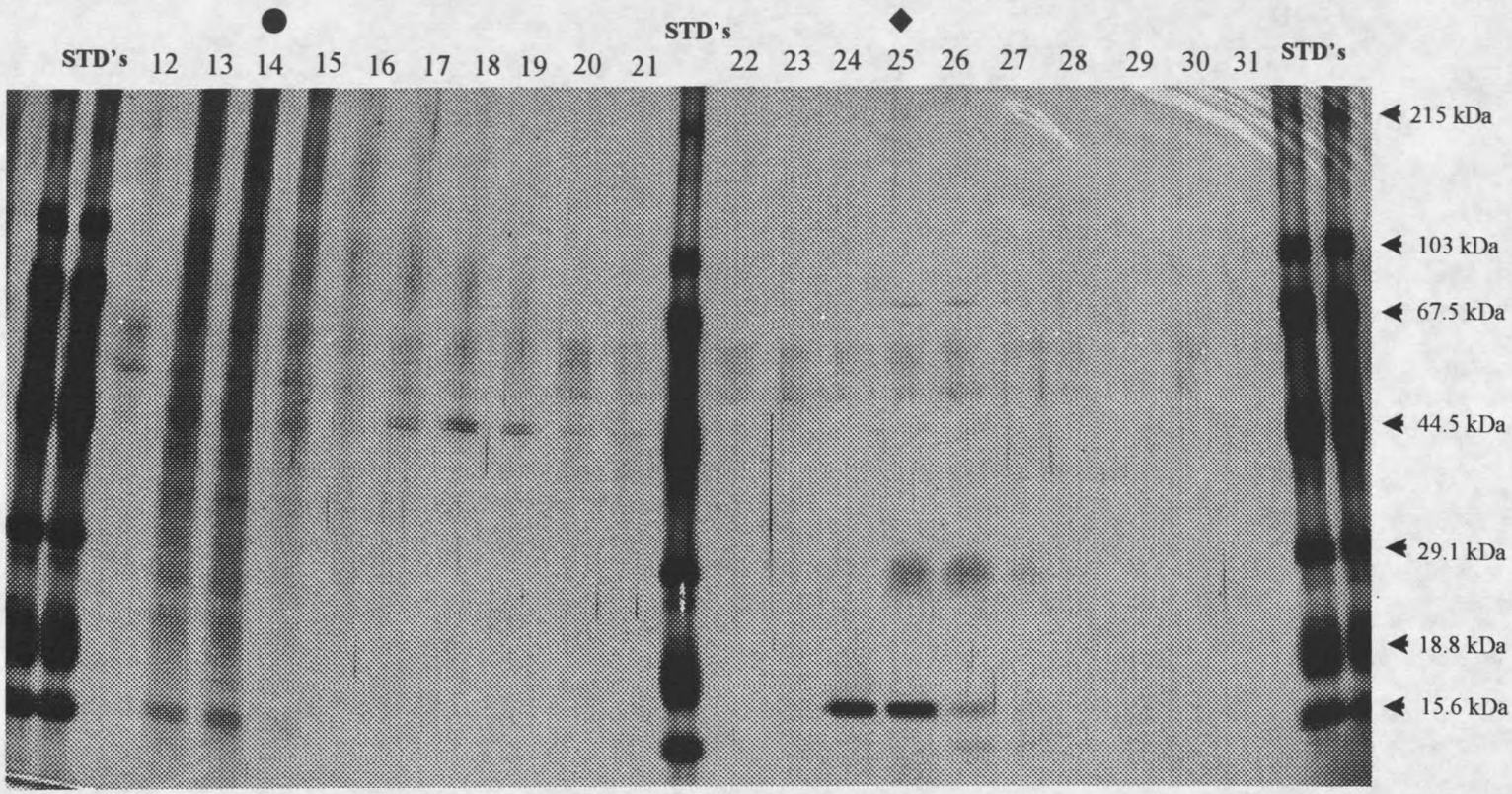


**Figure 53**. Silver stained 7-18% SDS-PAGE gel of fractions eluted from the gel filtration column after the injection of the OG solubilized cytochrome $b_{558}$ partially digested with trypsin. Lanes are labeled by the starting time for the collection of the sample. Components of the peak labeled (●) in Figure 52 are shown in lanes 13 and 14 while the components of the peak labeled (◆) are shown in lanes 24-26. The gel indicates that there is aggregation of heme containing fragments because of the broad range of molecular weights in lanes 13 and 14. The gel also shows that the peak labeled (◆) in Figure 52 is comprised of a much smaller number of fragments.

The UV/Visible absorbance detector for the HPLC system is a single wavelength monitor and thus cannot differentiate between different absorbing species. Hence absorbance spectra of oxidized and reduced fractions to detect heme absorbance characteristics were performed on a Hewlett Packard diode array spectrophotometer. Due to the low absorbance values of the samples, each fraction was concentrated from a volume of 800 $\mu$l to roughly 140 $\mu$l using a Centricon 10 protein concentrator. The absorbance spectra of the concentrated fractions were then measured directly by placing the samples into a micro-cuvette, having a 1cm pathlength and a minimum volume of 140 $\mu$l (filled till the meniscus was above the light path). Figure 54 shows the absorbance spectra of fractions 23 through 26, analyzed by SDS-PAGE in Figure 53. The change in the absorbance profile can readily be seen by the change in the 414 nm absorbance as the peak at 25 minutes elutes from the column. The actual absorbance for the peak after concentrating the fraction appears to be at 428 nm as seen in fractions 24 and 25. However, there is also a change in the baseline in fraction 26 where the broad peak has a maximum at 420 nm, suggesting that at least half of the absorbance measured at 414 nm represents a change in the background.

To determine the concentration of heme, fraction 24 was reduced with 4 $\mu$l of freshly prepared 1 M sodium dithionite. The dotted trace in Figure 55 represents the oxidized profile of the sample while the solid line depicts the reduced form. Clearly the peak at 428 nm is sensitive to the addition of reducing agent to the cuvette. However, since the peak at 428 nm disappears after reduction, it is difficult to compare this result with undigested cytochrome $b_{558}$. In the undigested protein, the Soret band observed at

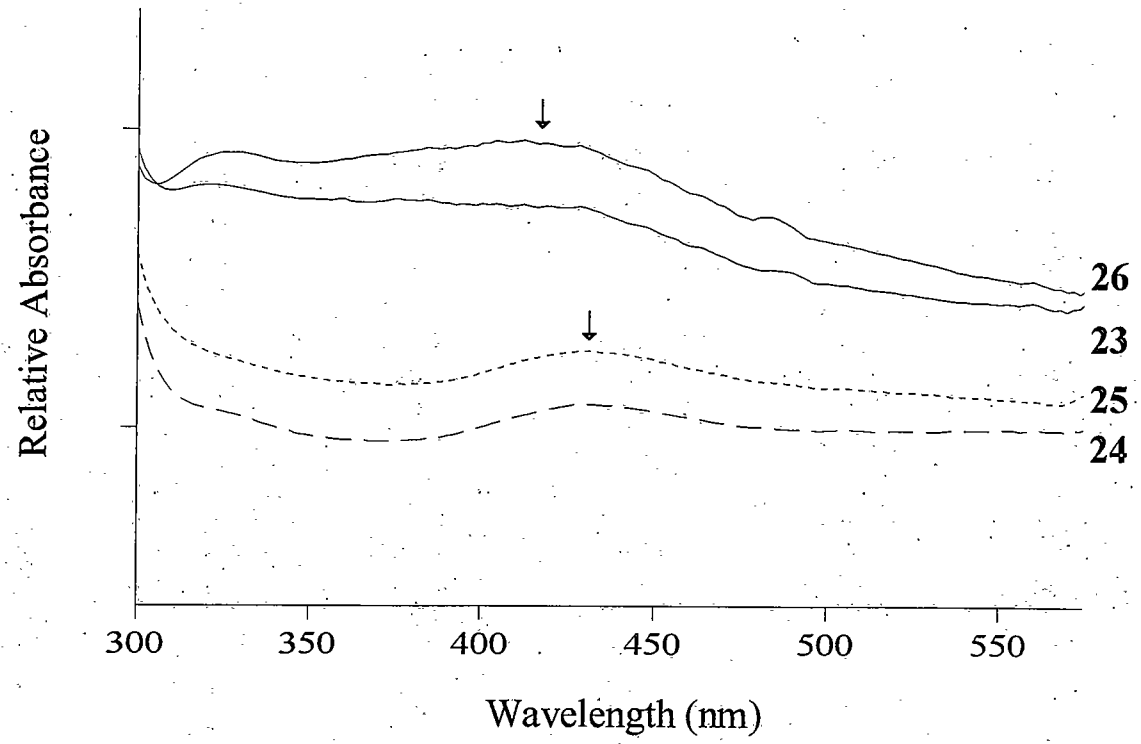


**Figure 54**. Oxidized absorbance spectra from fractions 23 thru 26 collected from the gel filtration column after the injection of cytochrome $b_{558}$ solubilized in OG and partially digested with trypsin. All spectra are normalized to each other. The spectra are displayed top-bottom: fraction 26, fraction 23, fraction 25 (short dashes), and fraction 24 (long dashes). The absorbance maximum for fraction 26 is 420 nm and the absorbance maximum for fractions 24 and 25 is 428 nm. The spectra displayed show that the absorbance observed from the peak at 24.8 min in Figure 52 had an absorbance maximum at 428 nm.

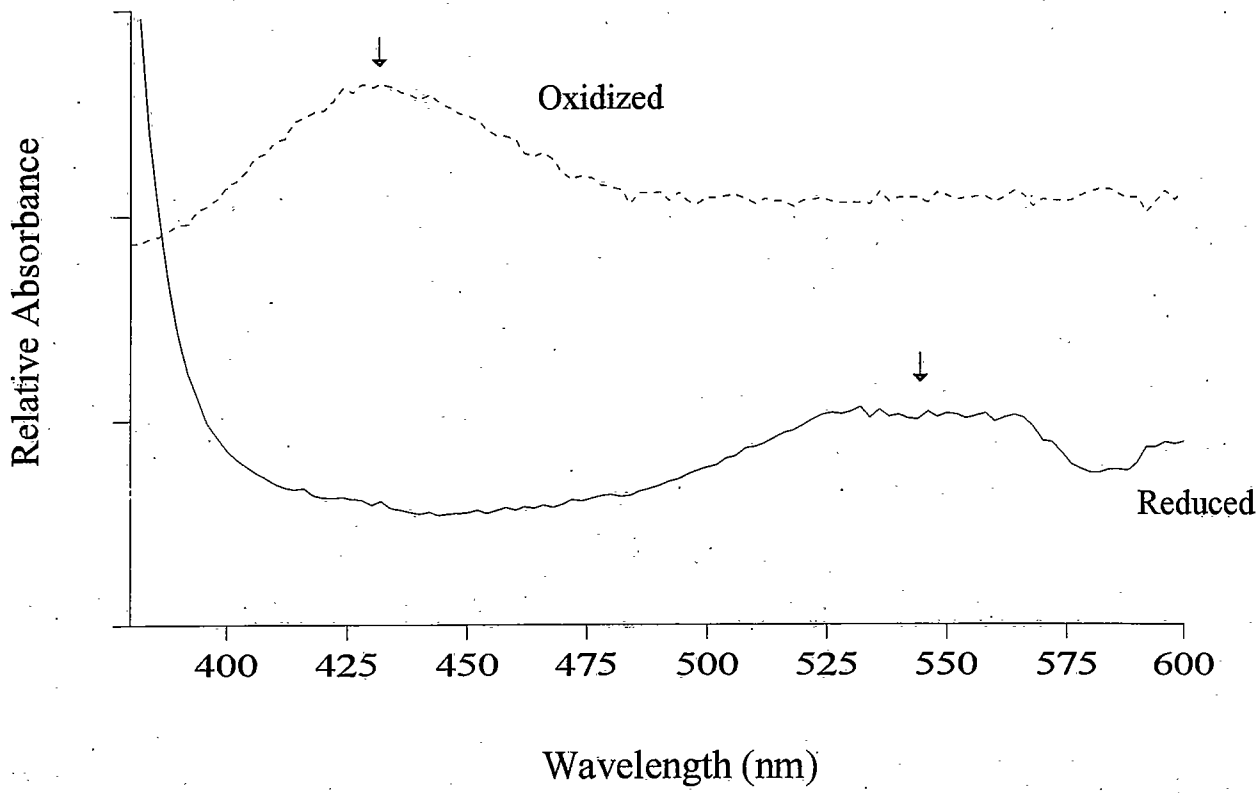


**Figure 55**. Absorbance spectra of fraction 24 oxidized (dotted line) and reduced (solid line). The absorbance maximum for the peak in the oxidized spectrum is 428 nm. This peak is not present in the reduced spectrum, however a broad band between 510 and 575 nm does appear after reduction of the sample with 4 $\mu$l of 1 M sodium dithionite. These spectra suggest the presence of a component sensitive to reduction by sodium dithionite.

414 nm shifts to a maximum at 426 nm after reduction. The small increase in the baseline between 520 to 570 nm suggests that α and β-like bands may be produced upon reduction of undigested cytochrome $b_{558}$. However, without a corresponding shift for the peak observed 428 nm, it is difficult to interpret these results. Controls carried out with gel filtration buffer show no change in the baseline upon addition of sodium dithionite at the same wavelengths.

Cytochrome $b_{558}$ is an oxidase (37) with a low electrochemical reduction potential, and can be reoxidized from the reduced state when exposed to ambient oxygen simply by bubbling air into the cuvette (7,8). Figure 56 documents the reoxidation of fraction 24 by bubbling air into the cuvette after the sample was reduced with sodium dithionite. The reoxidized spectrum (dotted line) clearly shows the reappearance of the peak at 428 nm. The solid line shows that the same sample can be reduced a second time by the addition of another 4 $\mu$l of sodium dithionite. The sample was reoxidized a second time and the peak at 428 nm appeared once again (data not shown). The disappearance upon reduction and the reappearance upon oxidation of the peak at 428 nm, strongly suggests the presence of a redox center. An upper estimate of the amount of heme present in the sample is 0.5 pmol using the extinction coefficient for the oxidized form of cytochrome $b_{558}$ (131 $mM^{-1}cm^{-1}$ @ 414nm). However, this estimate is based solely on the assumption that the extinction coefficient for the oxidized form of cytochrome $b_{558}$ is similar to the extinction coefficient for the material in fraction 24.

The data from oxidized and reduced absorbance spectra from fraction 24 indicate the presence of an optically sensitive redox center. Nevertheless, additional methodology

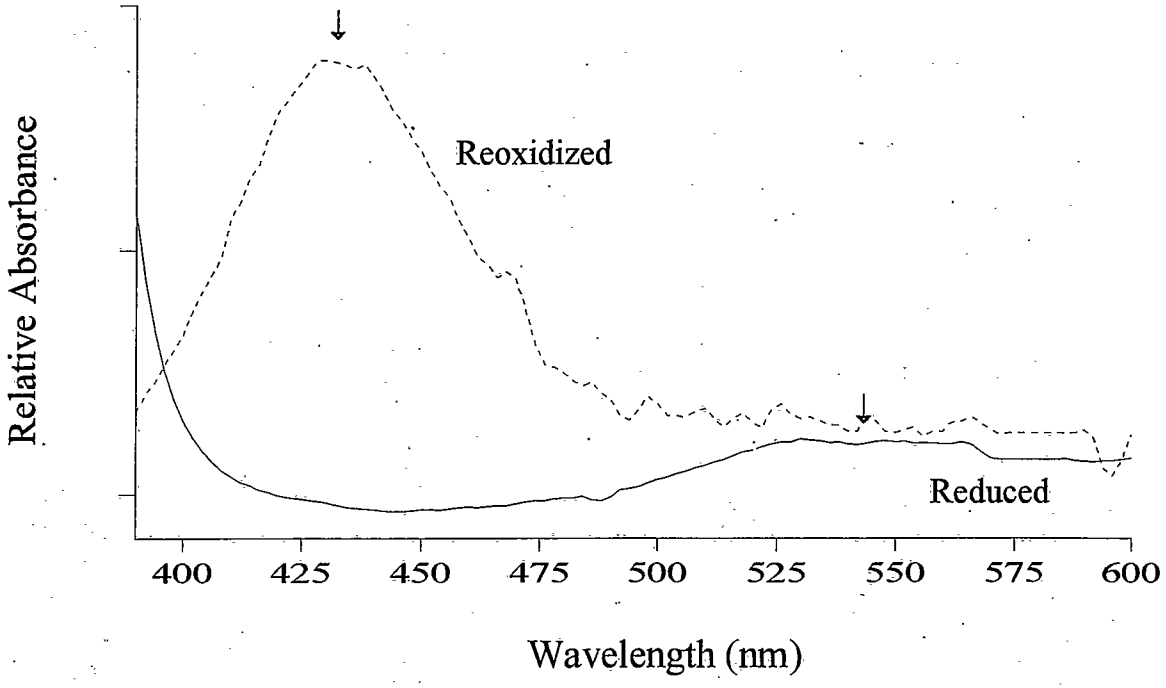


**Figure 56**. Absorbance spectrum of fraction 24 reoxidized (dotted line). The starting material is seen in the solid line spectrum shown in Figure 55. Ambient air was bubbled through the cuvette for ten seconds prior to taking the spectrum. The absorbance maximum for this spectrum is 428 nm. The sample was reduced again with 4 $\mu$l of 1 M sodium dithionite (solid line) and the resulting spectrum shows the broad band seen in Figure 55. These spectra confirm the reversible oxidation of the components present in the fraction.

was needed to characterize the contents of fractions 24-26. The small amount of material present in fraction 24 made it impractical to probe the fraction further by both immunological analysis and MALDI MS, and still have enough sample to submit for sequencing. Therefore, a small aliquot of fraction 24 was analyzed by MALDI MS and the rest was sent for sequencing. However, fraction 25 displayed absorbance characteristics comparable to fraction 24 and was thus used for Western blot and WGA binding assays.

Western Blot and WGA Binding Analysis of Fraction 25

Western blot analysis was performed on fraction 25 to characterize the components present in the sample using the rabbit polyclonal anti-peptide antibody α-EAR made against the peptide $^{162}$EARKKPSEEEAAA$^{174}$ from the carboxy terminus of the small subunit of cytochrome $b_{558}$ (5,38). Figure 57 shows an immunological analysis of fraction 25 using the antibody α-EAR, before and after reduction and alkylation. A band at a $M_r$ of 17 kDa is evident in lanes 1 and 2 and suggests that a fragment of the small subunit is present in the fraction. Figure 57 also shows the appearance of a band at ~26 kDa upon reduction and alkylation of the sample suggesting intra-chain disulfide mediated folding that is partially relaxed only under reducing conditions.

Previous experiments by Parkos et al. have shown that the small subunit is not glycosylated (5). We hypothesize that the large and small subunit are tightly bound via disulfide linkages and heme coordination near sites of glycosylation on the large subunit. If a fragment of this complex were stable to digestion and SDS-PAGE treatments, evidence of glycosylation should be found. Thus, an additional experiment was performed on

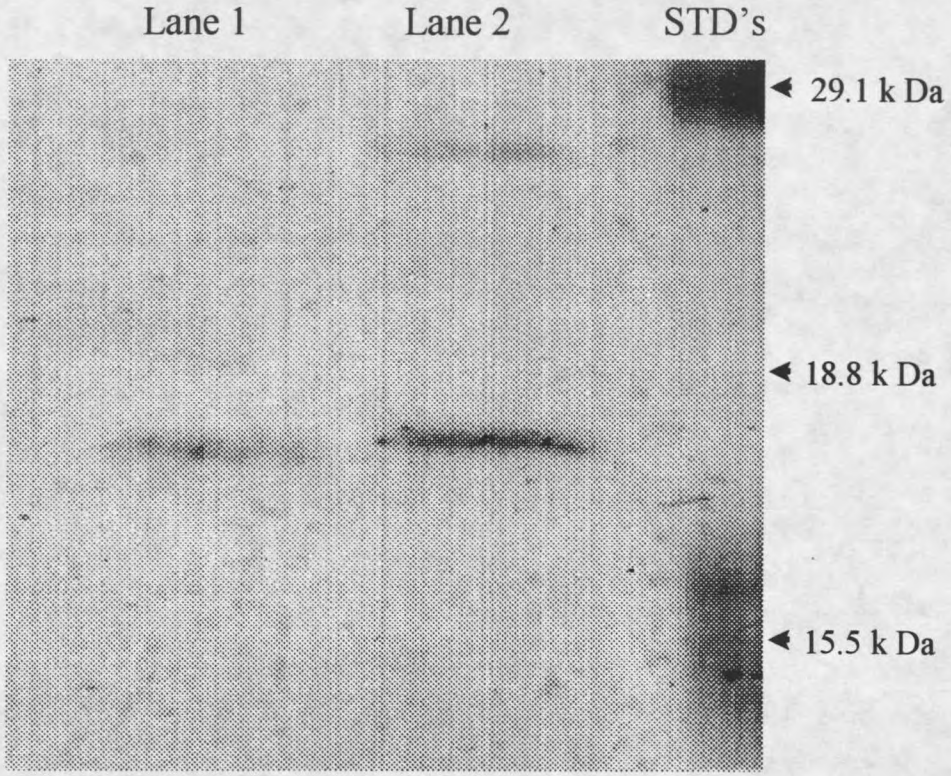


**Figure 57**. Western blot of gel filtration fraction 25 from the partial tryptic digest of OG solubilized cytochrome $b_{558}$. The primary antibody used was the anti-small subunit antibody α-EAR. Lane 1 contains sample prior to reduction and alkylation while Lane 2 contains the same amount of sample after reduction and alkylation. A volume of 20 $\mu$l from the concentrated fractions used in Figure 54 was applied to each lane. The antibody from serum was used at a dilution of 1:400. The blot indicates the presence of a fragment originating from the small subunit evident from the staining at $M_r$ = 17 kDa.

fraction 25 designed to evaluate the existence of carbohydrate on the fragments present in the fraction. The lectin binding protein wheat germ agglutinin (WGA) is used to purify cytochrome $b_{558}$ exploiting its carbohydrate binding affinity (5). By using WGA covalently labeled with a fluorescent dye such as Cascade Blue (CCB), it is possible to locate carbohydrate containing polypeptides immobilized on nitrocellulose since the dye will fluoresce when exposed to UV light. The specificity of this binding was examined by adding 200 mM *N*-acetylglucosamine to the WGA-CCB solution during incubation. The binding of the WGA-CCB to controls as well as samples, has been shown to be competitively inhibited by the presence of the free carbohydrate in solution (data not shown). To evaluate the hypothesis that disulfide linkages play a role in the heme coordination within the heme-binding domain, samples were reduced and alkylated prior to separation by SDS-PAGE to observe any changes in the $M_r$ of the fragments associated with the optical activity.

Figure 58 shows the effect on the binding of WGA-conjugated CCB to fraction 25 (Figure 53) with and without reduction and alkylation. The blot suggests that carbohydrate is associated with these samples. Since the band seen at 17 kDa has the same $M_r$ as the fragment recognized by the α-EAR antibody, these data suggest that the bands at 17 kDa (found in fractions 24 and 25) and 26 kDa (found in fractions 25 and 26) may contain both large and small subunit. As controls, similar experiments were performed using an undigested purified cytochrome $b_{558}$. These experiments indicated that the small subunit does not bind WGA-CCB while the large subunit does (data not shown). Thus, the presence of the small subunit, as indicated by Western blot analysis using the

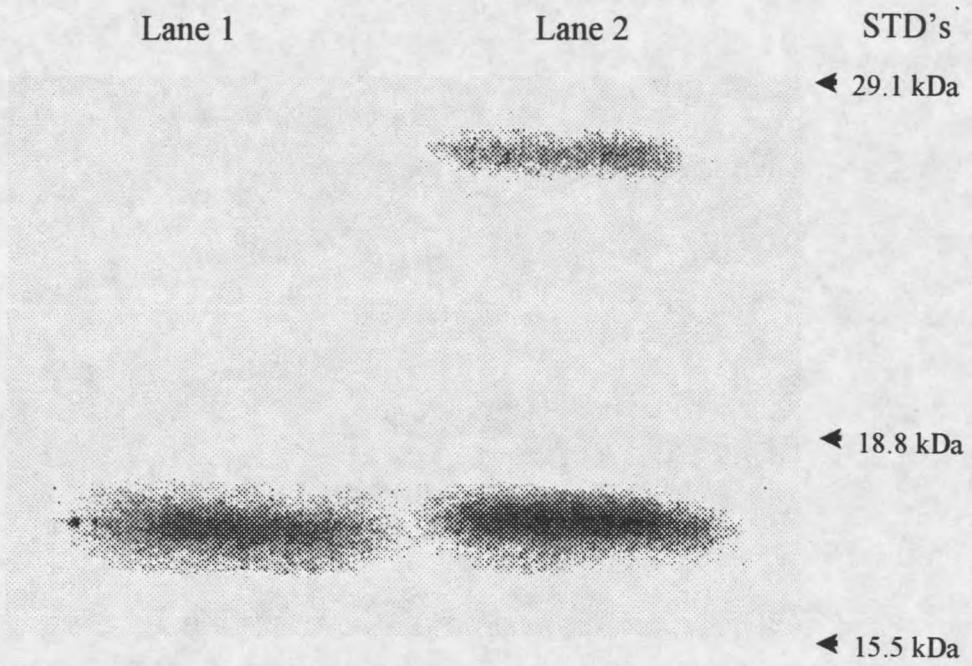


**Figure 58**. Wheat germ agglutinin-conjugated Cascade Blue affinty labeling blot. Lane 1 contains 20 $\mu$l of fraction 25 without reduction and alkylation while Lane 2 contains the same amount of material with reduction and alkylation. The blot represents the inverse image produced by illuminating immobilized sample with UV light after incubation with fluorescently labeled wheat germ agglutinin. The blot illustrates the binding of WGA to the band at 17 kDa, also recognized by the anti-small subunit Ab α-EAR, suggesting the presence of carbohydrate

small subunit antibody EAR, coupled with the fact that there is carbohydrate strongly suggest that fragments of both subunits exist in the 17 kDa band. These results suggest further that the 17 kDa species observed in the partial tryptic digest of cytochrome $b_{558}$ contains a fragment of both subunits that demonstrates high stability under the conditions of SDS-PAGE. In addition, the sensitivity of this fragment to reducing and alkylating conditions also suggests that this fragment contains a region of intra-chain disulfide linkages.

MALDI MS Analysis of Fractions 24, 25, and 26

MALDI MS analysis was conducted on fractions 24, 25, and 26 in an effort to obtain accurate mass of the tryptic fragments for comparison with the predicted tryptic fragments of cytochrome $b_{558}$. MALDI MS was also used to detect the presence of smaller peptides (< 10,000 Da). This aspect of the analysis was important since, under the SDS-PAGE conditions used, small peptides would not be detected. Additionally, MALDI MS could reveal non-covalent interactions not evident in SDS-PAGE analysis. Figure 59 is a MALDI mass spectrum of fraction 24. The mass range from 5,000 Da to 27,000 Da is shown in the figure. No ions were observed below 5,000 Da that were not seen in controls except for a mass peak at 616.5 Da from heme. There is no evidence for ions from intact trypsin (M.W. 23,309 Da), nor were ions observed above 27,000 Da. The mass spectrum in Figure 59 shows the 17 kDa fragment described previously labeled ***a*** with an accurate mass of 16,997 Da. There are clearly two other peaks that are present in this fraction near the prominent peak at 16,997 Da. This includes the peak lower in mass, at 16,705 Da and

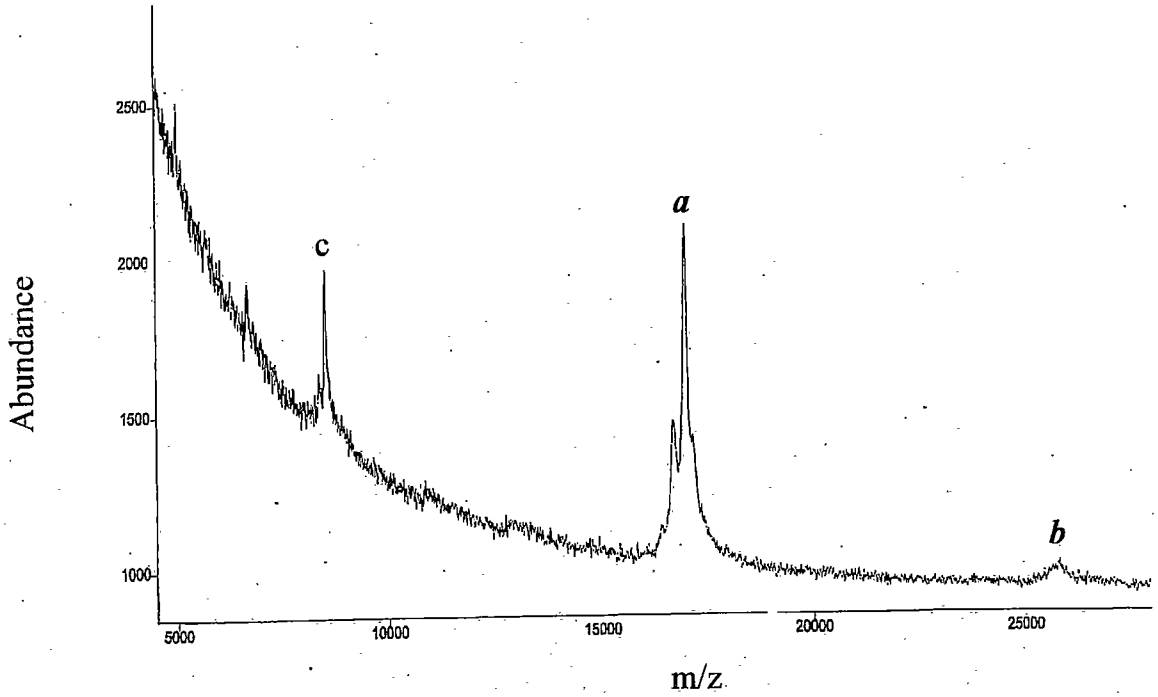


**Figure 59**. MALDI mass spectrum of gel filtration fraction 24 from the partial tryptic digest of cytochrome $b_{558}$ solubilized in OG. The peak labeled ***a*** is the has an accurate mass 16,997 Da. Peaks of lesser intensity can be seen peak ***a*** at a slightly lower mass (16,705 Da) and a slightly higher mass (17,089 Da). The peak labeled ***b*** at m/z 25,838 is the fragment at 26 kDa seen as a diffuse band by SDS-PAGE. The peak labeled *c* is the $MH_2^{+2}$ ion of the 17 kDa fragment. This MALDI MS spectrum clearly shows that the band at 17 kDa observed in SDS-PAGE analysis contains more than one component.

a shoulder peak higher in mass at 17,089 Da. The peak labeled ***c*** is presumably the doubly charged ion of peak ***a***. Figure 59 also shows a peak labeled ***b***, at m/z 25,838 Da. This probably corresponds to the band at $\approx M_r$ 26 kDa in fractions 25 and 26 in Figure 53, that was not seen in fraction 24. Most importantly, a mass peak at 616.5 Da, characteristic of heme, was observed in the low mass region of fraction 24 (data not shown) indicating the presence of heme in this fraction. The finding by MALDI MS that a mass indicative of heme is present in fraction 24 implies that one of the components in this fraction has a heme associated with it. This observation supports the evidence that the fragment at 17 kDa is associated with a heme-binding domain in cytochrome $b_{558}$. However, the fact that the absorbance profile for the fragment is not the same as intact cytochrome $b_{558}$ indicates that the heme is no longer in an environment similar to the intact protein. Western blot analysis for this fraction using the anti-small subunit antibody α-EAR indicates that at least one of these components is from the small subunit of cytochrome $b_{558}$. In addition, the WGA-CCB experiments serve to show that at least one of these components also contains carbohydrate, or a carbohydrate binding capacity.

The masses found for the peaks at 17 kDa do not match the expected masses for tryptic fragments from either the large or small subunits taking into account the possibility of skipped cleavage sites or stable heme-peptide complexes. A mass assignment cannot be made that takes into account the possibility that one of the MALDI MS peaks represents a disulfide-linked fragment of the large and small subunit since the exact mass of carbohydrate present on the large subunit is not known. The mass assignment for the band at ~26 kDa, obtained by MALDI, shows that the component present is heterogeneous. As

stated previously, the elution times for fractions 24 and 25 from the gel filtration column were similar to the elution time for the standard protein myoglobin (M.W. 17.5 kDa). This suggests that the species at 17 kDa in fractions 24 and 25 was not associated with the heterogeneous species observed at ~ 26 kDa in the same fractions, since the combined mass of the two species would be roughly 43 kDa.

The mass spectra obtained from these fractions were of good quality and serve to substantiate the finding that masses for samples solubilized in OG can be determined by MALDI MS with better resolution than SDS-PAGE (33). However, the application of accurate mass, in combination with immunological data, was not successful at determining the origin of the fragments present in fraction 24 due in part to the limitations in resolution of the mass spectrometer used for this analysis. Clearly, there are multiple components present at molecular weights ranging from 16,500 Da to 17,200 Da in fraction 24. Yet this mixture was too complex to be sufficiently resolved by MALDI MS with the resolution afforded by the instrument. Solutions to this problem include; 1) analyzing the sample on an instrument with higher resolution, or 2) separating the fragments using an alternative chromatographic technique such as reverse-phase HPLC. In addition, the observation that most of the 414 nm absorbance is present as aggregated material in fractions 13 and 14, indicates that further separation of this aggregated material could result in the isolation of heme-bearing fragments. One method that may be successful at disrupting this aggregation, without destroying the heme ligation, includes the use of a different detergent. Therefore, digests were carried out on Triton X-100 solubilized cytochrome $b_{558}$ to evaluate the stability of heme-containing proteolytic fragments.

Partial Digestion of Cytochrome $b_{558}$ Solubilized in Triton X-100

Experiments by Quinn et al. showed that cytochrome $b_{558}$ solubilized in Triton X-100 partially proteolyzed by V8, produced fragments with stable absorbance spectra, even after an hour of digestion (20). Accordingly, Triton X-100 was chosen as an alternative detergent to OG since it was shown to stabilize heme-bearing proteolytic fragments of cytochrome $b_{558}$. To avoid interference from TX-100 observed in previous MALDI MS experiments (unpublished data), the gel filtration column used to separate the proteolytic fragments was equilibrated in OG. This step minimizes TX-100 interference in MALDI and allows concentration by ultracentrifugation because of the smaller micellular molecular weight of OG (6,000 Da) vs. TX-100 (90,000).

Figure 60 shows the invariance of absorbance spectra taken at 10 minute intervals during a 1 hour tryptic digestion of 119 $\mu$g of purified oxidized cytochrome $b_{558}$ purified in TX-100. The sample contained 7 $\mu$g of trypsin and was run at 37°C in heparin column elution buffer containing 0.1% TX-100, 600 mM NaCl, and 5 mM HEPES pH 7.4. The inset shows the absorbance spectra of reduced sample from before (dotted line) and after (solid line) the digest. This figure confirms that stability of heme spectral activity of both reduced and oxidized fragments solubilized in TX-100 are stable after proteolysis as previously shown by Quinn et al. (20).

When mapping a protein using proteolytic cleavage, proteases with different cleavage specificity are used to produce fragments of different size. The mass difference of the fragments can then be determined by mass spectrometry to establish where they originated in the protein. Since the protease V8 was used in the study by Quinn et al., it

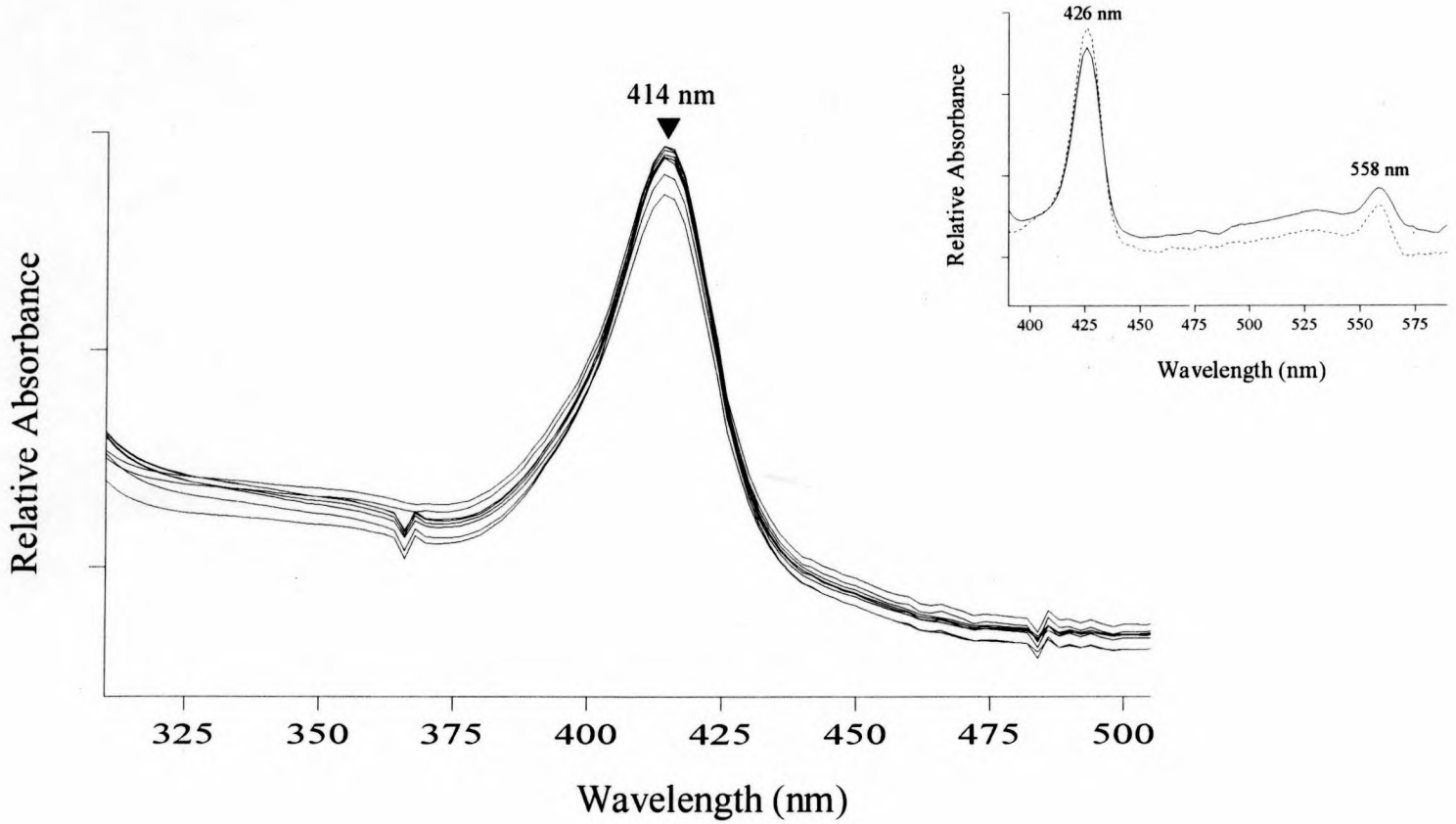


**Figure 60**. Invariance of cytochrome $b_{558}$ absorbance spectrum during a 1 hour tryptic digestion in TX-100. The spectra taken every 10 minutes conclusively show that the absorbance maximum (414 nm) and intensity is not significantly altered over 1 hour of digestion. The inset shows the reduced spectra before (dotted) and after (solid) tryptic digestion.

was used as an additional protease in this study in hopes of producing stable heme-containing fragments that could be compared to the fragments produced by trypsin. Figure 61 shows the time dependence of absorbance spectra taken during a 1 hour V8 digestion of purified oxidized cytochrome $b_{558}$ in TX-100. The conditions were the same as those listed above for the partial tryptic digest. The invariance in the absorbance intensity during the V8 digestion is similar to that observed for the tryptic digestion. Therefore, the heme containing proteolytic fragments produced, either by trypsin or V8, are spectrally stable in Triton X-100 under the conditions used for digestion. Upon comparison of Figure 50 with Figures 60 and 61, it is easy to see the difference in the spectral properties of the protein upon partial digestion in OG vs. TX-100. Cytochrome $b_{558}$ solubilized in TX-100 is much more stable to proteolysis than cytochrome $b_{558}$ solubilized in OG.

Isolation of Spectrally Active Fragments From Partially Digested Cytochrome $b_{558}$ Solubilized in Triton X-100 by Gel Filtration Chromatography

To isolate the fragments possessing spectral activity, and hence the heme-binding domain, both partially digested cytochrome $b_{558}$ samples shown in Figures 60 and 61 were subjected to gel filtration chromatography. Figure 62 shows the gel filtration elution profiles monitored at 414 nm for undigested cytochrome $b_{558}$ (top), cytochrome $b_{558}$ partially digested with trypsin (middle), and cytochrome $b_{558}$ partially digested with V8 (bottom). The non-aggregated undigested cytochrome $b_{558}$ labeled ■ in the top chromatogram has a retention time of 19.5 minutes. However, after 1 hour partial digestion with trypsin and V8 respectively, the retention time of this peak shifts to 21.4

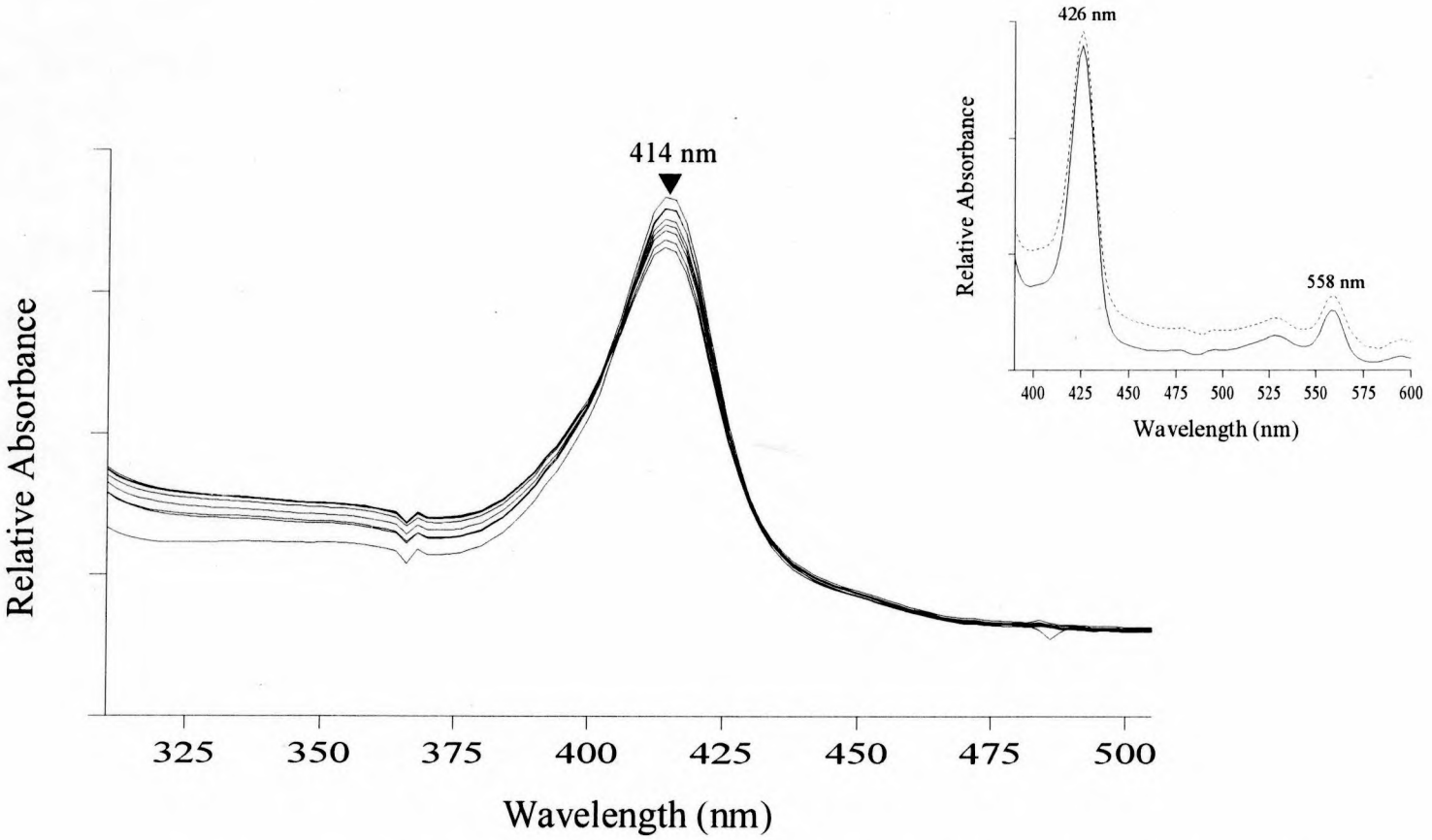


**Figure 61**. Invarianceof cytochrome $b_{558}$ absorbance spectrum during the V8 digestion in TX100. The spectra, taken every 10 minutes, conclusively show that the absorbance maximum (414 nm) and intensity is not altered over 1 hour of digestion. The inset shows the reduced spectra before (dotted) and after (solid) V8 digestion.

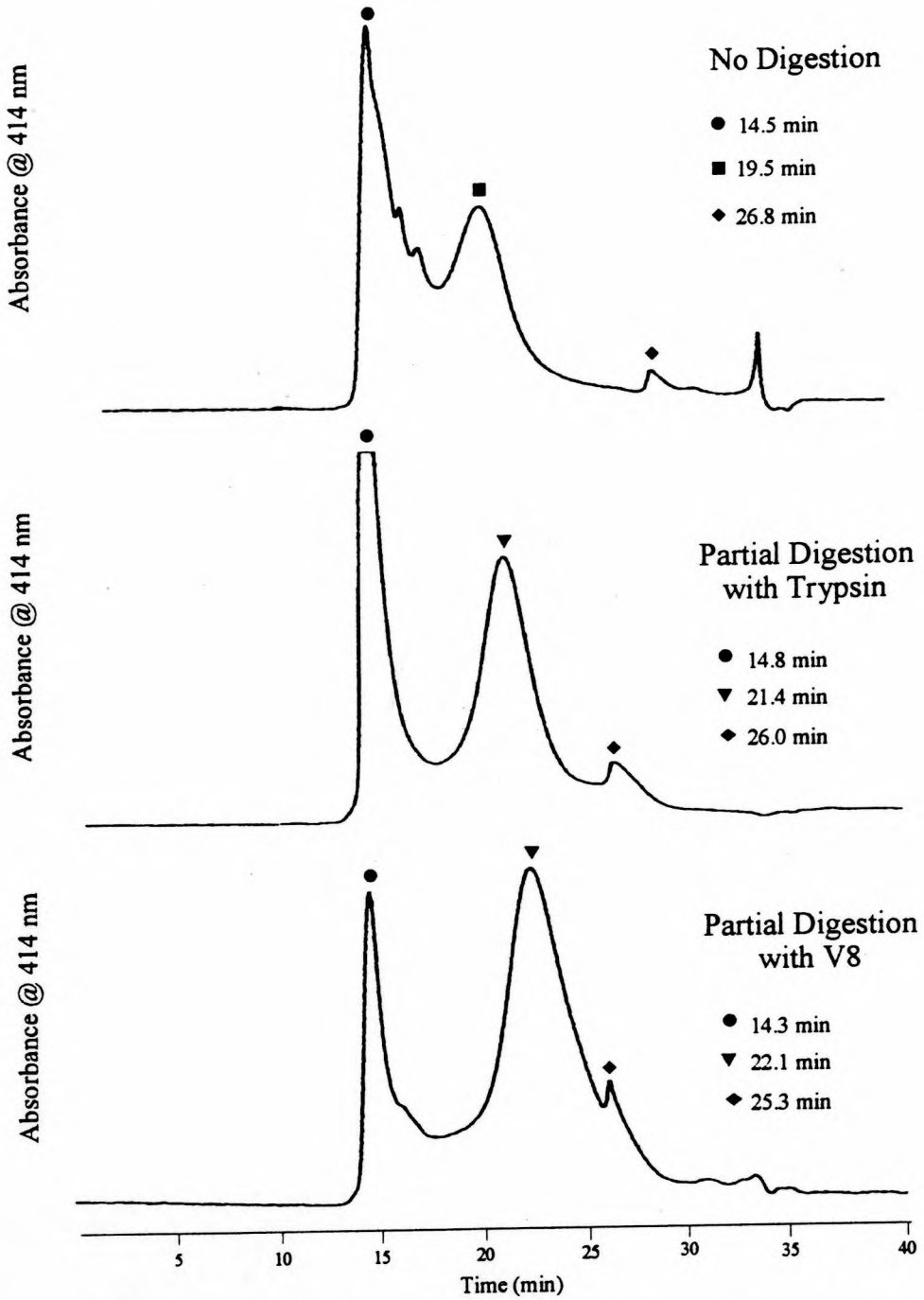


**Figure 62**. Gel filtration chromatography of undigested (top), trypsin digested (middle), and V8 digested (bottom) cytochrome $b_{558}$ solubilized in TX-100. The peak labeled ● is the aggregated form of both intact protein and fragments. The peak in the top chromatogram labeled ■ is non-aggregated intact cytochrome $b_{558}$. The peaks labeled ▼ and ◆ contain the proposed heme bearing fragments. All chromatograms have the same attenuation setting. The chromatograms show that after 1 hour of digestion, fragments with 414 nm absorbance shift to a lower molecular as compared to the undigested protein.

min for trypsin and 22.1 min for V8 indicated by the labeled peaks. This result indicates that although the use of different proteases for the partial digestion did not change the environment of the hemes, the proteases did produce different sized fragments. The elution times for these fractions (21.4 min and 22.1 min) are approximately the same as that of ovalbumin (M.W. ~ 45 kDa) run under the same conditions.

To correlate the 414 nm absorbance peaks with the elution of specific protein fragments, fractions were analyzed by SDS-PAGE. Figure 62 shows the results of fractions collected every minute and subjected to SDS-PAGE using a 7-18% gradient gel developed using silver stain. Figures 63, 64, and 65 show the SDS-PAGE analysis of the fractions from gel filtration column runs for undigested (Figure 63), trypsin digested (Figure 64), and V8 digested (Figure 65) cytochrome $b_{558}$. When bands in the SDS-PAGE of the undigested cytochrome $b_{558}$, Figure 63, are compared with the 414 nm peaks labeled ● and ■ in the top chromatogram of Figure 62 (undigested cytochrome $b_{558}$), there is a slight correlation between the intensity of the staining at $M_r$ ~91 kDa and the 414 nm absorbance. Although there is clearly staining in this molecular weight range throughout fractions 14-20, the most intense staining occurs in fractions 14 and 19. These fractions are the same fractions that include the highest 414 nm absorbance.

The different elution times for the maximum 414 nm absorbance suggests that the undigested cytochrome $b_{558}$ is eluting as both an aggregate and a monomer. However, the form of the aggregate (i.e. association of cytochrome b558 with itself vs. other protein) cannot be deduced from the gel. Apparent bands above $M_r$ 91 kDa in fraction 14 shows that there are other proteins present, including protein that did not penetrate into the gel.

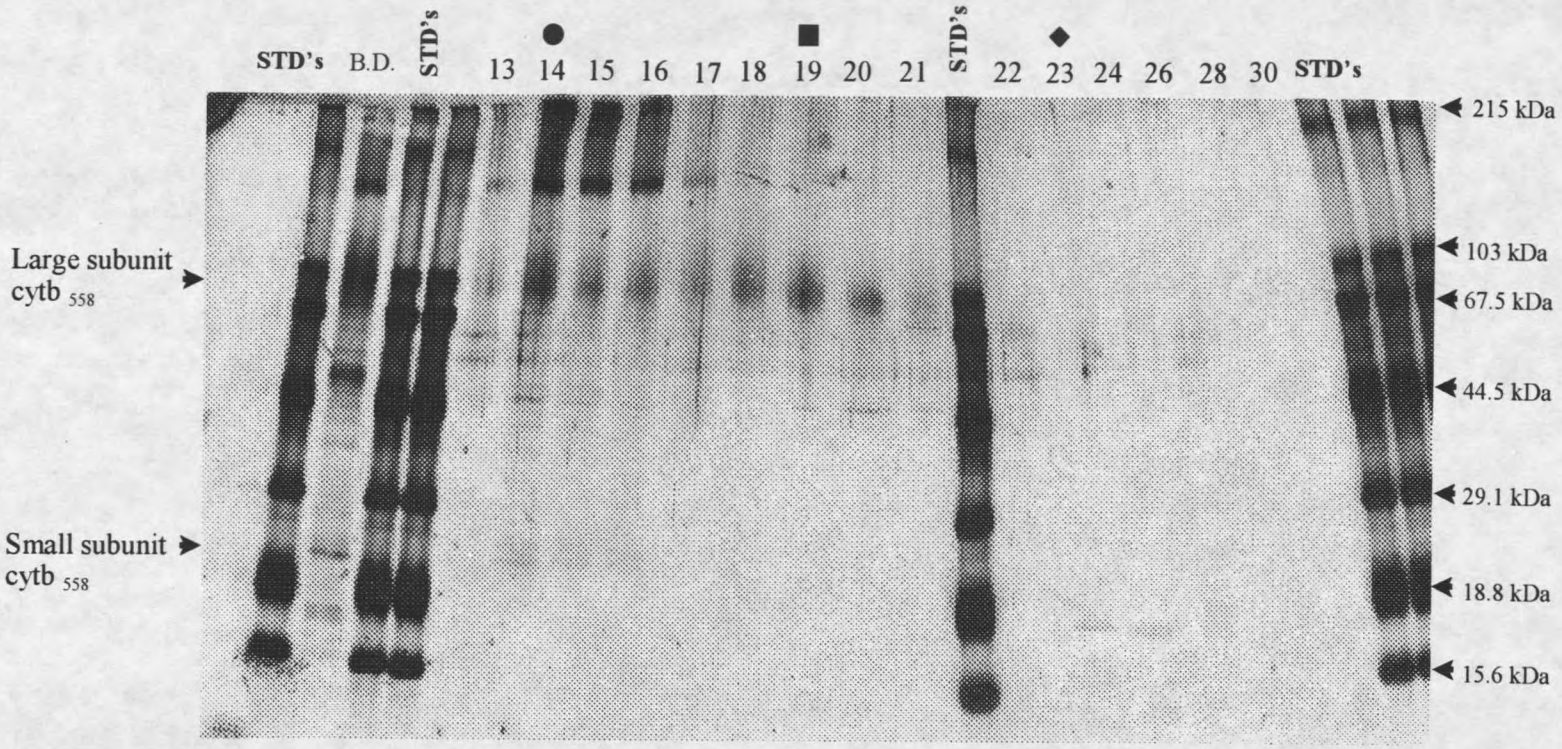


**Figure 63**. SDS-PAGE separation of components from gel filtration chromatography of undigested cytochrome $b_{558}$ solubilized in TX-100. Each lane contains 20 $\mu$l of sample from a total of 800 $\mu$l. Lanes are labeled by the starting time for the collection of the sample. The fractions corresponding to the labeled peaks in Figure 62 are marked by their matching symbols. The gel shows that the 414 nm absorbance peak at 14 min in Figure 62 is made up of aggregated protein while the peak at 19 minutes is unaggregated cytochrome $b_{558}$.

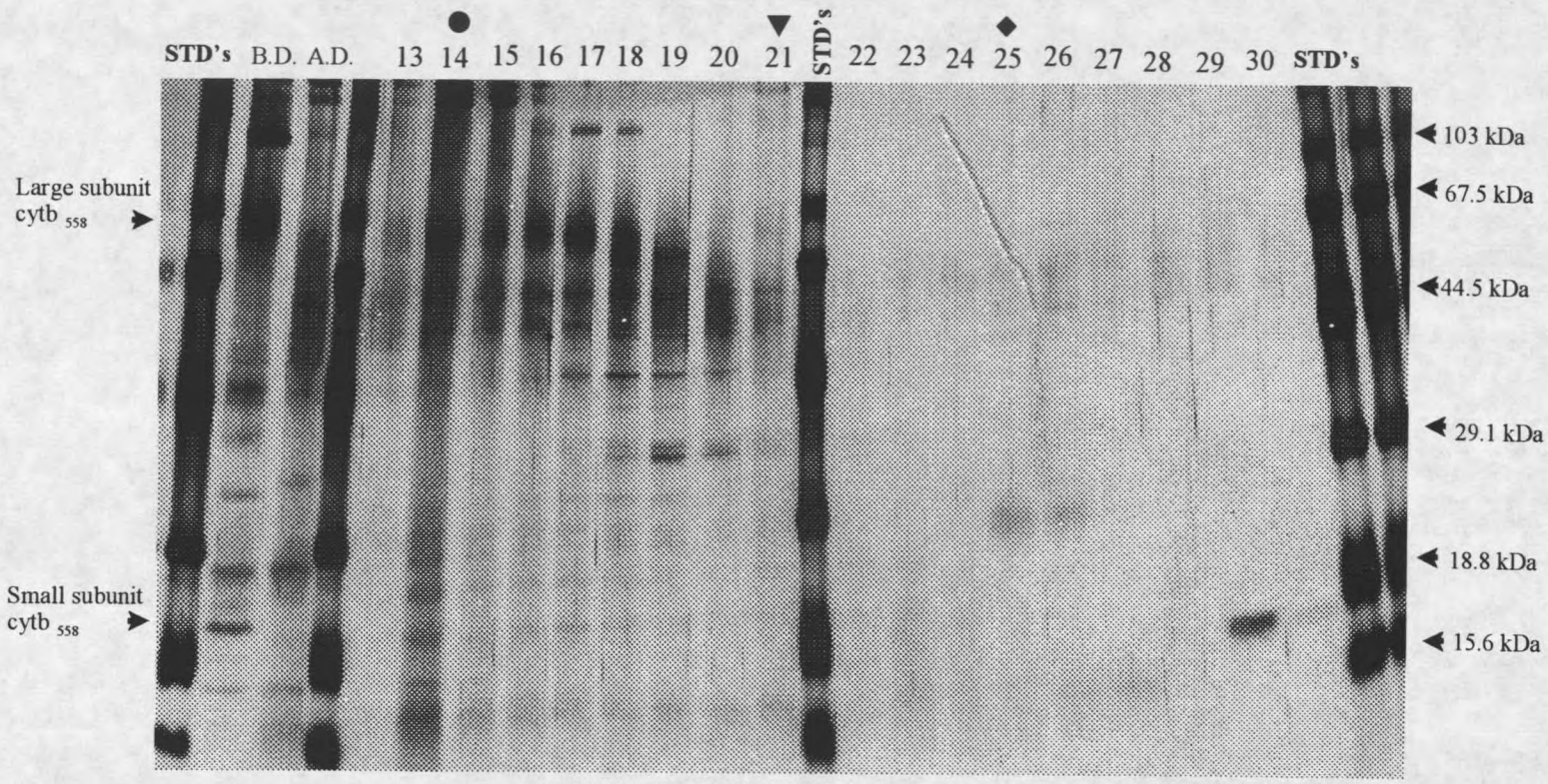


**Figure 64.** SDS-PAGE separation of gel filtration fractions from cytochrome $b_{558}$ solubilized in TX-100 subjected to digestion with trypsin for 1 hour. The gel was developed with silver stain and each lane contains 20 $\mu$l of sample from a total of 800 $\mu$l. Lanes are labeled by the starting time for the collection of the sample. The fractions corresponding to the labeled peaks in Figure 62 are marked by their matching symbols. Lanes B.D. and A.D. are before and after digestion respectively. The gel shows a change in the molecular weight for the large and small subunits after digestion. In addition, the gel illustrates aggregation within the fractions since the low molecular weight bands (<29 kDa) would not appear in early eluting fractions unless part of a complex.

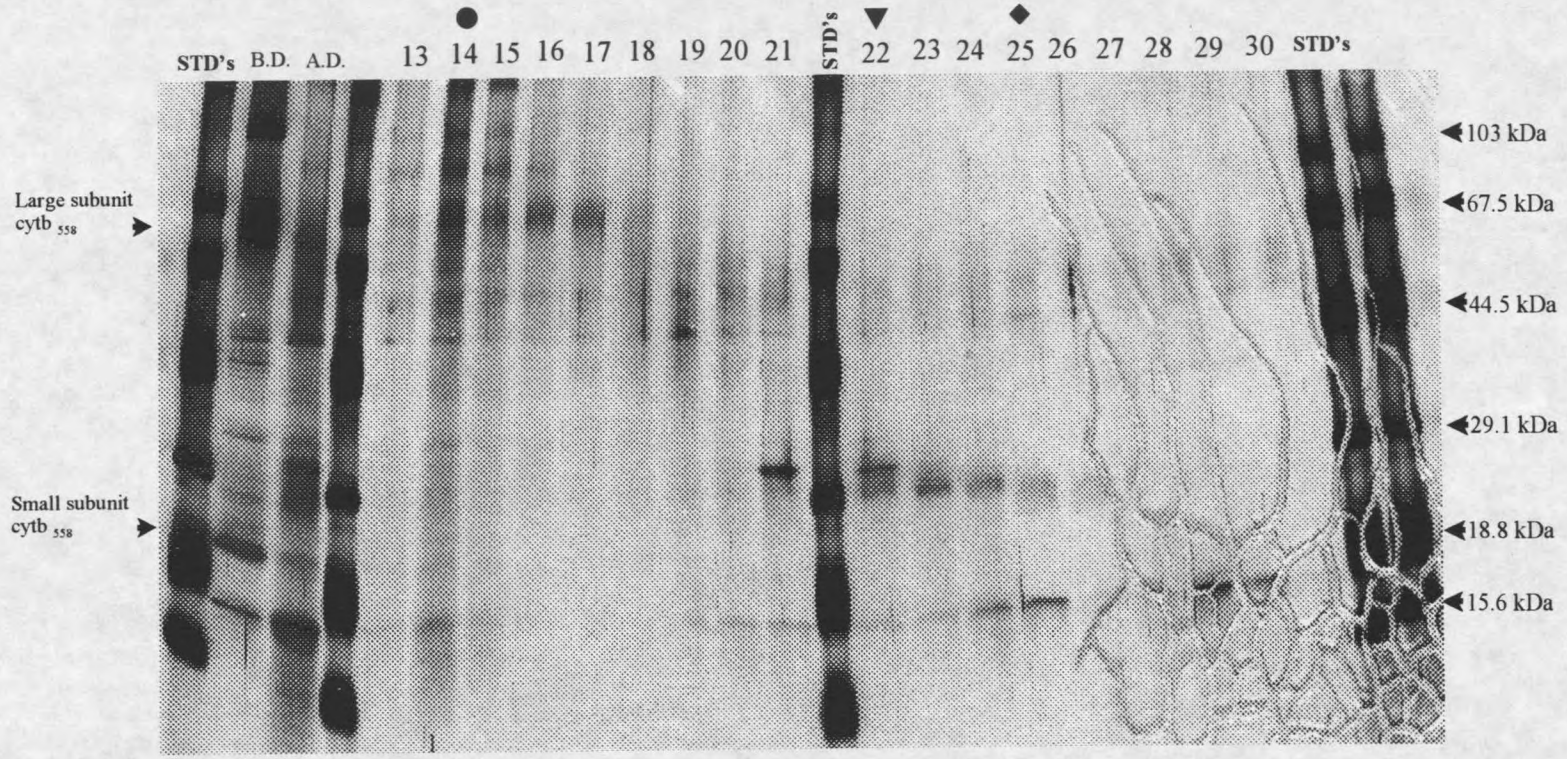


**Figure 65**. SDS-PAGE separation of gel filtration fractions from cytochrome $b_{558}$ solubilized in TX-100 subjected to digestion with V8 for 1 hour. The gel was developed with silver stain and each lane contains 20 $\mu$l of sample from a total of 800 $\mu$l. Lanes are labeled by the starting time for the collection of the sample. The fractions corresponding to the labeled peaks in Figure 62 are marked by their matching symbols. Lanes B.D. and A.D. are before and after digestion respectively. The gel shows a change in the molecular weight for the large and small subunits after digestion. In addition, the gel illustrates aggregation within the fractions since the low molecular weight bands (<29 kDa) would not appear in early eluting fractions unless part of a complex. The lines in the lower right hand corner of the gel are due to cracks formed during the drying procedure.

Comparison of the SDS-PAGE distribution of pre-digestion polypeptides with post-digestion polypeptides allows identification of proteolytic fragments. This type of comparison was done for pre- and post- digestion species for both the tryptic and V8 protease digestions. Figure 64 shows an SDS-PAGE separation of gel filtration fractions from the 1 hour tryptic digest of cytochrome $b_{558}$ solubilized in Triton X-100. The silver-stained gel has two lanes on the left-hand side, B.D. (Before Digest) and A.D. (After Digest), with the large and small subunit of cytochrome $b_{558}$ labeled next to these lanes. The large subunit at ~ 91 kDa can be seen as a diffuse band, in the lane labeled B.D., that appears to shift to a lower molecular weight after partial proteolysis. The small subunit at ~22 kDa, visible in the lanes labeled B.D., disappears at this $M_r$ after digestion. The lanes labeled 14 through 21 illustrate the size distribution of the majority of protein species resulting from partial digestion. However, some of the species are present throughout the remaining fractions. Notably, the bands at $M_r$ ~45-65 kDa, $M_r$ ~26 kDa, and 15.5 kDa. The appearance of small fragments (≤29 kDa), in fractions 14 through 21, indicate that they eluted as part of a complex. Standards run under the same conditions showed that the retention time for fraction 14 corresponds to the elution time for the standard thrombin (M.W. 650 kDa), while the retention time for fraction 21 corresponds to the elution time for the standard ovalbumin (M.W. 45 kDa). Fraction 25 has the same elution time as myoglobin (M.W. 17.5 kDa).

The species which show the highest degree of correlation with the maximum 414 nm absorbance in the gel filtration chromatogram, and are not seen in the preparation prior to digestion, represent the best candidates for further analysis. Furthermore, the species

should ideally be found in a fraction with the fewest number of components (in this case a later elution time). One of the predominant species observed after digestion can be seen in lanes 14 through 21 in Figure 64 at $M_r$ ~45-65 kDa. This diffuse band appears to shift to lower $M_r$'s in lanes 14 through 21 and is no longer apparent in lanes 22 through 30. The species observed at $M_r$ ~15 kDa in lanes 14 thru 21 in Figure 64 can be seen to change in intensity with each lane, but this intensity change cannot be explicitly shown to correlate with the 414 nm absorbance. Thus, the information from the SDS-PAGE separation of the gel filtration fractions does not conclusively show any fragment that is strictly correlated with the maximum 414 nm absorbance profile.

Figure 65 shows an SDS-PAGE separation of gel filtration fractions from the 1 hour V8 digest of cytochrome $b_{558}$ solubilized in Triton X-100. Examination of the lanes labeled B.D. (Before Digest) and A.D. (After Digest), show a change in the molecular weights of the large and small subunits after V8 digestion and are consistent with the findings from the digest done with trypsin. The size distribution of the fragments produced by V8 are readily observed in the SDS-PAGE separation of the gel filtration fractions. There is evidence for aggregation in more than one gel filtration fraction demonstrated by the presence of low molecular weight species similar to the fragments produced by tryptic digestion. Two of these species include the diffuse bands seen at $M_r$ ~ 91 kDa in fractions 14-17 (presumably undigested cytochrome $b_{558}$) and $M_r$ ~45-65 kDa in fractions 18-21. Other species include the sharp band at $M_r$ 30 kDa seen in fractions 21 and 22, along with the diffuse band seen below it at $M_r$ ~ 24-29 kDa observed in fractions 21-26. There is also a band at $M_r$ 17 kDa that is found in fraction 14 and fractions 20-29.

Other post-digestion species observed in the V8 digestion include the diffuse band at $M_r$ ~45-65 kDa, the sharp peak at $M_r$ 30 kDa, and the diffuse band below it at $M_r$ ~ 24-29 kDa. The diffuse band at $M_r$ ~45-65 in lanes 18-21 is similar to the diffuse band seen at the same $M_r$ in the tryptic digest. However, in this instance it appears to have little correlation with the maximum 414 nm absorbance in fraction 22. This band appears in the lanes at the lowest absorbance between the peaks at 14 minutes and 22 minutes, and throughout most of the lanes in the gel, suggesting that it is an artifact most likely caused from the common contaminant keratin. The component at $M_r$ 30 kDa, and the diffuse band at $M_r$ ~ 29 kDa, show some correlation with the peak 414 nm absorbance in fraction 22, however, they are difficult to observe in the aggregated material in fraction 14 which also displays peak 414 nm absorbance. It is possible that these species actually represent the protease V8 and would explain their absence in the starting material. Moreover, the molecular weight of the recombinant V8 from *S. aureus* is 30 kDa and controls performed on V8 separated by SDS-PAGE show a staining pattern between $M_r$ 25-35 kDa similar to that observed in fraction 22. The elution time of a molecule of $M_r$ ~30 kDa is expected to be approximately 21-23 min on the gel filtration column, thus it is not surprising to see evidence for the protease in this fraction. However, this does not rule out the possibility that these species are part of the heme-bearing complex present in these fractions.

The fragment at 17 kDa observed in fraction 14 and 20-29 does appear in the fractions having maximum absorbance at 414 nm. Yet this species appears in the starting material and is present in multiple fractions. Thus, no conclusions can be made on the role this fragment has in association with the heme-bearing fragment. There is a band at 17

kDa in the starting material, yet the intensity of this band increases upon digestion. Due to the resolution of the 7-18% SDS-PAGE gel, it is not possible to tell if this 17 kDa fragment is related to the 17 kDa fragment seen in the starting material, or if it is a new fragment produced by digestion. It is also not possible to tell by SDS-PAGE whether the 17 kDa band observed in fractions 14 and 20-29 are the same or different species with very similar molecular weights. It can only be stated that these species are found in both maximum 414 nm absorbance peaks, and that the species would not elute from the gel filtration column at 22 minutes unless it was complexed with either another fragment, with itself, or possibly non-specific interaction with the column matrix. As stated previously, the information from the SDS-PAGE separation cannot conclusively identify any species as being the heme bearing fragment responsible for the absorbance at 414 nm observed in fraction 22.

Absorption Spectroscopy of Gel Filtration Fractions

Fractions with 414 nm absorbance were concentrated and analyzed for reduced minus oxidized spectral activity to confirm that the absorbance observed was not due to scattering or contaminating chromophores. Figure 66 shows the oxidized absorbance spectra of fractions 17 through 23 from partially digested cytochrome $b_{558}$ solubilized in Triton X-100 subjected to gel filtration chromatography. The fraction with the highest concentration of 414 nm absorbing material was found to be fraction 21. The reduced minus oxidized spectrum of this fraction is shown in the inset and displays the same properties as undigested cytochrome $b_{558}$. Calculation of the recovery of activity in these

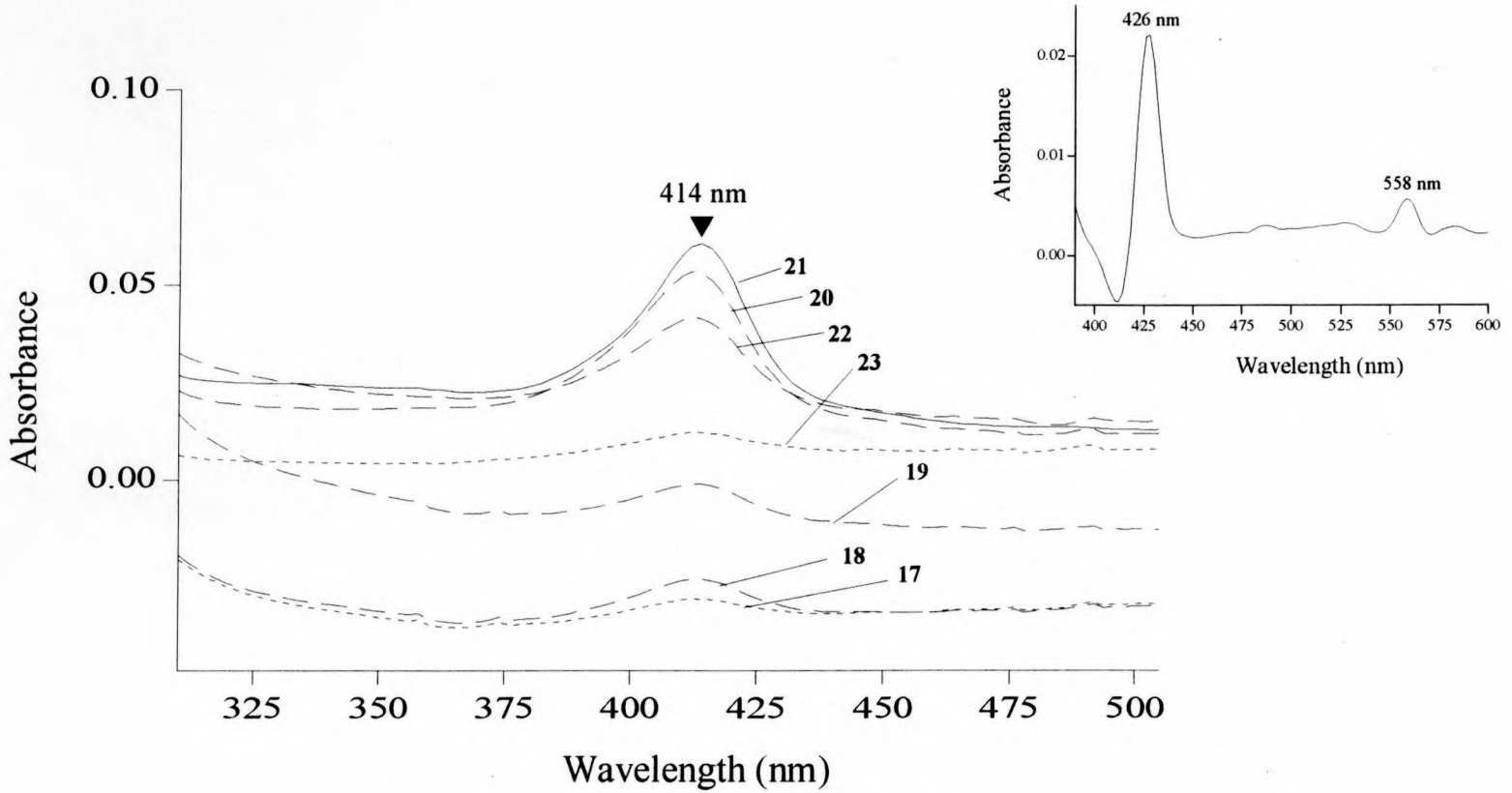


**Figure 66**. Absorbance spectra of concentrated gel filtration fractions 17 through 23 from the partial tryptic digestion of purified cytochrome $b_{558}$ solubilized in TX-100. The inset shows the results from the reduced minus oxidized absorbance spectrum of fraction 21. The results of this experiment suggest that fraction 21 contains a heme bearing fragment that exibits spectral activity identical to that of undigested cytochrome $b_{558}$.

fractions is problematic since the extinction coefficient and the molecular weights of the fragments are unknown. Assuming an extinction coefficient of 161 $mM^{-1}$ $cm^{-1}$ at 426 nm for intact cytochrome $b_{558}$ (12), and an average molecular weight of roughly 30 kDa, the concentration in the 140 $\mu$l cuvette can be estimated to be 700 ng. This amount represents a very small recovery (<1% of the total digested). The oxidized absorbance spectra from gel filtration fractions 18 through 24 minutes, of cytochrome $b_{558}$ partially digested with V8, can be seen in Figure 67. In this figure, fraction 22 has the highest absorbance value at 414 nm of the fractions shown. The inset shows the reduced minus oxidized spectra of this fraction. The calculated recovery is almost identical to that for fraction 21 of the partial tryptic digest.

The results of these experiments indicate that a fragment bearing heme is present in fraction 21 (tryptic digest) and in fraction 22 (V8 digest). The broad elution profile of these peaks also indicates the presence of heme-bearing species in the fractions eluting before and after the maximum 414 nm absorbance activity.

Immunological Analysis of Gel Filtration Fractions

To further characterize polypeptides found in the chromatographic fractions associated with heme absorbance, immunological assays using anti-cytochrome $b_{558}$ specific antibodies were performed. Figure 68 is a Western blot assay of undigested cytochrome $b_{558}$ probed with the anti-small subunit antibody α-EAR (specific for the carboxy-tail, a.a. 162-174). The blot demonstrates that no staining of a 17 kDa species in fractions eluting from the gel filtration column after the injection of undigested

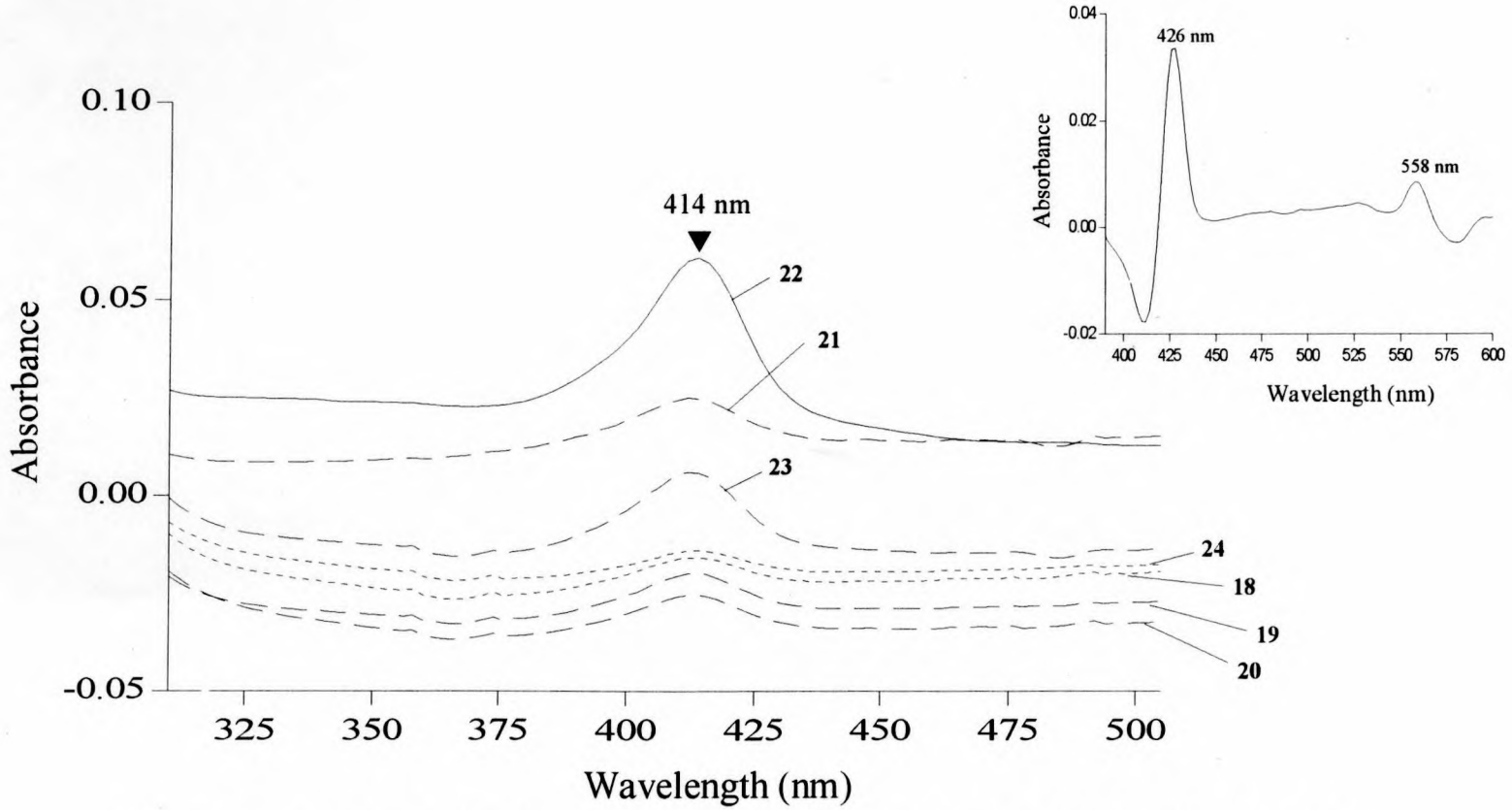


**Figur 67**. Absorbance spectra of concentrated gel filtration fractions 18 through 24 from the partial V8 digest on of purified cytochrome $b_{558}$ solubilized in TX-100. The inset shows the results from the reduced minus oxidized absorbance spectrum of fraction 22. The results of this experiment suggest that fraction 22 contains a heme bearing fragment that exibits spectral activity identical to that of undigested cytochrome $b_{558}$.

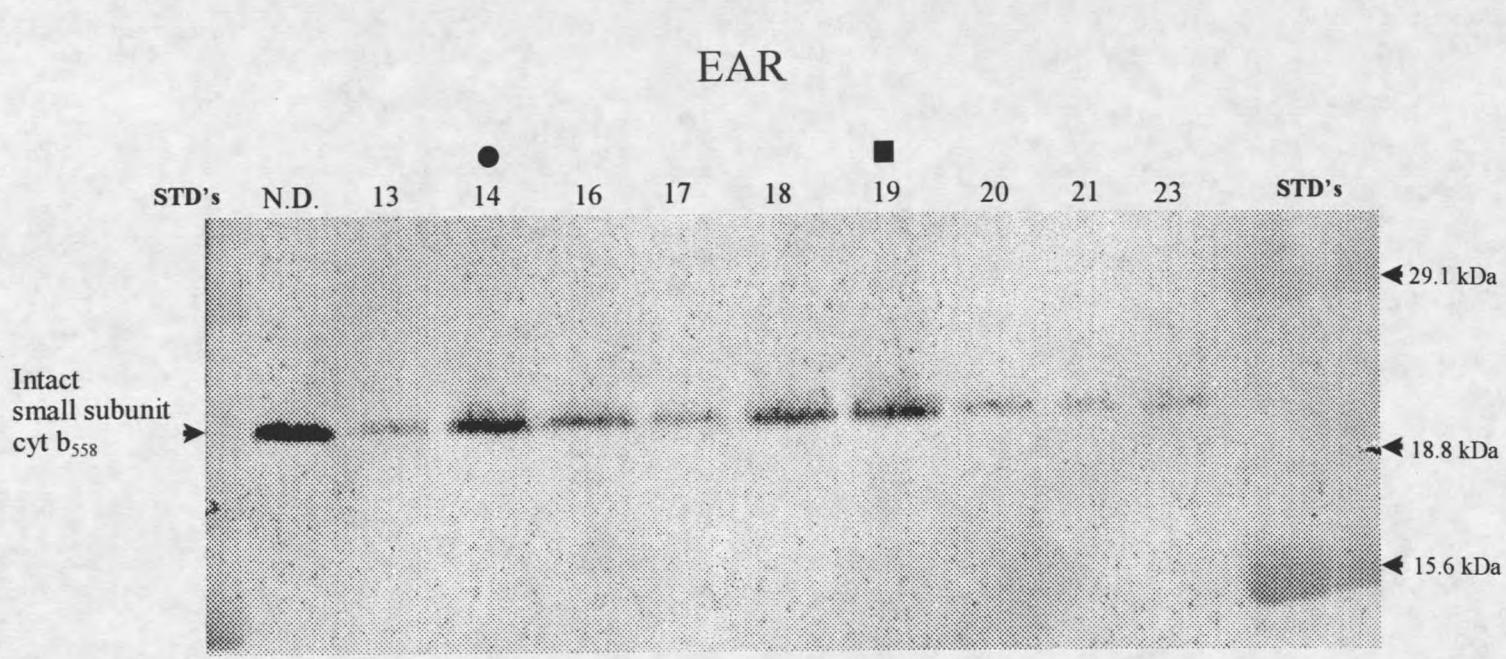


**Figure 68**. Western blot assay of fractions eluted from the gel filtration column after the injection of undigested cytochrome $b_{558}$ solubilized in TX-100. The primary antibody is the anti-small subunit antibody α-EAR at a dilution of 1:400. The lane labeled N.D. is the sample before application to the gel filtration column. The other lanes are labeled corresponding to the starting time for the collection of each fraction from the chromatogram shown in Figure 62 for undigested cytochrome $b_{558}$. The blot demonstrates that the17 kDa fragment is not present in undigested cytochrome $b_{558}$.

cytochrome $b_{558}$. It also shows the correlation between the absorbance of the 22 kDa species from the small subunit of cytochrome $b_{558}$ found in fractions 14 and 19, and an increase in absorbance at 414 nm, as shown in Figure 62.

To correlate absorbance observed after 1 hour of tryptic digestion of cytochrome $b_{558}$ with the fragments produced by the digestion, gel filtration fractions were probed by Western blot analysis using both large and small subunit antibodies. Figure 69 shows the results from probing chromatographic fractions with the anti-small subunit antibody α-EAR and the anti-large subunit antibody α-KIS (specific for a region near the glycosylation sites, a.a. 246-256). The blot labeled EAR clearly shows that the α-EAR epitope is lost after partial tryptic digestion of cytochrome $b_{558}$ under the conditions used. The portion of the figure showing the results using α-KIS demonstrates that the large subunit, shown in the lane marked B.D. (Before Digest), is cleaved into smaller heterogeneously glycosylated fragments at a lower $M_r$, shown in the lane marked A.D. (After Digest). These fragments are seen in gel filtration fractions 14, and 19-21, coinciding with the peaks having 414 nm absorbance in the gel filtration chromatogram in the middle of Figure 62. Bands between $M_r$ ~45-65 kDa recognized by α-KIS, indicate that fragments of the large subunit are present in the fractions with peak 414 nm absorbance. Furthermore, there was no apparent staining below $M_r$ ~45-65 kDa in these fractions indicating that the epitope recognized by α-KIS was only present on these fragments. In addition, the bands in these fractions are diffuse, suggesting the presence of carbohydrate, or possibly the presence of a heterogeneous mixture of cleavage products. Thus, these fragments are likely from the heme containing core region of the large subunit.

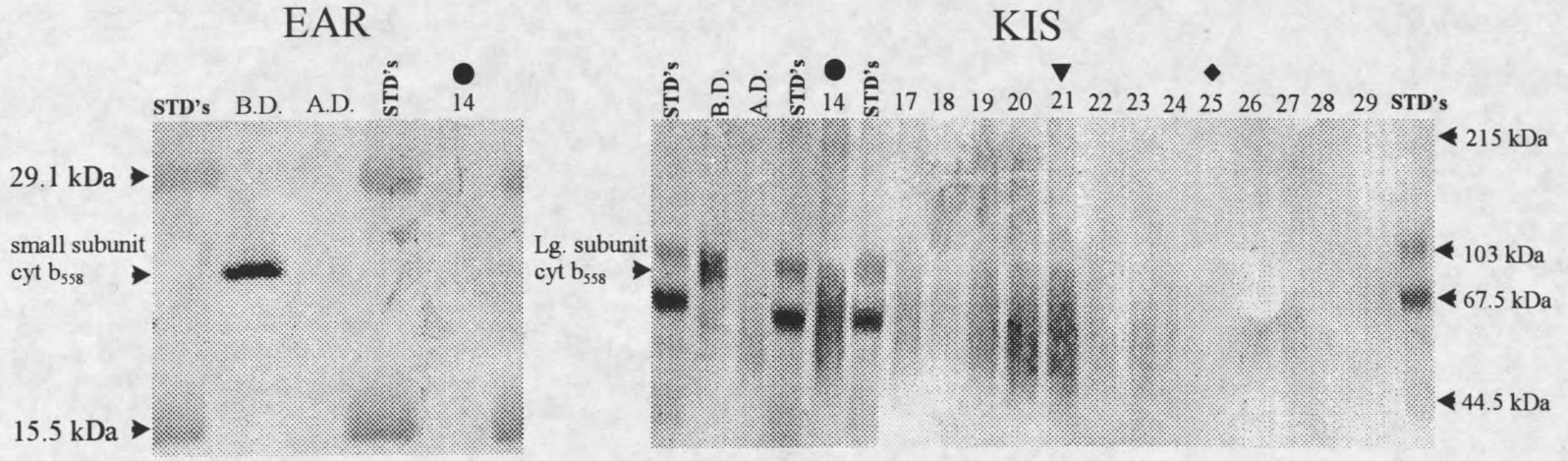


**Figure 69**. Western blot assay of fractions eluted from the gel filtration column after the injection of TX-100 solubilized cytochrome $b_{558}$ partially digested with trypsin. The primary antibodies used are the anti-small subunit antibody α-EAR at a 1:400 dilution and the anti-large subunit antibody α-KIS at a 1:150 dilution . The lanes labeled B.D. are the samples before digestion and the samples labeled A.D. are the same samples after digestion with equal amounts of sample in each lane. Numbered lanes are labeled by the starting time for the collection of the sample. Labeled lanes correspond to fractions with maximum 414 nm absorbance. The blot labeled EAR demonstrates the loss of the epitope recognized by α-EAR on the small subunit after digestion. The blot also shows the presence of proteolytic fragments from the large subunit containing the epitope recognized by α-KIS in fractions that also display heme absorbance.

The chromatographic fractions of the 1 hour V8 digest of cytochrome $b_{558}$ were also subjected to immunological analysis. Figure 70 shows the results from the fractions probed with α-EAR. It is clear from the figure that the 17 kDa fragment recognized by α-EAR appears only after digestion, lane A.D., and is not present in the undigested material, lane B.D. Additionally, a 17 kDa fragment is recovered in multiple fractions, including those with heme absorbance, seen in the bottom panel of Figure 62. Experiments carried out using the antibody α-KIS were inconclusive as insufficient material precluded repeated experiments. However, these results show that the 17 kDa species present before digestion, evident in the silver stained SDS-PAGE gel (Figure 68), is approximately the same molecular weight as the fragment produced after digestion with V8 protease. These results also suggest that a 17 kDa fragment recognized by α-EAR is associated with heme absorbance. Finally, the results of the Western blot analyses from both the 1 hour tryptic and V8 digests show that no intact small subunit is present after digestion. Additionally, the results show that there is a fragment present in fraction 22 from the V8 protease digest that contains the α-KIS epitope.

Detection of a Glycosylated Fragment of Cytochrome $b_{558}$

To determine if the fragments produced by partial digestion were glycosylated, gel filtration fractions were first run on SDS-PAGE gels then transferred onto nitrocellulose and probed with cascade blue-conjugated wheat germ agglutinin. Experiments performed on cytochrome $b_{558}$ partially digested with trypsin revealed that for fractions 19, 20, and 21, the same fractions that stained using the α-KIS antibody in Figure 69, exhibited

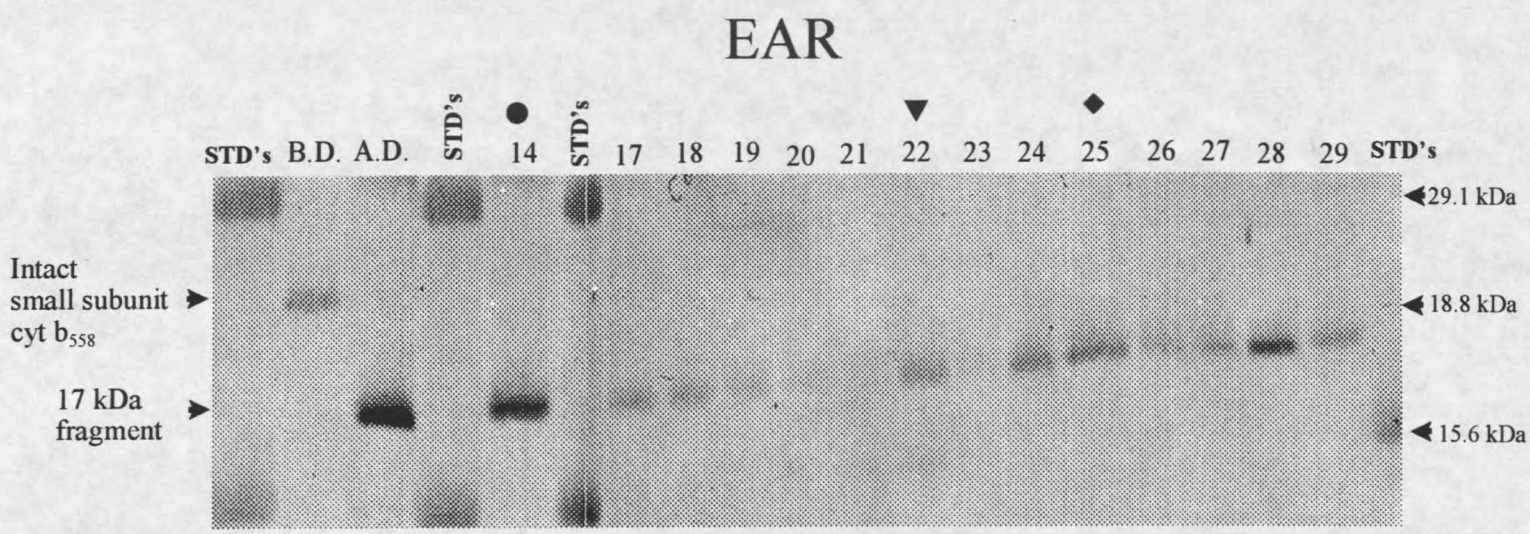


**Figure 70**. Western blot assay of fractions eluted from the gel filtration column after the injection of TX-100 solubilized cytochrome $b_{558}$ partially digested with V8. The primary antibody is the anti-small subunit antibody α-EAR at a 1:400 dilution. The lane labeled B.D. is the sample before digestion and the sample labeled A.D. is the same sample after digestion with equal amounts of sample in each lane. Numbered lanes are labeled by the starting time for the collection of the sample. Labeled lanes correspond to fractions with maximum 414 nm absorbance. The blot demonstrates the digestion of the small subunit clearly visible by the shift from 22 kDa in lane B..D. to 17 kDa in lane A.D. These results show that the 17 kDa fragment observed in the starting material is not recognized by α-EAR. In addition, the 17 kDa fragment recognized by α-EAR is found in multiple fractions, including the fractions associated with heme absorbance. The 'wobble' in the molecular weight in the gel is due to an anomalie in the SDS-PAGE gradient.

fluorescence when probed with WGA-CCB at a $M_r$ ~ 45-65 kDa (data not shown). The fluorescence that was observed for these fractions suggested that a portion of cytochrome $b_{558}$ digested with trypsin yielded a core region of the large subunit that contained sites of glycosylation, heme, and the epitope recognized by the α-KIS antibody. No WGA-CCB binding was observed for the band at 15.5 kDa seen in the silver-stained SDS-PAGE gel in Figure 64.

Gel filtration fractions 17 through 29 from TX-100 solubilized cytochrome $b_{558}$ partially digested with V8 were also examined for WGA-CCB binding, and the results are shown in Figure 71. A 17 kDa band is seen in fractions 24, 25 (◆), and 28. There was no discernible WGA-CCD staining for this 17 kDa band in samples examined before digestion (data not shown). There is only weak WGA-CCB staining for the band at 17 kDa in the fraction 22 (▼) that was recognized by the anti-small subunit antibody α-EAR and exhibited peak heme absorbance. Upon comparison of the results from the Western blot shown in Figure 69, and the WGA-CCB results in Figure 71, there is clearly a difference in the intensity of the staining patterns depending on the primary recognition modality (immunological vs. lectin). The α-EAR antibody used to probe the fractions in Figure 69 recognizes fragments in fractions 24-29. However, when these same fractions are probed with WGA-CCB, intense staining is only readily apparent in fractions 24, 25 and 28. The reason for this discrepancy is not known but may be due to the different sensitivities intrinsic to each assay. The observation of WGA-CCB fluorescence staining for a fragment at 17 kDa, that is also recognized by a small subunit antibody, is quite intriguing.

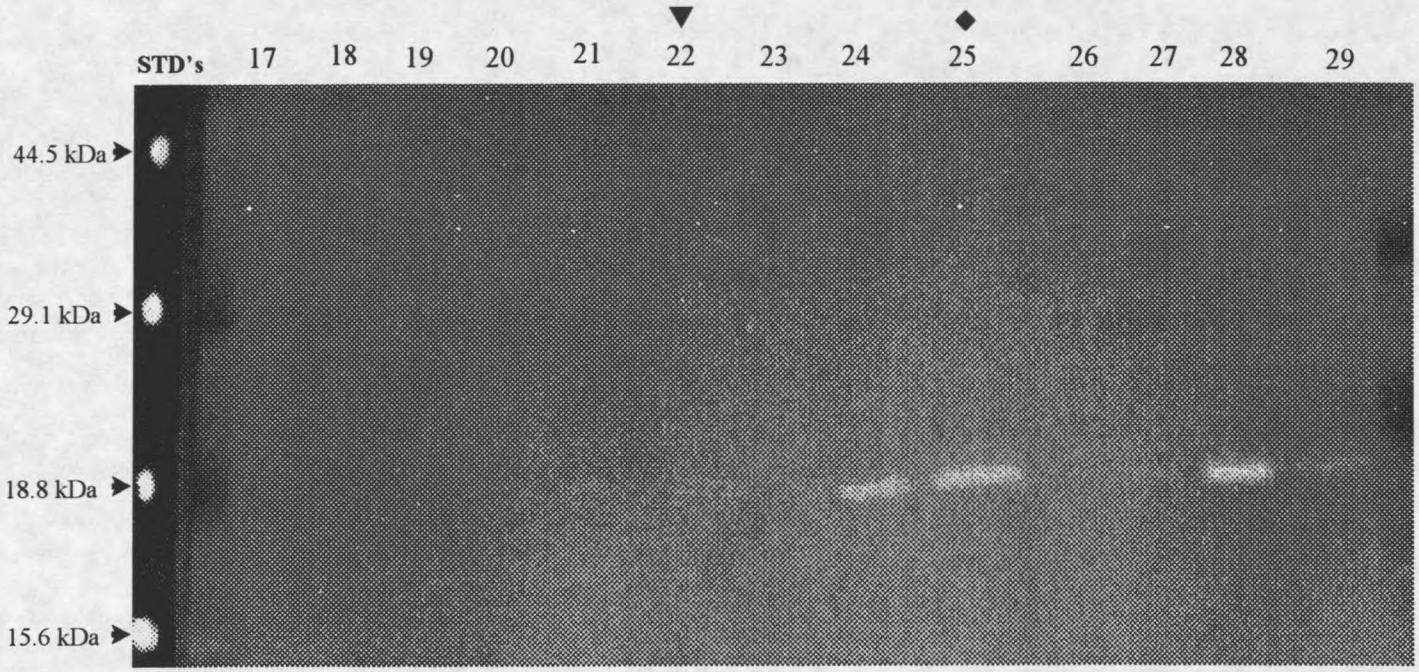


**Figure 71**. Wheat germ agglutinin-conjugated Cascade Blue affinity labeling blot of fractions 17 through 30 eluted from the gel filtration column after the injection of TX-100 solubilized cytochrome $b_{558}$ partially digested with V8. Labeled fractions correspond to fractions having maximum 414 nm absorbance in the bottom chromatogram of Figure 62. The blot demonstrates that the WGA binding capacity associated with 17 kDa fragment is readily apparent in fractions 24 and 25 (◆).

One hypothesis for this observation is that the fragment either has carbohydrate and is complexed with the α-EAR epitope, or has affinity for WGA not related to carbohydrate.

MALDI MS Analysis of Gel Filtration Fractions

Accurate mass determination of proteolytic digests can be used to unequivocally identify the fragments of proteins whose sequence is known (33). Mass data for proteolytic fragments from cytochrome $b_{558}$ were compared with the predicted amino acid sequences of fragments produced from a complete digestion of the protein by a protease of known specificity. To assist in characterizing the fragments associated with the heme absorbance from cytochrome $b_{558}$ digests, MALDI MS was performed on the peak heme absorbance fractions from both the tryptic and V8 digests. These fractions include fraction 21 from the partial tryptic digest and fraction 22 from the partial V8 digest.

Figure 72 shows a MALDI MS spectrum of fraction 21 from the 1 hour tryptic digest. The peak labeled ***a*** in the spectrum has a tentative assigned mass of 15,325 Da. A centroid assignment for this peak is compromised by the low intensity of the peak along with its asymmetric shape. The peak with a somewhat lower mass may be a product of an additional tryptic cleavage from peak ***a***. However determination of an accurate mass difference between the two peaks is not possible due to low intensity and low resolution. There are 2 speculative assignments for the location of the mass peak labeled ***a*** in Figure 72. The computer program General Protein Mass Analysis for Windows (GPMAW) is able to match the mass of possible fragments produced from a known protein sequence by comparing the known amino acid sequence to the mass of the unknown fragment.

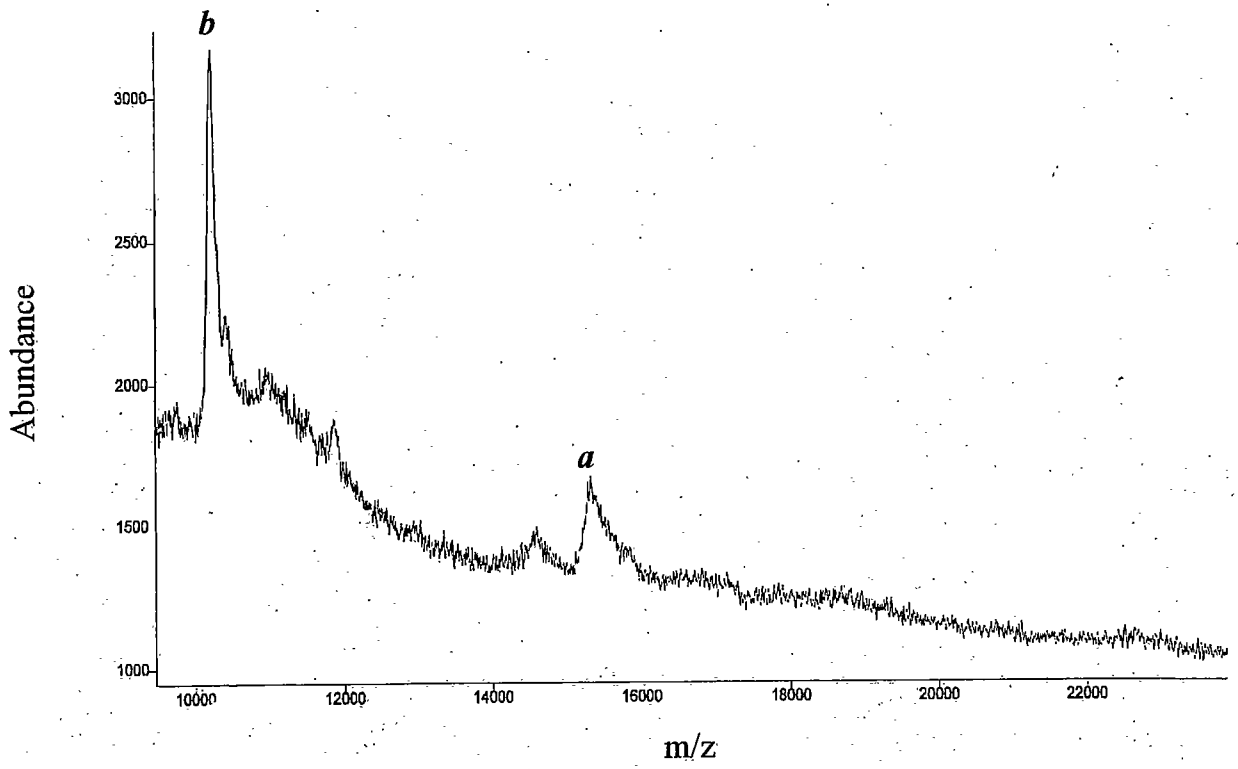


**Figure 72**. MALDI mass spectrum of gel filtration fraction 21 from the 1 hour tryptic digest of TX-100 solubilized cytochrome $b_{558}$. The peak labeled ***a*** is the 15.5 kDa fragment at m/z 15,325 while the peak labeled ***b*** at m/z 10,215 Da is an additional fragment not observed by SDS-PAGE. Tentative assigment for the peak at m/z 15,325 Da includes the region M 1 to R 139 from the small subunit. The asigment for the peak at m/z 10,215 Da includes the region from the small subunit from K72 to K165. The MALDI MS data shown in the figure suggest the presence of small subunit tryptic fragments in fraction 21.

There were two possible matches found using GPMAW at a mass error tolerance of 0.2% or roughly +/- 30 Da for the peak at 15,325 Da. These two matches were from the small subunit with residues M 1 to R 139 (m.w. 15,289 Da) and the large subunit with residues Q 92 to R 225 (m.w. 15,302 Da). The fragment from the small subunit would not include the epitope recognized by the α-EAR antibody. This analysis suggests that the α-EAR antibody would not recognize this fragment if it were indeed from the small subunit since the epitope specific for the antibody was cleaved away. The match for the large subunit also does not include the additional mass from glycosylation that should be present at arginine residues 131 and 146, thus it is unlikely that it represents fragment Q92 to R225 of the large subunit. In addition, Figure 72 also contains an additional peak labeled ***b*** at m/z 10,215 that is 7 Da higher in mass than the tryptic peptide including residues H 71 to K 165 from the small subunit. This fragment also does not contain the epitope for the α-EAR antibody. Confidence in the estimation of the mass for the peak labeled ***b*** in Figure 72 is high. Therefore, the results from the MALDI MS data suggest the existence of fragments originating from the small subunit in fraction 21 that should not be recognized by the α-EAR antibody.

The MALDI MS spectrum of the mass region from 15 kDa to 55 kDa for fraction 21 is shown in Figure 73. The figure clearly shows a broad mass peak with a center of mass at 40,000 Da. If this is the true mass of the fragment containing the epitope for the α-KIS antibody, seen in Figure 68, then the mass of the polypeptide chain present in the fraction, without the proposed glycosylation (roughly 26 kDa, estimated from SDS-PAGE results), is approximately 14,000 Da. Therefore, if the mass peak observed at 40,000 Da in

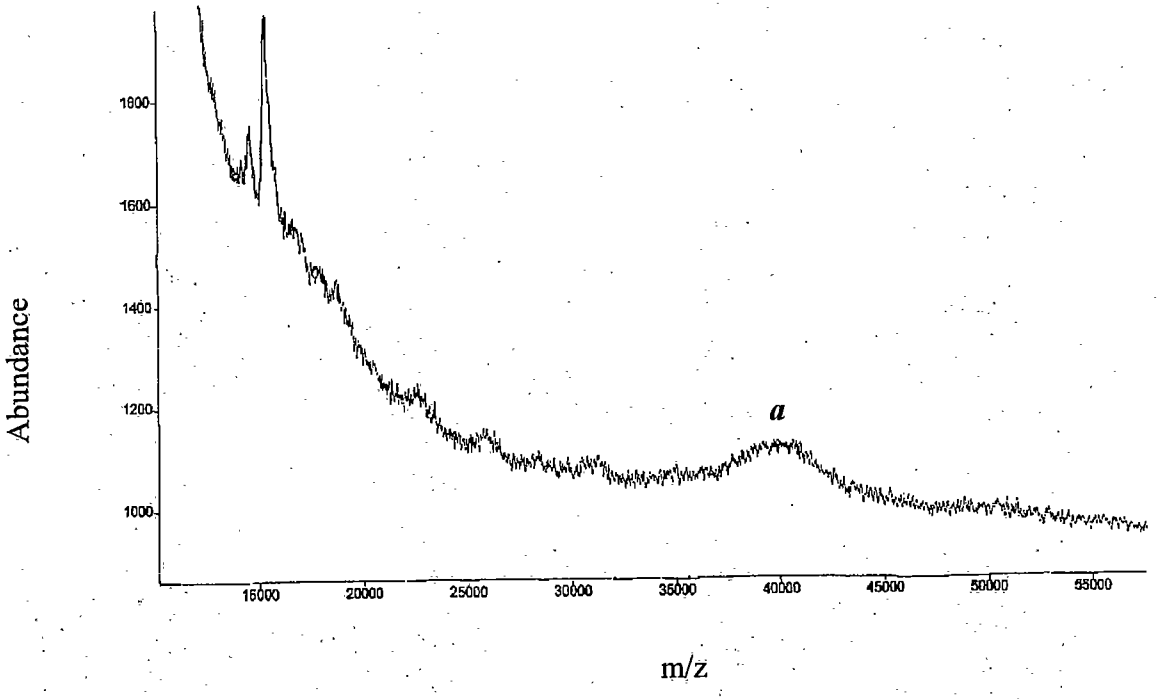


**Figure 73**. MALDI mass spectrum showing the region between m/z 15,000 to 55,000 of gel filtration fraction 21 from the 1 hour tryptic digest of cytochrome $b_{558}$. The peak labeled ***a*** presumably represents the broad 45-65 kDa fragment observed in the SDS-PAGE gel that also exhibited staining when probed with the large subunit antibody α-KIS. The peak is heterogeneous in mass likely due to the presence of glycosylation. The results from this spectrum show that the masses of the fragments recognized by α-KIS are actually lower than those observed by the Western blot analysis. In addition, these results suggest that the polypeptide chain containing the KIS epitope, and proposed sites of glycosyltaion, may include potential heme coordinating sites.

Figure 73 contains all the predicted extracellular sites of glycosylation on the large subunit, e.g. asparagines 131, 146, and 239, with approximately 14 kDa from the polypeptide chain, the fragment can only reasonably contain only residues 130 through 270 and still include the epitope for the α-KIS antibody. This tentative assignment for a position of this fragment in the large subunit would also include potential heme coordinating sites H 208, H 209, and H 221, all within the same proposed transmembrane region. Estimates for the position of the fragment represented by the peak labeled ***a*** in Figure 73 are based on the assumption that this peak was the same fragment recognized by the anti-large subunit antibody α-KIS shown in Figure 68. Nevertheless, there were no mass peaks observed in this fraction above 45,000 Da. This observation implies that the mass observed at 40,000 Da depicts all the high mass components (>35 kDa) ionized by MALDI and thus includes the fragments that contain the α-KIS epitope seen in Figure 68.

To compare the contents of fractions derived from the V8 digest with those observed from the tryptic digest, MALDI MS was performed on chromatographic fraction 22 which contained fragments associated with the highest absorbance at 414 nm after V8 digestion. The MALDI mass spectrum of gel filtration fraction 22 is shown in Figure 74. This spectrum contains a large peak at 15,237 Da that matches the mass of the doubly charged ion from the V8 protease labeled $MH_2^{+2}$. The smaller peaks between 14,000 Da and 15,200 Da are also from the protease and are due to heterogeneously cleaved Pro and Arg residues found in a repeated motif in the carboxy-terminal portion of the protease. The mass region above 20 kDa is not shown. However, it was clear from the higher mass region of the spectrum that V8 was the most easily ionized component of the fraction

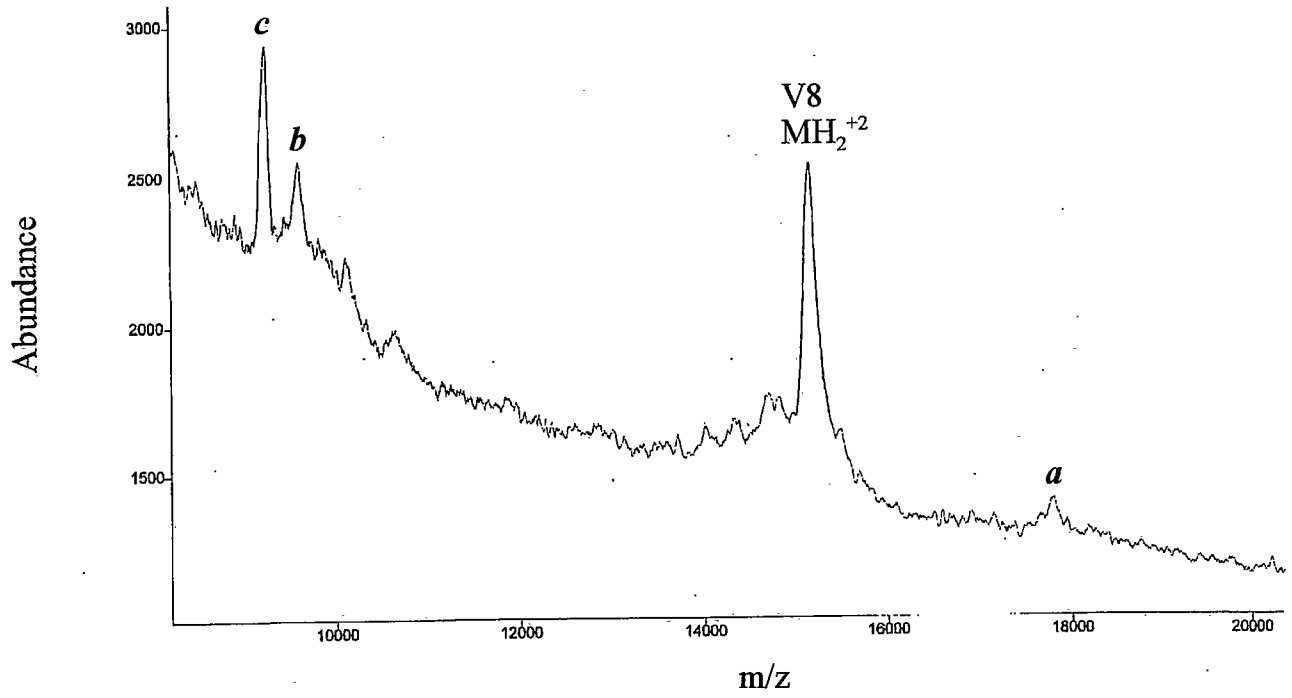


**Figure 74.** MALDI mass spectrum of gel filtration fraction 22 from the 1 hour V8 digest of TX-100 solubilized cytochrome $b_{558}$. The peak labeled *a* is the 17 kDa fragment at m/z 17,786. The peak labeled *b* at m/z 9,250 matches the mass of a V8 peptide of the large subunit from V203 to E282 while the peak labeled *c* at m/z 9,623 matches the mass of a V8 peptide from A378 to E 461 also from the large subunit. The main peak in the spectrum is due to the doubly charged ion from intact V8 protease. These results suggest the presence of fragments from the large subunit in fraction 22.

since a large peak at the exact mass for V8 dominated this region of the spectrum. The spectrum also shows a peak labeled ***a*** which is at the same mass as the band at 17 kDa observed in SDS-PAGE, Western blot, and WGA-CCB experiments. Since the intensity of this peak is low, the timed-ion selector option available in the instrument was utilized to try and obtain a better mass assignment. This option allows only ions with a predetermined flight-time to reach the detector. However, experiments that were performed on fraction 22 using the timed-ion selector did not produce a more intense peak at the mass for peak ***a*** to allow for a more accurate mass assignment. Yet, control mass spectra taken of the V8 protease showed no mass peaks at 17 kDa thus suggesting that this peak did not originate from the protease.

Nonetheless, using the tentative mass found in Figure 74 for peak ***a*** (17,786 Da), along with the GPMAW software, a match was determined for the fragment that would result from the cleavage of the carboxytail of the small subunit at E 162 (m.w. 17,734 Da) leaving a fragment that would include H 92 from the proposed transmembrane region of the small subunit. However, if this were the case the epitope for the α-EAR small subunit antibody would be cleaved away. This interpretation is thus in conflict with the Western blot results shown above which show staining for this 17 kDa species with the α-EAR antibody (see Figure 69). Yet this fragment could clearly not originate from the cleavage of hCAP-18 since there is no V8 cleavage product of hCAP-18 that remotely resembles the mass of this fragment. In addition, there were no V8 fragments that matched with the tentative mass of 17,786 Da that could have originated from the large subunit. An alternative explanation is that this fragment represents another form of the heme stabilized

complex of fragments from the large and small subunits. However, an accurate characterization of the fragment observed at 17,786 Da in relation to the large or small subunit is not possible using the MALDI MS data obtained on this fraction.

The MALDI mass spectrum in Figure 74 also contains two other distinct mass peaks not related to V8, labeled ***b*** and ***c***. The fragment labeled ***b*** at m/z 9,623 is 12 Da higher in mass than a V8 generated fragment of the large subunit consisting of residues A 378 to E 461. This fragment contains a proposed transmembrane region however, the only histidine in the fragment, H 448, is within a proposed cytosolic domain. The other fragment labeled ***c*** at m/z 9,256 Da is 14 Da higher in mass than a calculated V8 fragment from the large subunit consisting of residues V 203 to E 282. This fragment includes a proposed transmembrane region that contains histidines H 208, H 209, and H 22. However, it also contains a proposed glycosylation site at N239 and the mass that was found to match does not include the additional mass due to glycosylation. The MADLI MS high mass region of fraction 22 showed no other peaks than those of the protease.

Examination of the low mass regions in the MALDI MS spectrum from fraction 21 of the trypsin digest and fraction 22 of the V8 digest revealed the presence of heme in the sample verified by its mass at 616.5 Da. Figure 75 shows the MALDI mass spectrum from the low mass region of fraction 21 taken from the tryptic digest of cytochrome $b_{558}$ solubilized in Triton X-100. It is clear from the evidence of the mass of heme in fractions 21 from the tryptic digest and fraction 22 of the V8 digest, along with the spectral evidence in Figures 69 and 70, that fragments present in these fractions coordinated heme.

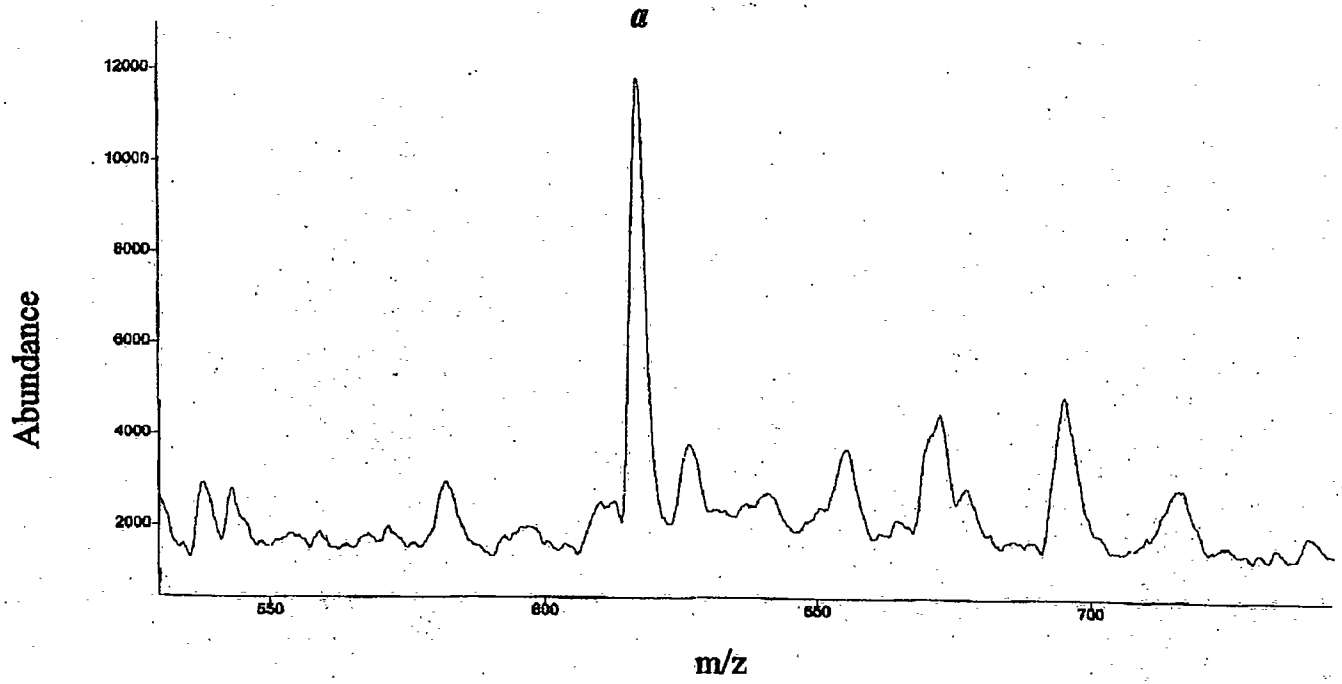


**Figure 75**. MALDI spectrum showing the low mass region of gel filtration fraction 21 from the partial tryptic digest of cytochrome $b_{558}$ solubilized in TX-100. The peak labeled ***a*** has an accurate mass of 616.5 Da, identical to the mass of heme. The results from the low mass region of Fraction 22 from the partial V8 digest of are equivalent to the spectrum show in the figure. These results show that heme is present in fractions 21 and 22 consistent with the absorbance spectroscopy data.

## Discussion

The differential protease sensitivity of cytochrome $b_{558}$ solubilized in the detergents octyl-glucoside (OG) and Triton X-100 plainly establishes the critical role played by detergent in stabilizing heme containing fragments when the protein is subjected to partial digestion. This conclusion is based on the results from structurally and optically stable heme-bearing proteolytic fragments isolated by high performance gel filtration chromatography. Characterization of the fragments was carried out using SDS-PAGE, immunological and lectin reactivity, and MALDI MS. Due to the extensive volume of data presented in this chapter, flow diagrams are presented to aid the discussion of the results. Salient points have been reiterated to facilitate the understanding of the argument for the identification of the heme-binding domain in cytochrome $b_{558}$. In addition, the flow diagrams include the results from SDS-PAGE, Western blot, WGA-CCB, and MALDI MS analyses for species in the gel filtration fractions exhibiting reduced minus oxidized heme absorbance properties.

### Condensed Summary of Experimental Procedures and Results

Figures 76, 77, and 78 summarize the experimental design and results of three different approaches aimed at identification of the heme-bearing domain of cytochrome $b_{558}$. In each figure the dashed boxes illustrate a key result found in the experimental series. The bold text after the arrows describes key experimental procedures leading to the boxed result.

The diagrams refer to the analysis of OG solubilized cytochrome $b_{558}$ digested with trypsin (Figure 76), Triton X-100 solubilized cytochrome $b_{558}$ digested with trypsin (Figure 77), and Triton X-100 solubilized cytochrome $b_{558}$ digested with V8 protease (Figure 78).

The first step in the experimental procedure, labeled 1) in the diagram, was the observation of the effect of partial digestion on the absorbance spectrum. It is clear that the absorbance spectrum deteriorates dramatically during the partial digestion of the protein solubilized in octyl-glucoside. This is in contrast to the identical digestion performed while the protein is solubilized in Triton X-100 where the absorbance spectrum does not change. This comparison is easily seen in Figures 50 and 60. The absorbance intensity at 414 nm of the partial tryptic digest performed in OG shows a loss of roughly 60% after 10 minutes of digestion as opposed to the partial tryptic digestion performed in Triton X-100 where the absorbance intensity at 414 nm does not change appreciably, even after 60 minutes. These data imply that OG renders the fragments produced unstable as compared to Triton X-100 and is true irrespective of the protease used.

The second step in the experimental procedure, labeled 2) in the flow diagrams, refers to the fragments produced as observed by SDS-PAGE. In each partial digestion experiment, the intact cytochrome $b_{558}$ starting material was cleaved into smaller fragments. This is supported by the disappearance of the bands at $M_r$ = 91 kDa (large subunit) and $M_r$ = 22 (small subunit) after 1 hour of digestion, clearly seen in Figures 51, 64, and 65 in the lanes labeled B.D. (Before Digest) and A.D. (After Digest). Proteolytic fragments produced include a 15.5 kDa band from the tryptic digestion and 17 kDa band from the digestion with V8 protease.

**Figure 76** **Flow Diagram of the Partial Tryptic Digestion of Cytochrome $b_{558}$ Solubilized in Octylglucoside**

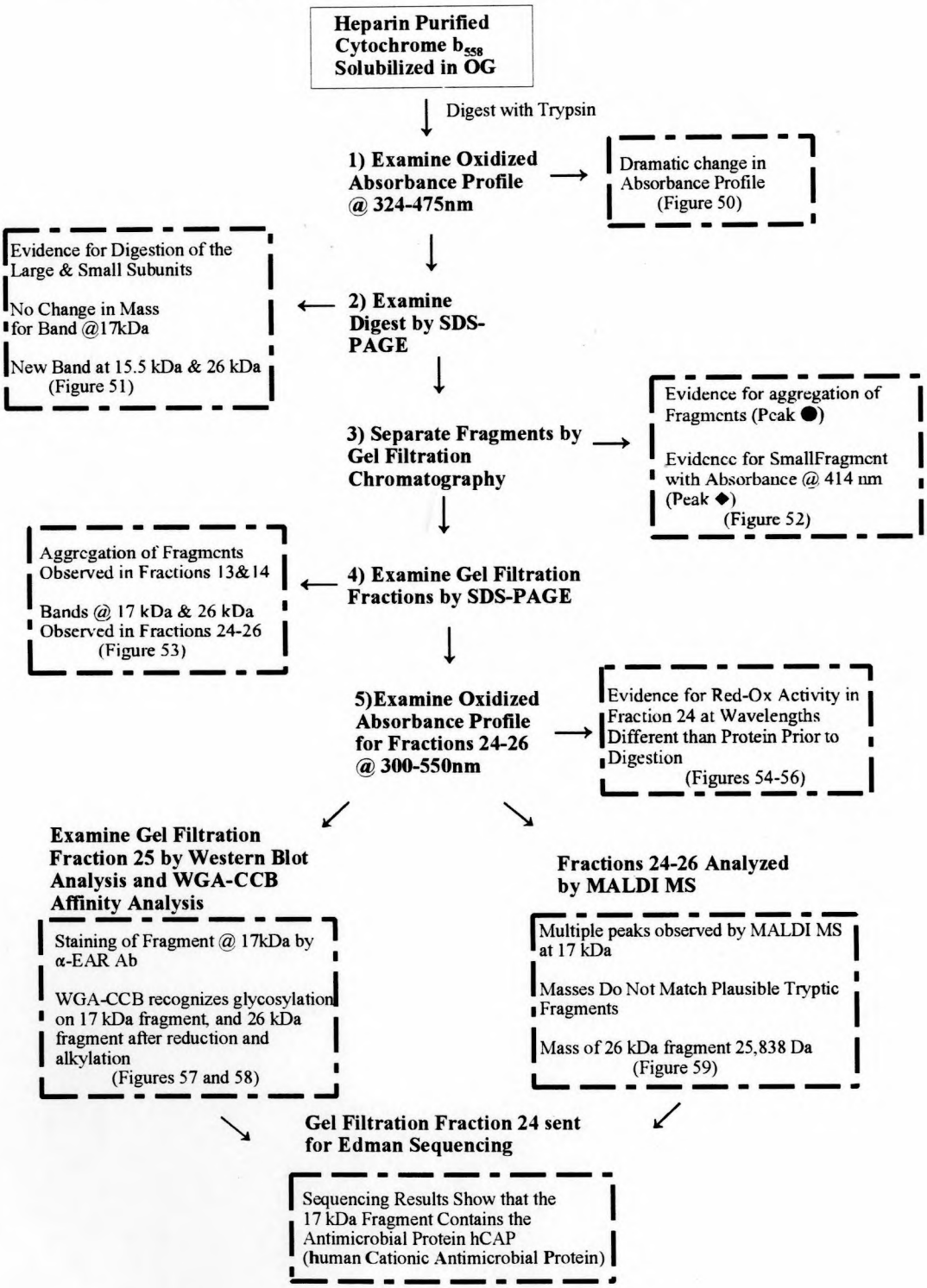

**Figure 77** **Flow Diagram of the Partial Tryptic Digestion of Cytochrome $b_{558}$ Solubilized in Triton X-100**

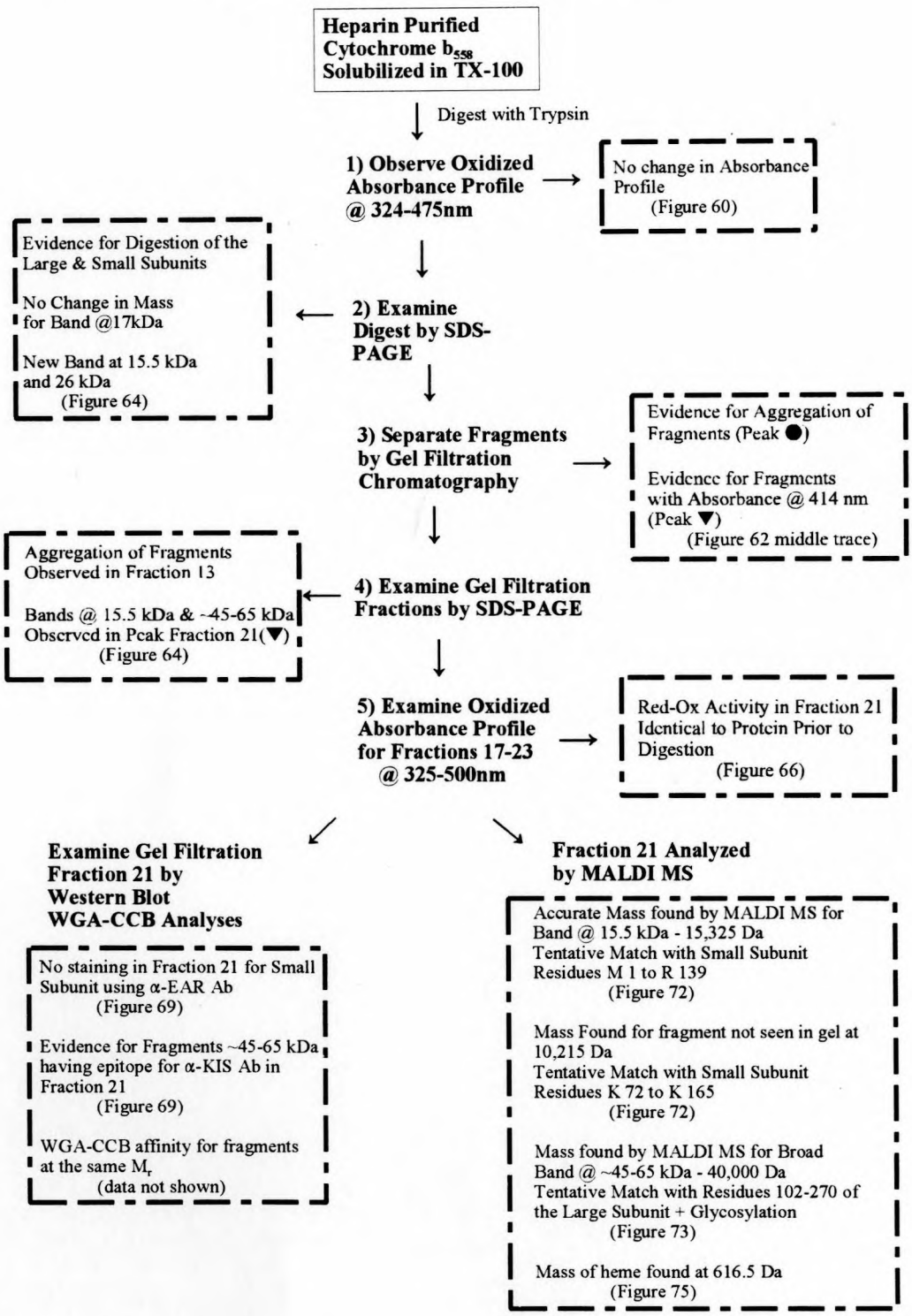

**Figure 78** **Flow Diagram of the Partial V8 Digestion of Cytochrome $b_{558}$ Solubilized in Triton X-100**

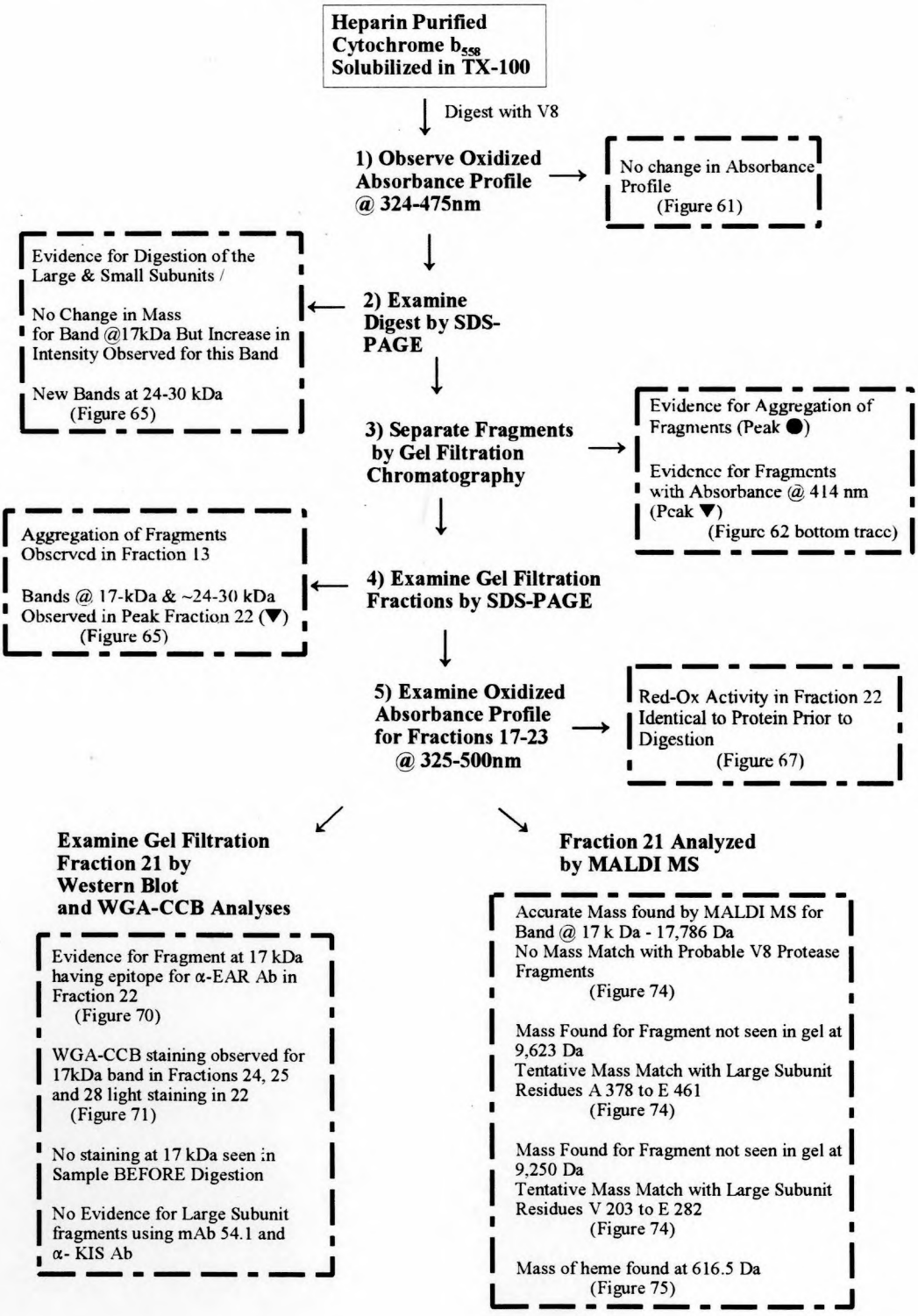

The third step in the experimental procedure, labeled 3), was separation of the proteolytic fragments by gel filtration chromatography. The separation was 'non ideal' since many fragments associated with the absorbance at 414 nm eluted as an aggregate, at or near the void volume of the column. Current experiments suggest that these aggregates existed in the crude detergent extract and can be dispersed by sonication without significant loss of heme absorbance (A. Jesaitis, personal communication). Figure 52 shows the gel filtration chromatogram from the partial digest of cytochrome $b_{558}$ in OG and confirms that a majority of the heme-containing species elutes as part of an aggregate and only a small amount of heme-bearing material elutes at a later retention time. This conclusion is derived from spectroscopic evidence including the 414 nm absorbance and tryptophan fluorescence chromatograms shown in Figure 52. The molecular size for the peak labeled ● in Figure 52 is approximately 657 kDa while that for the peak labeled ◆ is approximately 17.5 kDa, as determined by their retention times relative to standard proteins run under the same conditions. Control experiments with undigested cytochrome $b_{558}$ solubilzed in OG show that a majority of the protein elutes as an aggregate. Little or no 414 nm absorbance activity eluted at a later retention time (data not shown). Figure 62 illustrates the findings for the TX-100 digestions and clearly shows that new peaks containing heme bearing fragments were produced, and isolated, upon digestion with either trypsin or V8. The apparent molecular weight of the peak observed in each chromatogram labeled ●, at ~14 minutes, is approximately 675 kDa while the apparent molecular weight of the peak labeled ■ at 19.5 min in the undigested material is roughly 150 kDa. This distribution differs significantly after digestion, where the peak

at ~14 minutes has the same retention time but both the peak shape and intensity change. Furthermore, the peak observed at 19.5 minutes in the undigested material now shifts to a later retention time. This is evident by the new peaks observed in the partially digested samples labeled ▼, which have retention times of 21.4 minutes for the tryptic digest and 22.1 minutes for the V8 protease digest. The apparent molecular weight for these new peaks are approximately 60 kDa and 45 kDa, respectively.

The fourth procedure in the analysis, (labeled 4 in Figures 76-78), involved analysis of gel filtration fractions by SDS-PAGE. Separation of the components in the aggregate peak at ~14 minutes showed that the fractions contain many proteolyzed fragments of cytochrome $b_{558}$. Unaggregated proteolyzed fragments from cytochrome $b_{558}$, associated with 414 nm absorbance were separated by gel filtration. Fraction 24-26 of the tryptic digest in OG (Figure 53), fraction 21 of the tryptic digest in TX-100 (Figure 64), and fraction 22 of the V8 protease digest in TX-100 (Figure 65) all show evidence for fewer fragments than the peak at ~ 14 minutes. In addition, the $M_r$ 's for these fragments are different from those of the large and small subunit.

The fifth procedure in the analysis, (labeled 5 in Figures 76-78), was the absorbance spectroscopy of gel filtration fractions. This part of the analysis was necessary to rule out other sources of 414 nm absorbance and was central to confirming the presence of heme in the isolated proteolytic fragments. The reduced minus oxidized absorbance spectra for the peak fractions from the digestions carried out on TX-100 solubilized cytochrome $b_{558}$ (Figures 60 and 61) show that proteolytic fragments retain heme in an environment similar to the intact protein. When digestion was carried out in

OG the absorbance spectra obtained from fragments isolated by gel filtration (seen in Figures 54, 55, and 56) show that after partial digestion the species present no longer possess the same reduced minus oxidized spectra as the starting material. This result strongly supports the important role of TX-100 in stabilizing the heme-binding domain when the protein is subjected to partial proteolysis.

Finally, the last part of the analysis was aimed at determining the location in cytochrome $b_{558}$ of the fragments found in later eluting spectrally active gel filtration fractions. Using SDS-PAGE, Western blot analysis, fluorescent WGA affinity analysis, and MALDI MS, the fragments were characterized relative to their potential position in either the large subunit or small subunit of cytochrome $b_{558}$. Discussion of the results from these analyses follow for each of the digestion conditions.

Digestion in Octylglucoside

The oxidized absorbance spectra taken during the 1 hour digestion of cytochrome $b_{558}$ showed that the protein is not stable during proteolysis while solubilized in OG (Figure 50). However, after separation of the digested material by gel filtration chromatography, fraction 24 did show the presence of an uncharacterized absorbing species that was reversibly sensitive to reduction by dithionite (Figure 55 and 56). SDS-PAGE revealed two bands in fractions 24-26, a species with $M_r$ = 17 kDa and a species with $M_r$ = 26 kDa (Figure 53). The 17 kDa species was observed in fraction 24, but fractions 25 and 26 contained both. Microsequencing analysis was carried out on fraction 24 while immunological and lectin (WGA) affinity analysis were done on fraction 25.

The Western blot analysis shown in Figure 57, using the anti-small subunit antibody α-EAR, suggests that a 17 kDa fragment of the small subunit was present in fraction 25 and most likely in fraction 24, thus implicating the small subunit in the absorbance properties of the fractions. Additional support for the generation of this fragment comes from the observation that the 17 kDa species was not present in the starting material when probed with the α-EAR antibody.

WGA-CCB affinity labeling of the electrotransfer of gel filtration fraction 25 (Figure 58) shows that a band at 17 kDa also possesses WGA-CCB binding capacity and is thus glycosylated. This result suggests a fragment from the small subunit and the glycosylated large subunit were both present since previous work has shown that the small subunit does not contain glycosylation (5).

MALDI MS analysis of fraction 24, shown in Figure 59, revealed that the fraction consists of multiple components at 17 kDa, a smaller peak at 16,708 Da and a shoulder peak at 17,089 Da, along with the major peak at 16,997 Da. These masses, however, do not match any predicted cleavage products that would result from partial digestion of the small subunit by the protease trypsin. In summary, fractions 24 and 25 have these properties: 1) a fragment with $M_r$ = 17 kDa that is recognized by the small subunit antibody α-EAR; 2) a fragment with $M_r$ = 17 kDa that binds WGA-CCB suggesting that it is glycosylated; 3) at least three fragments at $M_r$ ~17 kDa when analyzed by MALDI MS none of which match a fragment of the small subunit cleaved by the protease trypsin.

Conclusions from the Partial Tryptic Digest of Cytochrome $b_{558}$ Solubilized in OG

In order to determine the amino acid sequence of the components of fraction 24, the fraction was sent for sequencing at the Harvard Microsequencing Facility located at Harvard University. The results showed that a component of the sample, i.e. the fragment with a mass of 16,997 Da (Figure 59), was from the lipopolysaccharide binding protein hCAP18 (**h**uman **C**ationic **A**ntimicrobial binding **P**rotein) with a small trpytic fragment removed from the N-terminus. Also, the peak slightly lower in mass at 16,705 Da in Figure 59, matches another tryptic fragment of hCAP-18. This protein is found in high concentrations in specific granules of human neutrophils and is either a contaminant of the cytochrome $b_{558}$ preparation used for these experiments due to its hydrophobic C-terminus (39,40) or it could conceivably be associated with cytochrome $b_{558}$ and thus copurify. Since there were multiple species present in fraction 24 (as observed by MALDI MS), numerous peptides were produced upon digestion of the fraction for microsequening analysis. Thus, not all peptides were subjected to amino acid sequencing due to the large number.

The results from the absorbance spectroscopy, Western blot, WGA-CCB, and MALDI MS analyses, leave a number of unanswered questions about the origin of the tryptic fragments detected in fractions 24 and 25. First, is the absorbance observed in fraction 24 from heme coordinated to one of the species present in the fraction? The spectral absorbance properties observed in this fraction do not match those of undigested cytochrome $b_{558}$ (428 nm vs. 414 nm for the oxidized Soret peak). One hypothesis to explain this observation is that the fragment(s) present no longer contain(s) the tertiary

structure surrounding the heme found in the undigested protein due to the instability of the fragments in OG. Since the findings from the tryptic digestion performed in TX-100 clearly show that the fragments are stable in this detergent, the hypothesis that the fragments produced in OG no longer possess a 'normal' tertiary structure seems plausible. The observation that a redox center, optically sensitive to reducing agent, and reoxidized by the introduction of oxygen to the system, is consistent with the presence of heme coordinated to one of the fragments. In addition, absorbance spectra of free hemin in gel filtration sample buffer were unlike those found for fraction 24 (data not shown).

One other question arises from the immunological analysis of the fragments associated with these fractions. Why does an antibody for the small subunit, and a carbohydrate binding probe, apparently recognize the same fragment? One possibility is that the binding of α-EAR, and WGA-CCB, to the 17 kDa species was non-specific. Previous experiments have shown that binding of α-EAR to undigested small subunit of cytochrome $b_{558}$ is competitively inhibited by the presence of EAR peptide, as is the binding of WGA-CCB which is competitively inhibited by the presence of *N*-acetylglucosamine. Moreover, neither α-EAR nor WGA-CCB recognize this species in the undigested material. Although it is possible that α-EAR non-specifically recognized a region of hCAP-18 that was exposed after partial digestion, it is unlikely. If this were the case then the staining seen in the Western blot using α-EAR antibody (Figure 57) would most likely be more intense than what was seen since there is a substantial amount of hCAP18 in the fraction.

Another possible explanation is that a fragment of the small subunit, along with a portion of the large subunit containing carbohydrate, are bound together in a complex that is stable when subjected to SDS-PAGE. It is clear from the results of the Western blot analysis performed using the α-EAR antibody, that when the fraction is reduced and alkylated, an increase in staining is observed at $M_r$ = 17 kDa (see Figure 57). In addition, a faint band becomes apparent at Mr ~ 26 kDa when the reduced and alkylated fraction is probed with α-EAR. If a stable complex of the large and small subunit bound tightly by intra- and inter-chain disulfide linkages exists in this fraction, due to the conditions of partial digestion, then the application of reducing and alkylating reagents would likely cause this complex to be partially disrupted and allow for the antibody to better recognize the specific epitope. This would only be true if the complex became more stable under conditions of partial digestion since the α-EAR epitope is recognized on the small subunit when undigested cytochrome $b_{558}$ is probed using Western blot analysis. Reduction and alkylation would unfold a polypeptide chain containing intra-chain disulfide linkages causing it to migrate at a slower rate in SDS-PAGE, thus giving rise to the band observed at $M_r$ ~ 26 kDa. The WGA-CCB results from fraction 25 show the presence of WGA binding species at $M_r$ = 17 kDa before reduction and alkylation, and at $M_r$ = 17 and $M_r$ ~ 26 kDa after reduction and alkylation (see Figure 58). The results are in accord with the α-EAR Western blot analysis seen in Figure 57 and support the hypothesis that a carbohydrate containing species, presumably from the large subunit, is present complexed through disulfide-stabilized interactions to a fragment of the small subunit.

MALDI MS analysis of fraction 24 shows that it contains multiple components (see Figure 59). However, the poor resolution obtained in this fraction does not allow accurate mass assignment for all the components. This was also the case for fraction 25 where the results were identical to those found for fraction 24 (data not shown). Since MALDI MS is not sensitive to folding by intra-chain disulfides, the masses observed in Figure 59 reflect the masses of the components independent of reduction and alkylation. If a fragment consisting of a portion of the large and small subunits were present in fraction 24, consistent with the Western blot and lectin affinity analyses, then the MALDI MS data should show two peaks corresponding to the two fragments, assuming they would dissociate under the conditions used. If the two fragments did not dissociate when subjected to MALDI, then the combined mass of the fragments should be close to ~ 26 kDa. The peaks observed in fraction 24 correspond to both these possibilities. There are peaks observed at m/z ~8,300 - 8,800 Da, 16,500 - 17,300 Da, and 25,700 - 25,900 Da (which also support the findings observed using SDS-PAGE). A combination of one of the mass peaks between 8,300 - 8,800 Da with one of the mass peaks at 16,500 - 17,300 Da, would result in a combined mass equal to that observed for the band at $M_r$ ~ 26 kDa in the Western blot and lectin affinity analyses upon reduction and alkylation. Furthermore, the mass peak observed between 25,700 - 25,900 Da would also match the observed band at $M_r$ ~ 26 kDa in the Western blot and lectin affinity analyses observed upon reduction and alkylation. However, an exact assignment for the mass peaks observed in the fraction are confounded by the presence of the singly charged ion of hCAP-18 at m/z 16,997 Da and its doubly charged ion at m/z 8,498 Da.

Thus the MALDI MS data cannot prove or disprove the existence of a large and small subunit complex in the fraction and support the reasonable explanation for both immunological and lectin binding activities for components in this molecular weight range (i.e. several components of the same approximate mass). Additional work is needed to conclusively determine if such a complex exists when cytochrome $b_{558}$ solubilized in OG is partially digested with trypsin. Experiments that could be performed to isolate and characterize such a complex include, shortening the digestion time (to reduce the problem of instability of the heme coordination), removal of hCAP-18 from the sample prior to digestion, or affinity isolation of the α-EAR epitope containing fragment by immuno-affinity methods.

Digestion of Cytochrome $b_{558}$ in Triton X-100

The use of Triton X-100 for solubilizing cytochrome $b_{558}$ prior to digestion proved essential for generating stable heme containing proteolytic fragments that could be further characterized. The flow diagrams showing the findings from these digestions using trypsin and V8 protease are shown in Figures 77 and 78. Summaries of the findings by Western blot and WGA-CCB analyses are presented at the lower left corner of the figures and findings from MALDI MS analyses are presented in the lower right-hand corner. The difference between the two detergent environments is the stability of the heme absorbance spectra. The stability furnished by the TX-100 resulted in reduced minus oxidized absorbance spectra in gel filtration fractions tryptic digestion and V8 protease digestion (see Figures 66 and 67) indicative of stable heme coordination.

Tryptic Digestion of Cytochrome $b_{558}$ in Triton X-100

Western blot analysis using the small subunit antibody α-EAR on gel filtration fractions from the 1 hour tryptic digest show that the epitope on the small subunit recognized by α-EAR (amino acids 162-174) has been cleaved away by the protease (Figure 69). This is easily observed by comparing the lanes labeled B.D. (Before Digest) and A.D. (After Digest). Gel filtration fractions were also probed with the small subunit mAb 44.1 and no labeling was observed (data not shown). These results indicate that at least the 33 carboxy-terminal residues containing the epitopes for the antibodies α-EAR and mAb 44.1 were not present in this fraction.

Gel filtration fractions were also probed with the anti-large subunit antibody α-KIS as shown in Figure 71. A broad band between $M_r$ ~45-65 kDa indicates that partially digested large subunit retains the KIS epitope (amino acids 246-256) and elutes in these fractions. A broad band of $M_r$ ~45-65 kDa is also evident in fraction 14 and in fraction 21 when separated by SDS-PAGE, both of which exhibited the reduced minus oxidized absorbance spectrum identical to cytochrome $b_{558}$. These same fractions were probed with the large subunit mAb 54.1 which recognizes residues 382-389 from the N-terminal half of the protein. No staining was observed. These results indicate that at least residues 381-569 were removed from this sample and that heme could not be coordinated by residues in the C-terminal portion of the large subunit. In addition, these results suggest that the heme-bearing fragment present in this sample contains the epitope for the α-KIS antibody in a polypeptide chain with a maximum molecular weight of ~ 39 kDa plus the additional mass of ~ 26 kDa from the carbohydrate.

Probing of the gel filtration fractions with WGA-CCB on a nitrocellulose transfer revealed that the broad band observed in the Western blot analysis was due to glycosylation since the WGA-CCB was found to bind to the same region recognized by α-KIS (data not shown). These results suggested that the portion of the large subunit, containing sites of glycosylation, was most likely responsible for the absorbance spectrum seen in Figure 68. An estimate for the average amount of carbohydrate on the protein is approximately 26 kDa (i.e. 91 kDa for the mass of the intact protein minus 65 kDa for the polypeptide chain). This calculation would place the maximum molecular weight of the polypeptide chain present in fraction 21 at ~ 39,000 and would include amino acids 246-256 from the epitope recognized by the α-KIS antibody. This is consistent with the present hypothesis that the hemes are ligated somewhere between residues 100-260 of the large subunit (25-29).

MALDI MS spectral data for fraction 21 revealed two tryptic fragments that could have originated from the small subunit of cytochrome $b_{558}$ (see Figure 72). One of these fragments has a mass of 15,325 Da, however the mass assignment for this fragment is tentative since the signal intensity was low. This fragment could have originated from the small subunit, since a tryptic fragment of the small subunit having a mass 15,289 Da containing residues M 1 to R 139 was within the mass error associated with the instrument. The mass for the fragment did not match any tryptic fragments from the large subunit. In addition, the 15,325 Da fragment observed in gel filtration fractions 14 and 21 (both of which had reduced minus oxidized absorbance spectra identical to intact cytochrome $b_{558}$) was not observed in fraction 17 (which had little or no absorbance

activity). These results are shown in Figure 79 along with the control digest of trypsin without substrate. A notably smaller fragment, with a mass of 10,215 Da, was found that was not readily observed in the SDS-PAGE seen in Figure 79. The confidence in the mass assignment for this fragment is quite high and moreover it matches a tryptic fragment of the small subunit containing residues H 72 to K 165 that would not be recognized by either α-EAR or mAb 44.1 . Both tentative assignments for these fragments contain H 92 which is in the proposed hydrophobic transmembrane region of the small subunit. Thus the MALDI MS data suggests that fragments of the small subunit are present in fraction 21. The elution time of these fragments suggest that they are somehow associated with other fragments since they would not elute at this retention time in monomeric form.

MALDI MS analysis provides higher accuracy than data derived from SDS-PAGE and Western blot analysis. Although bands observed by Western blot and WGA-CCB analyses suggest a fragment of the large subunit with $M_r$ between 45-65 kDa, the data for the high mass region using MALDI MS suggests that the true mass is closer to 40 kDa. When the mass of the carbohydrate present on the fragment is taken into account (roughly 25-30 kDa) the polypeptide backbone is approximately 10-15 kDa. As mentioned previously, this would implicate residues 130 through 270 of the large subunit, which includes the epitope for the α-KIS antibody and also H 208, H 209, and H 221 from the same proposed transmembrane region. The MALDI MS data thus suggest that the fragments isolated in fraction 21 contain fragments of both the large and small subunits.

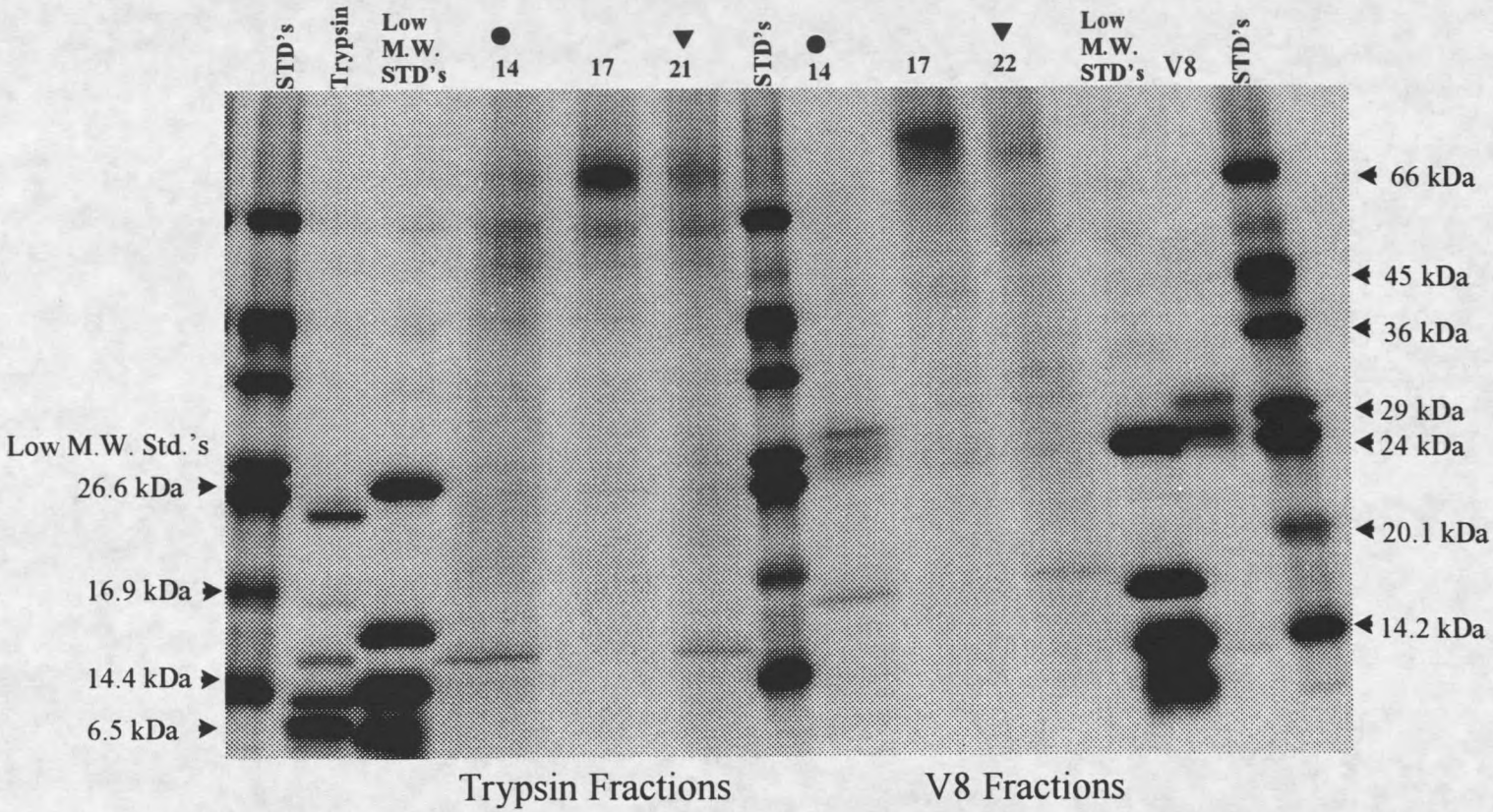


**Figure 79**. 7-18% gradient SDS-PAGE gel with gel filtration fractions from 1 hour tryptic and V8 digests of TX-100 solubilized cytochrome $b_{558}$. The lanes from the tryptic digest show a 15.5 kDa fragment that is seen in both of the fractions having reduced minus oxidized activity (14 and 21) but not in the fraction where there is little spectral activity (17). In addition, the lanes labeled V8 digest show the fragment at 17 kDa in both of the fractions having reduced minus oxidized activity (14 and 22) but not in the fraction were there is little spectral activity (17). These results illustrate that the 15.5 kDa tryptic fragment and the 17 kDa V8 fragment are not present in the fractions that do not have appreciable spectral activity.

V8 Protease Digestion of Cytochrome $b_{558}$ in Triton X-100

The results from the Western blot analysis of fraction 22 shows that a 17 kDa species containing the α-EAR epitope was produced after one hour of V8 protease exposure (Figure 70). These results are shown in the lanes labeled B.D. (Before Digest), where small subunit staining is plainly visible, and A.D. (After Digest), where staining for the 17 kDa species is plainly visible. The results from the gel filtration fractions in the same figure show that this 17 kDa species was present in a number of fractions, most importantly, in fractions 14 and 22 which exhibited reduced minus oxidized absorbance spectra identical to undigested cytochrome $b_{558}$. This species would not be present in these fractions unless it was associated with other fragments since a molecule with $M_r$ = 17 kDa should elute at a later retention time. Western blot analysis of fraction 22 using the α-KIS antibody produced only weak staining. This fraction was also probed with the mAb 54.1 which recognizes the N-terminal region of the large subunit containing amino acids 382-389. The results from this Western blot showed that intact large subunit, or any fragments containing the 54.1 epitope, were not detected (data not shown). This fraction was of interest since it contained a band at 17 kDa recognized by the small subunit antibody α-EAR and a reduced minus oxidized absorbance spectrum identical to cytochrome $b_{558}$.

Gel filtration fractions 14, 17, and 22 were also examined by SDS-PAGE to detect other major components produced by V8 digestion which were not evident by Western blot analysis (Figure 79). The spacing patterns in lanes containing fractions 14 and 22 show that below $M_r$ of 24 kDa, the band at 17 kDa is the major component. Furthermore, the 17 kDa fragment is present in these fractions but is not present in fraction 17 where

little or no absorbance at 414 nm was observed. This evidence, coupled with the data from Western blot analysis using α-EAR, is consistent with the small subunit participation of heme- binding in the molecule.

MALDI MS data on fraction 22 (Figure 74) demonstrated that the 17 kDa fragment has a mass of roughly 17,786 Da but interference from the doubly charged protease in the fraction made it difficult to obtain an accurate mass. In spite of the uncertainty introduced, there is no mass spectral evidence for this fragment originating from either hCAP-18, or from the large subunit of cytochrome $b_{558}$. The lack of accurate mass data for the 17 kDa fragment in this fraction is problematic, however the presence of this fragment in duplicate experiments (performed by T. Foubert and J. Burritt in the Jesaitis laboratory) is consistent with this polypeptide participating in the heme-binding domain. The mass of the fragment labeled ***b*** in the MALDI MS spectrum in Figure 74, matches the mass of a V8 fragment from the N-terminal half of the large subunit, residues V 203 to E 282. This result is questionable even though it corresponds to a predicted heme-bearing domain of the large subunit lacking its carbohydrate. Another unusual result is the presence of the fragment labeled ***c*** at m/z = 9,623 Da in Figure 79, which matches a V8 generated fragment composed of residues A 378 to E 461, that includes H 448 from the carboxy-tail region of the protein and the epitope for mAb 54.1. The results from the Western blot analysis on fraction 22 using mAb 54.1 did not include species with a molecular weight below 12 kDa since the lowest molecular weight standard was run to the bottom of the gel. These results suggest that portions of the N-terminal half of the large subunit are present in these fractions. However, the MALDI MS data do not provide

sufficient evidence to determine the origin of the 17 kDa species observed in the SDS-PAGE, Western blot, and lectin affinity analyses. This was due to low signal intensities for this species despite repeated attempts to optimize the signal by changing ionization parameters in the mass spectrometer.

## Conclusion

The findings presented in this chapter develop several features inherent to the isolation of the heme-binding sites within cytochrome $b_{558}$. The most important of these features is the stability of the proteolytic heme-bearing fragments in the detergent used for the digestion. The absorbance characteristics of cytochrome $b_{558}$ were used to illustrate the change in the protein upon partial digestion. Clearly, when compared to OG, the higher molecular weight and more hydrophobic detergent Triton X-100 (TX-100) appears to produce fragments of higher stability upon partial digestion with the proteases V8 or trypsin.

Another feature of the characterization of proteolytic digestion of cytochrome $b_{558}$ is the effectiveness of gel filtration chromatography for separating partially digested material while maintaining the integrity of the non-covalently bound heme prosthetic groups. The presence of aggregated material in the chromatograms of partially digested and undigested protein indicates that the starting material was not ideal and that non-specific interactions (e.g. hydrophobic interactions) may have been preserved when placed on the gel filtration column.

The properties of the solid support in the TSK G3000SW column used for separation may have contributed to this problem. The column, produced by TosoHass, uses a silica bead coated with a synthetic inert hydrophilic polymer. This type of support is somewhat different than the more common Sepharose bead support produced by Pharmacia Biotech (Uppsala, Sweden) which is based on the hydrophilic biopolymer agarose. Future work will focus on the ability of Sepharose to separate fragments from partially digested cytochrome $b_{558}$. Nonetheless, fragments isolated using the TSK G3000SW gel filtration column were stable for more that 24 hours as determined by their reduced minus oxidized absorbance spectra. This finding is fundamental to the characterization of the fragments after separation since exchange of the partially digested material from TX-100 to OG in the column was needed to successfully perform MALDI MS.

The use of MALDI MS to analyze fragments from the partial digestion of cytochrome $b_{558}$ was an essential step in the experimental design aimed at determining the heme-binding domain in cytochrome $b_{558}$. Mass spectrometry has been underutilized in the exploration of membrane protein structure due to the problems inherent in the use of detergents used to solubilize this class of hydrophobic biopolymers. The results presented here represent some of the first work employing MALDI MS to evaluate the products of digestion from cytochrome $b_{558}$. The data obtained from using MALDI MS did not conclusively determine the origin of the fragments associated with the reduced minus oxidized spectra observed in the gel filtration fractions. Nevertheless, they represent a fundamental first step in establishing the usefulness of mass spectrometry in the analysis of

functional domains in cytochrome $b_{558}$. MALDI MS has proven to be an effective analytical technique for identifying transmembrane tryptic fragments of rhodopsin isolated by RP-HPLC (33) and in the determination of the location of photo cross-linked ligand in recombinant n-formyl peptide receptor (41). In addition, the results from the MALDI MS experiments illustrated in this chapter show that MALDI MS can provide additional unique information on the composition of fractions from high-performance gel filtration chromatography, including the use of accurate mass data to identify the presence of heme.

Identification of Heme-binding Domains in Cytochrome $b_{558}$

The results described in this chapter confirm the evidence from previous studies which suggest that the small subunit of cytochrome $b_{558}$ is involved in binding heme within the protein. Quinn et al. demonstrated that fragments of cytochrome $b_{558}$, produced by partial digestion with V8 protease, are recognized by anti-small subunit antibodies and also exhibit heme staining (20). In addition, Yu et al. demonstrated that the expression of functional cytochrome $b_{558}$ is inhibited in myeloid cells undergoing differentiation upon the addition of the heme synthesis inhibitor, succinyl acetone (42). The authors propose that heme plays a crucial role in the stable expression of the large and small subunits of cytochrome $b_{558}$ by either aiding in the proper folding of the polypeptides or by allowing the two subunits to interact, i.e. dimerization via a heme group. This hypothesis counters an opposing hypothesis held by other groups, who suggest that only the large subunit is involved in binding the hemes (25-29). Cytochromes found in other systems have been shown to contain hemes bound by two separate transmembrane polypeptide

chains (30, 39-42). Furthermore, the small subunit of cytochrome $b_{558}$ shares homology with other heme-binding proteins (15). Therefore, the hypothesis that the small subunit is involved in heme-binding in cytochrome $b_{558}$ is the only one supported by direct evidence and thus is more tenable than the single subunit hypothesis.

MALDI MS results presented here for the high mass fragments isolated from the partial tryptic digestion of cytochrome $b_{558}$ solubilized in TX-100, supports a N-terminal locus for the heme-binding domain in the large subunit. These results narrow the residues most likely involved in the locus to those between 120-270 since the mass observed using MALDI MS is ~ 40 kDa, as opposed to 45-65 kDa when analyzed using SDS-PAGE. In addition, Quinn et al. found this same broadly distributed band between 45-65 kDa by lithium dodecyl sulfate-PAGE after partial digestion with V8 and they demonstrated that this band exhibits TMBZ/$H_2O_2$ heme staining.

Figure 80 is a speculative model showing the interchain heme-binding domain within cytochrome $b_{558}$ deduced from the findings presented in this chapter. This model is based upon the model shown in Figure 2 in Chapter 1 (3) and includes the tryptic fragment from the small subunit that was deduced from the observed mass of the peak labeled ***b*** in Figure 77. It also includes the tryptic fragment from the large subunit that was calculated from the observed high mass peak labeled ***a*** in Figure 78. Together they provide a picture of the most probable link, via a heme, between regions of the large and small subunit of cytochrome $b_{558}$. This model represents only the fragments observed by MALDI MS that could be assigned an accurate position within the protein and does not include the other arrangements that were observed in this fraction (i.e. peak ***a*** in Figure 77).

Figure 80

Model of Heme-binding Domain in Cytochrome $b_{558}$

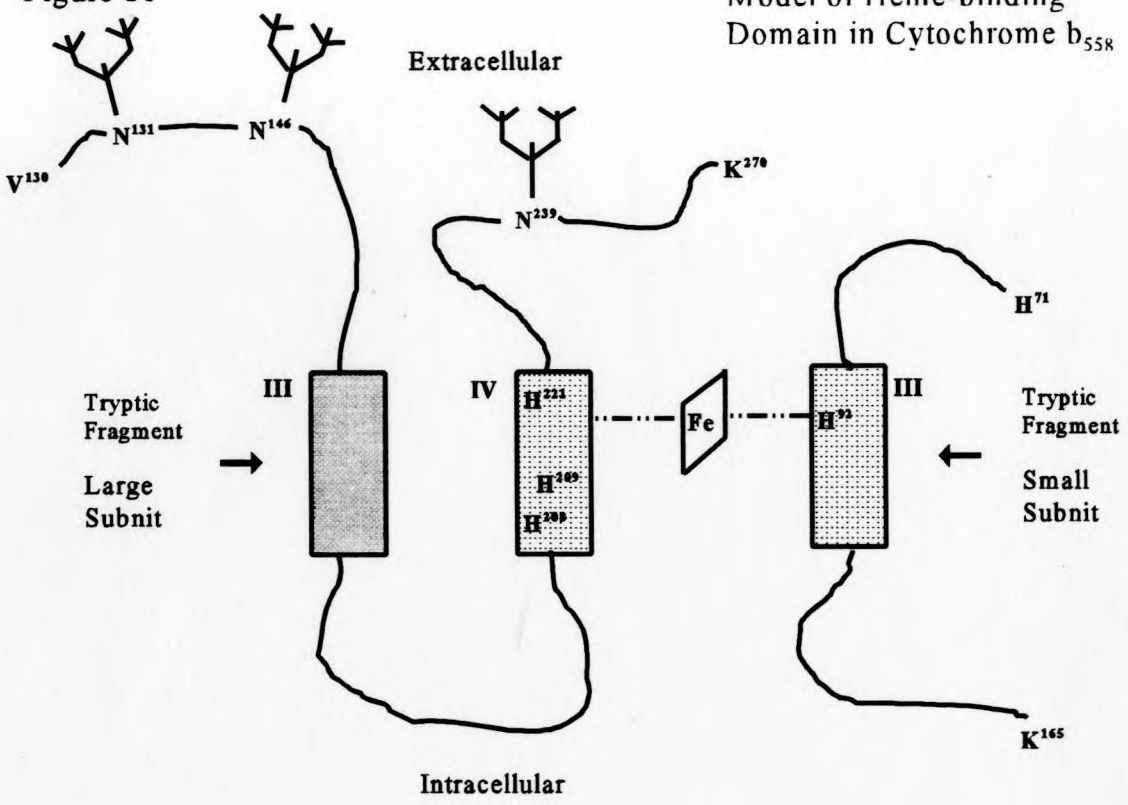


The partial digestion approach to isolating the heme-binding domains in cytochrome $b_{558}$ does not provide a satisfactory, conclusive description, of the positioning of the hemes in the molecule. Our data also weakly suggest that proposed transmembrane histidines 208, 209 and 221 from the large subunit is involved in heme-binding. Our data also show that small subunit fragments are always found in fractions that exhibit heme absorbance properties and these fragments copurify with large subunit fragments.

This conclusion is supported by the following observations:

1) Fraction 24 from the partial tryptic digest of cytochrome $b_{558}$ solubilized in OG contained a species ($M_r$ = 17 kDa) that was recognized by a small subunit antibody and by a lectin binding probe. Fraction 24 also contained species having masses, that together, could result in the species recognized by a small subunit antibody and by a lectin binding probe after reduction and alkylation ($M_r$ ~26 kDa).

2) Fragments in fraction 21 from the partial tryptic digest of cytochrome $b_{558}$ solubilized in TX-100, at m/z 15,325 Da and 10,215 Da, matched tryptic fragments of the small subunit. This fraction also contained a ~ 40 kDa species recognized by a large subunit antibody and by a lectin binding probe.

3) Fraction 22 from the partial V8 digest of cytochrome $b_{558}$ solubilized in TX-100 contained a 17 kDa fragment recognized by a small subunit antibody. This fraction also included two species at m/z 9,250 Da and 9,623 Da, which matched V8 protease fragments from the large subunit.

Future experiments using proteolytic methods must focus on improving the gel filtration separation of the fragments produced. This will necessitate exploring different column supports, such as Sepharose beads. Alternative separatory methods on the spectrally active fractions will help to avoid complications in the MALDI MS analysis from interference of added protease and detergent suppression effects. Additionally, the fragments separated by gel filtration should be further separated by SDS-PAGE, then subjected to in-gel digestion followed by sequencing analysis using nanospray MS/MS. Finally, fractions that exhibit reduced minus oxidized spectra, and show WGA-CCB

binding, should be treated with glycosidase to remove carbohydrate in order to provide more effective and accurate mass analysis. If these suggestions are implemented, the results should provide a definitive localization of the heme-binding domains in cytochrome $b_{558}$.

## Closing Remarks

The experiments described in this thesis performed on the proteins bacteriorhodopsin (BR), rhodopsin, and cytochrome $b_{558}$ have shown that mass spectrometry is a viable analytical technique for characterizing integral membrane proteins. The results obtained have demonstrated that mass spectrometry can provide accurate mass for intact membrane proteins, as well as proteolytic fragments, solubilized in detergent. Furthermore, this thesis illustrates that when data from techniques such as Western blot analysis and visible absorbance spectroscopy are coupled with mass spectral data the results can be compiled to produce meaningful structural information on integral membrane proteins.

## References


1. Dinauer, M. C. 1993. The respiratory burst oxidase and the molecular genetics of chronic granulomatous disease. *Crit. Rev. Clin. La. Sci.* 30:329-369.

2. Dinauer, M. C., S. H. Orkin, R. Brown, A. J. Jesaitis, and C. A. Parkos. 1987. The glycoprotein encoded by the X-linked chronic granulomatous disease locus is a component of the neutrophil cytochrome b complex. *Nature* 327:717-720.

3. Parkos, C. A., M. T. Quinn, and A. J. Jesaitis. 1992. Molecular basis of oxidative damage by leukocytes. A. J. Jesaitis and E. A. Dratz, editors. CRC Press, Boca Raton,FL.

4. Segal, A. W. and O. T. Jones. 1978. Novel cytochrome b system in phagocytic vacuoles of human granulocytes. *Nature (London)* 276:515-517.

5. Parkos, C. A., A. A. Allen, C. G. Cochrane, and A. J. Jesaitis. 1987. Purified cytochrome b from human granulocyte plasma membrane is comprised of two polypeptides with relative molecular weights of 91,000 and 22,000. *J. Clin. Invest.* 80:732-742.

6. Segal, A. W. 1989. The electron transport chain of the microbicidal oxidase of phagocytic cells and its involvment in the molecular pehtology of chronic granulomatous disease. *J. Clin. Invest.* 1057:281-298.

7. Cross, A. R., F. K. Higson, O. T. Jones, A. M. Harper, and A. W. Segal. 1982. The enzymic reduction and kinetics of oxidation of cytochrome b-245 of neutrophils. *Biochem. J.* 204:479-485.

8. Cross, A. R., O. T. Jones, A. M. Harper, and A. W. Segal. 1981. Oxidation-reduction properties of the cytochrome b found in the plasma-membrane fraction of human neutrophils. A possible oxidase in the respiratory burst. *Biochem. J.* 194:599-606.

9. Sumimoto, H., N. Sakamoto, M. Nozaki, Y. Sakaki, K. Takeshige, and S. Minakami. 1992. Cytochrome b558, a component of the phagocyte NADPH oxidase, is a flavoprotein. *Biochem. Biophys. Res. Commun.* 186:1368-1375.

10. Koshkin, V. and Pick, E. Generation of superoxide by purified and relipidated cytochrome b559 in the absence of cytosolic activators. *FEBS Lett.* 327(1):57-62, 1993.

11. Segal, A. W., I. West, F. Wientjes, J. H. Nugent, A. J. Chavan, B. Haley, R. C. Garcia, H. Rosen, and G. Scrace. 1992. Cytochrome b-245 is a flavocytochrome containing FAD and the NADPH-binding site of the microbicidal oxidase of phagocytes. *Biochem. J.* 284P781-8:781-788.

12. Rotrosen, D., C. L. Yeung, T. L. Leto, H. L. Malech, and C. H. Kwong. 1992. Cytochrome b558: the flavin-binding component of the phagocyte NADPH oxidase. *Science* 256:1459-1462.

13. Lutter, R., M. L. J. van Schaik, R. V. van Zwieten, R. Wever, D. Roos, and M. N. Hamers. 1985. Purification and partial characterization of the *b*-type cytochrome from human polymorphonuclear leukocytes. *J. Biol. Chem.* 260:2237-2244.

14. Harper, A. M., M. J. dunne, and A. W. Segal. 1984. Purification of cytochrome $b_{-245}$ from human neutrophils. *Biochem. J.* 219:519-527.

15. Royer-Pokora, B., L. M. Kunkel, A. P. Monaco, S. C. Goff, R. L. Newburger, R. L. Baehner, F. S. Cole, J. T. Curnutte, and S. H. Orkin. 1986. Cloning of the gene for an inherited human disorder-chronic granulomatous disease- on the basis of its chromosomal location. *Nature* 322:32-38.

16. Parkos, C. A., M. C. Dinauer, L. E. Walker, R. A. Allen, A. J. Jesaitis, and S. H. Orkin. 1988. Primary structure and unique expression of the 22-kilodalton light chain of human neutrophil cytochrome *b*. *Proc. Natl. Acad. Sci. U. S. A.* 85:3319-3323.

17. Parkos, C.A., M. T. Quinn, S. Sheets, and A. J. Jesaitis. 1992. The structure of human neutrophil b-type cytochrome involved in superoxide production. In: Molecular Basis of Oxidative Damage by Leukocytes. Jesaitis A. J., and E. A. Dratz, eds. CRC Press, Boca Raton, Fla. 45-55.

18. Jesaitis, A. J. 1995. The structure of human phagocyte cytochrome b and its relationship to microbicidal superoxide production. *J. Immunol.* 155:3286-3288.

19. Iizuka, T., S. Kanegasaki, R. Makino, T. Tanaka, and Y. Ishimura. 1985. Studies on neutrophil *b*-type cytochrome *in situ* by low tempurature absorption spectroscopy. *J. Biol. Chem.* 260:12049-12053.

20. Quinn, M. T., M. L. Mullen, and A. J. Jesaitis. 1992. Human neutrophil cytochrome b contains multiple hemes; evidence for heme associated with both subunits. *J. Biol. Chem.* 267:7303-7309.

21. Cross, A. R., J. Rae, and J. T. Curnutte. 1995. Cytochrome b-245 of the neutrophil superoxide-generating system contains two nonidentical hemes. Potentiometric studies of a mutant form of gp91phox. *J. Biol. Chem.* 270:17075-17077.

22. Cross, A. R., P. G. Heyworth, J. Rae, and J. T. Curnutte. 1995. A variant X-linked chronic granulomatous disease patient (X91+) with partially functional cytochrome b [published erratum appears in J Biol Chem 1995 Jul 14;270(28):17056]. *J. Biol. Chem.* 270:8194-8200.

23. Fujii, H. and K. Kakinuma. 1992. Electron paramagnetic resonance studies on cytochrome b-558 and peroxidases of pig blood granulocytes. *Biochim. Biophys. Acta* 1136:239-246.

24. Ueno, I., S. Fujii, H. Ohya Nishiguchi, T. Iizuka, and S. Kanegasaki. 1991. Characterization of neutrophil b-type cytochrome in situ by electron paramagnetic resonance spectroscopy. *FEBS Lett.* 281:130-132.

25. Hurst, J. K., T. M. Loehr, J. T. Curnutte, and H. Rosen. 1991. Resonance Raman and electron paramagnetic resonance structural investigations of neutrophil cytochrome b558. *J. Biol. Chem.* 266:1627-1634.

26. Doussiere, J., J. Gaillard, and P. V. Vignais. 1996. Electron transfer across the O2-generating flavocytochrome b of neutrophils. Evidence for a transition from a low-spin state to a high-spin state of the heme iron component. *Biochemistry* 35:13400-13410.

27. Miki, T., H. Fujii, and K. Kakinuma. 1992. EPR signals of cytochrome b558 purified from porcine neutrophils. *J. Biol. Chem.* 267:19673-19675.

28. Fujii, H., M. G. Finnegan, T. Miki, B. R. Crouse, K. Kakinuma, and M. K. Johnson. 1995. Spectroscopic identification of the heme axial ligation of cytochrome b558 in the NADPH oxidase of porcine neutrophils. *FEBS Lett.* 377:345-348.

29. Fujii, H., M. K. Johnson, M. G. Finnegan, T. Miki, L. S. Yoshida, and K. Kakinuma. 1995. Electron spin resonance studies on neutrophil cytochrome b558. Evidence that low-spin heme iron is essential for O2-. generating activity. *J. Biol. Chem.* 270:12685-12689.

30. Fujii, H., T. Yonetani, T. Miki, and K. Kakinuma. 1995. Modulation of the heme environment of neutrophil cytochrome b558 to a "cytochrome P450-like" structure by pyridine. *J. Biol. Chem.* 270:3193-3196.

31. Shatwell, K. P., A. Dancis, A. R. Cross, R. D. Klausner, and A. W. Segal. 1996. The FRE1 ferric reductase of Saccharomyces cerevisiae is a cytochrome b similar to that of NADPH oxidase. *J. Biol. Chem.* 271:14240-14244.

32. Finegold, A. A., K. P. Shatwell, A. W. Segal, R. D. Klausner, and A. Dancis. 1996. Intramembrane bis-heme motif for transmembrane electron transport conserved in a yeast iron reductase and the human NADPH oxidase. *J. Biol. Chem.* 271:31021-31024.

33. Babcock, G. T., W. R. Widger, W. A. Cramer, W. A. Oertling, and J. G. Metz. 1985. Axial ligands of chloroplast cytochrome b-559: identification and requirement for a heme-cross-linked polypeptide structure. *Biochemistry* 24:3638-3645.

34. Nauseef, W.M., Olsson, I., and Arnljots, K. Biosynthesis and processing of myeloperoxidase--a marker for myeloid cell differentiation. *Eur.J.Haematol.* 40(2):97-110, 1988.

35. Towbin, H., Staehelin, T., and Gordon, J. Electrophoretic transfer of proteins from polyacrylamide gels to nitrocellulose sheets: Procedure and some applications. *Proc. Natl. Acad. Sci.* 76:4350-4354, 1979.

36. Barnidge, D. R., E. A. Dratz, J. Sunner, and A. J. Jesaitis. 1997. Identification of transmembrane tryptic peptides of rhodopsin using matrix-assisted laser desorption/ionization time-of-flight mass spectrometry. *Protein Sci.* 6:816-824.

37. Koshkin, V. and E. Pick. 1994. Superoxide production by cytochrome b559. Mechanism of cytosol-independent activation. *FEBS Lett.* 338:285-289.

38. Quinn, M. T., C. A. Parkos, L. Walker, S. H. Orkin, M. C. Dinauer, and A. J. Jesaitis. 1989. Association of a ras-related protein with cytochrome b of human neutrophils. *Nature* 342:198-204.

39. Larrick, J.W., M. Hirata, J. Zhong, and S.C. Wright. 1995. Anti-microbial activity of human CAP18 peptides. *Immunotechnology* (1):65-72.

40. Sorensen, O., K. Arnljots, J.B. Cowland, D. F. Bainton, and N. Borregaard. 1997. The human antibacterial cathelicidin, hCAP-18, is synthesized in myelocytes and metamyelocytes and localized to specific granules in neutrophils. *Blood* (7):2796-2803.

41. Mills, J. S., Miettinen, H. M., Barnidge, D. R., Vlases, M. J., Wimer-Mackin, S., Dratz, E. A., and Jesaitis, A. J. 1998. Identification of a ligand binding site in the human neutrophil formyl peptide receptor using a site-specific fluorescent photoaffinity label and mass spectrometry. *J. Biol. Chem.* (273): 10428-10435.

42. Yu, L., L. Zhen, and M.C. Dinauer. 1997 Biosynthesis of the phagocyte NADPH oxidase cytochrome b558. Role of heme incorporation and heterodimer formation in maturation and stability of gp91phox and p22phox subunits. *J Biol Chem* (43):27288-27294